

Visible Light-induced Photo-redox Catalysis and Dual Catalysis for C–H Functionalization of 2-Phenyl-4*H*-pyrido[1,2-*a*]pyrimidin-4-one and 2-Aryl Heterocycles

Ph.D. Thesis

By

BHAWALE RAJESH TABAJEE



**DISCIPLINE OF CHEMISTRY
INDIAN INSTITUTE OF TECHNOLOGY INDORE
DECEMBER 2024**

Visible Light-induced Photo-redox Catalysis and Dual Catalysis for C–H Functionalization of 2-Phenyl-4*H*-pyrido[1,2-*a*]pyrimidin-4-one and 2-Aryl Heterocycles

A THESIS

*Submitted in partial fulfillment of the
requirements for the award of the degree
of*
DOCTOR OF PHILOSOPHY

by
BHAWALE RAJESH TABAJEE



**DISCIPLINE OF CHEMISTRY
INDIAN INSTITUTE OF TECHNOLOGY INDORE**

December 2024




INDIAN INSTITUTE OF TECHNOLOGY INDORE

CANDIDATE'S DECLARATION

I hereby certify that the work which is being presented in the thesis entitled “**Visible Light-induced Photo-redox Catalysis and Dual Catalysis for C–H Functionalization of 2-Phenyl-4*H*-pyrido[1,2-*a*]pyrimidin-4-one and 2-Aryl Heterocycles**” in the partial fulfillment of the requirements for the award of the degree of **DOCTOR OF PHILOSOPHY** and submitted in the **Department of Chemistry, Indian Institute of Technology Indore**, is an authentic record of my own work carried out during the time period from **January 2020** to **December 2024** under the supervision of **Dr. Umesh A. Kshirsagar, Associate Professor, Department of Chemistry, IIT Indore**.

The matter presented in this thesis has not been submitted by me for the award of any other degree of this or any other institute.


07/05/2025

Signature of the Student with date
(Bhawale Rajesh Tabajee)

This is to certify that the above statement made by the candidate is correct to the best of my/our knowledge.


07-05-2025

Signature of Thesis Supervisor with date
(Dr. Umesh A. Kshirsagar)

Mr. Bhawale Rajesh Tabajee has successfully given his Ph.D. Oral Examination held on **06/05/2025**


07-05-2025

Signature of Thesis Supervisor with date
(Dr. Umesh A. Kshirsagar)

ACKNOWLEDGEMENT

The completion of my Ph.D. research is not solely the result of my individual efforts but a culmination of the support, guidance, and generosity of many remarkable individuals. I would like to take this opportunity to express my heartfelt gratitude to all those who contributed to this achievement.

*I would like to begin by expressing my heartfelt gratitude to my venerable supervisor, **Dr. Umesh A. Kshirsagar**. I consider myself incredibly fortunate to have had such a mentor who allowed me the freedom to explore independently while offering invaluable guidance whenever I faced challenges. Their unwavering courage and conviction will always inspire me, and I hope to carry forward their noble vision in my future endeavors.*

I would like to extend my heartfelt thanks to my PSPC members, Prof. Satya S. Bulusu and Dr. Amrendra Kumar Singh, for their invaluable suggestions and guidance.

I am deeply thankful to Prof. Suhas S. Joshi, Director of the Indian Institute of Technology Indore, for giving me the opportunity to pursue my doctoral studies and providing the necessary facilities for my research.

I would like to express my thanks to IIT Indore for the financial support provided through the fellowship, and to the Ministry of Human Resource Development (MHRD) for the infrastructure support.

I wish to express my gratitude to Prof. Tushar Kanti Mukherjee (Head, Department of Chemistry, Indian Institute of Technology Indore) for his guidance and support. Also, I wish to express my gratitude to Prof. Rajneesh Misra, Prof. Suman Mukhopadhyay, Prof. Apurba K. Das, Prof. Sampak Samanta, Prof. Biswarup Pathak, Prof. Sanjay Kumar Singh, Dr. Tridib Kumar Sarma, Prof. Anjan Chakraborty, Prof. Shaikh M. Mobin, Prof. Satya Bulusu, Prof. Chelvam Venkatesh, Dr. Amrendra

Kumar Singh, Dr. Debayan Sarkar, Dr. Abhinav Raghuvanshi, Dr. Dipak Kumar Roy, Dr. Selvakumar Sermadurai and Dr. Pravarthana Dhanapal for their guidance and help during various activities.

I extend my gratitude to Dr. Soumen Ghosh (IIT Madras) for his valuable contributions to the theoretical DFT calculations.

I would like to take this opportunity to express my heartfelt gratitude to my group members Mr. Durgesh Sarothiya, Mr. Abhinay S. Chillal, Mr. Amol B. Kirwale, Mr. Shivaji V. Surve, Mr. Pandurang B. Hardas, Mr. Ganesh A. Kadam, Ms. Varsha Kumari, and Chandani, Biswajit, Shalini, Suresh for their generous cooperation and unwavering support. I was lucky to work in a very united, organized, and clean lab.

My special thanks to the members of Lab-1E-104 - Dr. Shivendu Mishra, Mr. Dilip Pandey, Mr. Rahul Kumar Yadav, Mr. Laxman Kharabe, Ms. Darakshan Praveen, Mr. Anirudh Mishra, Mr. Sarvesh Kumar Maurya, Mr. Ritesh Kumar Sahu, Ms. Jyoti Pannu, Ms. Radhika Shrivastava, and Ms. Dimpal Sharma for their valuable suggestions and insightful discussions.

I am grateful to Mr. Kinny Pandey, Mr. Ghanashyam Bhavsar, Mr. Manish Kushwaha, Mr. Parthiban P. K., Mr. Rameshwar, and Ms. Vinita Kothari for their valuable technical assistance and support.

I sincerely thank Dr. Rohit Jadhav and Dr. Dilip Pinjari for their invaluable guidance and support throughout my Ph.D. journey. I am also grateful to Mr. Kailas Chavan (IITJ) and Mr. Atul Nipate (IITDh) for their assistance and insightful discussions. My heartfelt thanks go to all my friends for their good wishes, as well as their direct and indirect support and help. I would like to express my gratitude to my wonderful juniors, and seniors, for their cooperation and invaluable assistance.

I would like to express my heartfelt gratitude to my family, especially my father, Tabajee Bhawale, and my mother, Nilavatee Bhawale, who has been a constant source of inspiration and unwavering moral support throughout my educational journey. I am also deeply grateful to my wife,

Pallavi Bhawale, and to the Almighty for blessing me with such a wonderful family. Additionally, I extend my sincere thanks to my brothers, sisters, and all other family members for their love and encouragement. Above all, none of this would have been possible without their unwavering prayers, support, and encouragement. Their efforts, sacrifices, and hard work are evident in my life.

My Ph.D. journey has been an exciting, fulfilling, and rewarding experience, shaped by the contributions of many individuals, both directly and indirectly. I am leaving with a wealth of experiences and cherished memories, and I would like to acknowledge everyone who played a part in this beautiful journey.

RAJESH...



**DEDICATED TO
MY TEACHERS, BELOVED
FAMILY AND FRIENDS**

- BHAWALE RAJESH TABAJEE

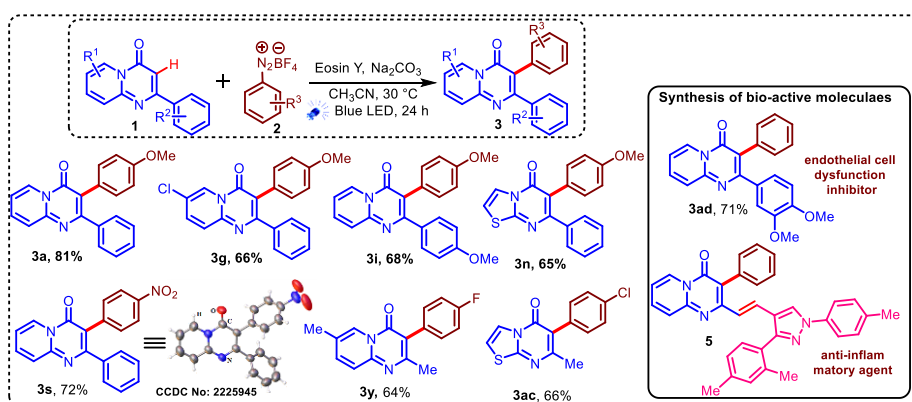
SYNOPSIS

This thesis aims to investigate the potential of modern advancements in carbon-carbon (C–C) bond formation, with a specific emphasis on C–H activation and functionalization facilitated by visible light-mediated photo-redox catalysis and transition metal catalysis. These innovative strategies enable the construction of C–C bonds under mild conditions, typically at room temperature, offering a greener and more sustainable approach to synthetic transformations. In **Chapter 1**, we introduced the literature study of coupling reactions, particularly for C–C bond formation facilitated by transition metal catalysts. This discussion was extended to include visible-light photoinduced pathways for C–H functionalization, highlighting their growing significance in modern organic synthesis. Furthermore, advanced methodologies that integrate photocatalysis with transition metal catalysis to achieve efficient C–C bond formation, emphasizing their innovative potential have been discussed. Finally, we briefly discussed the importance of 2-phenyl-4*H*-pyrido[1,2-*a*]pyrimidin-4-one and reviewed previous reports on the synthesis and functionalization of 2-phenyl-4*H*-pyrido[1,2-*a*]pyrimidin-4-one, providing a foundation for further exploration in this area. Current thesis work focuses on the regio-selective C–H activation and subsequent functionalization, such as arylation, acylation, alkylation, and alkenylation of 2-Phenyl-4*H*-pyrido[1,2-*a*]pyrimidin-4-one and related heterocycles under visible light photo-redox catalytic conditions or through the synergistic merging of photo-redox with transition metal catalysis.

Chapter 2: *Visible Light Assisted, Direct C3–H Arylation of Pyrido[1,2-*a*]pyrimidin-4-ones and Thiazolo[3,2-*a*]pyrimidin-5-ones*

In *Chapter 2*, we demonstrated the metal-free, visible light-induced photocatalyzed, direct C3-H arylation of 2-methyl and 2-aryl-4*H*-pyrido[1,2-*a*]pyrimidin-4-ones and 7-methyl and 7-aryl-5*H*-thiazolo[3,2-*a*]pyrimidin-5-ones with aryldiazonium salts (**Scheme 1**).

A nontoxic, inexpensive organic dye was utilized as a photo-redox catalyst for this operationally simple and mild C–H arylation reaction, showing good functional group tolerance and broad substrate scope. The synthetic and practical utility of this approach was demonstrated by synthesizing therapeutically important endothelial cell dysfunction inhibitors and anti-inflammatory agents, as well as successful gram-scale synthesis. For the mechanistic study, various control experiments were conducted, including fluorescence quenching experiments, radical trapping experiments, light-on-off experiments, and quantum yield calculations.



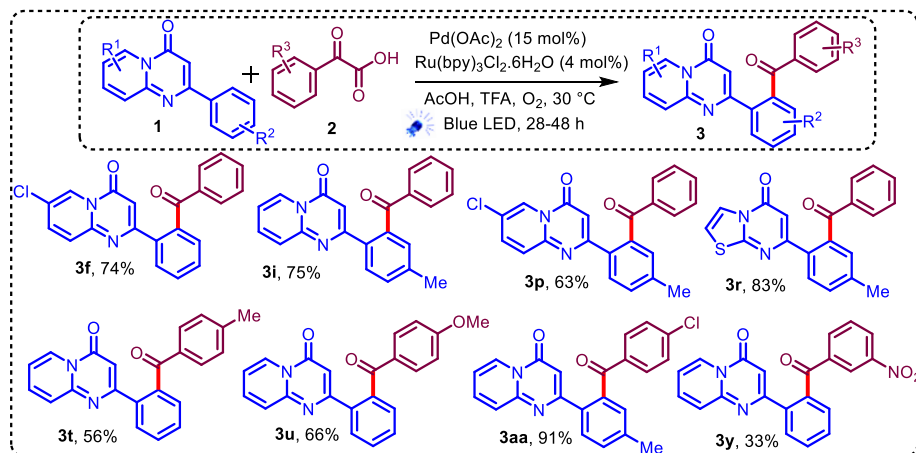
Scheme 1. Photoinduced C3-arylation of pyrido[1,2-*a*]pyrimidin-4-one and bio-active compounds.

Reference: Bhawale R. T., Kshirsagar U. A., *J. Org. Chem.*, **2023**, 88, 9537–9542.

Chapter 3: Synergistic Approach for Decarboxylative Ortho C–H Arylation of 2-Aryl-pyrido[1,2-*a*]pyrimidin-4-ones and Thiazolopyrimidinones

This chapter discussed a mild and efficient synergistic arylation of 2-aryl-pyrido[1,2-*a*]pyrimidin-4-ones and their derivatives. By merging palladium-catalyzed C–H activation with visible-light mediated photo-redox catalysis, regio-selective C–H arylation via decarboxylation of phenyl glyoxylic acid was carried out in the presence of oxygen as a green oxidant (**Scheme 2**). For the mechanistic study, several control experiment was carried out with radical scavengers, and trapped radical

intermediates were isolated and characterized using NMR and HRMS analysis.

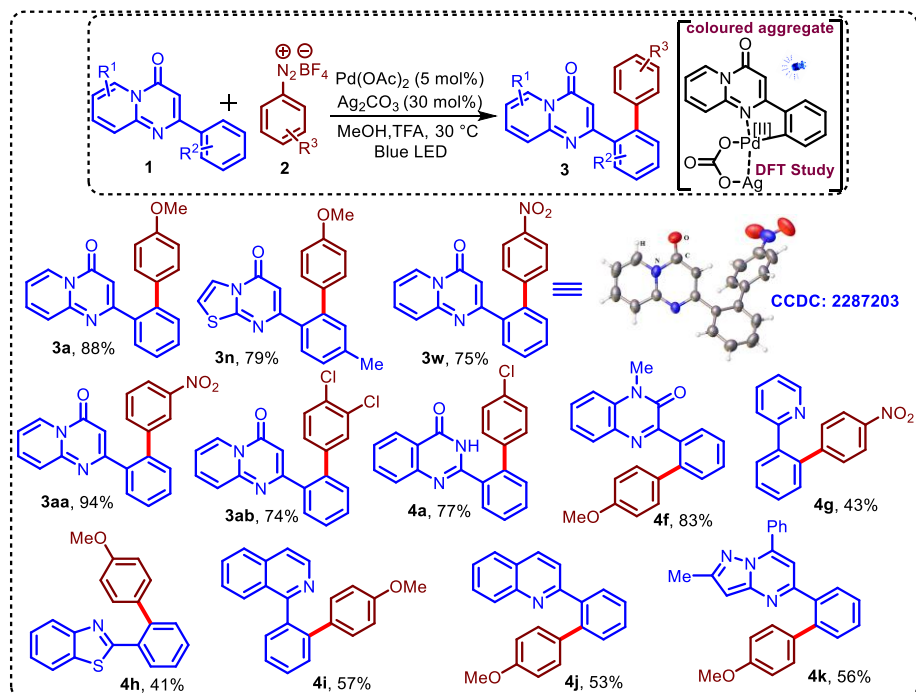


Scheme 2. Photoinduced ortho C-H acylation of pyrido[1,2-*a*]pyrimidin-4-one

Reference: Bhawale R. T., Sarothiya D., Kshirsagar U. A. *Asian J. Org. Chem* **2022**, e202200134.

Chapter 4: Visible-Light Induced Ag-Palladacycle-complex Mediated Regioselective C–H Arylation

In this chapter, we report the development of a photocatalyst-free, visible light-mediated, regioselective ortho C–H arylation of pyrido[1,2-



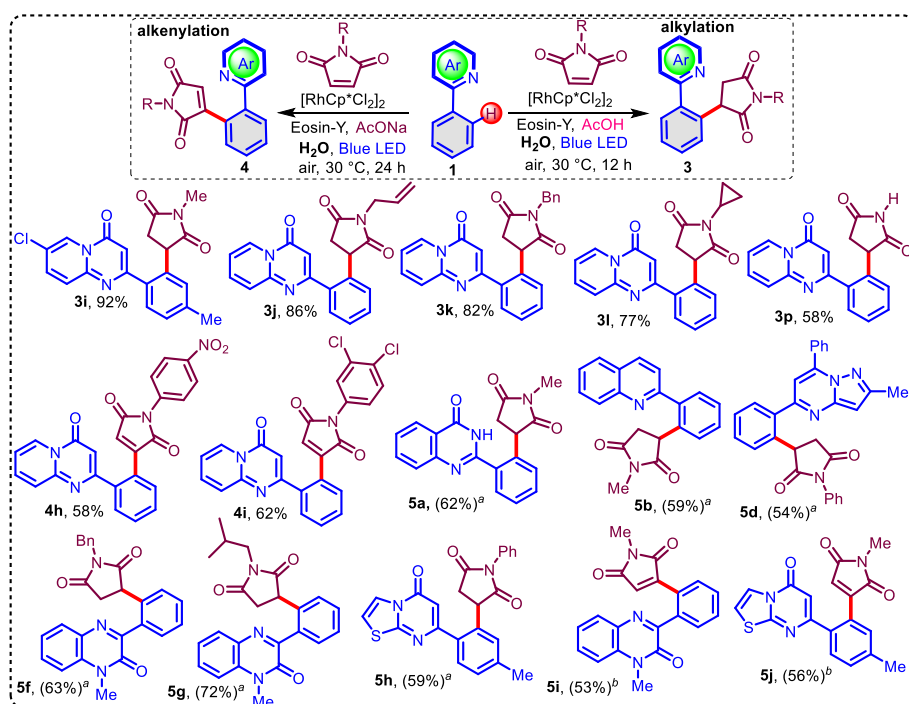
Scheme 3. Photoinduced Ag-Palladacycle-complex mediated arylation of pyrido[1,2-*a*]pyrimidin-4-one.

a]pyrimidin-4-ones and related heteroarenes at room temperature using a palladium (II) catalyst provided desired products in 41-95% yields (**Scheme 3**). A mechanistic study using control experiments, with radical scavengers, UV-visible study, DFT study, light-on-off experiments, kinetic isotopic effect, H/D labelling experiments, and quantum yield measurements was carried out.

Reference: Bhawale R. T., Chillal A. S., Ghosh S., Kshirsagar U. A. *Adv. Synth. Catal.* **2024**, 366, 3603–3609

Chapter 5: Visible-Light-Enabled Regioselective C–H alkylation and alkenylation of 2-Aryl Heterocycles using Dual Catalysis

In this chapter, we have discussed the dual catalytic, silver/copper-free, external oxidant-free, mild, and simple strategy for site-selective



Scheme 4. This approach for photoinduced alkylation and alkenylation of 2-aryl heterocycles.

alkylation as well as alkenylation of 4*H*-pyrido[1, 2-*a*]pyrimidin-4-ones and other related 2-aryl heterocycles with maleimides by merging of organic dyes with rhodium-catalyst, in the presence of acid or base under visible light irradiation at room temperature in an aqueous reaction condition (**Scheme 4**). This operationally simple and mild approach

enables the selective formation of alkylation and alkenylation products up to 92% yield under silver-free conditions with excellent substrate scope. For the mechanistic examination, control experiments such as KIE, H/D labelling experiments, light-on-off investigations, and quantum yield measurements were conducted to substantiate the proposed mechanistic pathways. Additionally, present conditions were found adequate for scale-up synthesis.

Reference: Bhawale R. T., Chillal A. S., Kshirsagar U. A. *Adv. Synth. Catal.* **2025**, 367, e202401294.

Conclusion:

The functionalization of fused heterocycles and nitrogen-containing heterocycles continues to be a compelling area of research in organic synthesis due to its broad applications across various fields, including medicinal chemistry, agrochemicals, pharmaceuticals, and materials science. The core focus of this thesis is to develop novel strategies for C–C bond formation via visible light-mediated C–H functionalization of 2-aryl heterocycles. Specifically, we have explored the reactivity of the 2-phenyl-4*H*-pyrido[1,2-*a*]pyrimidin-4-one scaffold, employing a photo-redox catalysis as well as a dual catalytic approach that synergistically merges photo-redox and transition metal catalysis to provide sustainable and mild pathways.

List of Publications

1. **Bhawale R.T.**, Kshirsagar U. A. (2023), Visible Light Assisted C-3 Arylation of Pyrido[1,2-*a*]pyrimidin-4-ones and Thiazolo[3,2-*a*]pyrimidin-5-ones, *J. Org. Chem.* 88, 9537-9542 (DOI: 10.1021/acs.joc.3c00780).
2. **Bhawale R. T.**, Sarothiya D., Kshirsagar U. A. (2022), Synergistic Approach for Decarboxylative Ortho C–H Aroylation of 2-Aryl-pyrido[1,2-*a*]pyrimidin-4-ones and Thiazolopyrimidinones by Merging Palladium Catalysis with Photo-catalysis, *Asian J. Org. Chem.* 11, e202200134 (DOI: 10.1002/ajoc.202200134).

3. **Bhawale R. T.**, Chillal A. S., Ghosh S., Kshirsagar U. A. (2024), Visible-Light Induced Ag-Palladacycle-Complex-Mediated Regioselective C–H Arylation, *Adv. Synth. Catal.* **366**, 3603-3609 (DOI:10.1002/adsc.202400466).
4. **Bhawale R. T.**, Chillal A. S., Kshirsagar U. A. (2025), Visible-Light-Enabled Regioselective C–H alkylation and alkenylation of 2-Aryl Heterocycles using Dual Catalysis, *Adv. Synth. Catal.* **367**, e202401294 (DOI: 10.1002/adsc.202401294).
5. **Bhawale R. T.**, Chillal A. S., Kshirsagar U. A. (2023), 4*H*-Pyrido[1,2-*a*]pyrimidin-4-one, biologically important fused heterocyclic scaffold: Synthesis and functionalization, *J. Heterocycl. Chem.* **60**, 1356-1373 (DOI: 10.1002/jhet.4637).

Additional Paper:

1. Sarothiya D., **Bhawale R. T.**, Kshirsagar U. A. (2022), Organic-Dye-Catalyzed Visible-Light-Mediated Regioselective C-3 Alkoxyacylation of Imidazopyridines by Carbazates, *J. Org. Chem.* **87**, 14915-14922 (DOI: 10.1021/acs.joc.2c01742).
2. Chillal A. S., **Bhawale R. T.**, Kshirsagar U. A. (2023), Photo-induced Regio-selective Chalcogenation and Thiocyanation of 4*H*-Pyrido[1,2-*a*]-pyrimidin-4-ones Under Benign Conditions, *Eur. J. Org. Chem.* **26**, e202300665 (DOI: 10.1002/ejoc.202300665).
3. Chillal A. S., **Bhawale R. T.**, Kshirsagar U. A. (2024), Oxone[®] Mediated Regioselective C(sp²)-H Selenylation and Thiocyanation of Pyrazolo[1,5-*a*]pyrimidines at room temperature, *Chemistryselect* **9**, e202304815 (DOI: 10.1002/slct.202304815).
4. Chillal A. S., **Bhawale R. T.**, Kshirsagar U. A. (2024), Regioselective C(sp²)-H halogenation of pyrazolo[1,5-*a*]pyrimidines facilitated by hypervalent iodine(III) under aqueous and ambient conditions, *RSC Adv.* **14**, 13095-13099 (DOI: 10.1039/d4ra02090a).

5. Chillal A. S., **Bhawale R. T.**, Sharma S., Kshirsagar U. A. (2024), Electrochemical Regioselective C(sp²)-H Bond Chalcogenation of Pyrazolo[1,5-*a*]pyrimidines via Radical Cross Coupling at Room Temperature, *J. Org. Chem.* 89, 14496-14504 (DOI: 10.1021/acs.joc.4c00856).

Conferences: Oral/Poster Presentation

Oral Presentation

1. IIT INDORE, *Chemistry In-House Symposium (CHEM 2022)*, 11 February 2022, Oral presentations (Best oral presentations award).
2. IGP- *Chemistry & Industry Colloquium 2024*, Department of Chemistry IIT Indore, held February 23-24, 2024.
3. *Sustainable Chemistry Conference-III*, 2025, Department of Chemistry, IIT Indore, held March 18-20, 2025.

Poster Presentation

1. National Conference, *CONTEMPORARY FACTS IN ORGANIC SYNTHESIS (CFOS 2022)*, IIT Roorkee, held from December 1-4, 2022.
2. *International Conference on Sustainable Chemistry- 2023* under Indo-German Higher Education Partnership held from 22-23 February 2023.

Participate

1. International Conference on *Emerging Trends in Synthetic Organic Chemistry - 2021 (ICETSOC-2021)* organized by the Department of Chemistry, National Institute of Technology Puducherry, Karaikal, held from 06-07 December 2021, through virtual mode.
2. Online National Conference on *Organic Chemistry NITT Organic Chemistry Conference*, organized by the National Institute of Technology Tiruchirappalli, held from 16-18 December 2021.

3. First Virtual **JNOST Symposium organized by the Indian Institute of Science**, Bangalore, held from October 31 - November 1, 2020.

TABLE OF CONTENTS

1. List of Figures	XII
2. List of Schemes	XV
3. List of Tables	XVIII
4. Acronyms	XIX
5. Nomenclature	XIX
6. Materials and Experimental Techniques	XX

Chapter 1 Introduction

1.1 Introduction	3
1.2 Transition Metal Catalyst For C–H Activation and Functionalization	4
1.2.1 C-C, C-X bond formation via C–H activation	5
1.2.2 Palladium-catalyzed C–H functionalization	6
1.2.3 Rhodium-catalyzed C–H functionalization	8
1.2.4 Ruthenium-catalyzed C–H functionalization	11
1.3 Visible Light-Mediated Photo-Redox Catalysis For C-C Bond Formation	12
1.3.1 A brief history of visible light in chemical transformations	12
1.3.2 Photo-redox catalysis: light-driven synthetic chemistry	14
1.3.3 Metal-based photo-redox catalysts	16
1.3.4 Organic photo-redox catalysts	16
1.3.5 Semiconductor photo-redox catalysts	18
1.3.6 Application of photo-redox catalyst in C–H functionalization	19
1.4 Merging Transition Metal Catalysis and Photo-Redox Catalysis	21
1.5 Innovation and Bioactivity of Heterocyclic Compounds	24
1.5.1 4 <i>H</i> -Pyrido[1,2- <i>a</i>]pyrimidin-4-ones: biological importance	26
1.5.2 A classical route for the synthesis of 4 <i>H</i> -pyrido[1,2- <i>a</i>]pyrimidin-4-one	27
1.5.3 Functionalization of 4 <i>H</i> -pyrido[1,2- <i>a</i>]pyrimidin-4-one scaffold	28
1.6 Aim of Thesis	30
1.7 References	31

Chapter 2 Visible Light Assisted, Direct C3–H Arylation of Pyrido[1,2-*a*]pyrimidin-4-ones and Thiazolo[3,2-*a*]pyrimidin-5-ones

2.1 Introduction	43
2.2 Previous reports	44
2.3 Objective	45
2.4 Result and Discussion	45
2.5 Summary	53
2.6 Experimental Section	54
2.7 Characterization data of 3a-3ae, 5	55
2.8 ¹ H and ¹³ C NMR spectra of selected compounds 3a-d, 3ad, 5	65
2.9 The single crystal X-ray diffraction data	71
2.10 References	72

Chapter 3 Synergistic Approach for Decarboxylative Ortho C–H Aroylation of 2-Aryl-pyrido[1,2-*a*]pyrimidin-4-ones and Thiazopyrimidinones

3.1 Introduction	81
3.2 Previous Reports	83
3.3 Objective	84
3.4 Result and Discussion	84
3.5 Summary	90
3.6 Experimental Section	90
3.7 Characterization data of 3a-ad	91
3.8 ¹ H and ¹³ C NMR spectra of selected compounds 3a-e	102
3.9 The single crystal X-ray diffraction data	107
3.10 References	108

Chapter 4 Visible-Light Induced Ag-Palladacycle-complex Mediated Regioselective C–H Arylation

4.1 Introduction	117
4.3 Previous Reports	118
4.2 Objective	119
4.4 Result and Discussion	119
4.5 Summary	129
4.6 Experimental Section	130
4.7 Mechanistic Insights into Product Formation (3a)	130
4.8 Characterization Data of 3a-3ab and 4a-4k	131
4.9 ¹ H and ¹³ C NMR spectra of selected compounds 3a-c , 4a , 4f	143
4.10 Computational Studies	148
4.11 The single crystal X-ray diffraction data	148
4.12 References	150

Chapter 5 Visible-Light-Enabled Regioselective C–H alkylation and alkenylation of 2-Aryl Heterocycles using Dual Catalysis

5.1 Introduction	161
5.2 Previous Reports	161
5.3 Objective	163
5.4 Result and Discussion	163
5.5 Summary	172
5.6 Experimental Section	172
5.7 Characterization Data of 3a-p , 4a-j and 5a-j	174
5.8 ¹ H and ¹³ C NMR spectra of compounds 3a-c , 5d , 4a , 5	188
5.9 References	194

Chapter 6 Conclusions and Future Scope

6.1 Conclusion	199
6.2 Future Scope	201

LIST OF FIGURES

Chapter 1 Introduction

Figure 1.1 Transition metal (TM) catalyzed cross-coupling reactions	3
Figure 1.2 Transition metal catalyzed C-H activation&Functionzation	5
Figure 1.3 Relation between energy and wavelength of light	13
Figure 1.4 Oxidative and reductive quenching cycle of photocatalyst	15
Figure 1.5 Metal-based photo-redox catalyst	17
Figure 1.6 Organic photo-redox catalyst	18
Figure 1.7 Merging of the TM catalyst with PC	22
Figure 1.8 Pyridine-based bioactive compounds	25
Figure 1.9 Pyridine-based heterocycles: essential building blocks in bioactive molecules	25
Figure 1.10 Biological active compounds of 4 <i>H</i> -pyrido[1,2- <i>a</i>]pyrimidin-4-one	27

Chapter 2 Visible Light Assisted, Direct C3–H Arylation of Pyrido[1,2-*a*]pyrimidin-4-ones and Thiazolo[3,2-*a*]pyrimidin-5-ones

Figure 2.1 Biologically active C-3 arylated pyrido[1,2- <i>a</i>]pyrimidin-4-ones	43
Figure 2.2 ¹ H NMR spectrum of compound 3a (500 MHz, CDCl ₃)	65
Figure 2.3 ¹³ C NMR spectrum of compound 3a (126 MHz, CDCl ₃)	65
Figure 2.4 ¹ H NMR spectrum of compound 3b (500 MHz, CDCl ₃)	66
Figure 2.5 ¹³ C NMR spectrum of compound 3b (126 MHz, CDCl ₃)	66

Figure 2.6 ^1H NMR spectrum of compound 3c (500 MHz, CDCl_3)	67
Figure 2.7 ^{13}C NMR spectrum of compound 3c (126 MHz, CDCl_3)	67
Figure 2.8 ^1H NMR spectrum of compound 3d (500 MHz, CDCl_3)	68
Figure 2.9 ^{13}C NMR spectrum of compound 3d (126 MHz, CDCl_3)	68
Figure 2.10 ^1H NMR spectrum of compound 3ad (500 MHz, CDCl_3)	69
Figure 2.11 ^{13}C NMR spectrum of compound 3ad (126 MHz, CDCl_3)	69
Figure 2.12 ^1H NMR spectrum of compound 5 (500 MHz, CDCl_3)	70
Figure 2.13 ^{13}C NMR spectrum of compound 5 (126 MHz, CDCl_3)	70
Figure 2.14 ORTEP plot of compound 3s (CCDC 2225945)	71

Chapter 3: Synergistic Approach for Decarboxylative Ortho C–H Aroylation of 2-Aryl-pyrido[1,2-*a*]pyrimidin-4-ones and Thiazolopyrimidinone

Figure 3.1 Biologically active pyrido[1,2- <i>a</i>]pyrimidin-4-ones	81
Figure 3.2 ^1H NMR spectrum of compound 3a (500 MHz, CDCl_3)	102
Figure 3.3 ^{13}C NMR spectrum of compound 3a (126 MHz, CDCl_3)	102
Figure 3.4 ^1H NMR spectrum of compound 3b (500 MHz, CDCl_3)	103
Figure 3.5 ^{13}C NMR spectrum of compound 3b (126 MHz, CDCl_3)	103
Figure 3.6 ^1H NMR spectrum of compound 3c (500 MHz, CDCl_3)	104
Figure 3.7 ^{13}C NMR spectrum of compound 3c (126 MHz, CDCl_3)	104
Figure 3.8 ^1H NMR spectrum of compound 3d (500 MHz, CDCl_3)	105
Figure 3.9 ^{13}C NMR spectrum of compound 3d (126 MHz, CDCl_3)	105
Figure 3.10 ^1H NMR spectrum of compound 3e (500 MHz, CDCl_3)	106
Figure 3.11 ^{13}C NMR spectrum of compound 3e (126 MHz, CDCl_3)	106

Chapter 4 Visible-Light Induced Ag-Palladacycle-complex Mediated Regioselective C–H Arylation

Figure 4.1 Optimized structure of the EDA complex	127
Figure 4.2 Orbitals involved -low-lying excited states in intermediate [E]	128
Figure 4.3 ^1H NMR spectrum of compound 3a (500 MHz, CDCl_3)	143
Figure 4.4 ^{13}C NMR spectrum of compound 3a (126 MHz, CDCl_3)	143
Figure 4.5 ^1H NMR spectrum of compound 3b (500 MHz, CDCl_3)	144
Figure 4.6 ^{13}C NMR spectrum of compound 3b (126 MHz, CDCl_3)	144
Figure 4.7 ^1H NMR spectrum of compound 3c (500 MHz, CDCl_3)	145
Figure 4.8 ^{13}C NMR spectrum of compound 3c (126 MHz, CDCl_3)	145
Figure 4.9 ^1H NMR spectrum of compound 4a (500 MHz, CDCl_3)	146
Figure 4.10 ^{13}C NMR spectrum of compound 4a (126 MHz, CDCl_3)	146
Figure 4.11 ^1H NMR spectrum of compound 4f (500 MHz, CDCl_3)	147
Figure 4.12 ^{13}C NMR spectrum of compound 4f (126 MHz, CDCl_3)	147
Figure 4.13 The ORTEP plot of sample 3w (CCDC 2287203)	149

Chapter 5 Visible-Light-Enabled Regioselective C–H alkylation and alkenylation of 2-Aryl Heterocycles using Dual Catalysis

Figure 5.1 ^1H NMR spectrum of compound 3a (500 MHz, CDCl_3)	188
Figure 5.2 ^{13}C NMR spectrum of compound 3a (126 MHz, CDCl_3)	188
Figure 5.3 ^1H NMR spectrum of compound 3b (500 MHz, CDCl_3)	189
Figure 5.4 ^{13}C NMR spectrum of compound 3b (126 MHz, CDCl_3)	189
Figure 5.5 ^1H NMR spectrum of compound 3c (500 MHz, CDCl_3)	190
Figure 5.6 ^{13}C NMR spectrum of compound 3c (126 MHz, CDCl_3)	190

Figure 5.7 ^1H NMR spectrum of compound 5d (500 MHz, CDCl_3)	191
Figure 5.8 ^{13}C NMR spectrum of compound 5d (126 MHz, CDCl_3)	191
Figure 5.9 ^1H NMR spectrum of compound 4a (500 MHz, CDCl_3)	192
Figure 5.10 ^{13}C NMR spectrum of compound 4a (126 MHz, CDCl_3)	192
Figure 5.11 ^1H NMR spectrum of compound 5i (500 MHz, CDCl_3)	193
Figure 5.12 ^{13}C NMR spectrum of compound 5i (126 MHz, CDCl_3)	193

LIST OF SCHEMES

Chapter 1 Introduction

Scheme 1.1 Palladium-catalyzed C-C bond formation reactions	7
Scheme 1.2 Rhodium-catalysed C-C bond formation reactions	10
Scheme 1.3 Ruthenium-catalyzed C-C bond formation reactions	11
Scheme 1.4 Photoinduced C-H functionalization	20
Scheme 1.5 Photoinduced C-H activation and functionalization	23
Scheme 1.6 Classical synthetic route of 4 <i>H</i> -pyrido[1,2- <i>a</i>]pyrimidin-4-one scaffolds	28
Scheme 1.7 Functionalization of pyrido[1,2- <i>a</i>]pyrimidin-4-one	30

Chapter 2 Visible Light Assisted, Metal-Free Direct C3–H Arylation of Pyrido[1,2-*a*]pyrimidin-4-ones and Thiazolo[3,2-*a*]pyrimidin-5-ones

Scheme 2.1 Previous reports on C3-arylation of pyrido[1,2- <i>a</i>]pyrimidin-4-ones	44
Scheme 2.2 Photoinduced C3-arylation of pyrido[1,2- <i>a</i>]pyrimidin-4-ones	45

Scheme 2.3 Substrate scope for arylation of pyrido[1,2- <i>a</i>]pyrimidin-4-ones	49
Scheme 2.4 Substrate scope of aryl diazonium tetrafluoroborate	50
Scheme 2.5 Synthesis of bioactive molecules and scale-up reaction	51
Scheme 2.6 Control experiments and Fluorescence quenching study	52
Scheme 2.7 Proposed Reaction Mechanism	53

Chapter 3: Synergistic Approach for Decarboxylative Ortho C–H Arylation of 2-Aryl-pyrido[1,2-*a*]pyrimidin-4-ones and Thiazolopyrimidinones by Merging Palladium Catalysis with Photo-catalysis

Scheme 3.1 C-H functionalization of <i>N</i> -containing heterocycles	83
Scheme 3.2 Photoinduced ortho C-H acylation of pyrido[1,2- <i>a</i>]pyrimidin-4-one	84
Scheme 3.3 Substrate scope for arylation of pyrido[1,2- <i>a</i>]pyrimidin-4-ones	87
Scheme 3.4 Substrate scope of α -oxo carboxylic acids	88
Scheme 3.5 Radical scavenger experiment	89
Scheme 3.6 Proposed mechanism for synergistic arylation	89

Chapter 4 Visible-Light Induced Ag-Palladacycle-complex Mediated Regioselective C–H Arylation

Scheme 4.1 Previous reports on visible light-mediated photoinduced arylation	118
Scheme 4.2 Photoinduced arylation of pyrido[1,2- <i>a</i>]pyrimidin-4-one	119
Scheme 4.3 Substrate scope arylation of pyrido[1,2- <i>a</i>]pyrimidin-4-ones	122

Scheme 4.4 Scope of aryl diazonium tetrafluoroborate	123
Scheme 4.5 Scope of various heterocyclic compound arylation	124
Scheme 4.6 Scale-up synthesis of compound 3w	124
Scheme 4.7 Control experiments, light on/off, color observation, and UV-visible study	125
Scheme 4.8 Plausible reaction mechanism	128
Scheme 4.9 Computed structure of intermediate [E]	129
Scheme 4.10 Mechanistic insights into product formation (3a)	131

Chapter 5 Visible-Light-Enabled Regioselective C–H alkylation and alkenylation of 2-Aryl Heterocycles using Dual Catalysis

Scheme 5.1 Previous reports for alkylation and alkenylation of heterocycles with maleimides	162
Scheme 5.2 Current approach for photoinduced alkylation and alkenylation of 2-aryl heterocycles	163
Scheme 5.3 Substrate scope for alkylation of pyrido[1,2- <i>a</i>]pyrimidin-4-ones with maleimides	166
Scheme 5.4 Substrate scope for alkenylation of pyrido[1,2- <i>a</i>]pyrimidin-4-ones with maleimides	167
Scheme 5.5 Substrate scope for alkylation and alkenylation of other heterocycles with maleimides	168
Scheme 5.6 Mechanistic findings: control experiments	169
Scheme 5.7 Light on-off experiments	170
Scheme 5.8 Proposed reaction mechanism for alkylation and alkenylation	171

LIST OF TABLES

Chapter 2 Visible Light Assisted, Direct C3–H Arylation of Pyrido[1,2-*a*]pyrimidin-4-ones and Thiazolo[3,2-*a*]pyrimidin-5-ones

Table 2.1 Optimization of the reaction conditions 47

Table 2.2 The single crystal X-ray diffraction data of compound **3s** 71

Chapter 3 Synergistic Approach for Decarboxylative Ortho C–H Arylation of 2-Aryl-pyrido[1,2-*a*]pyrimidin-4-ones and Thiazolopyrimidinone

Table 3.1 Optimization Table 85

Table 3.2 Crystal data and structure refinement for **3a** 107

Chapter 4 Visible-Light Induced Ag-Palladacycle-complex Mediated Regioselective C–H Arylation

Table 4.1 Optimization of the reaction conditions 120

Table 4.3 The crystallographic data for compound **3w** 149

Chapter 5 Visible-Light-Enabled Regioselective C–H alkylation and alkenylation of 2-Aryl Heterocycles using Dual Catalysis

Table 5.1 Selected optimization of reaction conditions 164

ACRONYMS

^1H NMR	Proton Nuclear Magnetic Resonance
^{13}C NMR	Carbon Nuclear Magnetic Resonance
CDCl_3	Deuterated Chloroform
DMSO-D_6	Deuterated dimethyl sulfoxide
UV-Vis	UV-Visible Spectroscopy
ESI-MS	Electrospray Ionization- Mass Spectrometry
IR	Infrared
m.p.	Melting Point
Calcd.	Calculated
CDC	Cross dehydrogenative coupling
LCMS	Liquid Chromatography Mass Spectrometry
HRMS	High-Resolution Mass Spectrometry
Ppm	Parts per million
PPA	Polyphosphoric acid
DMF	Dimethylformamide
Ph	Phenyl
EtOH	Ethanol
MeOH	Methanol
ACN	Acetonitrile
TLC	Thin Layer Chromatography

NOMENCLATURE

A	Alfa
Å	Angstrom
a. u.	Arbitrary Unit
β	Beta
Bn	Benzyl
δ	Chemical shift
cm	Centimeter
$^{\circ}\text{C}$	Degree Celsius
DCE	Dichloroethane
ϵ	Extinction coefficient

γ	Gamma
h	Hour
mmol	Millimole
mL	Milliliter
nm	Nanometer
ϕ	Quantum yield
λ	Wavelength
equiv.	equivalent
h	hour

Materials and Experimental Techniques:

All experiments were monitored by analytical thin-layer chromatography (TLC) using Merck silica gel 60F₂₅₄ precoated aluminum sheets. After elution, the TLC plates were visualized under UV light (254 nm). Organic solutions were concentrated under reduced pressure using a Heidolph rotary evaporator. Column chromatography purifications were performed using silica gel (100-200 mesh or 60-120 mesh) as the stationary phase, with ethyl acetate-hexane mixtures as the eluent, unless stated otherwise. All materials were purchased from commercial suppliers and used without further purification. A custom-built photoreactor equipped with a blue LED strip (wavelength range: 422–490 nm, λ_{max} = 458 nm) was used for the reactions. The emission wavelength of the LED light source was measured using an Open Spectrophotometer.

NMR Spectroscopy: Proton (¹H NMR, 500 MHz), carbon (¹³C NMR, 126 MHz), and Fluorine (¹⁹F NMR, 471 MHz) spectra were recorded on a Bruker Avance spectrometer, using appropriate solvents. The chemical shifts for protons are reported in parts per million (ppm), referenced to the residual proton signal in the NMR solvent. For ¹H NMR and ¹³C NMR in chloroform (CHCl₃), the residual proton signal is at δ 7.26 ppm, and the carbon signal is at δ 77.16 ppm. All chemical shifts (δ) are given on the ppm scale and coupling constants (*J*) are expressed in hertz (Hz).

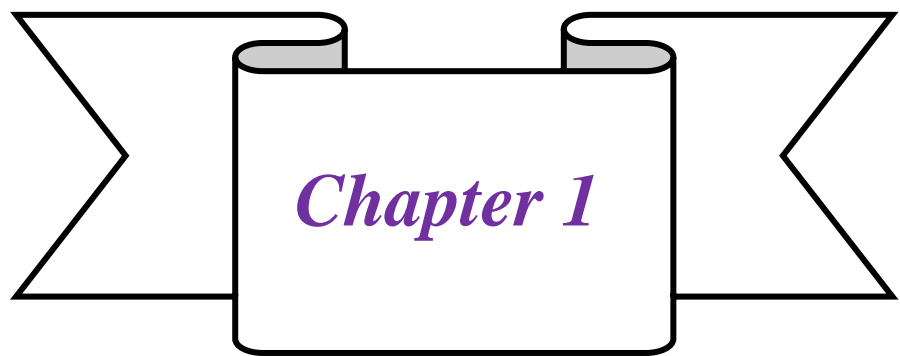
Multiplicities are denoted as: singlet (s), doublet (d), triplet (t), quartet (q), doublet of doublets (dd), and multiplet (m).

Mass Spectrometry: High-Resolution Mass Spectrometry (HR-MS) data were obtained using an ESI-TOF-MS instrument equipped with Electrospray Ionization (ESI) techniques (Models: Dionex Ultimate 3000 and YL9100).

UV-Vis Spectroscopy: Absorption spectra were recorded using a UV-visible spectrophotometer (Perkin Elmer Lambda 750).

IR analysis: Infrared spectra were collected using a Thermo Fisher Nicolet 6700 spectrometer, utilizing the Attenuated Total Reflectance (ATR) technique for efficient sample analysis.

Melting point: Melting points were determined using an Electrothermal melting point apparatus (Stuart SMP30) and are uncorrected.



Introduction

Chapter 1

1.1 Introduction

Organic synthesis plays a crucial role in chemical sciences and has emerged as a cornerstone for the development of versatile and essential classes of substrates. It contributes significantly to enhancing the quality of life by addressing social needs through innovative solutions. Over the past few decades, substantial progress in practical organic chemistry has revolutionized the field, enabling the precise design and efficient synthesis of target molecules. These advancements have paved the way for the creation of novel materials and products, driving scientific discovery and meeting the demands of modern society with enhanced specificity and functionality.^[1] Particularly, cross-coupling reactions, including Suzuki-Miyaura, Stille, Hiyama, Negishi, Mizoroki-Heck, Sonogashira, Kumada, etc.^[2-4] have been extensively employed with significant success in organic synthesis (**Figure 1.1**). These reactions facilitate the formation of C-C and C-X (C= N, O, S, P) bonds, allowing for the efficient construction of complex molecules from readily available starting materials. Their versatility and effectiveness in creating diverse functionalized products have made them indispensable tools in the area of medicinal chemistry and materials science. However, despite the growing emphasis on green chemistry principles, which promote synthetic designs focused on step and atom economy with

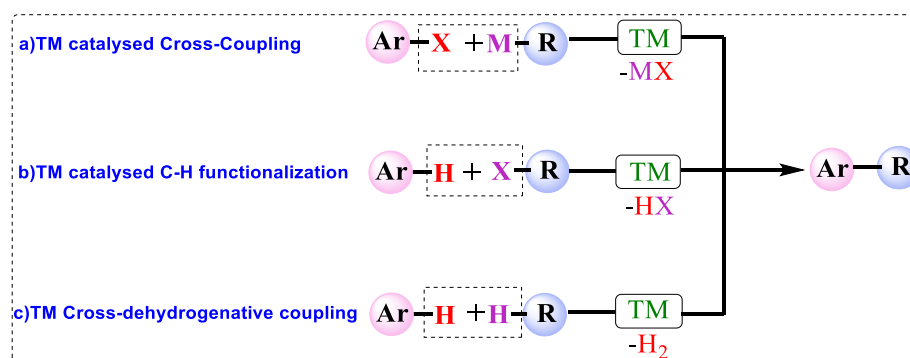


Figure 1.1 Transition metal (TM) catalyzed cross-coupling reactions

minimal waste, so many existing methods still depend on pre-functionalized starting materials. These include the use of aryl halides, pseudohalides, and organometallic reagents such as Grignard reagents (RMgX), stannanes (ArSnR_3), and zinc reagents (RZnX) (**Figure 1.1a**).^[2] Consequently, direct C–H bond functionalization of aryl (Ar-H) compounds with alkyl halides (R-X) is an emerging area in sustainable organic synthesis. This strategy avoids the need for pre-functionalization, which often generates waste, and makes the process more atom economical. By utilizing environmentally benign catalysts and mild reaction conditions, this method can align with sustainability goals, reducing waste and energy consumption while maintaining high efficiency (**Figure 1.1b**).^[3] Another intriguing approach for C–C bond formation is the cross-dehydrogenative coupling reaction (CDC), which enables direct bond formation between two C–H bonds. Conversely, this method generally necessitates the use of stoichiometric external oxidants, additives to facilitate the reaction, posing a challenge to sustainability and scalability (**Figure 1.1c**).^[4]

1.2 Transition metal catalyst for C–H activation and functionalization

Over the past decade, transition metal-catalyzed C–H activation and functionalization have emerged as powerful and efficient strategies for C–C and C–X ($\text{X} = \text{O}, \text{N}, \text{S}, \text{P}$) bond formation in synthetic organic chemistry.^[5] This approach eliminates the need for pre-functionalized substrates, reduces salt waste, and decreases production time and costs by enhancing step and atom economy. Using directing groups (DGs) containing coordinating atoms in heterocycles, metal catalysis facilitates the selective cleavage of C–H bonds at specific positions within molecules. While C–H activation traditionally occurs at the ortho position, recent advancements have enabled selective activation at the meta and para positions as well. These developments expand the scope of C–H functionalization, offering new avenues for various molecular modifications.^[6]

1.2.1 C-C, C-X bond formation via C-H activation^[7-9]

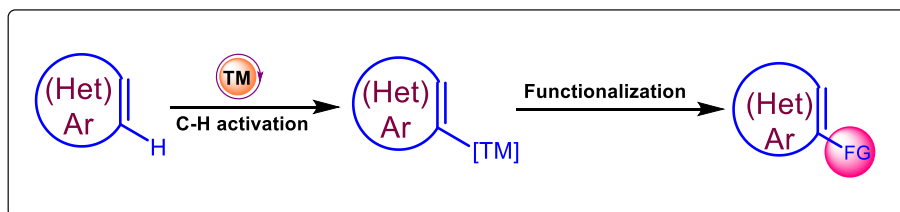


Figure 1.2 Transition metal (TM) catalyzed C-H activation/Functionalization.

Recent advancements have shown that direct C-H functionalization via C-H bond activation, facilitated by transition metal catalysis, leads to the formation of carbon-carbon bonds (**Figure 1.2**). Particularly, C-H bond activation refers to the process of cleaving the relatively inert C-H bond, which is one of the most stable and unreactive bonds in organic molecules due to its high bond dissociation energy and lack of polarity. Accordingly, the term "*C-H activation*" can be misleading, since it requires external intervention, typically in the form of a transition metal catalyst, to break these bonds. The primary objective of C-H activation strategies is to convert these unreactive bonds into more reactive intermediates, enabling further chemical transformations. After the C-H bond activation step, it forms a carbon-metal (C-M) containing intermediate, which can then undergo further transformations to produce a new C-C or C-X bond. This C-H functionalization protocol has become a valuable tool in organic synthesis, allowing for the overview of functional groups such as aryl, acyl, alkyl, amine, and many more substituents onto target molecules. This strategy not only simplifies the construction of complex molecular architectures but also aligns with the principles of green chemistry by reducing the need for pre-functionalized substrates and minimizing waste.

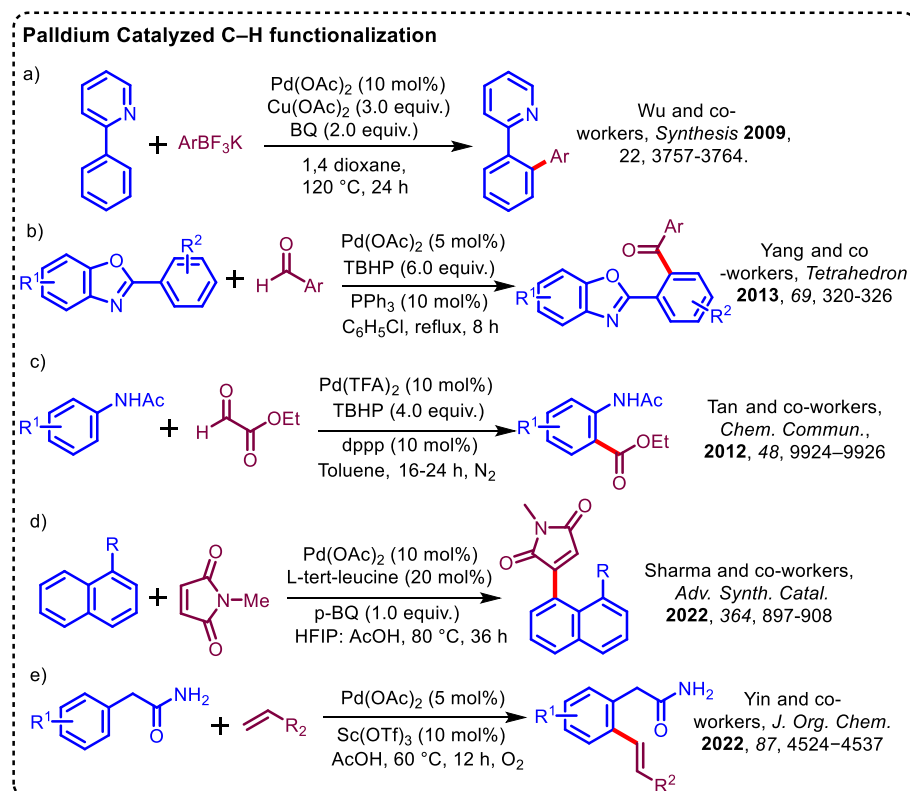
Transition metal catalysts, particularly palladium, rhodium, and ruthenium, have emerged as indispensable tools for C-H bond activation and functionalization, offering unparalleled efficiency and versatility in chemical transformations. Among the most prominent metals, palladium stands out for its remarkable ability to mediate assorted transformations such as oxidative addition, reductive elimination, and exhibit flexibility

for functionalization. These capabilities make palladium catalysts essential for constructing complex molecular architectures with precision. Similarly, rhodium catalysts have garnered significant attention for their exceptional reactivity and selectivity in C–H activation processes. Rhodium complexes are particularly effective in facilitating intramolecular and intermolecular reactions under mild conditions, thereby expanding the scope of accessible chemical frameworks. They have proven invaluable in synthesizing biologically active molecules and advanced materials. On the other hand, Ruthenium catalysts offer unique advantages due to their robustness and cost-effectiveness compared to other transition metals. Ruthenium-based systems excel in promoting challenging transformations, including regioselective C–H activation and functionalization of deactivated substrates. Their versatility has made them a cornerstone in developing sustainable and innovative synthetic methodologies.

1.2.2 Palladium-catalyzed C–H functionalization

Palladium-catalyzed C–H activation plays a crucial role in structural modification, particularly in the build-up of C–C bonds. Palladium catalysts are highly valued due to their ability to access multiple oxidation states, which facilitates the functionalization of inert C–H bonds into C–C, C–Heteroatom, and other essential bonds. This versatility makes palladium a critical catalyst for modern organic conversions. In the reaction mechanism, palladium catalysts operate through multiple oxidation states, enabling key transformations in organic synthesis, such as bond formation, C–H activation, and functional group interconversions. Typically, palladium (0) is oxidatively added to produce palladium (II), which allows C–H bond functionalization. As well, palladium (IV) intermediates can be formed by additional oxidation of palladium (II). In the mechanistic pathway, palladium is known to move between oxidation levels ranging from zero to four. The ability of palladium to achieve higher oxidation states, particularly palladium (IV), is critical for enhancing selectivity, especially in challenging C–H activation processes. Coordinating

ligands, including phosphines (PR₃), N-heterocyclic carbenes (NHCs), and pyridine-derived ligands, are frequently utilized with palladium catalysts to improve selectivity and enable challenging C–H activation. These ligands are essential in controlling palladium reactivity, stabilizing various oxidation states, and improving the catalyst's performance to facilitate more efficient and selective transformations in intricate synthetic processes.^[10] Here, discussing a few selected reports (Scheme 1.1). In 2009, Wu's and colleagues demonstrated a method for ortho C–H arylation of pyridine and 2-phenylpyridine derivatives. This process utilized transition metal catalysis, with potassium aryl trifluoroborates as arylating agents, copper as a co-catalyst, and *p*-benzoquinone. The reaction proceeded efficiently in the presence of an elevated temperature of 120 °C (Scheme 1.1a).^[11] Yang's and colleagues later reported a palladium-catalyzed acylation of 2-aryl benzoxazole using aldehydes. This reaction occurred under oxidative conditions with tert-butyl hydroperoxide (TBHP) as the oxidant and chlorobenzene as the solvent, enabling efficient C–C bond formation or



Scheme 1.1 Selected palladium-catalyzed C–C bond formation reactions

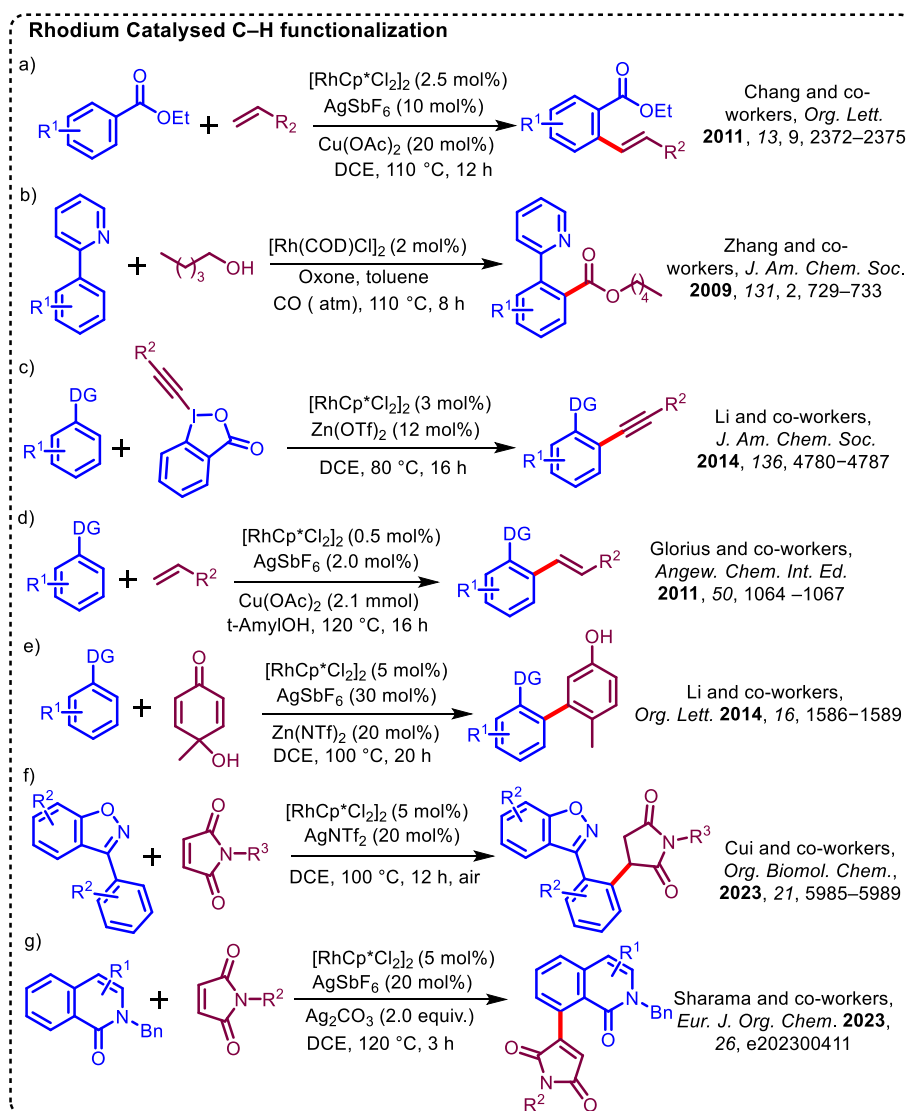
corresponding acylation of 2-aryl benzoxazoles (**Scheme 1.1b**).^[12] Afterward, Tan's and co-workers reported the synthesis of anthranilic ethyl esters from anilides through a palladium-catalyzed dehydrogenative coupling reaction, using TBHP as the oxidant. Under these conditions, a wide range of substrates were well tolerated, achieving yields between 40-66% (**Scheme 1.1c**).^[13] Further, cyclic and open-chain alkenylation of heteroarenes with *N*-methyl maleimides and substituted styrene derivatives. These reactions proceed with palladium-catalyzed functionalization under thermal conditions, demonstrating good functional group tolerance with acceptable yields of the corresponding alkenylated products. (**Scheme 1.1d-e**).^[14-15]

1.2.3 Rhodium-catalyzed C–H functionalization

In recent decades, transition metal-rhodium-catalyzed C–H functionalization has developed as a particularly effective methodology for constructing complex molecular architectures, including the functionalization of bioactive compounds. Rhodium catalysts are invaluable in modern synthetic chemistry due to their ability to selectively activate and functionalize inert C–H bonds. This strategy holds immense potential due to the abundance of C–H bonds in organic molecules, providing direct and atom-economical pathways for molecular diversification. Therefore, Pharmaceuticals, agrochemicals, and other industries benefit from its application, which has enabled them to synthesize a wide range of structurally various and functionally complex compounds from simple precursors. Rhodium catalysts play a critical role in the formation of new bonds within chemical feedstocks due to their versatility like, the Rh(I) or Rh(III) species can form rhodium-carbon bonds through C–H activation for further conversion. This transformation usually involves an initial oxidative addition, followed by reductive elimination, ultimately forming C–C or C–X bonds. The catalyst is then regenerated, enabling it to participate in further catalytic cycles.^[16-22]

Rhodium-catalyst-based C–H functionalization exhibits high regio- and chemo-selectivity, which can be fine-tuned by the presence or absence of directing ligands. Incorporating ligands or directing groups into the catalytic system profoundly influences the selectivity of these transformations. Exploring the diversity of rhodium catalyst ligands includes cyclopentadienyl, pentamethylcyclopentadienyl derivatives, and substituted phosphine oxides. Additionally, directing groups such as phosphines, dendritic phosphonated ligands, pyridyl, and oxazoline derivatives play a crucial role in guiding the activation site, allowing for controlled, selective bond formation. Classically, C–H functionalization reactions proceed via chelation-assisted mechanisms, whereby the directing group coordinates to the rhodium center, steering activation towards a specific C–H bond. This precise control over bond formation makes rhodium catalysts highly valued for their efficiency in constructing complex molecules and provides high selectivity with minimal waste. A few selected C–C bond-forming examples are discussed in (**Scheme 1.2**).

In 2011, Chang's and colleagues demonstrated a rhodium-catalyzed ortho C–H olefination of benzaldehydes and benzoates utilizing silver hexafluoroantimonate, copper acetate, and 1,2-dichloroethane (DCE) as a solvent, using 110 °C temperatures for 12 hours (**Scheme 1.2a**).^[16] Further, Zhang and colleagues developed that arenes and heteroarenes get oxidative carbonylated by rhodium-catalyzed directing groups, effectively converting them into esters under oxidative CO atmospheric conditions (**Scheme 1.2b**).^[17] In 2014, Li's and co-workers explored the rhodium(III)-catalyzed ortho C–H alkynylation of heteroaromatic substrates using hypervalent iodine-alkyne reagents in the presence of zinc triflate under thermal conditions for directing group-assisted alkynylation (**Scheme 1.2c**).^[18] In 2011, the Glorius group reported a Rh(III)-catalyzed ortho-olefination of key structural motifs such as acetophenones and benzamides, employing styrene as the olefin source, in the presence of silver salts and copper acetate as co-catalysts at 120 °C for 16 hours. This transformation exhibited excellent tolerance towa-



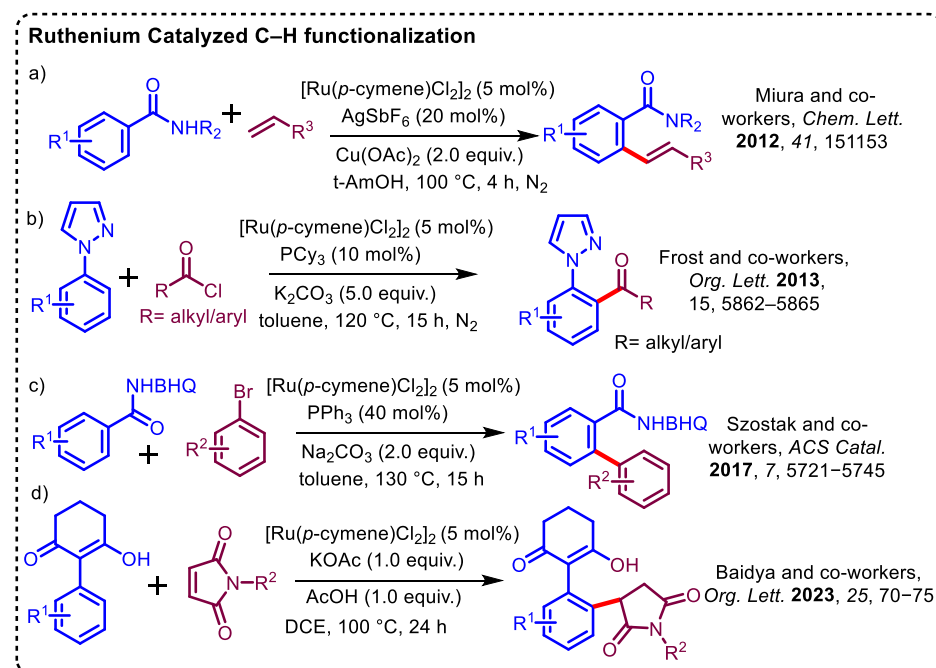
Scheme 1.2 Selected rhodium-catalyzed C–C bond formation reactions

–rd both electron-rich and electron-deficient substrates, delivering high yields with remarkable regioselectivity (**Scheme 1.2d**).^[19] In a complementary study, Li and co-workers described a rhodium-catalyzed, directing group-assisted C–H arylation with 4-hydroxycyclohexa-2,5-dienones as arylating source, where aromatization served as the driving force for product formation. The author performed this arylation, using silver salts, zinc catalysts, and 1,2-dichloroethane (DCE) as the solvent at 100 °C, which enabled the efficient synthesis of di- and tri-substituted phenols, with yields reaching up to 78% (**Scheme 1.2e**).^[20] Furthermore, an alkylation and alkenylation strategy was developed using *N*-alkyl maleimides with heteroarenes under Rh(III)-catalyzed conditions. The reaction employed silver salts and 1,2-

dichloroethane (DCE) as the solvent, conducted at temperatures ranging from 100-120 °C, showing a wide substrate scope. The methodology provided 3-arylbenzo[*d*]isoxazoles derivatives in yields ranging from 51% to 99%, while isoquinolones derivatives were obtained in yields of 19-96% (**Schemes 1.2f & g**).^[21,22]

1.2.4 Ruthenium-catalyzed C–H functionalization^[23-26]

Synthetic chemists are attracted to ruthenium-catalyzed C–H functionalization because of its low cost, selectivity, versatility, sustainability, and mild reaction conditions. The Miura and co-workers developed the ruthenium-catalyzed ortho C–H alkenylation of benzamide substrates using alkene reagents. The reaction was conducted under thermal conditions in the presence of silver salts and copper catalysts under a nitrogen atmosphere (**Scheme 1.3a**).^[23] Furthermore, Frost's, Szostak's, and Baidya's groups discovered that a range of C–C bond-forming reactions, including acylation, alkylation, and arylation, were achieved using ruthenium catalysts in combination with various ligands, bases, or acids. These transformations were typically carried out at temperatures of 100-130 °C with 15–24 hours of the reaction times (**Scheme 1.3b-d**).^[24-26]



Scheme 1.3 Selected ruthenium-catalyzed C–C bond formation reactions

Recently, organic chemists have increasingly prioritized the development of eco-friendly and sustainable methodologies and technologies. The traditional reliance on thermal energy to drive chemical reactions is gradually being supplemented and, in some cases, replaced by alternative energy sources. These include electrochemical, microwave, photochemical, and sonochemical methods, among others. Such innovations represent a paradigm shift towards greener and more efficient approaches in chemical synthesis, aligning with broader goals of sustainability and environmental stewardship.^[27]

1.3 Visible light-mediated photo-redox catalysis for C-C bond formation

The recent renaissance of photo-redox-catalyzed C–H functionalization has emerged as a prevailing strategy in drug discovery, particularly for forming C–C bonds via various reaction pathways. This method offers significant advantages, as it operates under mild conditions, typically at room temperature using visible light as a traceless and sustainable energy source to achieve efficient product formation. This approach has garnered considerable attention for its potential to enable selective and efficient chemical transformations, making it a valuable tool in modern organic synthesis.^[28]

1.3.1 A brief history of visible light in chemical transformations

For millennia, civilizations have understood the essential role of light in supporting life on Earth. As the primary light source and energy driving biological processes, the sun has been revered and studied throughout history. Various traditional remedies, some dating back centuries, suggest that sunlight exposure was an essential component of medical treatments. In the 19th century, significant advancements were made in the understanding of light and its properties. William Herschel discovered infrared radiation while investigating the thermal effects of sunlight, identifying a form of radiation beyond the visible red spectrum. Similarly, Johann Ritter uncovered ultraviolet (UV) radiation by

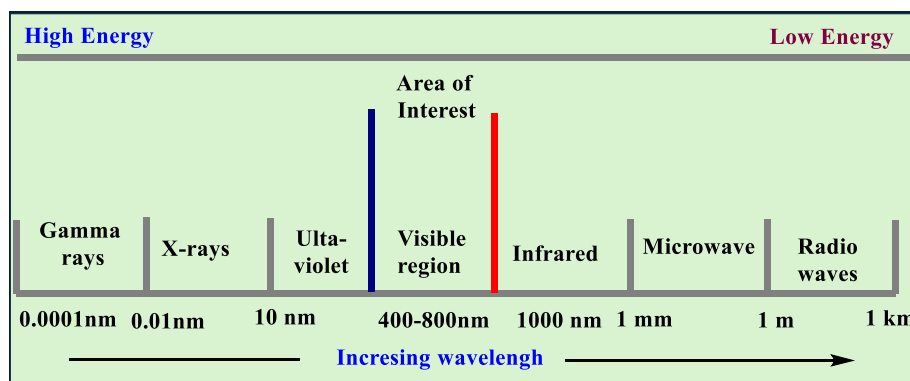


Figure 1.3 Relationship Between Energy and Wavelength of Light

studying the chemical reactions of silver chloride when exposed to sunlight, thus marking the opposite end of the visible spectrum. Further, James Clerk Maxwell combined the law of electricity and magnetism, resulting in the development of classical electromagnetism, which unifies the theory of electromagnetic waves, including visible light. The reaction of energy with a wavelength of light is shown in **Figure 1.3**. The first practical incandescent light bulb invented by Thomas Edison revolutionized artificial lighting and provided the foundation for modern lighting systems. In the early 20th century, Albert Einstein introduced the concept of photons-discrete packets of light energy to explain the photoelectric effect. As a result of this discovery, the quantum theory of light was established, making visible light more understandable at the atomic level.^[29] With the invention of fiber-optic technology in the late 20th century, Charles K. Kao revolutionized telecommunications by using light to transmit data over long distances with minimal loss. Light-emitting diode (LED) technology advanced dramatically in the 1990s when blue LEDs were invented, enabling the development of white LEDs. As a consequence of this breakthrough, highly energy-efficient and durable light sources were developed, revolutionizing modern lighting. Recently, visible light has been sporadically employed and gained attention for its role in photo-redox chemistry, enabling sustainable chemical transformations under mild, environmentally benign conditions. Photocatalysis techniques are particularly important in processes such as C–H functionalization, where visible light-driven

reactions facilitate the straightforward route of Carbon-Carbon bond through greater efficiency and selectivity. As green chemistry advances, visible-light-induced photo-redox catalysis has become a key component, offering innovative synthesis methodologies. It includes application in our own research, where visible light can be used to drive the C–H functionalization in heterocyclic compounds, making chemical processes more sustainable and energy-efficient.^[30]

1.3.2 Photo-redox Catalysis: Light-driven synthetic chemistry

Photo-redox catalysis is the process in which a catalyst absorbs light energy either visible or UV light to drive oxidation-reduction (redox) reactions and enable single-electron transfer reactions (SETs). As a result of irradiation, the catalyst undergoes transitions between its excited oxidative and reductive states, allowing electron transfer between the catalyst and substrate to occur. The precise control of redox potentials results in the generation of reactive radical intermediates, which promote the activation of traditionally inert chemical bonds in an energy-efficient environment. As a modern organic synthesis strategy, photo-redox catalysis has become increasingly important because it allows the previously inaccessible reaction pathways and enables the construction of structurally complex molecules with high chemoselectivity and regioselectivity.^[31,32] The photo-redox strategy has become integral to the advancement of sustainable methodologies, offering novel opportunities for selective functionalization in the context of green chemistry.^[33] As demonstrated in **Figure 1.4**, photocatalysts are excited under visible light to generate an excited state photocatalyst (PC)*, which initiates an oxidative cycle involving oxidizing agents. The excited photocatalyst (PC)* first reacts with oxidizing agent OA₁, resulting in the formation of a photocatalytic cation radical (PC)^{+•} and an anion radical (OA₁)^{•-}. Afterward, the ground state photocatalyst (PC) is regenerated by a reducing agent (RA₂, electron donor) generating a cation radical of (RA₂)^{+•}. Concomitantly, in the reductive quenching

cycle, the photocatalyst is excited under visible light to generate the excited state photocatalyst (PC)*, which then reacts with a reducing agent (RA₁), generating an anion radical of the photocatalyst (PC)^{•-} and a cation radical of RA₁^{+•}. This anion radical, (PC)^{•-} reacts with an oxidizing agent (OA₂) restoring the ground state of the photocatalyst (PC) with anion radical of OA₂^{•-}. [34]

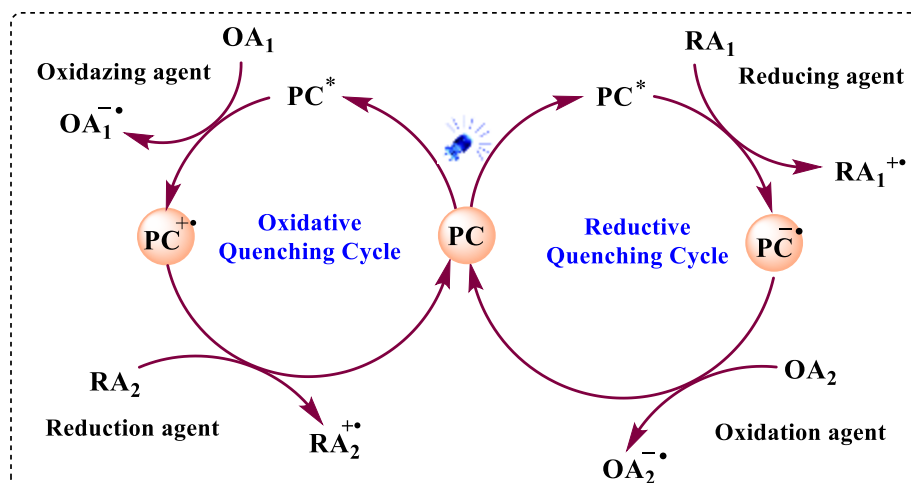


Figure 1.4 Oxidative and Reductive quenching cycle of photocatalyst

For a compound to function efficiently as a photo-redox catalyst in the visible light spectrum, it must meet several key criteria.

1. The catalyst should absorb visible light effectively within the range (400-700 nm) to ensure optimal photoexcitation by readily accessible light sources, such as sunlight or LEDs, facilitating the effective initiation of photo-redox processes.
2. The single-electron transfer (SET) processes should be achieved by the catalyst having sufficient redox potential to enable both oxidative and reductive interactions with the substrates.
3. The catalyst should exhibit redox potentials compatible with facilitating single-electron transfer (SET) reactions, ensuring that its excited state possesses sufficient energy to participate in both oxidation and reduction with the intended substrates.
4. The excited state (PC*) must exhibit a sufficiently long lifetime to enable productive interactions with substrates before relaxation to the

ground state. Additionally, the excited state should facilitate efficient energy transfer to substrates or intermediates, driving the desired chemical transformations.

5. The photocatalyst should demonstrate high photostability, resisting decomposition or degradation under prolonged light exposure and multiple redox cycles, to maintain sustained catalytic activity. Furthermore, it should exhibit efficient renewability after each catalytic cycle, ensuring continuous turnover without significant loss of performance.

1.3.3 Metal-based photo-redox catalysts ^[34,35]

Metal-based photo-redox catalysts are a class of catalysts that integrate the properties of both organometallic complexes and photo-redox systems. These catalysts typically feature a central transition metal, such as iridium, ruthenium, copper, and other metals (Fe, Ni, Au etc.) coordinated with organic ligands like phenylpyridine, bipyridyl etc. (**Figure 1.5**). Due to their unique photochemical properties, these coordination complexes have gathered significant attention as photo-redox catalysts. Under visible light irradiation, these metal-based catalysts are promoted from their ground state to an electronically excited state (PC*), transforming into an active species capable of initiating key reaction pathways. This excitation enables the catalyst to facilitate single-electron transfer (SET) processes, which can proceed through either oxidative or reductive mechanisms, depending on the reaction conditions. The effectiveness of these catalysts is further enhanced by their well-tuned redox potentials and relatively long-lived excited states, making them highly versatile for photo-redox catalysis in the presence of suitable oxidizing or reducing agents.

1.3.4 Organic photo-redox catalysts ^[34,35,36]

Organic photo-redox catalysts are a class of purely organic compounds (carbon-based) capable of mediating photo-redox reactions under light irradiation. These catalysts enable a wide range of otherwise thermally

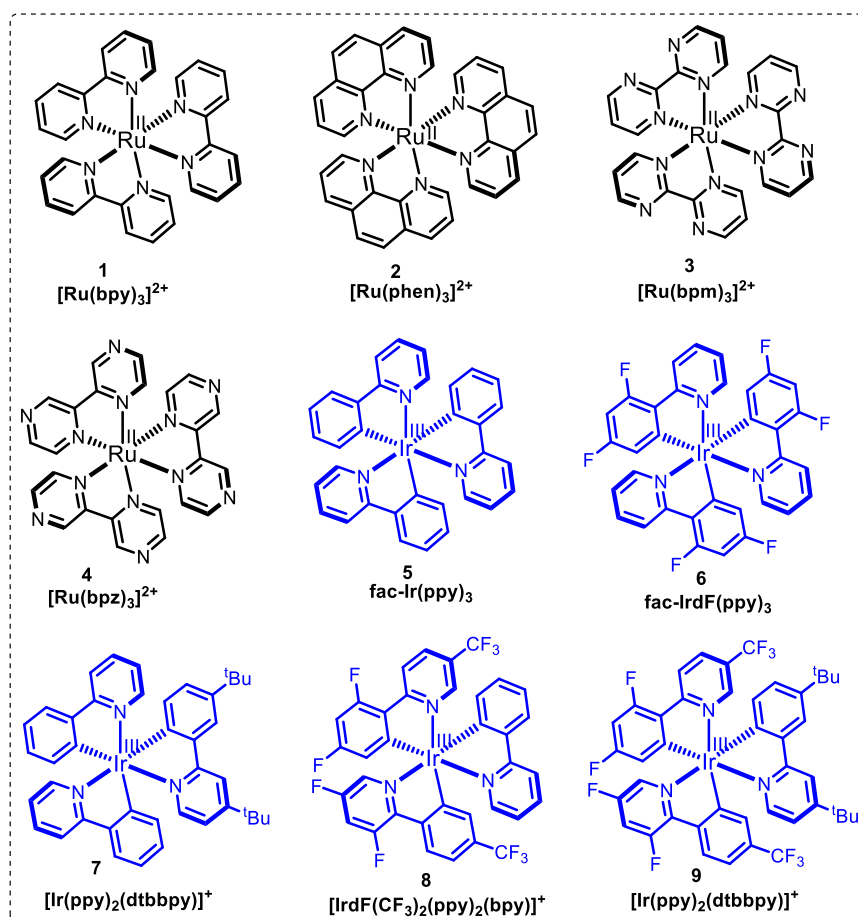


Figure 1.5 Metal-based photo-redox catalyst

inaccessible transformations by harnessing the energy of ultraviolet (UV) or visible light. By facilitating challenging oxidation and reduction reactions, organic photo-redox catalysts play a crucial role in advancing modern synthetic chemistry. The major advantages of organic photo-redox catalysts work without requiring metals, making them an attractive alternative due to their sustainability, cost-effectiveness, and reduced environmental impact. They are particularly valuable in promoting substrate activation and driving key transformations such as C–C, and C–X bond formation. Additionally, their versatility allows them to mediate various reaction types, including cross-coupling C–H functionalization, and more. Some organic photo-redox catalysts that absorb UV light (**Figure 1.6a**) have traditionally been used in chemical reactions. However, the reliance on UV light presents notable drawbacks, including high energy requirements, safety concerns, and limited functional group compatibility. To address these challenges,

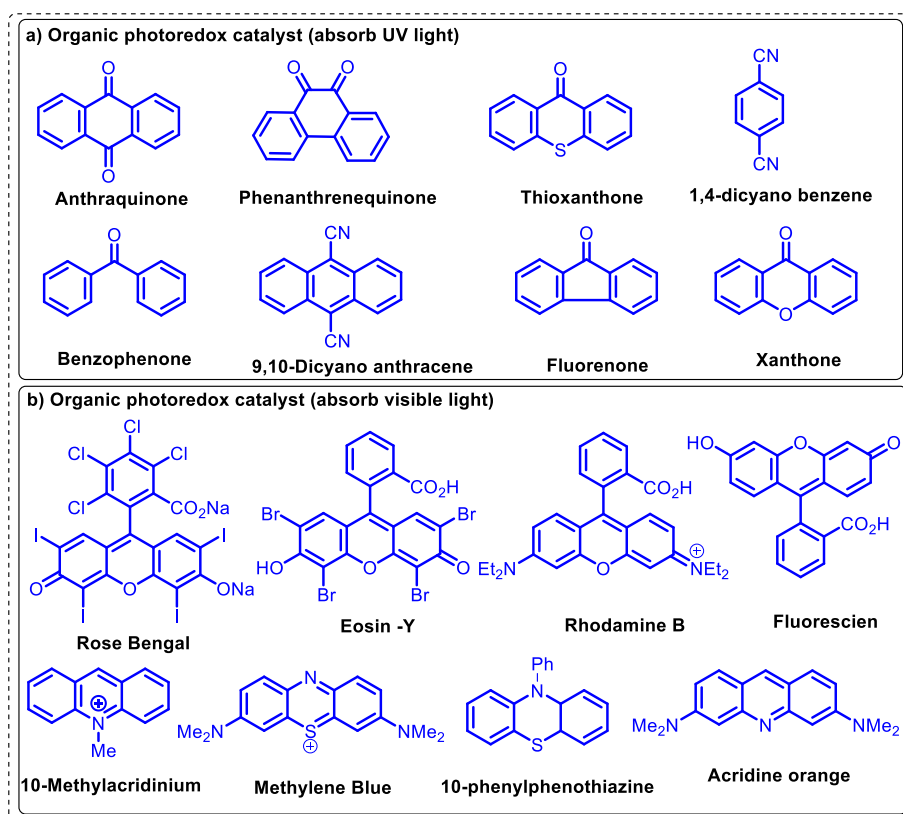


Figure 1.6 Organic photo-redox catalyst (a) & (b)

recent advancements have focused on the use of organic dyes as photocatalysts (**Figure 1.6b**). These dyes absorb visible light, providing a sustainable and efficient alternative for chemical transformations.

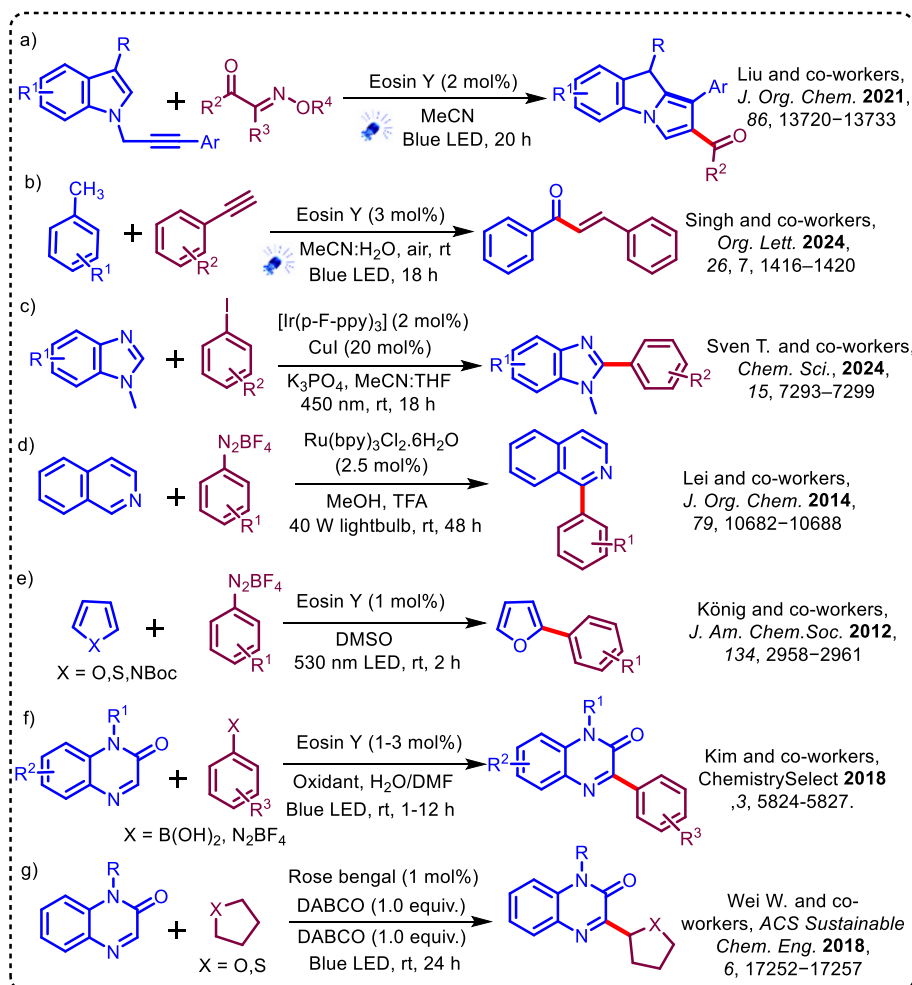
1.3.5 Semiconductor photo-redox catalysts

An additional type of photo-redox catalyst is a semiconductor photo-redox catalyst. It utilizes the unique electronic properties of semiconductors to facilitate redox reactions, specifically C–H functionalization of organic molecules, under light irradiation. This process involves activating inert carbon-hydrogen (C–H) bonds and transforming them into diverse chemical modifications. Examples of semiconductor photo-redox catalysts include Titanium dioxide (TiO_2), Zinc oxide (ZnO), Zinc sulfide (ZnS), Cadmium sulfide (CdS), Antimony trioxide (Sb_2O_3) which are used to promote these transformations under UV or visible light, depending on their bandgap properties.^[37]

1.3.6 Application of photo-redox catalyst in C–H functionalization

Photo-redox-catalyzed C–H functionalization has significant applications in drug discovery, particularly in the formation of C–C bonds through arylation, arylation, and alkylation.^[38,39] The scheme 1.4 illustrates several selected examples of C–H functionalization reactions. One notable example is the work by Liu and co-workers in 2021. A novel photo-redox catalyzed method was developed using eosin Y as a photocatalyst to promote cyclization and acylation reactions of *N*-propargyl indoles. This approach employs aryl or alkyl-substituted oxime esters as acyl donors, facilitating the efficient synthesis of 2-acylated 9*H*-pyrrolo[1,2-*a*]indoles under visible light irradiation at ambient temperature for 20 hours (**Scheme 1.4a**).^[40] The Singh group demonstrated an effective approach for synthesizing α,β -unsaturated ketone derivatives through the C(sp³)–H functionalization of toluene and phenylacetylene substrates. Utilizing an organic dye as the catalyst, this reaction selectively transforms various methyl arenes and aromatic alkynes into the target products with the source of visible light (**Scheme 1.4b**).^[41] Additionally, the Trienes group demonstrated coupling reactions in the presence of aryl halides and 1,3-azoles using photo-redox conditions under visible light irradiation, foremost to the formation of arylated products (**Scheme 1.4c**).^[42] These transformations highlight the versatility of visible-light-induced processes in synthesizing valuable organic molecules. Next, Lei and co-workers developed an arylation strategy for isoquinoline using Ru(bpy)₃Cl₂·6H₂O as a photocatalyst under visible light irradiation at room temperature. This photo-redox catalyzed approach enabled the efficient synthesis of isoquinoline derivatives, including alkaloids such as menisporphine and daurioxoisoporphine C. The method showcases the utility of Ru-based photo-redox catalysis in the functionalization of heterocycles and the synthesis of biologically relevant compounds (**Scheme 1.4d**).^[43] In addition to other photo-redox, organic dyes have been extensively employed in C–H functionalization. Notably, several

reports highlight using eosin Y as a photocatalyst for C–H arylation under visible light conditions, additional two significant studies are highlighted. König's and groups developed a metal-free C–H arylation methodology involving diazonium salts and heterocycles. Similarly, Kim's groups reported the C–H arylation of quinoxalin-2(1*H*)-ones using diazonium salts and aryl boronic acids under visible light irradiation. These studies demonstrate the versatility of eosin Y in



Scheme 1.4 Selected Examples of Photoinduced C-H Functionalization

facilitating C–H bond arylation reactions (**Scheme 1.4e & f**).^[44–45] Wei's and co-workers reported a C–H alkylation methodology employing organic photocatalysts, such as rose bengal, under visible light irradiation. This approach facilitated the alkylation of quinoxalin-2(1*H*)-ones using simple ethers as alkylating agents. Quinoxalin-2(1*H*)-ones were employed as the limiting reagents, demonstrating the efficacy of

organic photocatalysts in promoting C–H alkylation under visible light irradiation (**Scheme 1.4g**).^[46]

1.4 Merging of transition metal catalysis and photo-redox catalysis

Recently, photo-redox catalysts have been employed in conjunction with other catalytic systems, such as transition metal catalysis, in dual catalytic strategies to enhance reactivity and broaden the scope of transformations. This merging of transition metal catalysis with photo-redox catalysis has become a more advanced strategy for developing novel chemical bond formation pathways using visible light. In this dual catalysis strategy, traditionally inert C–H bonds are efficiently activated through the synergistic action of a transition metal catalyst and a photo-redox catalyst. The photo-redox catalyst facilitates the generation of reactive radical intermediates, enabling subsequent C–C bond formation or other bond-forming reactions. Notably, these transformations occur under exceptionally mild conditions, highlighting the approach's practicality and versatility in complex chemical synthesis. Mechanically, photocatalysts absorb visible light, excited from the ground state to an excited state. These excited photocatalysts can then engage in single-electron transfer (SET) events, either through oxidative or reductive quenching pathways, to activate unreactive substrates. Upon activation, the substrate generates radical intermediates that can further react with corresponding coupling partners, facilitating the desired functionalization under mild, energy-efficient conditions. This synergistic blend between transition metal catalysis and photo-redox catalysis is especially advantageous for challenging substrates such as those with unreactive C–H bonds or substrates requiring alkyl, aryl, acyl, etc. radical intermediates enabling regioselective and stereoselective transformations with high efficiency. The merging of photocatalysis and transition metal catalysis offers distinct mechanistic pathways for C–H functionalization, such as (1) C–H activation driven by photocatalysts and transition metal catalysts, (2) radical-radical cross

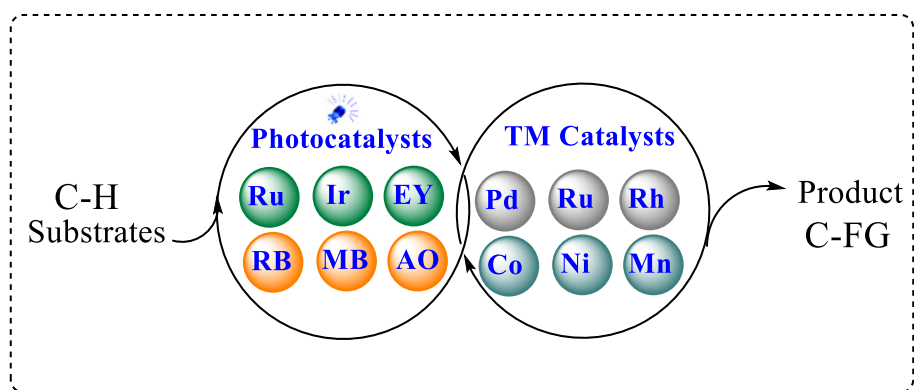
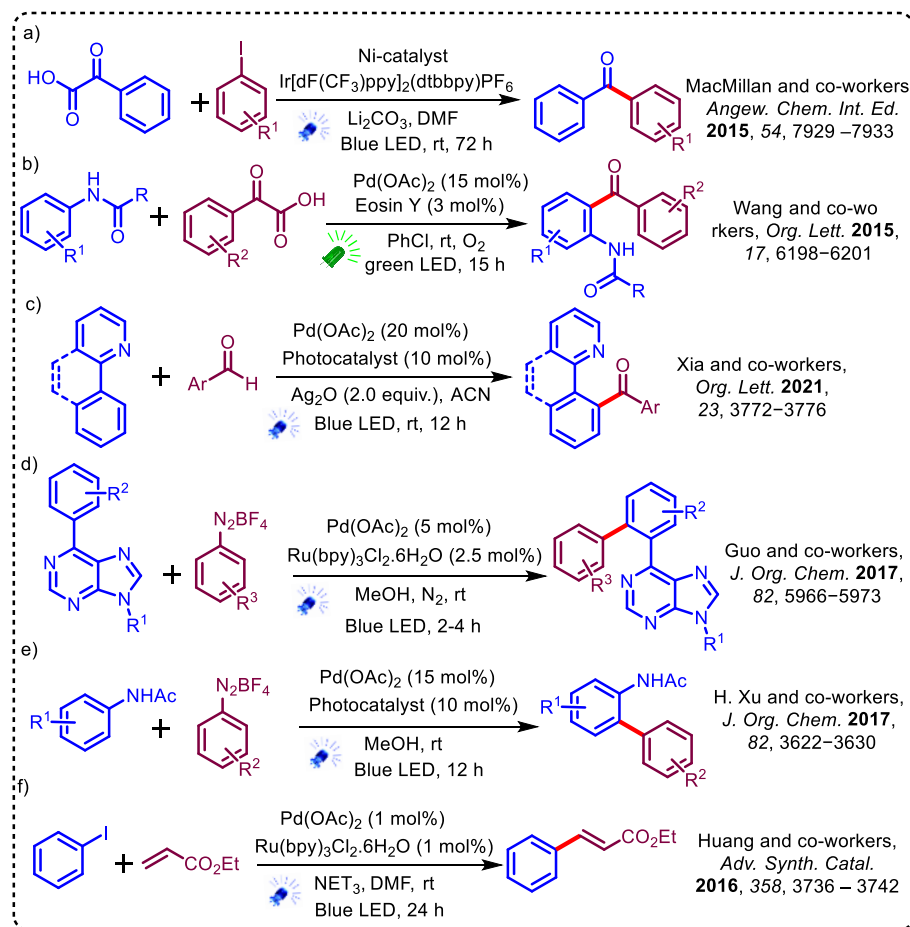


Figure 1.7 Merging of TM catalyst with PC

-coupling, and (3) dual catalysis (as predicted in **Figure 1.7**). Each pathway exploits the synergistic roles of light and transition metals to promote efficient bond formation under mild, sustainable conditions.^[47] In the C–H activation path, a photocatalyst absorbs visible light to reach an excited state, facilitating the generation of radical intermediates from substrates containing carbon or heteroatoms (e.g., acyl, aryl, alkyl, or heteroatoms such as N, O, and S). Concurrently, a transition metal catalyst (e.g., Pd, Ni, Au, Ru, Rh, Co) activates the C–H bond, initiating a catalytic cycle. In the presence of the transition metal catalyst, the radical intermediate is converted into the desired product by doing an interaction with it. In radical cross-coupling, the photocatalyst generates reactive radicals through either hydrogen atom transfer (HAT) processes or single electron transfer (SET). These radicals can then be intercepted by the transition metal catalyst, accelerating the chemical transformation. This approach provides access to complex molecular architectures via radical intermediates. Finally, in dual catalysis, the transition metal catalyst activates otherwise inert C–H bonds, while the photocatalyst supplies the necessary redox equivalents to drive the catalytic cycle under visible light. This dual catalytic strategy lowers the energy barrier for bond formation and enhances the efficiency of C–H functionalization.^[48]

Overall, these approaches expand the toolkit for developing novel, green synthetic methodologies, enabling the construction of molecular scaffolds under mild, visible-light-driven conditions. Since the early

breakthroughs in acylation reactions, research groups led by MacMillan,^[49] Wang,^[50] and Xia^[51] have pioneered transition metal-catalyzed, photo-redox-catalyzed acylation reactions under visible light irradiation (typically using blue or green LEDs), resulting in various carbonyl-containing products (**Scheme 1.5a-c**). In 2017, both Gau's^[52] and Xu's^[53] research groups independently reported the palladium-catalyzed, photo-redox-driven C–H arylation of heteroarenes



Scheme 1.5 Photoinduced C–H Activation and Functionalization

using aryl diazonium salts under blue LED irradiation, with methanol as the solvent (**Scheme 1.5d-e**). It was demonstrated that visible light-driven catalysis was successful in forming C–C bonds through C–H activation. Since then, several methodologies have emerged employing this dual catalytic system for C–C and C–X bond formation. Huang and co-workers^[54] developed an alkenylation approach via a Heck-type

reaction, combining a palladium catalyst and a photo-redox catalyst in the presence of visible light (**Scheme 1.5f**).

1.5 Innovation and bioactivity of heterocyclic compounds

Heterocyclic compounds represent a ubiquitous and integral class of substrates in pharmaceutical chemistry. Heterocyclic compounds, a cornerstone in the realm of organic synthesis, are characterized by ring structures comprising at least two distinct types of atoms. Specifically, when a ring system contains carbon atoms in conjunction with heteroatoms such as nitrogen (N), oxygen (O), or sulfur (S), it is classified as an organic heterocyclic compound. These compounds are highly significant in advanced organic synthesis due to their widespread presence in bioactive molecules. Heterocyclic chemistry is a crucial and captivating field, primarily due to the widespread presence of heterocycles in abundant therapeutic compounds. These compounds are extensively utilized across pharmaceuticals, veterinary medicine, and agrochemicals, making them indispensable in these industries. The development of new synthetic methods and the progress in medicinal chemistry have led to the design of drug molecules with enhanced efficacy and targeted drug delivery.^[55-57]

As a result, heterocyclic chemistry remains a central area of research, driving the discovery and improvement of compounds with wide-ranging applications across various scientific fields. A few selected naturally occurring pyridine derivatives, along with drugs and bioactive compounds that incorporate pyridine as a core structure, are shown in **Figure 1.8**.^[58,59]

Approximately 85% of physiologically active medications contain at least one heteroatom, such as nitrogen, with pyridine being a key structural component in many of these pharmaceutical compounds. Pyridine serves as a critical core in many drug molecules, playing a significant role in their biological activity, enzymatic inhibition, antimicrobial activity, and anti-cancer properties, highlighting their significance in medicinal chemistry. The pyridine core is a fundamental

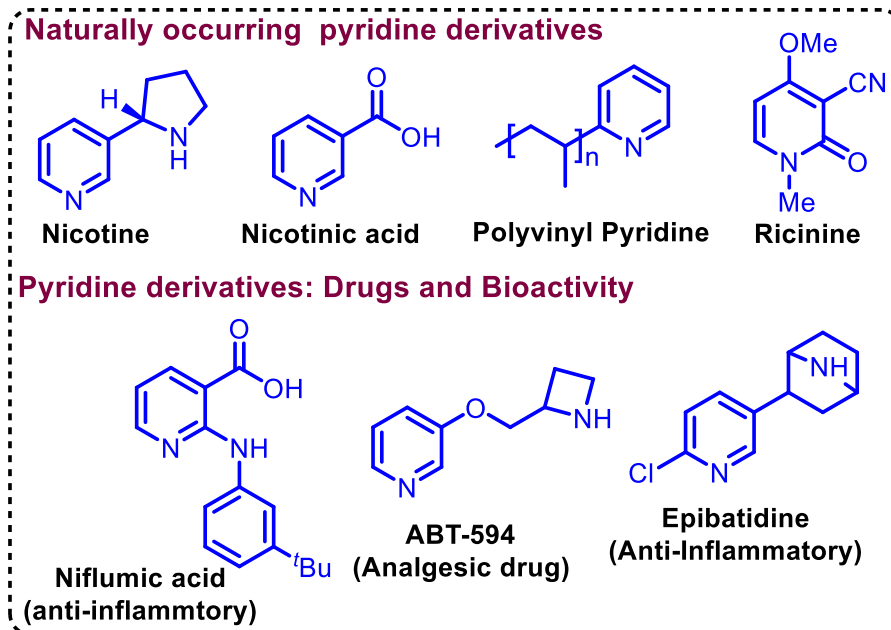


Figure 1.8 Pyridine-based bioactive compounds

structure found in a wide array of heterocyclic compounds and is commonly present in various bioactive molecules (**Figure 1.9**). Examples include heterocycles like quinoline, imidazo[1,2-*a*]pyridine, pyrimido[1,2-*a*]indole, 4*H*-pyrido[1,2-*a*]pyrimidin-4-one, pyrido[2,3-*b*]pyrazine, 1*H*-pyrazolo[3,4-*b*]pyridine, 3*H*-imidazo[4,5-*b*]pyridine,

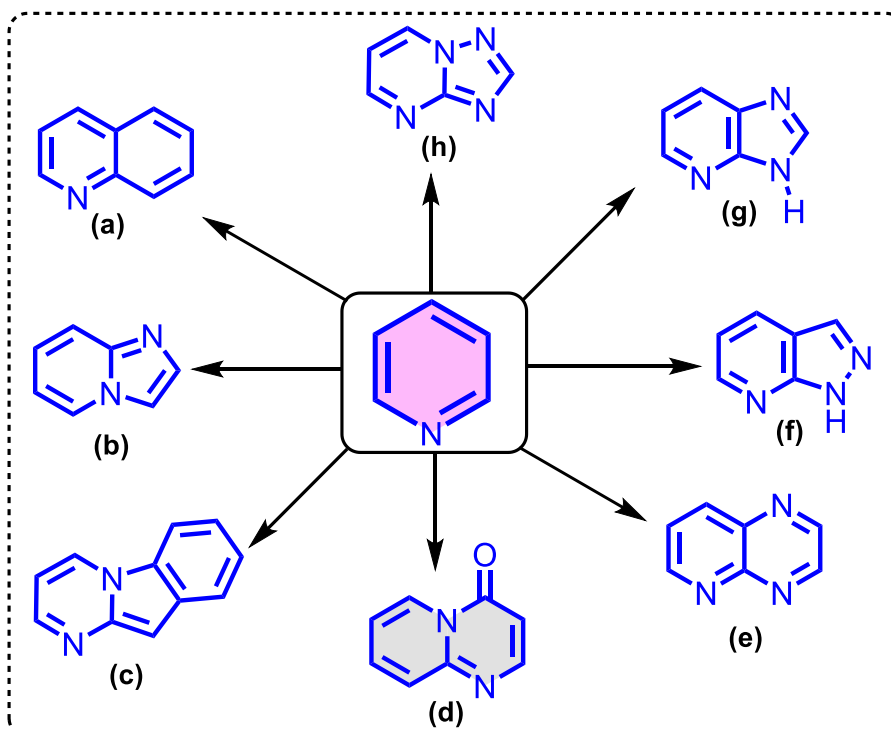


Figure 1.9 Pyridine-Based Heterocycles: Essential Building Blocks in Bioactive Molecules

and [1,2,4]triazolo[1,5-*a*]pyrimidine. These compounds play essential roles in various biological activities.^[60-64]

1.5.1 **4*H*-Pyrido[1,2-*a*]pyrimidin-4-ones: Biologically importance**

The 4*H*-pyrido[1,2-*a*]pyrimidin-4-one scaffold stands out as a distinct nitrogen-containing heterocycle, featuring a fused pyridine and pyrimidine ring structure. This structure is composed of a 4*H*-pyridine fused with 1,2-diazine (pyrimidine), where the carbonyl group at the fourth position defines the "4-one" nomenclature, while the "4*H*" signifies the hydrogen located on the nitrogen of the pyrimidine ring. 4*H*-pyrido[1,2-*a*]pyrimidin-4-ones, a type of fused heterocycle, are structurally and chemically versatile. The 4*H*-pyrido[1,2-*a*]pyrimidin-4-one scaffold, first investigated in the mid-20th century, has garnered significant attention due to its rigid and planar architecture, which facilitates interactions with various biological targets. This structural feature has made these compounds highly attractive in drug discovery and development.^[65]

4*H*-pyrido[1,2-*a*]pyrimidin-4-ones scaffold or their derivatives are recognized for their potent bioactivity and multifunctional utility, serving as critical motifs in diverse fields such as natural product chemistry, pharmaceuticals, agrochemicals, materials science, and medicinal compounds. The unique structural attributes of this scaffold make it a valuable target for research in these areas. A wide range of medicinal applications have been investigated for 4*H*-pyrido[1,2-*a*]pyrimidin-4-ones, which are illustrated in **Figure 1.10**. The therapeutic versatility of these compounds is noteworthy, including anti-allergic activity (e.g., Permirolast, endothelial cell dysfunction inhibition, and tranquilizing effects, as seen in Pirenperone. Furthermore, they have shown promising anticancer activity, function as ERPα reverse agonists, and are used in the treatment of spinal muscular atrophy, exemplified by Evrysdi. Other notable activities include CXCR3 antagonism, efflux pump inhibition, PI3K inhibition,

antidepressant effects e.g., Lusaperidone, aldose reductase inhibition, EPIs in *Pseudomonas aeruginosa*, Quorum sensing inhibitor. With these wide-ranging biological functions, scaffolds are highly valuable for drug development due to their broad therapeutic potential.^[65]

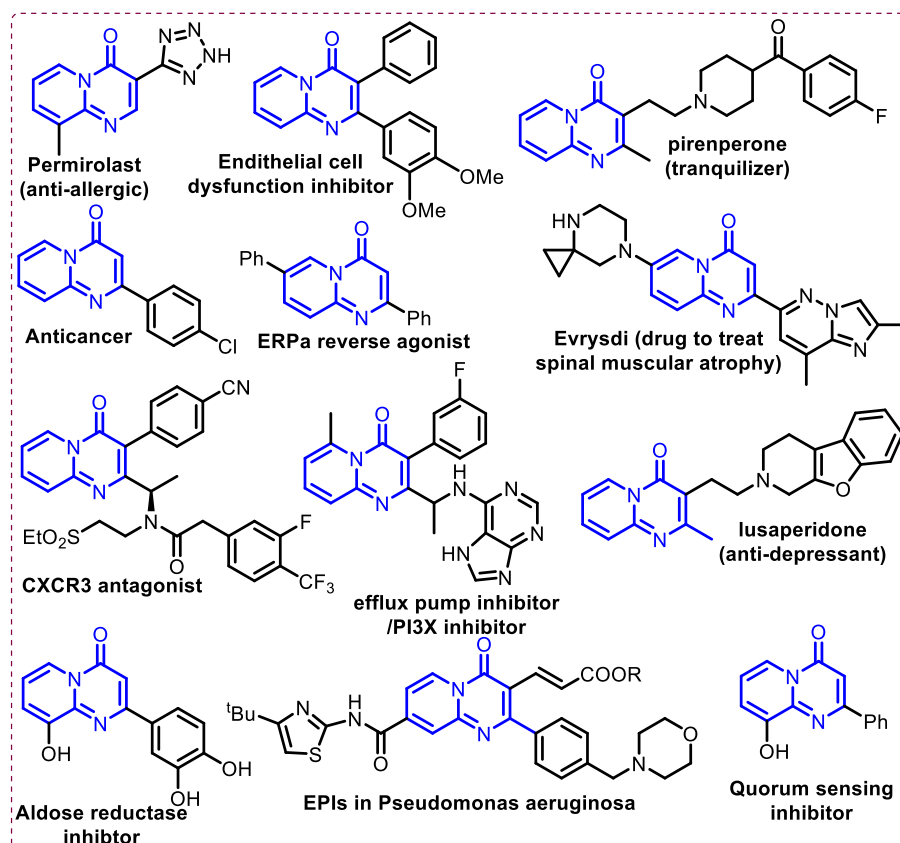
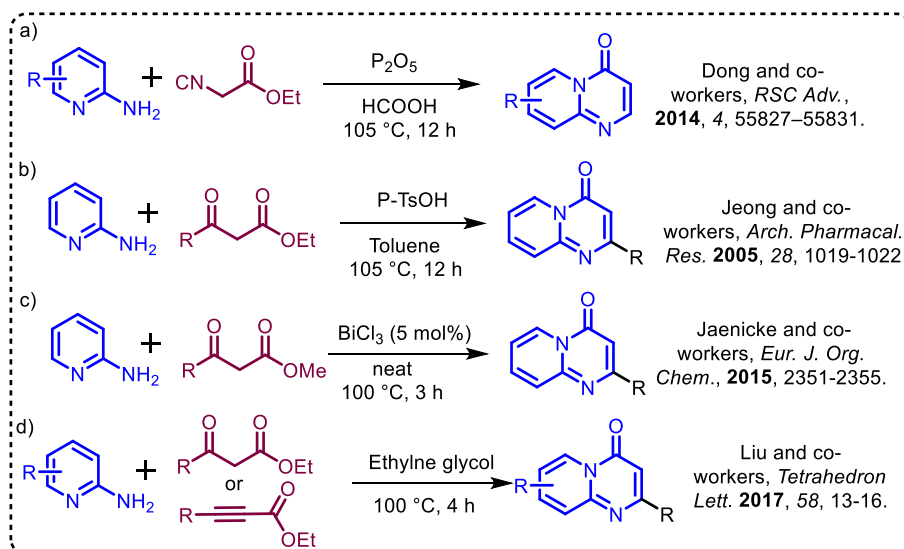


Figure 1.10 Biological active compounds of 4*H*-pyrido[1,2-*a*]pyrimidin-4-one

1.5.2 A classical route for the synthesis of 4*H*-pyrido[1,2-*a*]pyrimidin-4-one

A classical synthesis route and functionalization of the 4*H*-pyrido[1,2-*a*]pyrimidin-4-one scaffold have been extensively covered in the existing literature.^[65] Scheme 1.6 discusses selected synthetic routes for preparing pyrido[1,2-*a*]pyrimidin-4-ones and highlights key methodologies. In 2014, Dong and colleagues reported a cyclization strategy utilizing a 2-aminopyridine derivative and malononitrile in the presence of phosphorus pentoxide (P₂O₅) and formic acid as solvent. This reaction was conducted at 105 °C for 12 hours (**Scheme 1.6a**).^[66] Similarly, in 2005, Jeong *et al.* employed a related approach to

synthesize 4*H*-pyrido[1,2-*a*]pyrimidin-4-one scaffolds (**Scheme 1.6 b**). They used 2-aminopyridine as a key substrate, reacting it with ethyl acetoacetate under acidic conditions, specifically with *p*-toluene sulfonic acid (PTSA) in toluene, under reflux conditions.^[67] In 2015, the



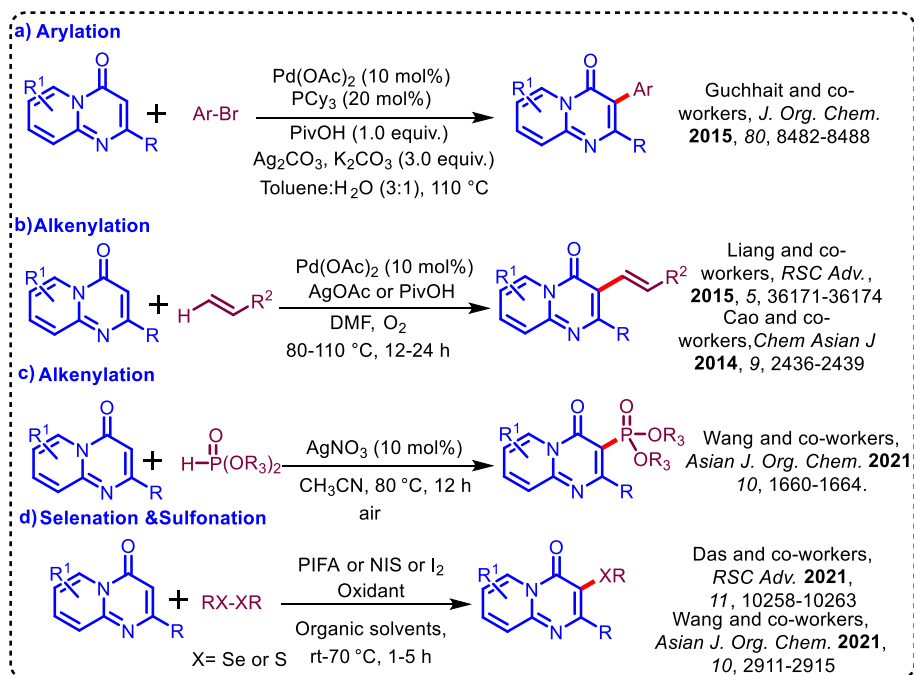
Scheme 1.6 Classical synthetic route of 4*H*-pyrido[1,2-*a*]pyrimidin-4-one scaffolds

Jaenicke group introduced a novel methodology utilizing bismuth chloride neat conditions at 100 °C for 3 hours to synthesize derivatives of 4*H*-pyrido[1,2-*a*]pyrimidin-4-one (**Scheme 1.6c**).^[68] Subsequently, in 2017, Liu and colleagues developed another synthetic route using either a beta-keto ester or a beta-diketone in combination with the aminopyridine derivative (**Scheme 1.6d**).^[69]

1.5.3 Functionalization of 4*H*-pyrido[1,2-*a*]pyrimidin-4-one scaffold

As discussed in the previous section and supported by the literature, 4*H*-pyrido[1,2-*a*]pyrimidin-4-one serves as a crucial structural core in many essential medicinal compounds. Not only does the 4*H*-pyrido[1,2-*a*]pyrimidin-4-one core exhibit bioactivity, but its functionalized derivatives also demonstrate significant biological effects in various compounds. As a result, several researchers have focused on developing novel functionalization strategies for this moiety. In 2015, *Guchhait et al.* pioneered an arylation methodology for the pyrido[1,2-*a*]pyrimidin-

4-one scaffold, offering a robust approach to introduce aryl groups, achieving efficient transformations at a reaction temperature of 110 °C (**Scheme 1.7a**).^[70] Subsequent progress was made by both the Cao's^[71] and Liang^[72] groups, who independently developed palladium-catalyzed C3 alkenylation of the 4*H*-pyrido[1,2-*a*]pyrimidin-4-one derivatives. The reactions, performed at 80 °C to 110 °C, resulted in valuable alkenylated products that display substantial synthetic and pharmacological potential (**Scheme 1.7b**). Functionalization strategies have been employed to investigate the formation of C-S, C-Se, and C-P bonds. Wang's group^[73] and Das's group^[74,75] reported efficient selenylation and sulfenylation reactions, conducted at temperatures spanning from room temperature to 110 °C, offering versatile tools for further scaffold diversification (**Scheme 1.7c**). In 2021, Guo's co-workers developed a silver-catalyzed C3 phosphorylation of the 4*H*-pyrido[1,2-*a*]pyrimidin-4-one core, achieving high selectivity at a reaction temperature of 80 °C (**Scheme 1.7d**).^[76] These developments underscore the growing versatility of functionalization strategies for the pyrido[1,2-*a*]pyrimidin-4-one framework, with various methods available for the introduction of alkenyl, aryl, selenyl, sulfonyl, and phosphoryl groups under a wide range of reaction conditions, from ambient temperature to elevated temperatures. The demand for novel heterocyclic compounds is driving the development of heterocyclic compounds through environmentally friendly methods, such as reactions at room temperature and under cost-effective conditions, which is a significant area of research. This thesis focuses on visible light photoinduced C–H functionalization of 2-aryl heterocycles via a dual catalytic system, merging photo-redox catalysis with transition metal catalysis under visible light irradiation at ambient temperature. The existing approach aims to achieve sustainable and efficient synthetic transformations.



Scheme 1.7 Functionalization of pyrido[1,2-*a*]pyrimidin-4-one

1.6 Aim of thesis

This thesis aims to explore the C-C bond functionalized methodologies in heterocyclic compounds, highlighting their importance in medicinal chemistry. In the past several years, cross-coupling reactions and transition metal-catalyzed thermal reactions have become widely utilized for C-C bond formation. However, these approaches often require pre-functionalized substrates and mostly rely on high temperatures, stoichiometric amounts of oxidants, ligands, and other additives, and sensitivity of certain functional groups (amine, hydroxyl, etc.) which pose challenges in terms of sustainability and operational simplicity, especially in environmentally conscious chemistry.

Looking at these requirements, in this thesis we focused on the C-H activation and functionalization, facilitated by visible light-mediated photo-induced pathways for C-C bond formation via direct C-H arylation, acylation, alkylation, and alkenylation of bioactive 2-phenyl-4*H*-pyrido[1,2-*a*]pyrimidin-4-ones and other related 2-aryl heterocycles. Further, by merging photo-redox catalysis with transition metal catalysis, we introduced novel approaches that enable C-C bond

formation at ambient conditions providing a more sustainable alternative to the classical synthetic transformations.

1.7 References

1. Blakemore D. C., Castro L., Churcher I., Rees D. C., Thomas A. W., Wilson D. M., Wood A. (2018), Organic synthesis provides opportunities to transform drug discovery, *Nat. Chem.* *10*, 383-394 (DOI: 10.1038/s41557-018-0021-z)
2. Ackermann L., Vicente R., Kapdi A. R. (2009), Transition-Metal-Catalyzed Direct Arylation of (Hetero)Arenes by C–H Bond Cleavage, *Angew. Chem. Int. Ed.* *48*, 9792-9826. (DOI: 10.1002/anie.200902996)
3. Seregin I. V., Gevorgyan V. (2007), Direct transition metal-catalyzed functionalization of heteroaromatic compounds, *Chem. Soc. Rev.* *36*, 1173-1193 (DOI: 10.1039/B606984N)
4. Liu C., Yuan J., Gao M., Tang S., Li W., Shi R., Lei A. (2015), Oxidative Coupling between Two Hydrocarbons: An Update of Recent C–H Functionalizations, *Chem. Rev.* *115*, 12138-12204 (DOI: 10.1021/cr500431s)
5. Rej S., Das A., Chatani N. (2021), Strategic evolution in transition metal-catalyzed directed C–H bond activation and future directions, *Coord. Chem. Rev.* *431*, 213683, (DOI: 10.1016/j.ccr.2020.213683)
6. Zhao Q., Poisson T., Pannecoucke X., Besset T. (2017), The Transient directing group strategy: A new trend in transition-metal-catalyzed C–H bond functionalization, *Synthesis* *49*, 4808-4826 (DOI: 10.1055/s-0036-1590878)
7. Chen Z., Wang B., Zhang J., Yu W., Liu Z., Zhang Y. (2015), Transition metal-catalyzed C–H bond functionalizations by the use of diverse directing groups, *Org. Chem. Front.* *2*, 1107-1295 (DOI: 10.1039/C5QO00004A)
8. Docherty J. H., Lister T. M., Mcarthur G., Findlay M. T., Domingo-Legarda P., Kenyon J., Choudhary S., Larrosa I. (2023), Transition-metal-catalyzed C–H bond activation for the

- formation of C–C bonds in complex molecules, *Chem. Rev.* **123**, 7692-7760 (DOI: 10.1021/acs.chemrev.2c00888)
9. Gandeepan P., Cheng C. H. (2015), Transition-Metal-Catalyzed π -Bond-Assisted C–H Bond Functionalization: An Emerging Trend in Organic Synthesis, *Chem. Asian J* **10**, 824-838 (DOI: 10.1002/asia.201403224)
 10. Chen X., Engle K. M., Wang D. H., Yu J. Q. (2009), Palladium (II)-catalyzed C–H activation/C–C cross-coupling reactions: versatility and practicality, *Angew. Chem. Int. Ed.* **48**, 5094-5115 (DOI: 10.1002/anie.200806273)
 11. Chu J.-H., Tsai S.-L., Wu M.-J. (2009), Palladium (II)-Catalyzed ortho Arylation of 2-Phenylpyridines with Potassium Aryl trifluoroborates by C-H Functionalization, *Synthesis* **2009**, 3757-3764 (DOI: 10.1055/s-0029-1217014)
 12. Zhang Q., Li C., Yang F., Li J., Wu Y. (2013), Palladium-catalyzed ortho-acylation of 2-arylbenzoxazoles, *Tetrahedron* **69**, 320-326 (DOI: 10.1016/j.tet.2012.10.033)
 13. Wang S., Yang Z., Liu J., Xie K., Wang A., Chen X., Tan Z. (2012), Efficient synthesis of anthranilic esters via Pd-catalyzed dehydrogenative/decarbonylative coupling of anilides and glyoxylates, *Chem. Commun.* **48**, 9924-9926 (DOI: 10.1039/C2CC34473D)
 14. Kumar R., Chandra D., Sharma U. (2022), Pd-Catalyzed Atropselective C–H Olefination Promoted by a Transient Directing Group, *Adv. Synth. Catal.* **364**, 897-908 (DOI: 10.1002/adsc.202101242)
 15. Zeng M., Jiang H., Li K., Chen Z., Yin G. (2022), Palladium(II)/Lewis Acid-Catalyzed Olefination of Arylacetamides with Dioxygen, *J. Org. Chem.* **87**, 4524-4537 (DOI: 10.1021/acs.joc.1c02783)
 16. Park S. H., Kim J. Y., Chang S. (2011), Rhodium-catalyzed selective olefination of arene esters via C–H bond activation, *Org. Lett.* **13**, 2372-2375 (DOI: 10.1021/ol200600p)

17. Guan Z.-H., Ren Z.-H., Spinella S. M., Yu S., Liang Y.-M., Zhang X. (2009), Rhodium-Catalyzed Direct Oxidative Carbonylation of Aromatic C–H Bond with CO and Alcohols, *J. Am. Chem. Soc.* *131*, 729-733 (DOI: 10.1021/ja807167y)
18. Xie F., Qi Z., Yu S., Li X. (2014), Rh (III)-and Ir (III)-catalyzed C–H alkynylation of arenes under chelation assistance, *J. Am. Chem. Soc.* *136*, 4780-4787 (DOI: 10.1021/ja501910e)
19. Patureau F. W., Besset T., Glorius F. (2011), Rhodium-Catalyzed Oxidative Olefination of C–H Bonds in Acetophenones and Benzamides, *Angew. Chem. Int. Ed.* *5*, 1064-1067 (DOI: 10.1002/anie.201006222)
20. Zhang X., Wang F., Qi Z., Yu S., Li, X. (2014), Rhodium (III)-catalyzed redox-neutral C–H arylation via rearomatization, *Org. Lett.* *16*, 1586-1589 (DOI: 10.1021/ol500186j)
21. Yue X., Zhao X., Huang J., Gao Y., Feng Y., Cui X. (2023), Rhodium(III)-catalyzed redox neutral alkylation of 3-arylbenzo[d]isoxazoles: easy access to substituted succinimides, *Org. Biomol. Chem.* *21*, 5985-5989 (DOI: 10.1039/D3OB00851G)
22. Manisha, Chandra D., Sharma U. (2023), Rhodium-Catalyzed C8-Alkenylation of Isoquinolones with Maleimides, *Eur. J. Org. Chem.* *26*, e202300411 (DOI: 10.1002/ejoc.202300411)
23. Hashimoto Y., Ortloff T., Hirano K., Satoh T., Bolm C., Miura M. (2012), Ru/Ag-Catalyzed Oxidative Alkenylation of Benzamides and Phenylazoles through Regioselective C–H Bond Cleavage, *Chem. Lett.* *41*, 151-153 (DOI: 10.1246/cl.2012.151)
24. Liu P. M., Frost C. G. (2013), Ruthenium-catalyzed C–H functionalization of arylpyrazoles: regioselective acylation with acid chlorides, *Org. Lett.* *15*, 5862-5865 (DOI: 10.1021/ol402936c)
25. Nareddy P., Jordan F., Szostak M. (2017), Recent developments in ruthenium-catalyzed C–H arylation: Array of mechanistic

- manifolds, *ACS Catal.* **7**, 5721-5745 (DOI: 10.1021/acscatal.7b01645)
26. Mondal S., Bera R., Chowdhury D., Dana S., Baidya M. (2022), Redox-Neutral Ruthenium (II)-Catalyzed Enol-Directed Arene C–H Alkylation with Maleimides, *Org. Lett.* **25**, 70-75 (DOI: 10.1021/acs.orglett.2c03858)
 27. Ali S. K., Althikrallah H. A., Alluhaibi M. S., Hawsawi M. B., Hakami O., Shariq M., Hassan D. A., Hussain M. (2024), Electrochemical and Photocatalytic Synthesis of Organic Compounds Utilizing a Greener Approach, *Mol. Catal.* **559**, 114087 (DOI: 10.1016/j.mcat.2024.114087)
 28. Venturi M., Balzani V., Gandolfi M. T. (2005), Fuels from solar energy. A dream of Giacomo Ciamician, the father of photochemistry, Proceedings ISES Solar World Congress, Orlando (USA), 2005
 29. Prier C. K., Rankic D. A., MacMillan D. W. (2013), Visible light photo-redox catalysis with transition metal complexes: applications in organic synthesis, *Chem. Rev.* **113**, 5322-5363 (DOI: 10.1021/cr300503r)
 30. Ramamurthy V., Turro, N. J. (1993), Photochemistry: Introduction, *Chem. Rev.* **93**, 1-2 (DOI: 10.1021/cr00017a600)
 31. Sordello F., Calza P., Minero C., Malato S., Minella M. (2022), More than One Century of History for Photocatalysis, from Past, Present and Future Perspectives, *Catalysts* **12**, 1572 (DOI: 10.3390/catal12121572)
 32. Azhar M. (2024), Historical Overview and Future Prospects of Photocatalysis. In *Graphene-Based Photocatalysts: From Fundamentals to Applications*, M.R. Johan, M.N. Naseer, M. Ikram, A.A. Zaidi, and Y. Abdul Wahab, eds. (*Springer Nature Switzerland*), pp. 47-65 (DOI: 10.1007/978-3-031-66260-7_3)
 33. Bell J. D., Murphy J. A. (2021), Recent advances in visible light-activated radical coupling reactions triggered by (I) ruthenium, (II) iridium and (III) organic photo-redox agents, *Chem. Soc. Rev.* **50**, 9540-9685 (DOI: 10.1039/D1CS00311A)

34. Bonardi A.-H., Dumur F., Noirbent, G., Lalevé J., Gigmes D. (2018), Organometallic vs organic photo-redox catalysts for photocuring reactions in the visible region, *Beilstein J. Org. Chem.* **14**, 3025-3046 (DOI: 10.3762/bjoc.14.282)
35. Romero N.A., Nicewicz D.A. (2016), Organic Photo-redox Catalysis, *Chem. Rev.* **116**, 10075-10166 (DOI: 10.1021/acs.chemrev.6b00057)
36. Holmberg-Douglas N., Nicewicz D. A. (2021), Photo-redox-catalyzed C–H functionalization reactions, *Chem. Rev.* **122**, 1925-2016 (DOI: 10.1021/acs.chemrev.1c00311)
37. Franchi D., Amara Z. (2020), Applications of Sensitized Semiconductors as Heterogeneous Visible-Light Photocatalysts in Organic Synthesis, *ACS Sustainable Chem. Eng.* **8**, 15405-15429 (DOI: 10.1021/acssuschemeng.0c05179)
38. Saha P. S., Gopinath P. (2022), Dual Palladium-Photo-redox Catalyzed C–H functionalization, *Eur. J. Org. Chem.* **2022**, e202200733 (DOI: 10.1002/ejoc.202200733)
39. Wang C.-S., Dixneuf P. H., Soulé J.-F. (2018), Photo-redox Catalysis for Building C–C Bonds from C(sp²)–H Bonds, *Chem. Rev.* **118**, 7532-7585 (DOI: 10.1021/acs.chemrev.8b00077)
40. Yu W.-Q., Xie J., Chen Z., Xiong B.-Q., Liu Y., Tang K.-W. (2021), Visible-Light-Induced Transition-Metal-Free Nitrogen-Centered Radical Strategy for the Synthesis of 2-Acylated 9*H*-Pyrrolo[1,2-*a*]indoles, *J. Org. Chem.* **86**, 13720-13733 (DOI: 10.1021/acs.joc.1c01834)
41. Kushwaha A. K., Kamal A., Singh H. K., Maury S. K., Mondal T., Singh, S. (2024), Photoinduced, Metal-Free Hydroacylation of Aromatic Alkynes for Synthesis of α,β -Unsaturated Ketones via C(sp³)–H Functionalization, *Org. Lett.* **26**, 1416-1420 (DOI: 10.1021/acs.orglett.4c00031)
42. Trienes S., Xu J., Ackermann L. (2024), Photoinduced C–H arylation of 1, 3-azoles via copper/photo-redox dual catalysis, *Chem. Sci.* **15**, 7293-7299 (DOI: 10.1039/D4SC00393D)

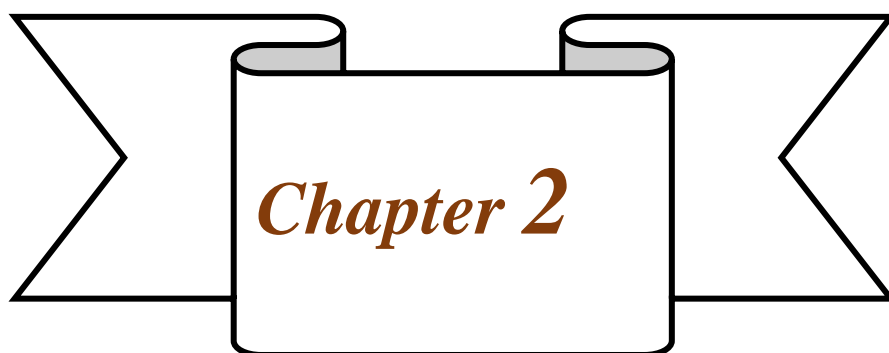
43. Zhang J., Chen J., Zhang X., Lei X. (2014), Total Syntheses of Menisporphine and Daurioxoisoporphine C Enabled by Photo-redox-Catalyzed Direct C–H Arylation of Isoquinoline with Aryldiazonium Salt, *J. Org. Chem.* **79**, 10682-10688 (DOI: 10.1021/jo5020432)
44. Hari D. P., Schroll P., König B. (2012), Metal-free, visible-light-mediated direct C–H arylation of heteroarenes with aryl diazonium salts, *J. Am. Chem. Soc.* **134**, 2958-2961 (DOI: 10.1021/ja212099r)
45. Kwon S. J., Jung H.I., Kim D. Y. (2018), Visible Light Photo-redox-Catalyzed Arylation of Quinoxalin-2(1*H*)-ones with Aryldiazonium Salts, *ChemistrySelect* **3**, 5824-5827 (DOI: 10.1002/slct.201801431)
46. Wei W., Wang L., Yue H., Bao P., Liu W., Hu C., Yang D., Wang H. (2018), Metal-Free Visible-Light-Induced C–H/C–H Cross-Dehydrogenative-Coupling of Quinoxalin-2(H)-ones with Simple Ethers, *ACS Sustain. Chem. Eng.* **6**, 17252-17257 (DOI: 10.1021/acssuschemeng.8b04652)
47. Chan A. Y., Perry I. B., Bissonnette N. B., Buksh B. F., Edwards G. A., Frye L. I., Garry O. L., Lavagnino M. N., Li B. X., Liang Y., *et al.* (2022), Metallaphotoredox: The Merger of Photo-redox and Transition Metal Catalysis, *Chem. Rev.* **122**, 1485-1542 (DOI: 10.1021/acs.chemrev.1c00383)
48. Prier C. K., Rankic D. A., MacMillan, D.W.C. (2013), Visible Light Photo-redox Catalysis with Transition Metal Complexes: Applications in Organic Synthesis, *Chem. Rev.* **113**, 5322-5363 (DOI: 10.1021/cr300503r)
49. Chu L., Lipshultz J. M., MacMillan D.W.C. (2015), Merging Photo-redox and Nickel Catalysis: The Direct Synthesis of Ketones by the Decarboxylative Arylation of α -Oxo Acids, *Angew. Chem. Int. Ed.* **54**, 7929-7933 (DOI: 10.1002/anie.201501908)
50. Zhou C., Li P., Zhu X., Wang L. (2015), Merging Photo-redox with Palladium Catalysis: Decarboxylative ortho-Acylation of

- Acetanilides with α -Oxocarboxylic Acids under Mild Reaction Conditions, *Org. Lett.* **17**, 6198-6201 (DOI: 10.1021/acs.orglett.5b03192)
51. Wang H., Li T., Hu D., Tong X., Zheng L., Xia C. (2021), Acylation of arenes with aldehydes through dual C–H activations by merging photocatalysis and palladium catalysis, *Org. Lett.* **23**, 3772-3776 (DOI: 10.1021/acs.orglett.1c01184)
 52. Liang L., Xie M.-S., Wang H.-X., Niu H.-Y., Qu G.-R., Guo H.-M. (2017), Visible-light-mediated monoselective ortho C–H arylation of 6-arylpyrimidine nucleosides with diazonium salts, *J. Org. Chem.* **82**, 5966-5973 (DOI: 10.1021/acs.joc.7b00659)
 53. Jiang J., Zhang W.-M., Dai J.-J., Xu J., Xu H.-J. (2017), Visible-light-promoted C–H arylation by merging palladium catalysis with organic photo-redox catalysis, *J. Org. Chem.* **82**, 3622-3630 (DOI: 10.1021/acs.joc.7b00140)
 54. Zhang H., Huang X. (2016), Ligand-Free Heck Reactions of Aryl Iodides: Significant Acceleration of the Rate through Visible Light Irradiation at Ambient Temperature, *Adv. Synth. Catal.* **358**, 3736-3742 (DOI: 10.1002/adsc.201600704)
 55. Fang F., Vogel M., Hines J. V., Bergmeier S. C. (2012), Fused ring aziridines as a facile entry into triazole fused tricyclic and bicyclic heterocycles, *Org. Biomol. Chem.* **10**, 3080-3091 (DOI: 10.1039/C2OB07042A)
 56. Hajós G., Riedl Z., Kollenz G. (2001), Recent Advances in Ring Transformations of Five-Membered Heterocycles and Their Fused Derivatives, *Eur. J. Org. Chem.* **2001**, 3405-3414 (DOI: 10.1002/1099-0690(200109)2001:18<3405::AID-EJOC3405>3.0.CO;2-Y)
 57. Qadir T., Amin A., Sharma P. K., Jeelani I., Abe H. (2022), A review on medicinally important heterocyclic compounds, *Open J. Med. Chem.* **16**(1) (DOI: 10.2174/18741045-v16-e2202280)
 58. M P. H., Al-Ostoot F.H., Vivek H. K., Khanum S. A. (2022), Design, docking, synthesis, and characterization of novel N'(2-phenoxyacetyl) nicotinohydrazide and N'(2-

- phenoxyacetyl)isonicotinohydrazide derivatives as anti-inflammatory and analgesic agents, *J. Mol. Struct.* **1247**, 131404 (DOI: 10.1016/j.molstruc.2021.131404)
59. De S., SK A. K., Shah S. K., Kazi S., Sarkar N., Banerjee S., Dey S. (2022), Pyridine: the scaffolds with significant clinical diversity, *RSC Adv.* **12**, 15385-15406 (DOI: 10.1039/D2RA01571D)
60. Afzal O., Kumar S., Haider M. R., Ali M. R., Kumar R., Jaggi M., Bawa S. (2015), A review on anticancer potential of bioactive heterocycle quinoline, *Eur. J. Med. Chem.* **97**, 871-910 (DOI: 10.1016/j.ejmech.2014.07.044)
61. Rao R. N., Mm B., Maiti B., Thakuria R., Chanda K. (2018), Efficient access to imidazo[1, 2-*a*] pyridines/pyrazines/pyrimidines via catalyst-free annulation reaction under microwave irradiation in green solvent, *ACS Comb. Sci.* **20**, 164-171 (DOI: 10.1021/acscombsci.7b00173)
62. Niaz L., Saddique F. A., Aslam S., Ahmad M., Mohsin N.u.A. (2020), Recent synthetic methodologies for pyridopyrazines: An update, *Synth. Commun.* **50**, 2755-2786 (DOI: 10.1080/00397911.2020.1786123)
63. Aggarwal R., Kumar S., Sumran G., Sharma D. (2024), One-pot synthesis and in vitro bioactivity of novel 4-aminopyrazolo [3, 4-*b*] pyridine derivatives as potential antimicrobial compounds, *Med. Chem. Res.* **33**, 117-126 (DOI: 10.1007/s00044-023-03161-4)
64. Krause M., Foks H., Gobis, K. (2017), Pharmacological potential and synthetic approaches of imidazo [4, 5-*b*] pyridine and imidazo [4, 5-*c*] pyridine derivatives, *Molecules* **22**, 399 (DOI: 10.3390/molecules22030399)
65. Bhawale R. T., Chillal A. S., Kshirsagar U. A. (2023), 4*H*-Pyrido [1,2-*a*] pyrimidin-4-one, biologically important fused heterocyclic scaffold: Synthesis and functionalization, *J. Heterocycl. Chem.* **60**, 1356-1373 (DOI: 10.1002/jhet.4637)

66. Dong H.-R., Gao Z.-L., Li R.-S., Hu Y.-M., Dong H.-S., Xie Z.-X. (2014), One-pot synthesis of 5*H*-1,3,4-thiadiazolo[3,2-*a*]pyrimidin-5-one derivatives, *RSC adv.* 4, 55827-55831 (DOI: 10.1039/C4RA02714K)
67. Kim D.-m., Kang M.-S., Kim J. S., Jeong J.-H. (2005), An efficient synthesis of risperidone via stille reaction: Antipsychotic, 5-HT₂, and dopamine-D₂-antagonist, *Arch. Pharmacol Res.* 28, 1019-1022 (DOI: 10.1007/BF02977394)
68. Roslan I. I., Lim Q. X., Han A., Chuah G. K., Jaenicke S. (2015), Solvent-Free Synthesis of 4*H*-Pyrido [1, 2-*a*] pyrimidin-4-ones Catalyzed by BiCl₃: A Green Route to a Privileged Backbone, *Eur. J. Org. Chem.* 2015, 2351-2355 (DOI: 10.1002/ejoc.201500227)
69. Chen Z., Wen Y., Ding H., Luo G., Ye M., Liu L., Xue J. (2017), Silver-catalyzed highly efficient synthesis of pyrido[1,2-*a*]pyrimidin-4-ones from 2-aminopyridines and alkynoates, *Tetrahedron Lett.* 58, 13-16 (DOI: 10.1016/j.tetlet.2016.11.079)
70. Guchhait S. K., Priyadarshani G. (2015), Pd-Catalyzed Ag (I)-promoted C3-arylation of pyrido[1,2-*a*]pyrimidin-4-ones with bromo/iodo-arenes, *J. Org. Chem.* 80, 8482-8488 (DOI: 10.1021/acs.joc.5b01573)
71. Liu W., Wang S., Zhang Q., Yu J., Li J., Xie Z., Cao H. (2014), Regioselective C3 Alkenylation of 4*H*-pyrido[1,2-*a*]pyrimidin-4-ones via Palladium-Catalyzed C–H Activation, *Chem. Asian J.* 9, 2436-2439 (DOI: 10.1002/asia.201402455)
72. Lv J., Liang Y., He P., Cai Z., Liu J., Huang F. (2015), Palladium-catalyzed direct alkenylation of 2-methyl-4*H*-pyrido[1,2-*a*]pyrimidin-4-ones using oxygen as the oxidant, *RSC Adv.* 5, 36171-36174 (DOI: 10.1039/C5RA02932E)
73. Liu W., Wang S., Cai Z., Li Z., Liu J., Wang A. (2018), Iodine-catalyzed regioselective sulfenylation of 4*H*-pyrido[1,2-*a*]pyrimidin-4-ones with sulfonyl hydrazides, *Synlett* 29, 116-120 (DOI: 10.1055/s-0036-1588549)

74. Ghosh P., Chhetri G., Das, S. (2021), Metal free C-3 chalcogenation (sulfenylation and selenylation) of 4*H*-pyrido[1,2-*a*]pyrimidin-4-ones, *RSC adv.* *11*, 10258-10263 (DOI: 0.1039/D1RA00834J)
75. Ghosh P., Chhetri G., Perl E., Das S. (2021), [Bis (trifluoroacetoxy) iodo] benzene Mediated C-3 Selenylation of Pyrido[1,2-*a*]pyrimidin-4-Ones Under Ambient Conditions, *Adv. Synth. Catal.* *363*, 2148-2156 (DOI: 10.1002/adsc.202001426)
76. Guo L., Su M., Zhan H., Liu W., Wang S. (2021), Silver-Catalyzed Direct Regioselective C3 Phosphonation of 4*H*-pyrido[1,2-*a*]pyrimidin-4-ones With H-phosphites, *Asian J. Org. Chem.* *10*, 1660-1664 (DOI: 10.1002/ajoc.202100235)



*Visible Light Assisted, Direct
C3–H Arylation of Pyrido[1,2-
a]pyrimidin-4-ones and
Thiazolo[3,2-a]pyrimidin-5-ones*

Chapter 2

Visible Light Assisted, Direct C3–H Arylation of Pyrido[1,2-*a*]pyrimidin-4-ones and Thiazolo[3,2-*a*]pyrimidin-5-ones

2.1 Introduction

The fused heterocyclic compounds are prevalent structural motifs in several clinical drugs and therapeutic agents and are widely utilized across various pharmaceutical and agrochemical applications.^[1-4] The bioactivity and drug-like properties of pyrido[1,2-*a*]pyrimidin-4-ones make it an attractive scaffold in drug discovery.^[5-9] For example 2,3-Diaryl-4*H*-pyrido[1,2-*a*]pyrimidin-4-one derivatives act as an endothelial cell dysfunction inhibitor and smooth muscle cell activator (Figure 2.1).^[10]

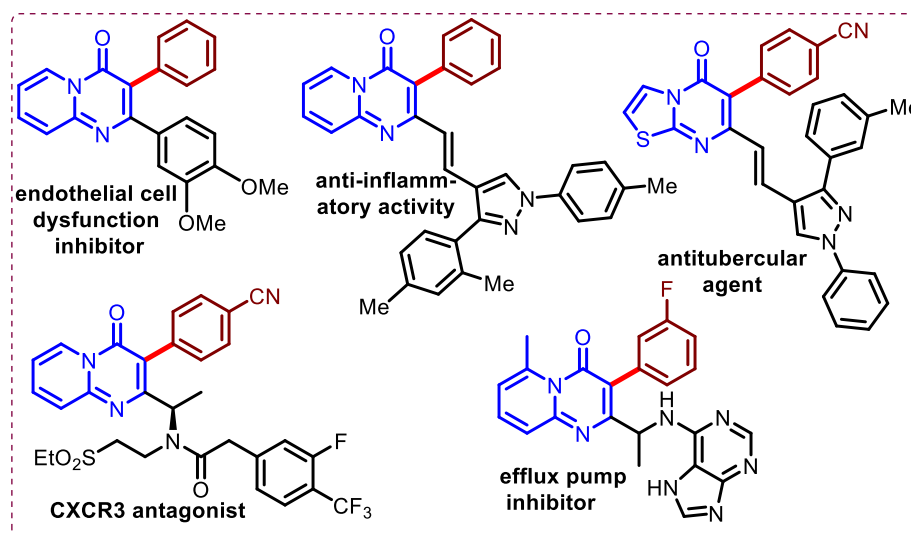


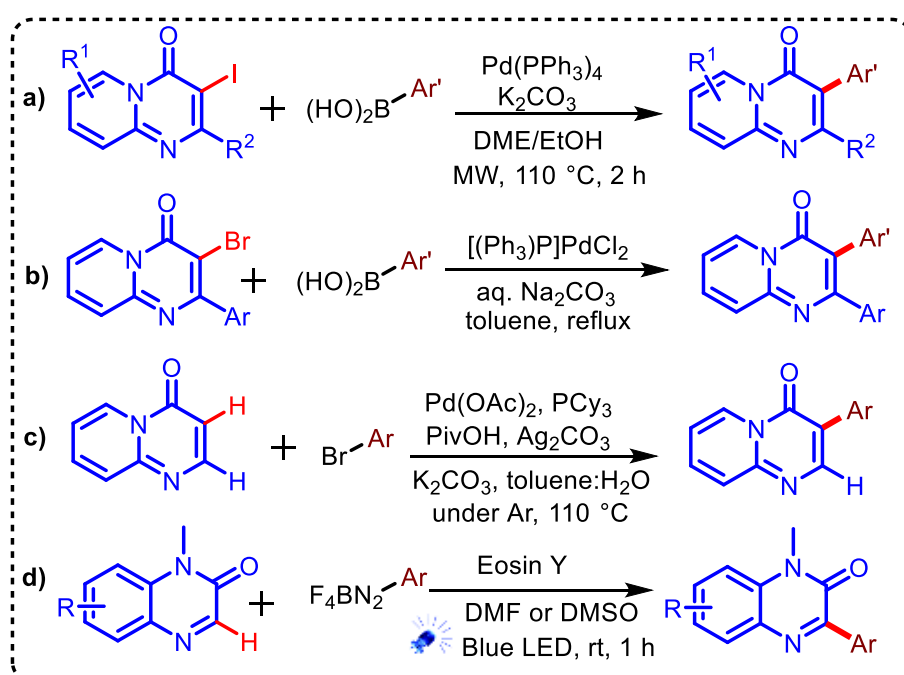
Figure 2.1 Biologically active C-3 arylated pyrido[1,2-*a*]pyrimidin-4-ones.

Additionally, C3-H arylated pyrido[1,2-*a*]pyrimidin-4-one showed various biological activities as shown in (Figure 2.1), such as modulator of platelet activation and aggregation,^[11] anti-inflammatory,^[12] antitubercular,^[13] CXCR3 antagonist,^[14] antiallergic activities

(pemirolast),^[15] and efflux pump inhibition,^[16] as well as acetylcholinesterase,^[17] antioxidants,^[18] and antipsychotics.^[19]

2.2 Previous Reports

The C3-H Arylation reaction of pyrido[1,2-*a*]pyrimidin-4-one has been previously reported via transition metal-catalyzed cross-coupling reactions at elevated temperatures (**Scheme 2.1**).^[20,10,21,22,23] The first reports that Vanelle and co-workers developed a Pd-catalyzed Suzuki-Miyaura cross-coupling reaction for C3-H arylated



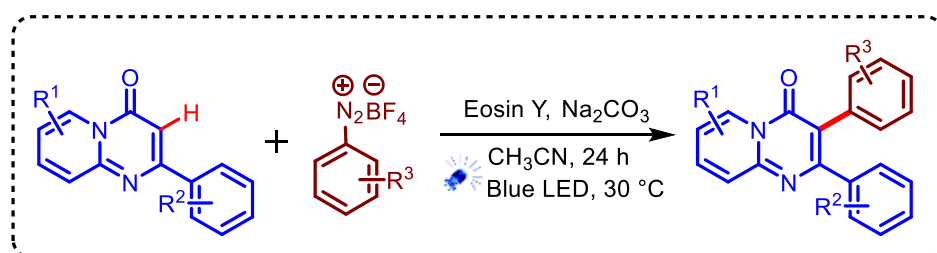
Scheme 2.1 Previous reports on C3-arylation of pyrido[1,2-*a*]pyrimidin-4-one

pyrido[1,2-*a*]pyrimidin-4-one by reacting 3-iodo-pyrido[1,2-*a*]pyrimidin-4-ones with aryl boronic acids under microwave irradiation at 100 °C for 2 h (**Scheme 2.1a**).^[20] Whereas, the La Motta research team reported the synthesis of 2,3-diaryl-4H-pyrido[1,2-*a*]pyrimidin-4-ones compounds via Pd-catalyzed cross-coupling of 3-bromo-2-aryl-4H-pyrido[1,2-*a*]pyrimidin-4-ones with aryl boronic acid by refluxing it in using toluene as solvent (**Scheme 2.1 b**).^[10,21] Furthermore, for the C-3 arylation of pyrido[1,2-*a*]pyrimidin-4-one framework, Guchhait co-workers developed Ag-promoted, Pd-catalyzed C–H coupling of 4H-pyrido[1,2-*a*]pyrimidin-4-one with bromo-arenes and acids, silver salt,

ligands, bases under argon atmosphere to generate 3-aryl-4*H*-pyrido[1,2-*a*]pyrimidin-4-one using 100 °C of reaction temperature (**Scheme 2.1 c**).^[22] Lately, the Kim group and later Wei group developed visible light-induced photocatalyzed C–H arylation of Quinoxalin-2(*H*)-ones with aryl diazonium salts and DMSO or DMF as a solvent (**Scheme 2.1 d**).^[23] Nevertheless, these transformations suffer from certain disadvantages such as required transition metal catalysts and ligands, high temperature, pre-functionalized starting materials, high cost^[24] etc. Moreover, the susceptible nature of the pyrido[1,2-*a*]pyrimidin-4-one framework to the harsh conditions results in decomposition or thermal rearrangement of the main skeletal structure, which is the deterring factor for suitable derivatization of this class of scaffold.^[22,25-27]

2.3 Objective

Development of transition-metal-free, convergent, mild, and efficient methods for direct C3-H arylation of 4*H*-pyrido[1,2-*a*]pyrimidin-4-one is highly essential. Visible light-promoted photo redox catalysis has been developed as a powerful synthetic tool and attracted significant interest from the synthetic community for a wide range of synthetic transformations under mild conditions.^[24,28-31] We have developed the visible light-promoted, eosin-Y-catalyzed, direct C3-H arylation of 4*H*-pyrido[1,2-*a*]pyrimidin-4-one using aryl diazonium compounds under very mild reactions conditions (**Scheme 2.2**).^[32]

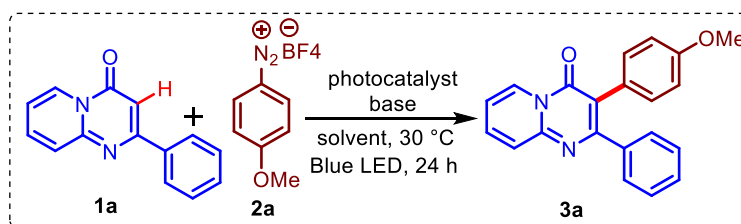


Scheme 2.2 Photoinduced C3-arylation of pyrido[1,2-*a*]pyrimidin-4-one

2.4 Result and Discussion

A preliminary investigation of the reaction condition was initiated by irradiating the mixture of 2-phenyl-4*H*-pyrido[1,2-*a*]pyrimidin-4-one

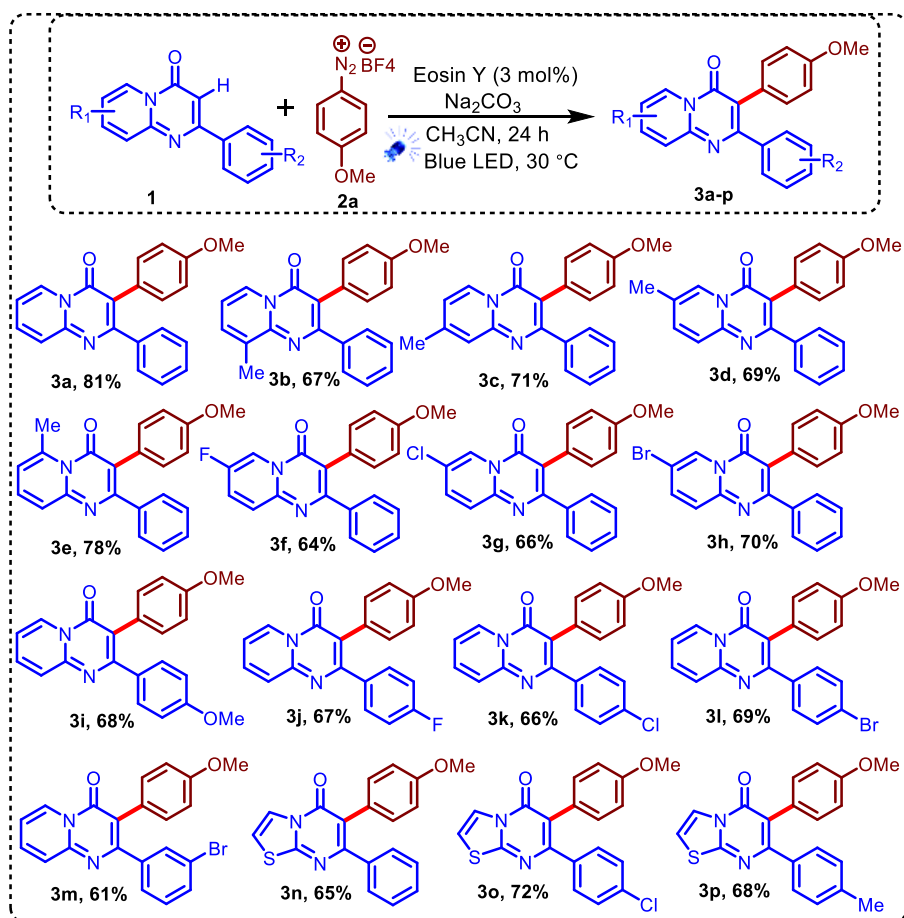
(**1a**, 0.2 mmol) with 4-methoxybenzenediazonium tetrafluoroborate (**2a**, 0.6 mmol) in presence of acridinium salt (3 mol%) as a photocatalyst in acetonitrile (2.0 mL) under blue light at room temperature (**Table 2.1**; entry 1). After irradiating the stirring reaction mixture for 24 h, product **3a** was isolated in 24% yields. The structure of product **3** was confirmed with the help of NMR spectroscopy and single crystal x-ray (CCDC No. 2225945 of **3s**).^[33] With this result, further optimization of the reaction condition was performed. When the reaction was performed in the presence of Na₂CO₃ (0.4 mmol) as a base, it delivered the expected product in 47% after 24 h (entry 2). Reaction with other organic dyes as photocatalysts (entries 3-7) such as fluorescein, rhodamine, methylene blue, eosin-Y, and rose bengal provided the desired product in progressive yields, amongst which eosin-Y provided the best yield (81%, entry 6). Reaction in the presence of other inorganic bases such as K₂CO₃, Cs₂CO₃, and NaHCO₃ gave slightly lower yields (entries 8-10), whereas organic bases such as DBU and Et₃N were unable to produce the desired product in encouraging yields (entries 11 and 12). The reaction was performed in different solvents. Results revealed that the replacement of acetonitrile with chlorinated solvents (DCE or DCM), 1,4-Dioxane, or other polar solvents such as methanol, acetic acid, or dimethyl formamide provided the desired product in very poor yield (5-20%, entries 13-18), except methanol (38%, entry 16). Apart from acetonitrile, the reaction delivered the expected product in moderate yield when dimethyl sulfoxide was used as a solvent (66%, entry 19). Upon performing the reaction in the absence of photocatalyst (entry 20) or light (entry 21) or in the absence of both, photo-catalyst and light (entry 22), product yield drastically drops to 27%, 21%, and 19% respectively. The reaction using NaOAc as a base in the absence of a photocatalyst and light (entry 23) produced the desired product with a 23% yield. With a lower amount of 4-methoxy benzene diazoniumtetrafluoroborate (2.0 and 1.0 equiv.), the yield of the desired product was diminished to 50% and 36% respectively (entry 24-25). When the light source was changed from blue to green, it was observed that the desired product yield decreased to 62% (entry 26).

Table 2.1 Optimization of the reaction conditions.^[a]

entry	photocatalyst	base	solvent	yield (%) ^[b]
1	acridinium salt	-	CH ₃ CN	24
2	acridinium salt	Na ₂ CO ₃	CH ₃ CN	47
3	fluorescein	Na ₂ CO ₃	CH ₃ CN	39
4	rhodamine	Na ₂ CO ₃	CH ₃ CN	58
5	methylene blue	Na ₂ CO ₃	CH ₃ CN	61
6	eosin Y	Na₂CO₃	CH₃CN	81
7	rose bengal	Na ₂ CO ₃	CH ₃ CN	64
8	eosin Y	K ₂ CO ₃	CH ₃ CN	67
9	eosin Y	Cs ₂ CO ₃	CH ₃ CN	53
10	eosin Y	NaHCO ₃	CH ₃ CN	48
11	eosin Y	DBU	CH ₃ CN	42
12	eosin Y	Et ₃ N	CH ₃ CN	38
13	eosin Y	Na ₂ CO ₃	DCE	10
14	eosin Y	Na ₂ CO ₃	DCM	12
15	eosin Y	Na ₂ CO ₃	dioxane	20
16	eosin Y	Na ₂ CO ₃	methanol	38
17	eosin Y	Na ₂ CO ₃	AcOH	17
18	eosin Y	Na ₂ CO ₃	DMF	7
19	eosin Y	Na ₂ CO ₃	DMSO	66
20 ^c	-	Na ₂ CO ₃	CH ₃ CN	27
21 ^d	eosin Y	Na ₂ CO ₃	CH ₃ CN	21
22 ^e	-	Na ₂ CO ₃	CH ₃ CN	19
23 ^e	-	NaOAc	CH ₃ CN	23
24 ^f	eosin Y	Na ₂ CO ₃	CH ₃ CN	50
25 ^g	eosin Y	Na ₂ CO ₃	CH ₃ CN	36
26 ^h	eosin Y	Na ₂ CO ₃	CH ₃ CN	62

^[a]Reaction conditions: **1a** (0.2 mmol), **2a** (0.6 mmol), photo-catalyst (3 mol%), base (0.4 mmol), solvent (2.0 mL), blue LED, rt, 24 h. ^[b]isolated yields. ^[c]No photo-catalyst. ^[d]No light. ^[e]No light, no photo-catalyst. ^[f]0.4 mmol of **2a**. ^[g]0.2 mmol of **2a**. ^[h]green LED. DCE =1,2 dichloroethylene; DCM = dichloromethane; dioxane = 1,4-Dioxane; DMF = N,N-dimethylformamide; DMSO = dimethyl sulfoxide.

Scheme 2.3 Substrate scope for arylation of pyrido[1,2-*a*]pyrimidin-4-ones^[a]



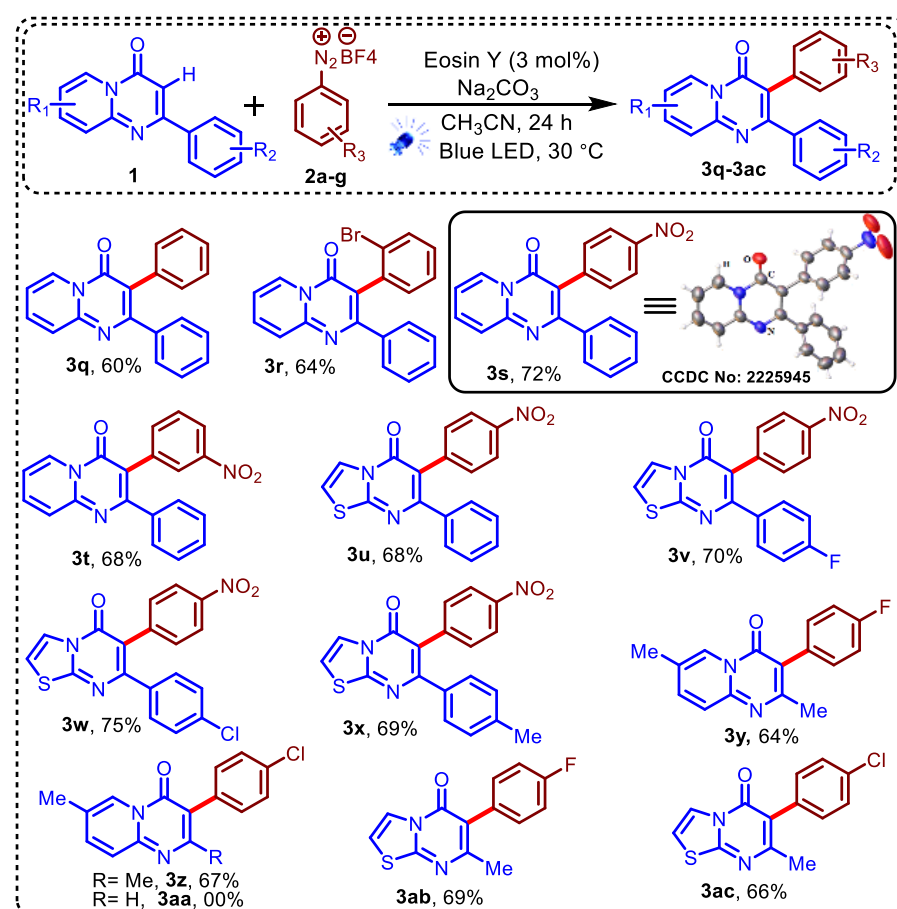
^[a]Reaction conditions: **1a** (0.2 mmol), **2a** (0.6 mmol), eosin Y (3 mol%), Na₂CO₃ (0.4 mmol), CH₃CN (2.0 mL), blue LED, rt, 24 h.

With the optimization of reaction conditions, further study of the substrate scope of direct C–H arylation of various 2-aryl-pyrido[1,2-*a*]pyrimidin-4-ones with 4-methoxybenzenediazonium tetrafluoroborate was pursued (**Scheme 2.3**). Substitutions of methyl groups on different positions of 2-phenyl-pyrido[1,2-*a*]pyrimidin-4-ones yielded the desired products **3b–e** in good yields (67%, 71%, 69%, and 78%, respectively). Halo-substituted (-F, -Cl, -Br) 2-phenyl-pyrido[1,2-*a*]pyrimidin-4-ones delivered expected products **3f–h** in good to moderate yields (64%, 66%, and 70% respectively). 2-Aryl-pyrido[1,2-*a*]pyrimidin-4-ones having substitution on the 2-phenyl ring (-OMe, -F, -Cl, -Br) also delivered desired C3 arylated products **3i–m** in good yields (68%, 67%, 66%, 69% and 61%, respectively). Because of the biological importance of 6-aryl-5*H*-thiazolo[3,2-*a*]pyrimidin-5-

ones (Figure 2.1), various 7-aryl-5*H*-thiazolo[3,2-*a*]pyrimidin-5-ones were selectively arylated at the C6 position using the above-mentioned reaction conditions in good yields to afford corresponding C6 arylated products **3n-p** (65-72%).

Further, the suitability of other substituted aryldiazonium salts (**2a-g**) for visible light mediated C3 arylation reaction of 2-aryl-pyrido[1,2-*a*]pyrimidin-4-ones and 7-aryl/alkyl-5*H*-thiazolo[3,2-*a*]pyrimidin-5-ones were investigated (**Scheme 2.4**). Reaction of benzenediazonium tetrafluoroborate with 2-phenyl-4*H*-pyrido[1,2-*a*]pyrimidin-4-one gave corresponding arylated product **3q** in 60% yield. Further, 2-phenyl-4*H*-pyrido[1,2-*a*]pyrimidin-4-one was allowed to react with 2-bromo-, 4-nitro-, and 3-nitro-diazonium tetrafluoroborate under optimized reaction conditions, which delivered corresponding C3 arylated 2-phenyl-4*H*-pyrido[1,2-*a*]pyrimidin-4-one derivatives **3r-t** in good yields (64%,

Scheme 2.4 Substrate Scope of aryl diazonium tetrafluoroborate^[a]

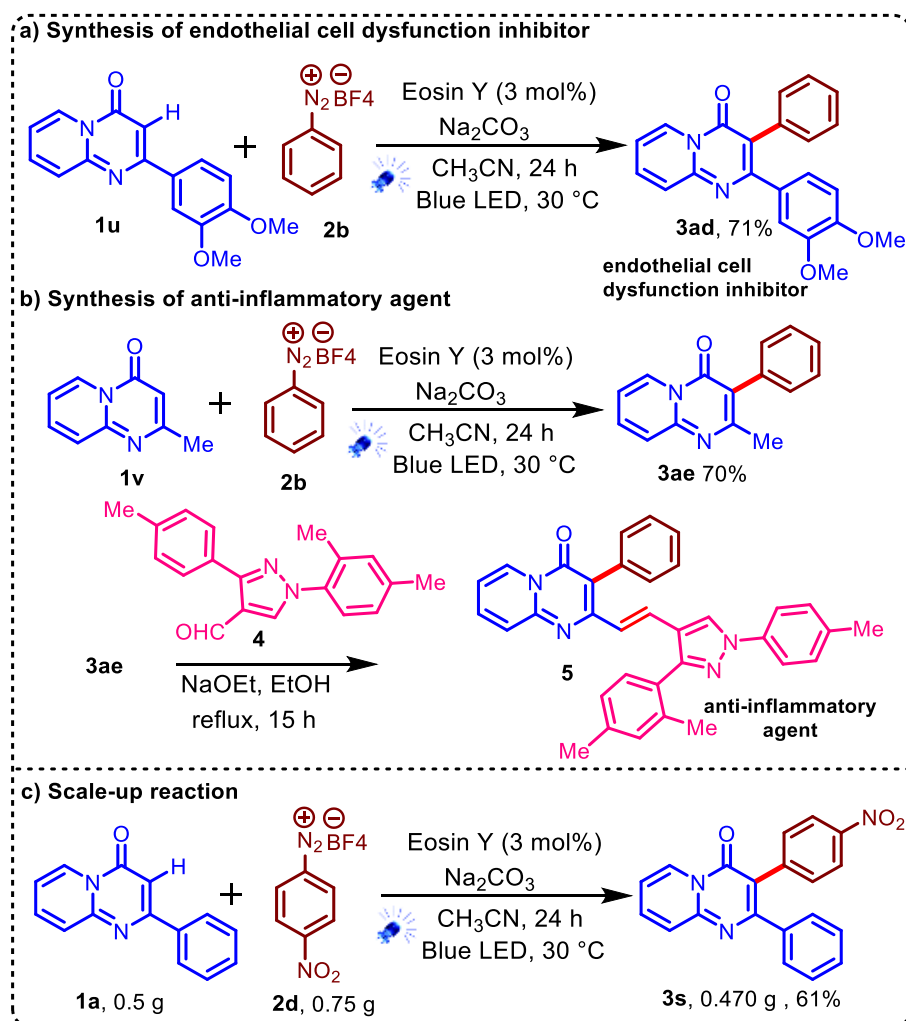


^[a]Reaction conditions: **1a** (0.2 mmol), **2a** (0.6 mmol), eosin Y (3 mol%), Na₂CO₃ (0.4 mmol), CH₃CN (2.0 mL), blue LED, rt, 24 h.

72% and 68% respectively). Later, different 7-aryl-5*H*-thiazolo[3,2-*a*]pyrimidin-5-ones were selectively arylated at the C6 position with 4-nitro-diazonium tetrafluoroborate under optimized reaction conditions to provide corresponding C6 arylated products **3u-x** in good to excellent yields (68%,70%,75% and 69% respectively). We were delighted to observe that the above-mentioned visible light-assisted C–H arylation strategy could be extended to the 2-methyl-4*H*-pyrido[1,2-*a*]pyrimidin-4-ones and 7-methyl-5*H*-thiazolo[3,2-*a*]pyrimidin-5-ones. 2-Methyl-4*H*-pyrido[1,2-*a*]pyrimidin-4-one was reacted with halogenated (F, Cl) diazonium tetrafluoroborate to produce **3y** and **3z** in 64% and 67% yield respectively. The reaction was unable to produce the desired C3-arylated product **3aa** with 7-methyl-4*H*-pyrido[1,2-*a*]pyrimidin-4-one. In this reaction, the starting material was found to be unreacted. 7-Methyl-5*H*-thiazolo[3,2-*a*]pyrimidin-5-one with halogenated (F, Cl) diazonium tetrafluoroborate delivered corresponding C6 arylated products **3ab** and **3ac** in 69% and 66% yield respectively.

Application of the present protocol was demonstrated in the synthesis of biologically active compounds (**Scheme 2.5**). When 2-(3,4-dimethoxyphenyl)-4*H*-pyrido[1,2-*a*]pyrimidin-4-one (**1u**) and benzenediazonium tetrafluoroborate were irradiated with blue light in the presence of eosin-Y, it produced endothelial cell dysfunction inhibitor^[10] **3ad** in 71% yield (**Scheme 2.5a**). In addition to this, 2-methyl-4*H*-pyrido[1,2-*a*]pyrimidin-4-one (**1v**) was reacted with benzenediazonium tetrafluoroborate under optimized reaction conditions to produce **3ae** in 70% yield. Product **3ae** was further converted into anti-inflammatory compound **5** using a previously reported method (**Scheme 2.5b**).^[12] Moreover, to determine the practical utility of the developed approach, a scale-up reaction was carried out on a 2.25 mmol scale with 2-phenyl-4*H*-pyrido[1,2-*a*]pyrimidin-4-one providing a 61% yield of corresponding C3 arylated product **3s** (**Scheme 2.5c**).

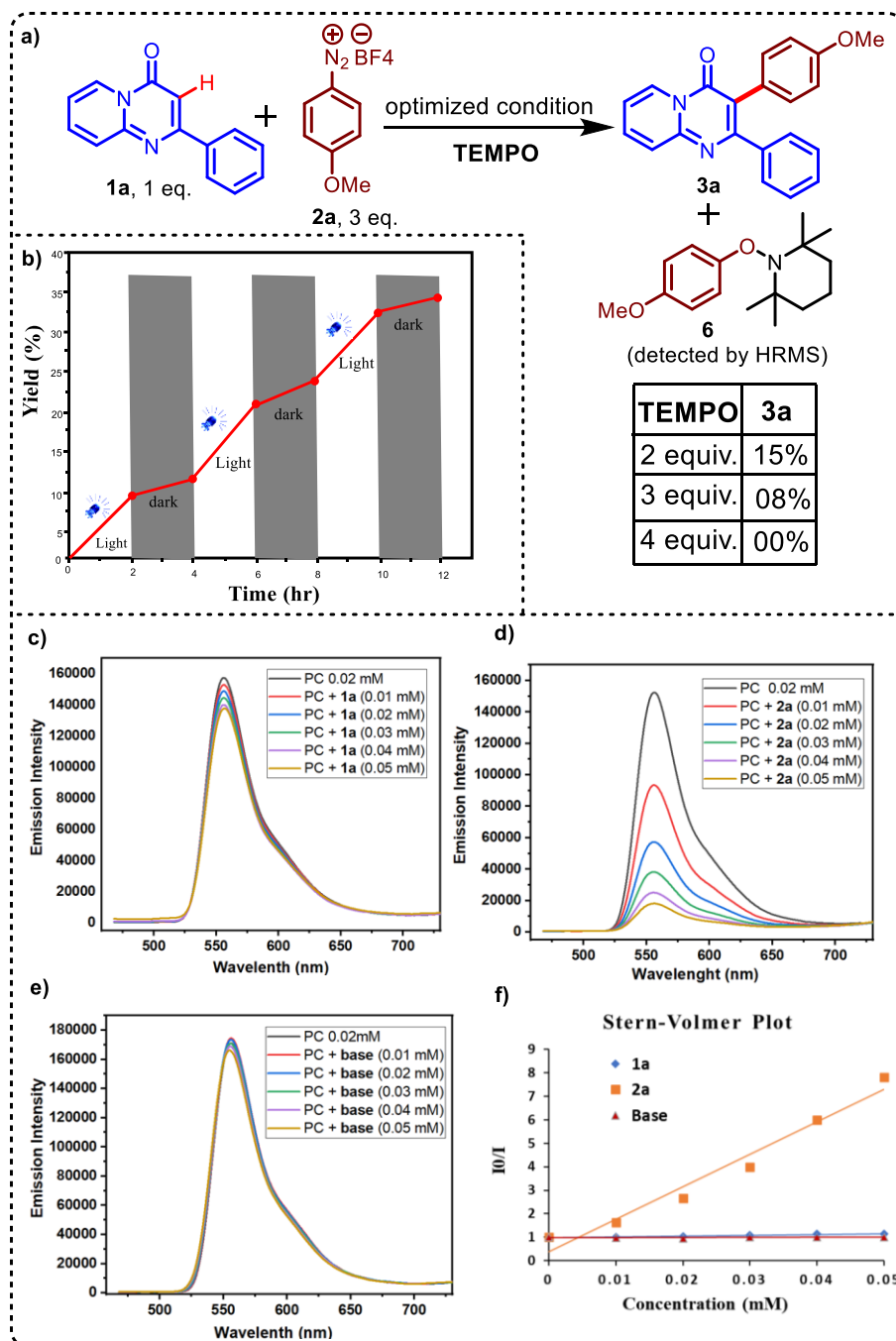
Scheme 2.5 Synthesis of bioactive molecules and Scale-up reaction



To gain more insights into this visible light-mediated photocatalyzed radical reaction mechanism, a series of control experiments were performed (**Scheme 2.6**). The reaction was performed under standard conditions in the presence of 2,2,6,6-tetramethylpiperidine-1-oxyl (TEMPO) as a radical scavenger. In the presence of 2.0 and 3.0 equiv. of TEMPO, product formation was drastically reduced to 13% and 08% respectively, whereas complete inhibition of product formation was observed in the presence of 4.0 equivalent of TEMPO. Additionally, the TEMPO trapped aryl radical intermediates **6** was detected by HRMS (**Scheme 2.6a**). A light on-off experiment was performed to investigate the light-dependent radical reaction. Results suggested most of the product, formation takes place with constant light irradiation (**Scheme 2.6b**). A fluorescence quenching study of photo-catalyst was performed with **1a**, **2a**, and base. 4-methoxybenzenediazonium tetrafluoroborate

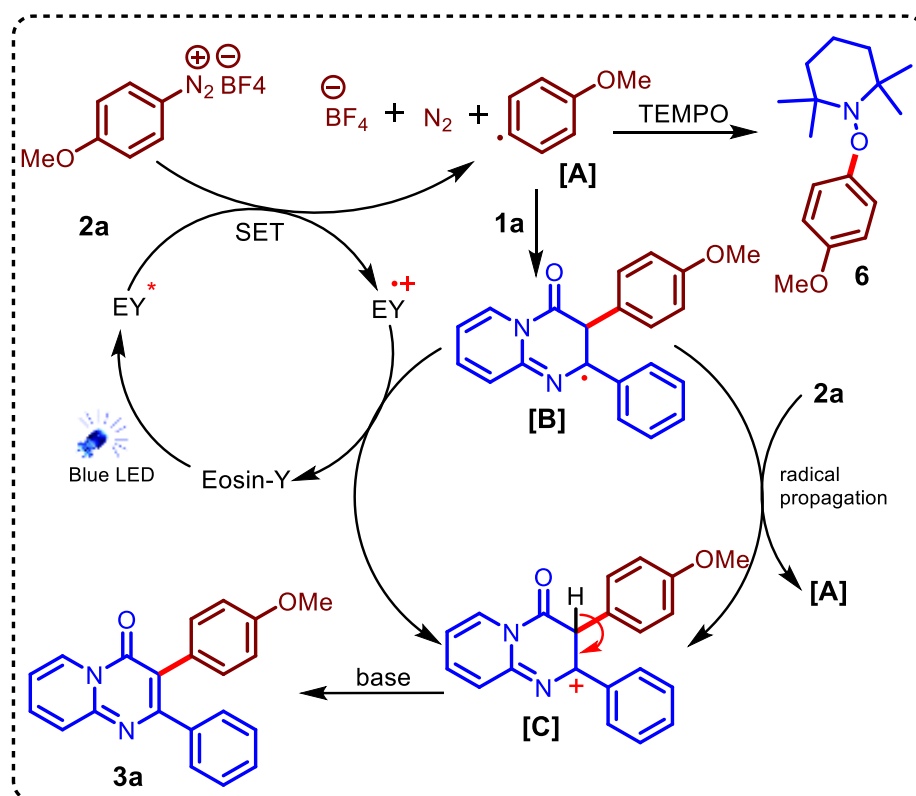
2a was observed as a potential fluorescence quencher (**Scheme 2.6c-f**). Further, the quantum yield (QY) of the model reaction was measured to be $\Phi = 5.98$ which supports the radical chain propagation of the reaction.

Scheme 2.6 Control experiments and Fluorescence quenching study.



Based on the above results of control experiments and mechanistic study available in the literature,^[24,28,34] a plausible visible light-mediated radical reaction mechanism for C3 arylation is outlined (**Scheme 2.7**).

Scheme 2.7 Proposed reaction mechanism.



It is speculated that the excited state of eosin-Y (EY*) generated upon blue light irradiation underwent oxidative quenching through single electron transfer (SET) with 4-methoxybenzenediazonium tetrafluoroborate **2a** to form methoxybenzene radical [A]. Methoxybenzene radical [A] reacted with 2-phenyl-4H-pyrido[1,2-a]pyrimidin-4-one (**1a**) generating a radical intermediate [B]. Intermediate [B] may react with EY⁺ or undergo radical-chain propagation with 4-methoxybenzenediazonium tetrafluoroborate **2a** to generate cation intermediate [C]. This cation intermediate [C] delivered the final C3 arylated product **3a** after a base-mediated deprotonation event.

2.5 Summary

To conclude, we developed the metal-free, visible light-induced photocatalyzed C3-H arylation of 2-methyl and 2-aryl-4H-pyrido[1,2-

a]-pyrimidin-4-ones with aryldiazonium salts. In addition to this, 7-methyl and 7-aryl-5H-thiazolo[3,2-*a*]pyrimidin-5-ones were found suitable substrates for direct C6-H arylation. A nontoxic, inexpensive organic dye was utilized as a photo-redox catalyst for this operationally simple and mild C–H arylation reaction showing good functional group tolerance and broad substrate scope. The synthetic and practical utility of this approach was demonstrated by synthesizing therapeutically important endothelial cell dysfunction inhibitors and anti-inflammatory agents as well as successful gram-scale synthesis. Further, extensions of this approach and their application in complex bioactive molecules are currently being investigated.

2.6 Experimental section

The general procedure for synthesis of 2-methyl-4*H*-pyrido[1,2-*a*]pyrimidin-4-one derivatives (1):^[35] All 2-methyl-4*H*-pyrido[1,2-*a*]pyrimidin-4-ones (**1**) were prepared using the reported procedure and confirmed by NMR analysis. A mixture of substituted 2-aminopyridine (**7**, 20.0 mmol, 1.0 equiv.) and ethyl acetoacetate (**9**, 40.0 mmol, 2.0 equiv.) and BiCl₃ (5 mol%, 1 mmol) was heated in an oil bath at 100 °C temperature for 5 h. After 5 h the mixture was cooled to room temperature and was diluted with ethanol (5 mL). The solid was filtered, and filtrate was purified by silica-gel column chromatography (ethyl acetate: petroleum ether) to give 2-methyl-4*H*-pyrido[1,2-*a*]pyrimidin-4-ones (**1**).

The general procedure for synthesis of aryl diazonium salts (2a-g):^[36] The aryl diazonium salts **2a-g** were synthesized according to the literature procedure. In a 50 mL of the round-bottom flask containing aniline (**10**, 20.0 mmol, 1.0 equiv.) in 8 mL of distilled water, was added a solution of HBF₄ (50 wt.% in H₂O, 90.0 mmol, 4.5 equiv.) at 0-5 °C temperature. Then, a precooled solution of NaNO₂ (46.0 mmol, 2.3 equiv.) in water (4 mL) was added dropwise into the above reaction mixture. During the addition, the temperature was carefully kept

between 0-5 °C and then the resulting mixture was left to stir at 0 °C for another 1 h. The resulting precipitate was collected by filtration. The crude product was dissolved in acetone, recrystallized by adding diethyl ether, and isolated by filtration. Recrystallization may be repeated again to obtain a white/light pink powder and dried under vacuum at room temperature.

Procedure for synthesis of 3-(4-methoxyphenyl)-2-phenyl-4H-pyrido[1,2-*a*]pyrimidin-4-one (3a): Acetonitrile (2.0 mL) was added to the mixture of 2-phenyl-4H-pyrido[1,2-*a*]pyrimidin-4-one (**1a**, 45 mg, 0.2 mmol, 1.0 equiv.), 4-methoxybenzenediazonium tetrafluoroborate (**2a**, 135 mg, 0.6 mmol, 3.0 equiv.), eosin Y (4 mg, 3 mol%), and Na₂CO₃ (43 mg, 0.4 mmol, 2.0 equiv.) in an oven dried reaction vessel equipped with magnetic stirring bar. Resulting reaction mixture was stirred at room temperature under irradiation of blue LED for 24 h. Reaction was quenched by adding H₂O (2 mL) and resulting reaction mixture was extracted with EtOAc (3 × 25 mL) and was washed with brine solution and dried over Na₂SO₄. Combined organic layer was concentrated under reduced pressure to yield crude product which was further purified by silica gel column chromatography (ethyl acetate: petroleum ether) to give desired product **3a** in 81% (53 mg).

2.7 Characterization data of 3a-3ae, 5

3-(4-Methoxyphenyl)-2-phenyl-4H-pyrido[1,2-*a*]pyrimidin-4-one (3a): Light green solid; 81% (53 mg); m.p.180-182 °C; ¹H NMR (500 MHz, CDCl₃): δ 9.11 (d, *J* = 7.5 Hz, 1H), 7.74 – 7.68 (m, 2H), 7.44 – 7.42 (m, 2H), 7.27 – 7.24 (m, 3H), 7.21 (d, *J* = 8.7 Hz, 2H), 7.14 – 7.11 (m, 1H), 6.82 (d, *J* = 8.8 Hz, 2H), 3.78 (s, 3H); ¹³C{¹H} NMR (126 MHz, CDCl₃): δ = 161.0, 158.8, 158.5, 149.4, 139.3, 135.6, 132.5, 129.9, 128.7, 128.0, 127.6, 126.9, 126.7, 115.6, 115.4, 113.7, 55.3; **HRMS** (ESI, *m/z*): calcd for C₂₁H₁₇N₂O₂ [M+H]⁺: 329.1285, found : 329.1284.

3-(4-Methoxyphenyl)-9-methyl-2-phenyl-4H-pyrido[1,2-*a*]pyrimidin-4-one (3b): Light yellow solid; 67% (46 mg); m.p.178-180 °C; ¹H NMR (500 MHz, CDCl₃): δ 9.00 (d, *J* = 6.7 Hz, 1H), 7.57 (d, *J* = 6.9 Hz, 1H), 7.52 (d, *J* = 6.2 Hz, 2H), 7.28 – 7.21 (m, 5H), 7.03 (t, *J* = 7.0 Hz, 1H), 6.85 (d, *J* = 8.6 Hz, 2H), 3.80 (s, 3H), 2.65 (s, 3H); ¹³C NMR (126 MHz, CDCl₃): δ = 159.6, 159.2, 158.8, 148.9, 139.6, 135.4, 134.2, 132.5, 130.4, 128.8, 127.9, 127.4, 125.7, 115.1, 114.9, 113.8, 55.3, 18.2; **IR (ATR):** 1656, 1510, 1247, 1025, 766, 692 cm⁻¹; **HRMS (ESI, *m/z*):** calcd for C₂₂H₁₉N₂O₂[M+ H]⁺: 343.1441, found : 342.1454.

3-(4-Methoxyphenyl)-8-methyl-2-phenyl-4H-pyrido[1,2-*a*]pyrimidin-4-one (3c): Yellow solid; 71% (48 mg); m.p.170-172 °C; ¹H NMR (500 MHz, CDCl₃): δ 9.01 (d, *J* = 7.3 Hz, 1H), 7.51 (s, 1H), 7.42 – 7.40 (m, 2H), 7.26 – 7.24 (m, 3H), 7.19 (d, *J* = 7.3 Hz, 2H), 6.98 (d, *J* = 7.3 Hz, 1H), 6.81 (d, *J* = 8.7 Hz, 2H), 3.78 (s, 3H), 2.49 (s, 3H); ¹³C NMR (126 MHz, CDCl₃): δ = 161.4, 158.7, 158.6, 149.5, 147.7, 139.5, 132.6, 129.9, 128.7, 128.0, 127.2, 127.0, 124.8, 118.2, 114.8, 113.7, 55.3, 21.6; **IR (ATR):** 1654, 1506, 1234, 1171, 696, 538 cm⁻¹; **HRMS (ESI, *m/z*):** calcd for C₂₂H₁₉N₂O₂[M+ H]⁺: 343.1441, found : 343.1457.

3-(4-Methoxyphenyl)-7-methyl-2-phenyl-4H-pyrido[1,2-*a*]pyrimidin-4-one (3d): Light green solid; 69% (46 mg); m.p.180-182 °C; ¹H NMR (500 MHz, CDCl₃): δ 8.90 (s, 1H), 7.65 (d, *J* = 9.0 Hz, 1H), 7.57 (d, *J* = 9.2 Hz, 1H), 7.41 – 7.39 (m, 2H), 7.25 – 7.23 (m, 3H), 7.19 (d, *J* = 8.7 Hz, 2H), 6.81 (d, *J* = 8.7 Hz, 2H), 3.77 (s, 3H), 2.43 (s, 3H); ¹³C NMR (126 MHz, CDCl₃): δ = 160.7, 158.7, 158.4, 148.4, 139.5, 138.6, 132.5, 129.8, 128.6, 128.0, 127.2, 126.2, 125.7, 124.9, 115.3, 113.5, 55.3, 18.6; **HRMS (ESI, *m/z*):** calcd for C₂₂H₁₉N₂O₂[M+ H]⁺: 343.1441, found: 343.1444.

3-(4-Methoxyphenyl)-6-methyl-2-phenyl-4H-pyrido[1,2-*a*]pyrimidin-4-one (3e): White solid; 78% (53 mg); m.p.176-178 °C; ¹H NMR (500 MHz, CDCl₃): δ 7.47 – 7.40 (m, 4H), 7.26 – 7.16 (m, 5H), 6.82 (d, *J* = 8.2 Hz, 2H), 6.65 (d, *J* = 6.8 Hz, 1H), 3.77 (s, 3H), 3.05 (s, 3H); ¹³C NMR (126 MHz, CDCl₃): δ = 162.7, 159.2, 158.6, 151.8, 143.9, 138.9,

134.7, 132.4, 129.7, 128.6, 127.9, 127.3, 125.6, 118.2, 117.3, 113.7, 55.2, 24.8; **IR (ATR)**: 1662, 1506, 1243, 1029, 803, 700 cm^{-1} ; **HRMS** (ESI, m/z): calcd for $\text{C}_{22}\text{H}_{19}\text{N}_2\text{O}_2[\text{M} + \text{H}]^+$: 343.1441, found: 343.1456.

7-Fluoro-3-(4-methoxyphenyl)-2-phenyl-4H-pyrido[1,2-*a*]pyrimidin-4-one (3f): Yellow solid; 64% (44 mg); m.p.186-188 $^{\circ}\text{C}$; **^1H NMR** (500 MHz, CDCl_3): δ 9.00 (d, $J = 4.8$ Hz, 1H), 7.75 – 7.72 (m, 1H), 7.64 – 7.60 (m, 1H), 7.42 (d, $J = 7.3$ Hz, 2H), 7.27 – 7.25 (m, 3H), 7.20 (d, $J = 8.8$ Hz, 2H), 6.82 (d, $J = 8.2$ Hz, 2H), 3.78 (s, 3H); **^{13}C NMR** (126 MHz, CDCl_3): $\delta = 160.7, 158.9, 158.1$ (d, $J_{\text{CF}} = 1.9$ Hz), 155.2 (d, $J_{\text{CF}} = 245$ Hz), 147.3, 139.1, 132.5, 129.9, 128.9, 128.7 (d, $J_{\text{CF}} = 7.4$ Hz), 128.3, 128.1, 126.6, 115.5, 113.8 (d, $J_{\text{CF}} = 4.7$ Hz), 113.4, 55.3; **^{19}F NMR** (471 MHz, CDCl_3) δ -132.98 (s, 1F); **IR (ATR)**: 1662, 1514, 1241, 1029, 836, 540 cm^{-1} ; **HRMS** (ESI, m/z): calcd for $\text{C}_{21}\text{H}_{16}\text{FN}_2\text{O}_2[\text{M} + \text{H}]^+$: 347.1190, found: 347.1204.

7-Chloro-3-(4-methoxyphenyl)-2-phenyl-4H-pyrido[1,2-*a*]pyrimidin-4-one (3g): Pale yellow solid; 66% (47 mg); m.p.184-186 $^{\circ}\text{C}$; **^1H NMR** (500 MHz, CDCl_3): δ 9.12 (s, 1H), 7.69 – 7.64 (m, 2H), 7.42 (d, $J = 6.9$ Hz, 2H), 7.29 – 7.25 (m, 3H), 7.20 (d, $J = 8.2$ Hz, 2H), 6.84 (d, $J = 8.3$ Hz, 2H), 3.80 (s, 3H); **^{13}C NMR** (126 MHz, CDCl_3): $\delta = 160.9, 159.0, 157.7, 147.7, 139.0, 136.9, 132.5, 129.9, 129.0, 128.1, 127.8, 126.6, 125.3, 124.1, 116.3, 113.8, 55.3$; **IR (ATR)**: 1664, 1514, 1245, 1029, 823, 540 cm^{-1} ; **HRMS** (ESI, m/z): calcd for $\text{C}_{21}\text{H}_{16}\text{ClN}_2\text{O}_2[\text{M} + \text{H}]^+$: 363.0894, found: 363.0907.

7-Bromo-3-(4-methoxyphenyl)-2-phenyl-4H-pyrido[1,2-*a*]pyrimidin-4-one (3h): Light green solid; 70% (62 mg); m.p.186-188 $^{\circ}\text{C}$; **^1H NMR** (500 MHz, CDCl_3): δ 9.21 (s, 1H), 7.73 (d, $J = 9.5$ Hz, 1H), 7.60 (d, $J = 9.5$ Hz, 1H), 7.41 (d, $J = 7.0$ Hz, 2H), 7.29 – 7.23 (m, 3H), 7.19 (d, $J = 8.1$ Hz, 2H), 6.83 (d, $J = 8.8$ Hz, 2H), 3.79 (s, 3H); **^{13}C NMR** (126 MHz, CDCl_3): $\delta = 160.9, 159.0, 157.6, 147.8, 139.0, 138.9, 132.5, 129.9, 129.0, 128.1, 127.8, 127.7, 126.6, 116.4, 113.8, 110.7, 55.3$; **IR (ATR)**: 1656, 1510, 1245, 1029, 823, 540 cm^{-1} ; **HRMS** (ESI, m/z): calcd for $\text{C}_{21}\text{H}_{16}\text{BrN}_2\text{O}_2[\text{M} + \text{H}]^+$: 407.0389, found: 407.0405.

2,3-Bis(4-methoxyphenyl)-4H-pyrido[1,2-a]pyrimidin-4-one (3i):

Pale yellow solid; 68% (48 mg); m.p.186-188 °C; ¹H NMR (500 MHz, CDCl₃): δ 9.08 (d, *J* = 7.2 Hz, 1H), 7.69 – 7.68 (m, 2H), 7.42 (d, *J* = 8.9 Hz, 2H), 7.23 (d, *J* = 8.8 Hz, 2H), 7.11 – 7.08 (m, 1H), 6.86 (d, *J* = 8.8 Hz, 2H), 6.78 (d, *J* = 8.8 Hz, 2H), 3.80 (s, 3H), 3.78 (s, 3H); ¹³C NMR (126 MHz, CDCl₃): δ = 160.5, 160.1, 158.7, 158.6, 149.3, 135.5, 132.5, 131.6, 131.6, 127.6, 127.4, 126.7, 115.2, 114.9, 113.8, 113.5, 55.3, 55.3; IR (ATR): 1668, 1508, 1234, 1025, 828, 760 cm⁻¹; HRMS (ESI, *m/z*): calcd for C₂₂H₁₉N₂O₃ [M+ H]⁺: 359.1390, found: 359.1404.

2-(4-Fluorophenyl)-3-(4-methoxyphenyl)-4H-pyrido[1,2-a]pyrimidin-4-one (3j):

Brown solid; 67% (46 mg); m.p.186-188 °C; ¹H NMR (500 MHz, CDCl₃): δ 9.10 (d, *J* = 7.1 Hz, 1H), 7.74 – 7.70 (m, 2H), 7.44 – 7.41 (m, 2H), 7.19 (d, *J* = 8.8 Hz, 2H), 7.15 – 7.12 (m, 1H), 6.94 (t, *J* = 8.7 Hz, 2H), 6.84 (d, *J* = 8.7 Hz, 2H), 3.80 (s, 3H); ¹³C NMR (126 MHz, CDCl₃): δ = 164.0 (d, *J*_{CF} = 249.1 Hz), 159.9, 158.9, 158.5, 149.5, 135.8, 135.4, 135.37, 132.5, 132.0 (d, *J*_{CF} = 8.4 Hz), 127.7, 126.8, 126.7, 115.5, 115.2 (d, *J*_{CF} = 21.6 Hz), 113.9, 55.3; ¹⁹F NMR (471 MHz, CDCl₃) δ -112.27 (s, 1F); IR (ATR): 1660, 1510, 1234, 1029, 830, 772 cm⁻¹; HRMS (ESI, *m/z*): calcd for C₂₁H₁₆FN₂O₂ [M+ H]⁺: 347.1190, found: 347.1208.

2-(4-Chlorophenyl)-3-(4-methoxyphenyl)-4H-pyrido[1,2-a]pyrimidin-4-one (3k):

Brown solid; 66% (47 mg); m.p.188-190 °C; ¹H NMR (500 MHz, CDCl₃): δ 9.09 (d, *J* = 7.2 Hz, 1H), 7.74 – 7.69 (m, 2H), 7.38 (d, *J* = 8.5 Hz, 2H), 7.23 (d, *J* = 8.5 Hz, 2H), 7.19 (d, *J* = 8.7 Hz, 2H), 7.15 – 7.12 (m, 1H), 6.84 (d, *J* = 8.7 Hz, 2H), 3.80 (s, 3H); ¹³C NMR (126 MHz, CDCl₃): δ = 159.6, 158.9, 158.5, 149.5, 137.8, 135.8, 134.9, 132.4, 131.3, 128.3, 127.6, 126.7, 126.6, 115.6, 115.6, 113.9, 55.3; IR (ATR): 1658, 1508, 1243, 1023, 828, 821 cm⁻¹; HRMS (ESI, *m/z*): calcd for C₂₁H₁₆ClN₂O₂ [M+ H]⁺: 363.0895, found: 363.0899.

2-(4-Bromophenyl)-3-(4-methoxyphenyl)-4H-pyrido[1,2-a]pyrimidin-4-one (3l):

White solid; 69% (55 mg); m.p.186-188 °C; ¹H NMR (500 MHz, CDCl₃): δ 9.10 (d, *J* = 7.1 Hz, 1H), 7.75 – 7.70 (m, 2H), 7.39

(d, $J = 8.2$ Hz, 2H), 7.32 (d, $J = 8.2$ Hz, 2H), 7.19 – 7.14 (m, 3H), 6.85 (d, $J = 8.4$ Hz, 2H), 3.80 (s, 3H); ^{13}C NMR (126 MHz, CDCl_3): $\delta = 159.7, 159.0, 158.5, 149.5, 138.3, 135.8, 132.5, 131.6, 131.3, 127.7, 126.7, 126.6, 123.3, 115.6, 115.6, 113.9, 55.3$; HRMS (ESI, m/z): calcd for $\text{C}_{21}\text{H}_{16}\text{BrN}_2\text{O}_2$ $[\text{M} + \text{H}]^+$: 407.0390, found: 407.0393.

2-(3-Bromophenyl)-3-(4-methoxyphenyl)-4H-pyrido[1,2-*a*]pyrimidin-4-one (3m): Yellow solid; 61% (49 mg); m.p.184-186 °C; ^1H NMR (500 MHz, CDCl_3): δ 9.10 (d, $J = 7.2$ Hz, 1H), 7.74 – 7.72 (m, 3H), 7.40 (d, $J = 8.1$ Hz, 1H), 7.20 – 7.14 (m, 4H), 7.04 (t, $J = 7.9$ Hz, 1H), 6.84 (d, $J = 8.7$ Hz, 2H), 3.79 (s, 3H); ^{13}C NMR (126 MHz, CDCl_3): $\delta = 159.1, 159.0, 158.4, 149.4, 141.2, 136.0, 132.7, 132.4, 131.7, 129.3, 128.6, 127.6, 126.6, 126.3, 122.2, 115.8, 115.7, 113.9, 55.3$; IR (ATR): 1668, 1512, 1243, 1175, 1029, 760 cm^{-1} ; HRMS (ESI, m/z): calcd for $\text{C}_{21}\text{H}_{16}\text{BrN}_2\text{O}_2$ $[\text{M} + \text{H}]^+$: 407.0390, found: 407.0399.

6-(4-Methoxyphenyl)-7-phenyl-5H-thiazolo[3,2-*a*]pyrimidin-5-one (3n): Light green solid; 65% (45 mg); m.p.168-170 °C; ^1H NMR (500 MHz, CDCl_3): δ 8.04 (d, $J = 4.9$ Hz, 1H), 7.37 (d, $J = 7.1$ Hz, 2H), 7.26 – 7.23 (m, 3H), 7.16 (d, $J = 8.2$ Hz, 2H), 7.01 (d, $J = 5.0$ Hz, 1H), 6.82 (d, $J = 8.3$ Hz, 2H), 3.78 (s, 3H); ^{13}C NMR (126 MHz, CDCl_3): $\delta = 160.3, 159.8, 159.2, 158.9, 138.7, 132.5, 129.8, 128.8, 128.0, 126.1, 122.4, 116.5, 113.8, 111.8, 55.3$; IR (ATR): 1649, 1512, 1241, 1175, 1027, 733 cm^{-1} ; HRMS (ESI, m/z): calcd for $\text{C}_{19}\text{H}_{15}\text{N}_2\text{O}_2\text{S}$ $[\text{M} + \text{H}]^+$: 335.0848, found: 335.0863.

7-(4-Chlorophenyl)-6-(4-methoxyphenyl)-5H-thiazolo[3,2-*a*]pyrimidin-5-one (3o): Yellow solid; 72% (52 mg); m.p.178-180 °C; ^1H NMR (500 MHz, CDCl_3): δ 8.03 (d, $J = 4.9$ Hz, 1H), 7.32 (d, $J = 8.4$ Hz, 2H), 7.21 (d, $J = 8.5$ Hz, 2H), 7.14 (d, $J = 8.6$ Hz, 2H), 7.03 (d, $J = 5.0$ Hz, 1H), 6.83 (d, $J = 8.6$ Hz, 2H), 3.79 (s, 3H); ^{13}C NMR (126 MHz, CDCl_3): $\delta = 160.4, 159.1, 159.0, 158.4, 137.0, 134.9, 132.4, 131.3, 128.2, 125.7, 122.4, 116.5, 114.0, 112.0, 55.3$; IR (ATR): 1658, 1512, 1241, 1025, 838, 719 cm^{-1} ; HRMS (ESI, m/z): calcd for $\text{C}_{19}\text{H}_{14}\text{ClN}_2\text{O}_2\text{S}$ $[\text{M} + \text{H}]^+$: 369.0459, found: 369.0474.

6-(4-Methoxyphenyl)-7-(*p*-tolyl)-5*H*-thiazolo[3,2-*a*]pyrimidin-5-one (3p): Yellow solid; 68% (46 mg); m.p.178-180 °C; ¹H NMR (500 MHz, CDCl₃): δ 8.02 (d, *J* = 4.9 Hz, 1H), 7.28 (d, *J* = 8.1 Hz, 2H), 7.17 (d, *J* = 8.3 Hz, 2H), 7.04 (d, *J* = 7.9 Hz, 2H), 7.00 (d, *J* = 4.9 Hz, 1H), 6.83 (d, *J* = 8.2 Hz, 2H), 3.79 (s, 3H), 2.30 (s, 3H); ¹³C NMR (126 MHz, CDCl₃): δ = 160.2, 159.8, 159.3, 158.8, 138.9, 135.7, 132.4, 129.8, 128.7, 126.3, 122.4, 116.1, 113.8, 111.7, 55.3, 21.4; **IR (ATR):** 1645, 1510, 1247, 1027, 807, 743 cm⁻¹; **HRMS** (ESI, *m/z*): calcd for C₂₀H₁₇N₂O₂S [M+ H]⁺: 349.1005, found: 349.1019.

2,3-Diphenyl-4*H*-pyrido[1,2-*a*]pyrimidin-4-one (3q): Light green solid; 60% (35 mg); m.p.178-180 °C; ¹H NMR (500 MHz, CDCl₃): δ 9.11 (d, *J* = 7.2 Hz, 1H), 7.74 – 7.71 (m, 2H), 7.41 – 7.39 (m, 2H), 7.27 – 7.20 (m, 8H), 7.15 – 7.11 (m, 1H); ¹³C NMR (126 MHz, CDCl₃): δ = 161.4, 158.3, 149.6, 139.2, 135.9, 134.9, 131.4, 129.9, 128.8, 128.1, 128.0, 127.7, 127.3, 126.8, 115.9, 115.5; **IR (ATR):** 1664, 1454, 1269, 1078, 758, 700, 534 cm⁻¹; **HRMS** (ESI, *m/z*): calcd for C₂₀H₁₅N₂O [M+H]⁺: 299.1179, found: 299.1193.

3-(2-Bromophenyl)-2-phenyl-4*H*-pyrido[1,2-*a*]pyrimidin-4-one (3r): White solid; 64% (48 mg); m.p.182-184 °C; ¹H NMR (500 MHz, CDCl₃): δ 9.14 (d, *J* = 7.2 Hz, 1H), 7.79 (d, *J* = 4.2 Hz, 2H), 7.62 – 7.61 (dd, *J* = 7.9, 1.3 Hz, 1H), 7.46 – 7.44 (m, 2H), 7.25 – 7.12 (m, 7H); ¹³C NMR (126 MHz, CDCl₃): δ = 161.9, 157.3, 150.2, 138.7, 136.5, 136.3, 133.0, 132.9, 129.4, 129.3, 129.1, 128.0, 127.9, 127.5, 126.9, 126.0, 116.0, 115.7; **HRMS** (ESI, *m/z*): calcd for C₂₀H₁₄BrN₂O [M+ H]⁺: 377.0284, found: 377.0299.

3-(4-Nitrophenyl)-2-phenyl-4*H*-pyrido[1,2-*a*]pyrimidin-4-one (3s): Yellow solid; 72% (49 mg); m.p.174-176 °C; ¹H NMR (500 MHz, CDCl₃): δ 9.14 (d, *J* = 7.2 Hz, 1H), 8.11 (d, *J* = 8.9 Hz, 2H), 7.84 – 7.77 (m, 2H), 7.47 (d, *J* = 8.8 Hz, 2H), 7.37 (d, *J* = 6.7 Hz, 2H), 7.33 – 7.30 (m, 1H), 7.28 – 7.22 (m, 3H); ¹³C NMR (126 MHz, CDCl₃): δ = 162.3, 157.7, 150.1, 146.6, 142.4, 138.4, 136.9, 132.5, 129.8, 129.5, 128.4, 127.8, 126.9, 123.3, 116.2, 113.4; **IR (ATR):** 1660, 1508, 1331, 1088,

770, 692 cm^{-1} ; **HRMS** (ESI, m/z): calcd for $\text{C}_{20}\text{H}_{14}\text{N}_3\text{O}_3[\text{M} + \text{H}]^+$: 344.1030, found: 344.1034.

3-(3-Nitrophenyl)-2-phenyl-4H-pyrido[1,2-*a*]pyrimidin-4-one (3t): Dark brown solid; 68% (46 mg); m.p.180-182 °C; **^1H NMR** (500 MHz, CDCl_3): δ 9.14 (d, $J = 7.1$ Hz, 1H), 8.21 (t, $J = 2.0$ Hz, 1H), 8.09 (d, $J = 8.1$ Hz, 1H), 7.84 – 7.79 (m, 2H), 7.57 (d, $J = 7.8$ Hz, 1H), 7.42 (d, $J = 8.0$ Hz, 1H), 7.39 – 7.35 (m, 2H), 7.31 – 7.24 (m, 4H); **^{13}C NMR** (126 MHz, CDCl_3): $\delta = 162.3, 157.9, 150.1, 148.1, 138.3, 137.7, 136.9, 136.8, 129.8, 129.4, 128.9, 128.4, 127.8, 126.9, 126.6, 122.2, 116.2, 113.3$; **IR (ATR)**: 1668, 1522, 1341, 1072, 752, 688 cm^{-1} ; **HRMS** (ESI, m/z): calcd for $\text{C}_{20}\text{H}_{14}\text{N}_3\text{O}_3[\text{M} + \text{H}]^+$: 344.1029, found: 344.1039.

6-(4-Nitrophenyl)-7-phenyl-5H-thiazolo[3,2-*a*]pyrimidin-5-one (3u): Off-white solid; 68% (47 mg); m.p.180-182 °C; **^1H NMR** (500 MHz, CDCl_3): δ 8.11 (d, $J = 8.8$ Hz, 2H), 8.08 (d, $J = 4.9$ Hz, 1H), 7.42 (d, $J = 8.8$ Hz, 2H), 7.32 – 7.29 (m, 3H), 7.26 – 7.23 (m, 2H), 7.12 (d, $J = 4.9$ Hz, 1H); **^{13}C NMR** (126 MHz, CDCl_3): $\delta = 161.8, 161.1, 158.2, 146.8, 141.6, 137.7, 132.4, 129.8, 129.7, 128.4, 123.3, 122.5, 114.5, 112.6$; **IR (ATR)**: 1641, 1506, 1337, 858, 700, 513 cm^{-1} ; **HRMS** (ESI, m/z): calcd for $\text{C}_{18}\text{H}_{12}\text{N}_3\text{O}_3\text{S} [\text{M} + \text{H}]^+$: 350.0593, found: 350.0609.

7-(4-Fluorophenyl)-6-(4-nitrophenyl)-5H-thiazolo[3,2-*a*]pyrimidin-5-one (3v): Brown solid; 70% (51 mg); m.p.188-190 °C; **^1H NMR** (500 MHz, CDCl_3): δ 8.13 (d, $J = 8.7$ Hz, 2H), 8.07 (d, $J = 4.9$ Hz, 1H), 7.42 (d, $J = 8.7$ Hz, 2H), 7.33 – 7.30 (m, 2H), 7.14 (d, $J = 4.9$ Hz, 1H), 6.94 (t, $J = 8.6$ Hz, 2H); **^{13}C NMR** (126 MHz, CDCl_3): $\delta = 164.3$ (d, $J_{\text{CF}} = 251.3$ Hz), 161.8, 159.8, 158.1, 146.8, 141.5, 133.7 (d, $J_{\text{CF}} = 3.3$ Hz), 132.4, 132.0 (d, $J_{\text{CF}} = 8.6$ Hz), 123.4, 122.4, 115.6 (d, $J_{\text{CF}} = 21.7$ Hz), 114.3, 112.7; **^{19}F NMR** (471 MHz, CDCl_3) δ -110.26 (s, 1F); **IR (ATR)**: 1643, 1508, 1339, 1232, 842, 737 cm^{-1} ; **HRMS** (ESI, m/z): calcd for $\text{C}_{18}\text{H}_{11}\text{FN}_3\text{O}_3\text{S} [\text{M} + \text{H}]^+$: 368.0500, found: 368.0504.

7-(4-Chlorophenyl)-6-(4-nitrophenyl)-5H-thiazolo[3,2-*a*]pyrimidin-5-one (3w): Pale yellow solid; 75% (57 mg); m.p.176-178 °C; **^1H NMR** (500 MHz, CDCl_3): δ 8.15 (d, $J = 8.3$ Hz, 2H), 8.08 (d, $J = 5.0$ Hz, 1H),

7.43 (d, J = 8.1 Hz, 2H), 7.28 – 7.22 (m, 4H), 7.13 (d, J = 5.0 Hz, 1H); **^{13}C NMR** (126 MHz, CDCl_3): δ = 161.9, 159.7, 158.2, 147.0, 141.3, 136.1, 136.0, 132.4, 131.3, 128.7, 123.6, 122.6, 114.6, 112.7; **IR (ATR)**: 1662, 1506, 1339, 1101, 846, 741 cm^{-1} ; **HRMS** (ESI, m/z): calcd for $\text{C}_{18}\text{H}_{11}\text{ClN}_3\text{O}_3\text{S}$ $[\text{M}+\text{H}]^+$: 384.0204, found: 384.0204.

6-(4-Nitrophenyl)-7-(*p*-tolyl)-5*H*-thiazolo[3,2-*a*]pyrimidin-5-one

(3x): Brown solid; 69% (50 mg); m.p.178-180 °C; **^1H NMR** (500 MHz, CDCl_3): δ 8.12 – 8.0 (dd, J = 8.9, 2.1 Hz, 2H), 8.07 – 8.04 (dd, J = 4.9, 1.8 Hz, 1H), 7.43 – 7.41 (m, 2H), 7.21 (d, J = 7.5 Hz, 2H), 7.10 (d, J = 4.9 Hz, 1H), 7.05 (d, J = 7.8 Hz, 2H), 2.31 (s, 3H); **^{13}C NMR** (126 MHz, CDCl_3): δ = 161.6, 161.2, 158.3, 146.7, 141.9, 140.0, 134.7, 132.4, 129.9, 129.1, 123.3, 122.4, 114.2, 112.5, 21.4; **IR (ATR)**: 1639, 1508, 1335, 1105, 828, 739 cm^{-1} ; **HRMS** (ESI, m/z): calcd for $\text{C}_{19}\text{H}_{14}\text{N}_3\text{O}_3\text{S}$ $[\text{M}+\text{H}]^+$: 364.0750, found: 364.0754.

3-(4-Fluorophenyl)-2,7-dimethyl-4*H*-pyrido[1,2-*a*]pyrimidin-4-one

(3y): Off-white solid; 64% (34 mg); m.p.140-142 °C; **^1H NMR** (500 MHz, CDCl_3): δ 8.83 (s, 1H), 7.58 – 7.52 (m, 2H), 7.34 – 7.31 (m, 2H), 7.13 (t, J = 8.5 Hz, 2H), 2.41 (s, 3H), 2.34 (s, 3H); **^{13}C NMR** (126 MHz, CDCl_3): δ = 163.3 (d, J_{CF} = 206 Hz), 161.6, 157.3, 148.4, 139.0, 132.2 (d, J_{CF} = 7.9 Hz), 131.1 (d, J_{CF} = 3.3 Hz), 125.5, 125.4, 125.0, 115.7, 115.6 (d, J_{CF} = 21.4 Hz), 23.8, 18.5; **^{19}F NMR** (471 MHz, CDCl_3) δ - 114.60 (s, 1F); **HRMS** (ESI, m/z): calcd for $\text{C}_{16}\text{H}_{14}\text{FN}_2\text{O}$ $[\text{M}+\text{H}]^+$: 269.1085, found: 269.1085.

3-(4-Chlorophenyl)-2,7-dimethyl-4*H*-pyrido[1,2-*a*]pyrimidin-4-one

(3z): Pale yellow solid; 67% (38 mg); m.p.158-160 °C; **^1H NMR** (500 MHz, CDCl_3): δ 8.83 (s, 1H), 7.60 – 7.55 (m, 2H), 7.42 (d, J = 8.4 Hz, 2H), 7.30 (d, J = 8.4 Hz, 2H), 2.42 (s, 3H), 2.35 (s, 3H); **^{13}C NMR** (126 MHz, CDCl_3): δ = 161.5, 157.1, 148.4, 139.3, 133.6, 133.5, 131.9, 128.8, 125.8, 125.2, 125.1, 115.6, 23.7, 18.5; **HRMS** (ESI, m/z): calcd for $\text{C}_{16}\text{H}_{14}\text{ClN}_2\text{O}$ $[\text{M}+\text{H}]^+$: 285.0789, found: 285.0788.

6-(4-Fluorophenyl)-7-methyl-5*H*-thiazolo[3,2-*a*]pyrimidin-5-one

(3ab): Pale yellow solid; 69% (36 mg); m.p.144-146 °C; **^1H NMR** (500

MHz, CDCl₃): δ 7.97 (d, J = 4.9 Hz, 1H), 7.30 – 7.27 (m, 2H), 7.12 (t, J = 8.7 Hz, 2H), 6.98 (d, J = 4.9 Hz, 1H), 2.28 (s, 3H); **¹³C NMR** (126 MHz, CDCl₃): δ = 163.4 (d, J_{CF} = 246.1 Hz), 161.0, 160.6, 158.3, 132.2 (d, J_{CF} = 8.0 Hz), 130.0 (d, J_{CF} = 3.6 Hz), 122.4, 116.8, 115.7 (d, J_{CF} = 21.3 Hz), 111.3, 23.4; **¹⁹F NMR** (471 MHz, CDCl₃) δ -114.3 (s, 1F); **HRMS** (ESI, m/z): calcd for C₁₃H₉FN₂OSNa[M+Na]⁺: 283.0312, found: 283.0312.

6-(4-Chlorophenyl)-7-methyl-5H-thiazolo[3,2-*a*]pyrimidin-5-one

(3ac): Pale yellow solid; 66% (37 mg); m.p.146-148 °C; **¹H NMR** (500 MHz, CDCl₃): δ 7.98 (d, J = 4.9 Hz, 1H), 7.43 (d, J = 8.0 Hz, 2H), 7.28 (d, J = 7.9 Hz, 2H), 6.99 (d, J = 4.9 Hz, 1H) 2.29 (s, 3H); **¹³C NMR** (126 MHz, CDCl₃): δ = 161.0, 160.7, 158.1, 133.8, 132.6, 131.9, 128.8, 122.4, 116.6, 111.3, 23.4; **HRMS** (ESI, m/z): calcd for C₁₃H₉ClN₂OSNa[M+Na]⁺: 299.0016, found: 299.0012.

2-(3,4-Dimethoxyphenyl)-3-phenyl-4H-pyrido[1,2-*a*]pyrimidin-4-one

(3ad): White solid; 71% (50 mg); m.p.178-180 °C; **¹H NMR** (500 MHz, CDCl₃): δ 9.09 (d, J = 7.2 Hz, 1H), 7.72 (d, J = 3.3 Hz, 2H), 7.33 – 7.29 (m, 4H), 7.26 – 7.20 (m, 2H), 7.13 – 7.10 (m, 1H), 6.84 (d, J = 2.0 Hz, 1H), 6.79 (d, J = 8.5 Hz, 1H), 3.85 (s, 3H), 3.53 (s, 3H); **¹³C NMR** (126 MHz, CDCl₃): δ = 160.4, 158.4, 149.7, 149.5, 148.0, 135.8, 135.5, 131.3, 131.3, 128.4, 127.6, 127.3, 126.7, 123.2, 115.3, 115.2, 113.6, 110.6, 55.9, 55.6; **IR (ATR)**: 1660, 1508, 1253, 1134, 754, 595 cm⁻¹; **HRMS** (ESI, m/z): calcd for C₂₂H₁₈N₂O₃Na[M+Na]⁺: 381.1210, found: 381.1218.

2-Methyl-3-phenyl-4H-pyrido[1,2-*a*]pyrimidin-4-one

(3ae): brown solid; 70% (33 mg); m.p.130-132 °C; **¹H NMR** (500 MHz, CDCl₃): δ 9.06 (d, J = 8.4 Hz, 1H), 7.73 – 7.70 (m, 1H), 7.63 (d, J = 7.8 Hz, 1H), 7.47 – 7.44 (m, 2H), 7.38 – 7.36 (m, 3H), 7.13 – 7.10 (m, 1H), 2.38 (s, 3H); **¹³C NMR** (126 MHz, CDCl₃): δ = 162.2, 157.5, 149.4, 135.9, 135.0, 130.4, 128.6, 127.8, 127.7, 125.9, 117.1, 115.2, 23.9; **HRMS** (ESI, m/z): calcd for C₁₅H₁₃N₂O [M+H]⁺: 237.1022, found: 237.1023.

(E)-2-(2-(3-(2,4-dimethylphenyl)-1-(*p*-tolyl)-1*H*-pyrazol-4-yl)vinyl)-3-phenyl-4*H*-pyrido[1,2-*a*]pyrimidin-4-one (5): Yellow solid; 37% (55 mg); m.p. 158-160 °C; ¹H NMR (500 MHz, CDCl₃): δ 8.96 (d, *J* = 6.1 Hz, 1H), 8.04 (s, 1H), 7.87 (d, *J* = 15.6 Hz, 1H), 7.63 – 7.55 (m, 4H), 7.42 – 7.39 (m, 3H), 7.31 – 7.29 (m, 2H), 7.24 (d, *J* = 8.1 Hz, 2H), 7.19 (d, *J* = 8.1 Hz, 1H), 7.00 – 6.97 (m, 3H), 6.59 (d, *J* = 15.6 Hz, 1H), 2.38 (s, 3H), 2.37 (s, 3H), 2.22 (s, 3H); ¹³C NMR (126 MHz, CDCl₃): δ = 158.2, 156.4, 152.8, 149.2, 138.1, 137.5, 136.9, 136.6, 135.4, 134.1, 131.4, 131.0, 130.3, 130.0, 129.5, 128.4, 128.3, 127.5 (2C), 126.5, 126.4, 126.1, 123.5, 120.1, 119.0, 115.5, 114.3, 21.5, 21.1, 20.1; **HRMS** (ESI, *m/z*): calcd for C₃₄H₂₈N₄O [M+H]⁺: 509.2336, found: 509.2331.

2.8 ^1H and ^{13}C NMR spectra of selected compounds

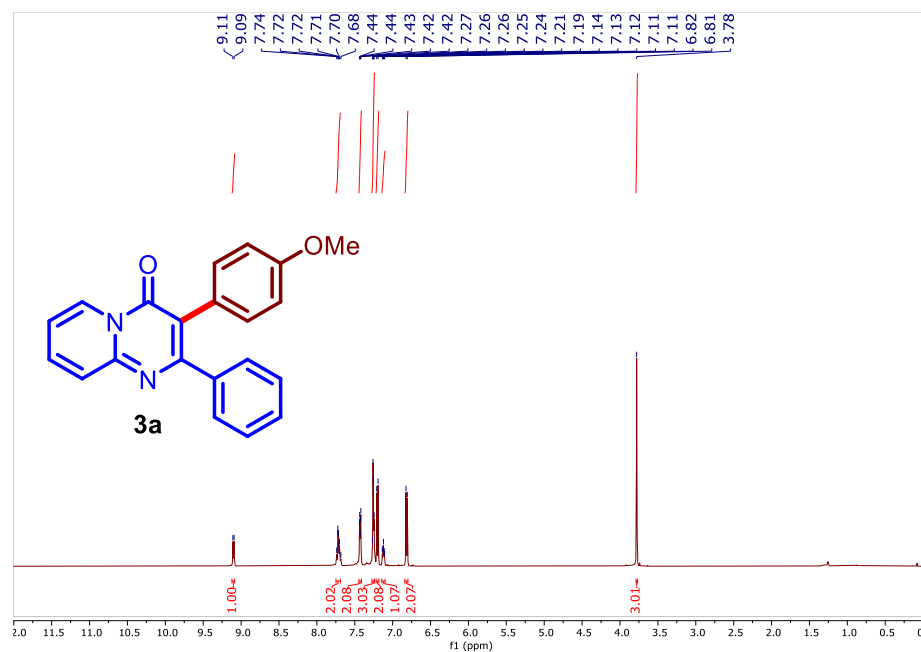


Figure 2.2 ^1H NMR spectrum of compound **3a** (500 MHz, CDCl_3)

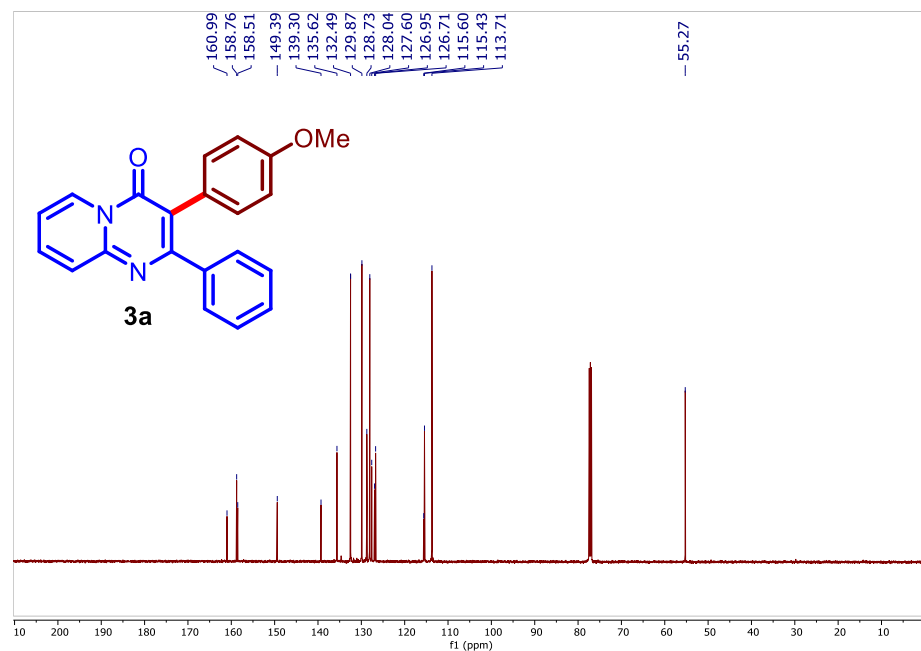


Figure 2.3 ^{13}C NMR spectrum of compound **3a** (126 MHz, CDCl_3)

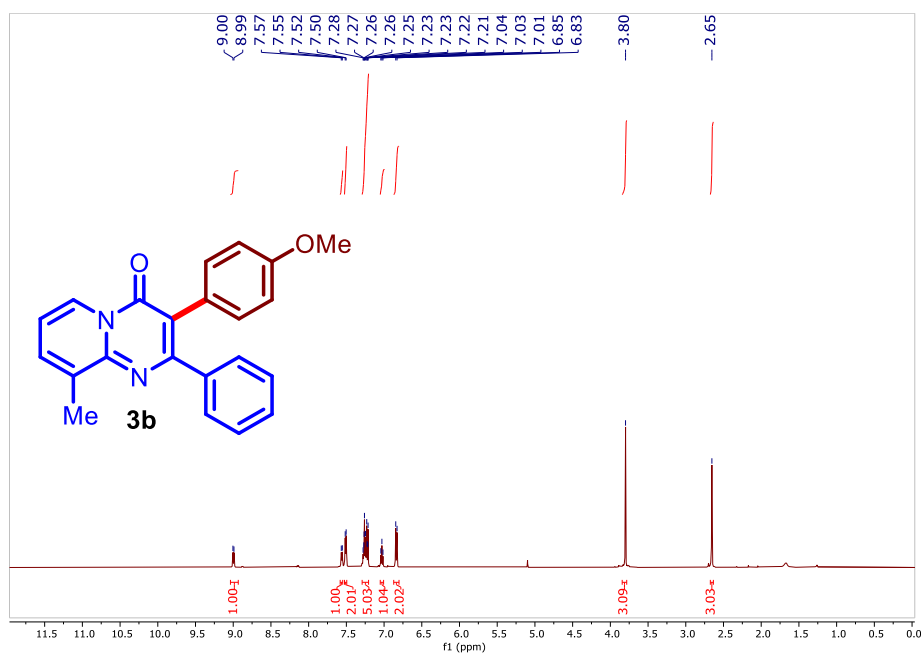


Figure 2.4 ¹H NMR spectrum of compound **3b** (500 MHz, CDCl₃)

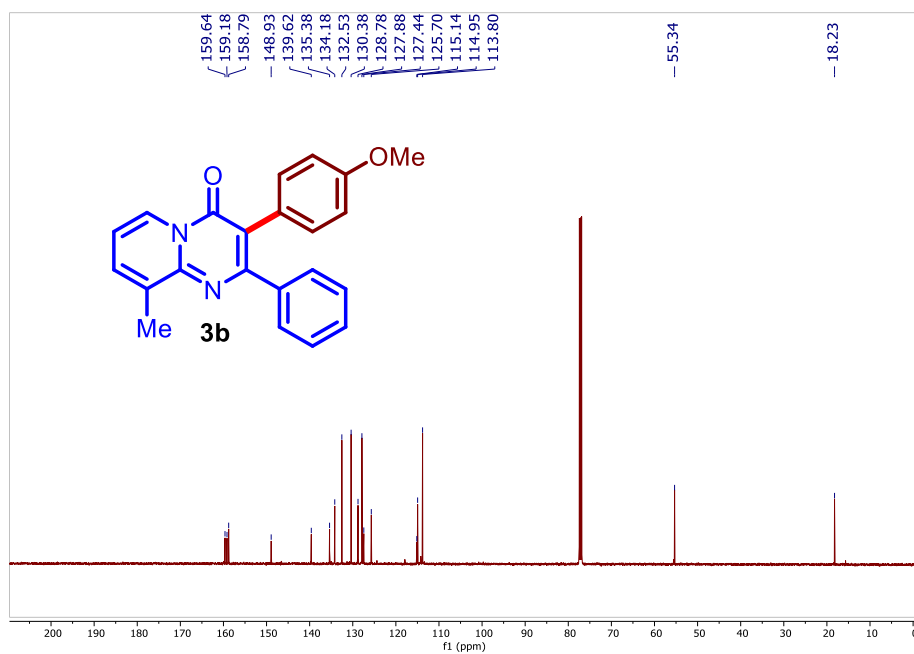


Figure 2.5 ¹³C NMR spectrum of compound **3b** (126 MHz, CDCl₃)

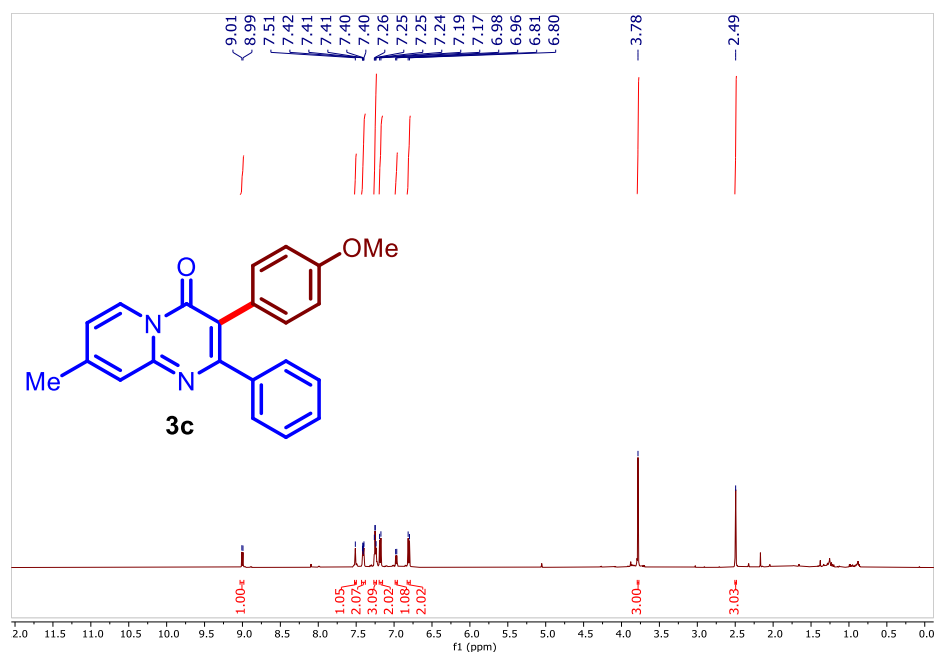


Figure 2.6 ¹H NMR spectrum of compound **3c** (500 MHz, CDCl₃)

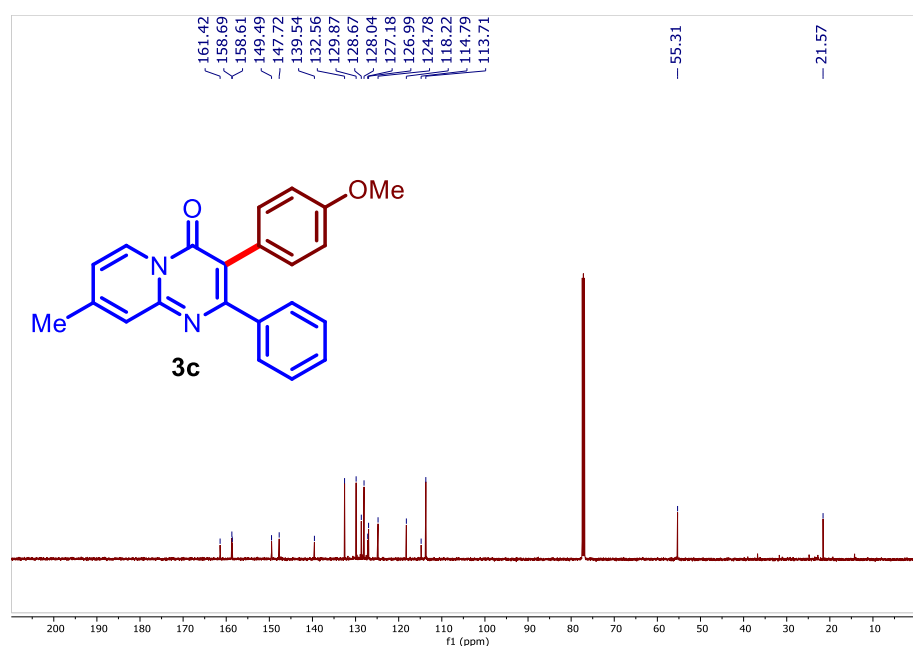
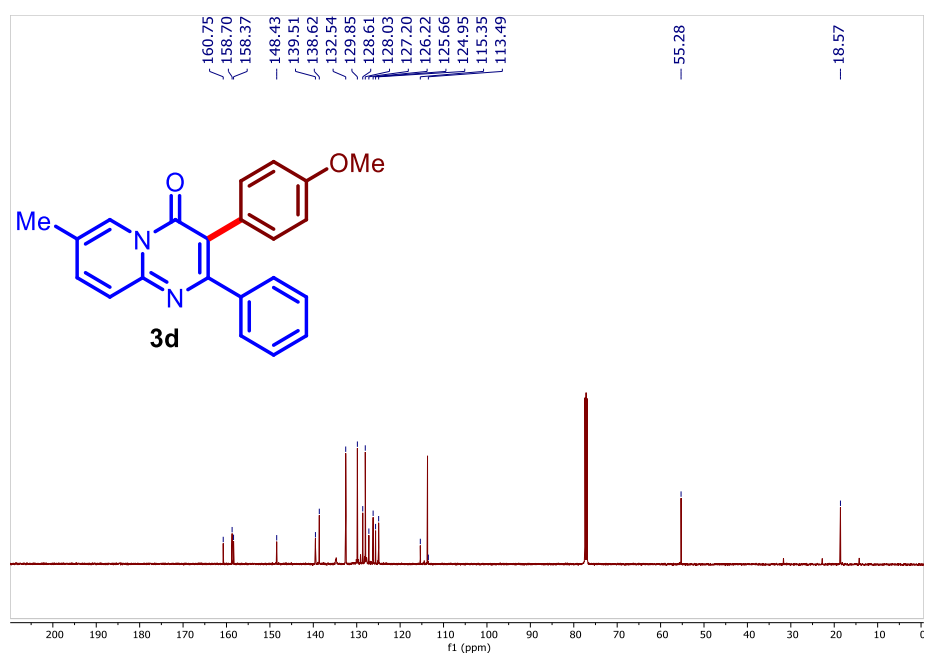
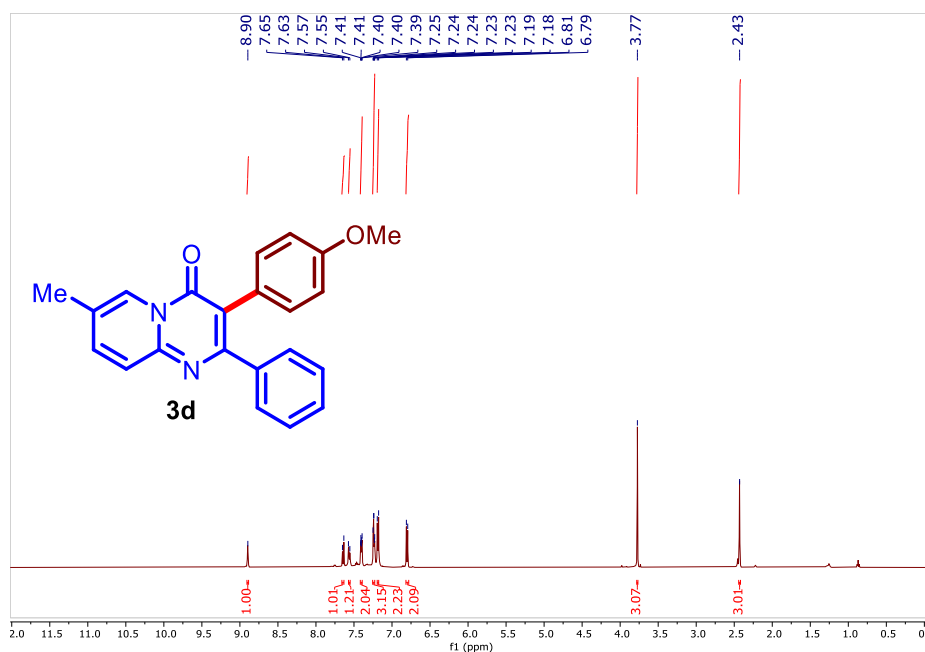


Figure 2.7 ¹³C NMR spectrum of compound **3c** (126 MHz, CDCl₃)



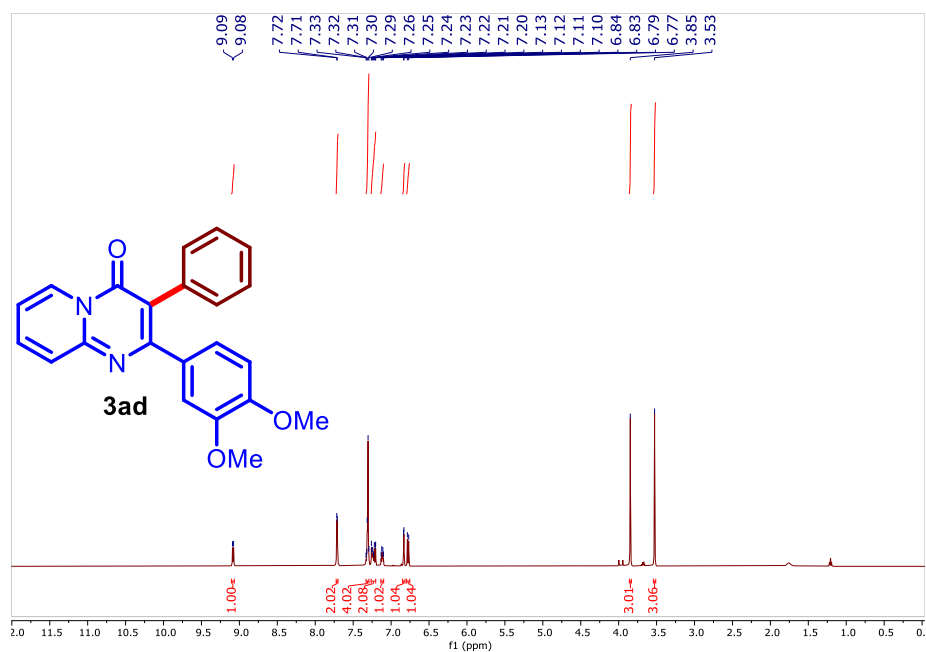


Figure 2.10 ¹H NMR spectrum of compound **3ad** (500 MHz, CDCl₃)

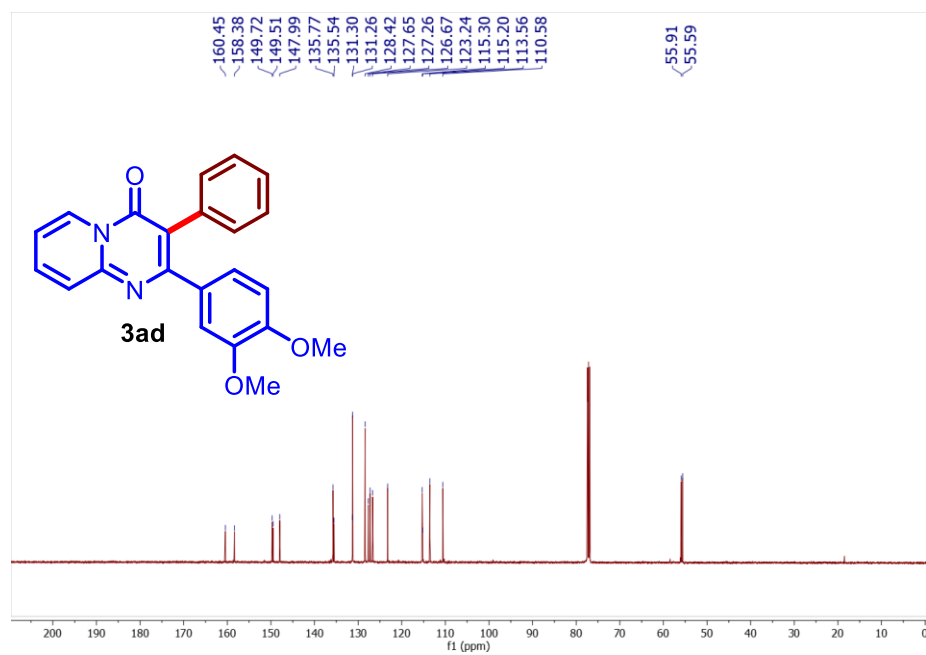
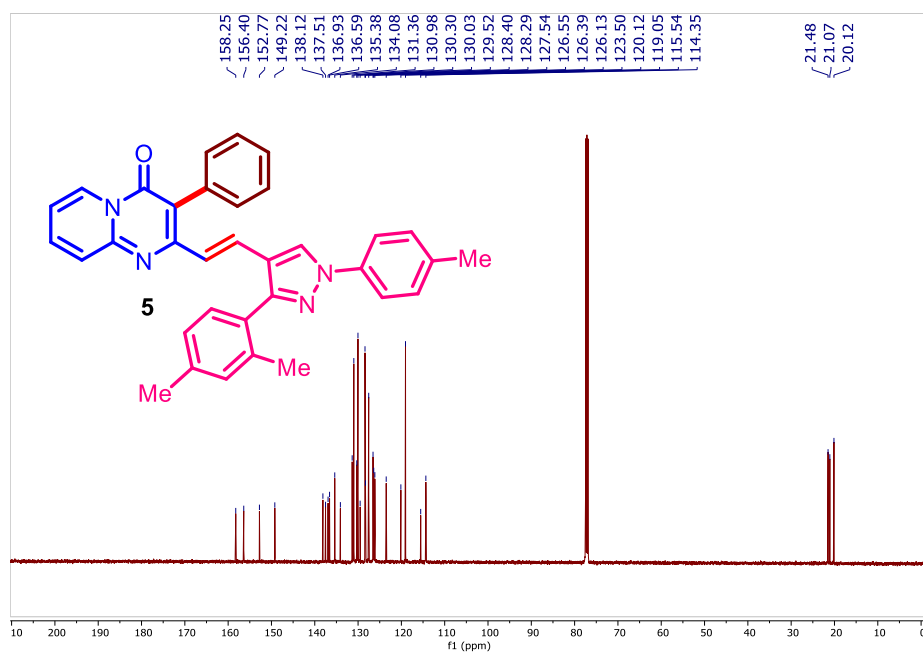
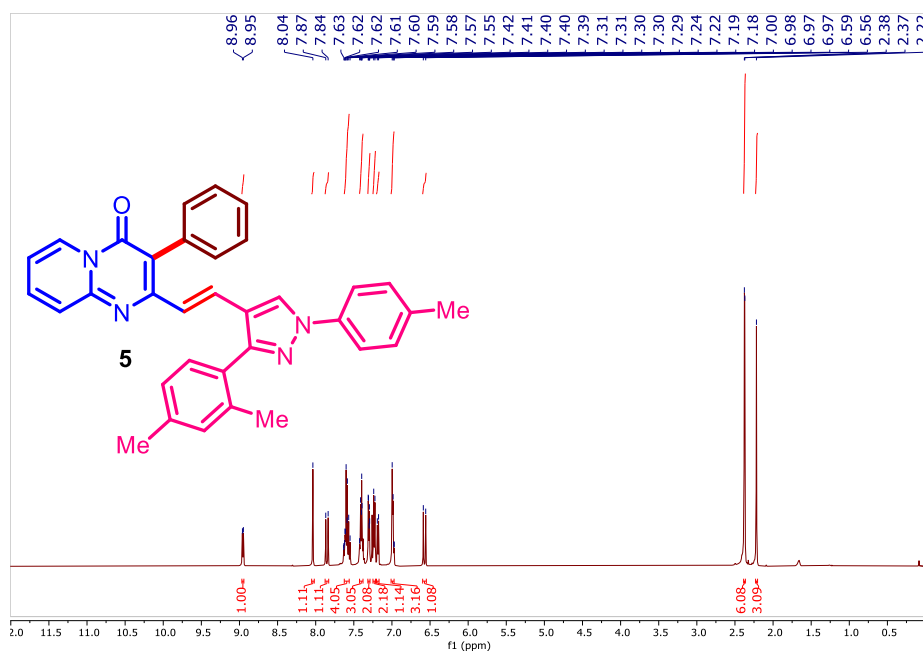


Figure 2.11 ¹³C NMR spectrum of compound **3ad** (126 MHz, CDCl₃)



2.9 The Single Crystal X-ray Diffraction data

The Single crystal X-ray Diffraction study of compound **3s** and which was readily crystalized from the mixture of dichloromethane and acetonitrile.

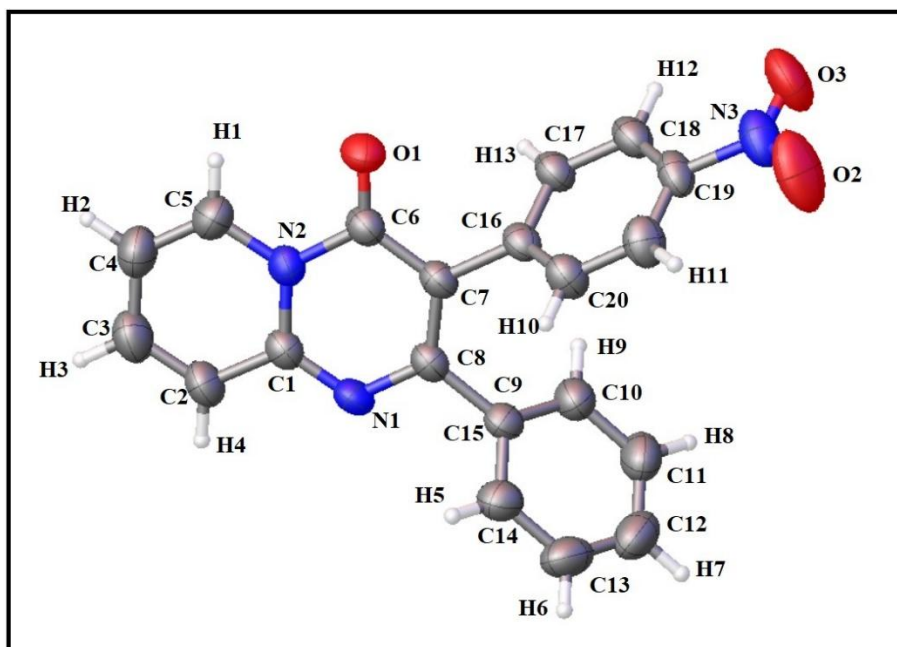


Figure 2.14 ORTEP plot of compound **3s** (CCDC 2225945) with 50% ellipsoid probability

Table 2.2 The single crystal X-ray diffraction data of compound **3s**

Compound name	3-(4-Nitrophenyl)-2-phenyl-4 <i>H</i> -pyrido[1,2- <i>a</i>]pyrimidin-4-one
Empirical formula	C ₂₀ H ₁₃ N ₃ O ₃
Formula weight	343.0957
Temperature/K	293(2)
Wavelength (Å)	0.71073 Å
Crystal system	triclinic
Space group	P-1
a/Å	12.3173(6)
b/Å	12.8009(7)
c/Å	13.8376(7)
α/°	87.743(4)
β/°	65.867(5)

$\gamma/^\circ$	66.105(5)
Volume/ \AA^3	1799.50(18)
Z	2
$\rho_{\text{calc}}/\text{g cm}^{-3}$	1.343
μ/mm^{-1}	0.093
F (000)	756.0
Radiation	MoK α ($\lambda = 0.71073$)
2 Θ range for data collection/ $^\circ$	5.902 to 49.996
Index ranges	$-14 \leq h \leq 14$, $-15 \leq k \leq 15$, $-16 \leq l \leq 16$
Reflections collected	17883
Independent reflections	6299 [$R_{\text{int}} = 0.0425$, $R_{\text{sigma}} = 0.0445$]
Data/restraints/parameters	6299/0/498
Goodness-of-fit on F^2	1.120
Final R indexes [$I \geq 2\sigma(I)$]	$R_1 = 0.0615$, $wR_2 = 0.1738$
Final R indexes [all data]	$R_1 = 0.0908$, $wR_2 = 0.1907$
Largest diff. peak/hole / $e \text{\AA}^{-3}$	0.20/-0.34

2.10 References

1. Baviskar A. T., Madaan C., Preet R., Mohapatra P., Jain V., Agarwal A., Guchhait S. K., Kundu C. N., Banerjee U. C., Bharatam P. V. (2011), N-Fused Imidazoles as Novel Anticancer Agents That Inhibit Catalytic Activity of Topoisomerase II α and Induce Apoptosis in G1/S Phase, *J. Med. Chem.* **54**, 5013-5030 (DOI: 10.1021/jm200235u)
2. Kumar K. A., Kannaboina P., Das P. (2017), Ruthenium-catalyzed site-selective C–H arylation of 2-pyridones and 1-isoquinolinones, *Org. Biomol. Chem.* **15**, 5457-5461 (DOI: 10.1039/C7OB01277B)
3. Zhang B., Studer A. (2015), Recent advances in the synthesis of nitrogen heterocycles via radical cascade reactions using

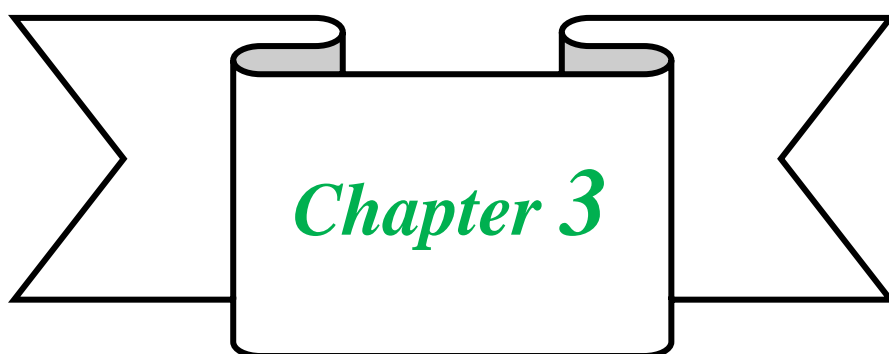
- isonitriles as radical acceptors, *Chem. Soc. Rev.* **44**, 3505-3521 (DOI: 10.1039/C5CS00083A)
4. Chernyak D., Gadamsetty S. B., Gevorgyan V. (2008), Low Temperature Organocopper-Mediated Two-Component Cross Coupling/Cycloisomerization Approach Toward *N*-Fused Heterocycles, *Org. Lett.* **10**, 2307-2310 (DOI: 10.1021/ol8008705)
 5. Bhawale R. T., Chillal A. S., Kshirsagar U. A. (2023), 4*H*-Pyrido[1,2-*a*]pyrimidin-4-one, biologically important fused heterocyclic scaffold: Synthesis and functionalization, *J. Heterocycl. Chem.* **60**, 1356-1373 (DOI: 10.1002/jhet.4637)
 6. Priyadarshani G., Amrutkar S., Nayak A., Banerjee U. C., Kundu C. N., Guchhait S. K. (2016) Scaffold-hopping of bioactive flavonoids: Discovery of aryl-pyridopyrimidinones as potent anticancer agents that inhibit catalytic role of topoisomerase II α , *Eur. J. Med. Chem.* **122**, 43-54 (DOI: 10.1016/j.ejmech.2016.06.024)
 7. Liang Y. F., Steinbock R., Münch A., Stalke D., Ackermann L. (2018), Manganese-Catalyzed Carbonylative Annulations for Redox-Neutral Late-Stage Diversification. *Angew. Chem. Int. Ed.* **130**, 5482-5486 (DOI: 0.1002/ange.201801111)
 8. Peng L., Gao X., Duan L., Ren X., Wu D., Ding K. (2011), Identification of pyrido [1, 2- α] pyrimidine-4-ones as new molecules improving the transcriptional functions of estrogen-related receptor α , *J. Med. Chem.* **54**, 7729-7733 (DOI: 10.1021/jm200976s)
 9. Zhang Z., Wang Z., Li Z. (2022), Three-Component One-Pot Construction of 2-Aryl-4 *H*-benzo [4, 5] thiazolo [3, 2-*a*] pyrimidines Using Solid Calcium Carbide as a Surrogate of Gaseous Acetylene, *Org. Lett.* **24**, 5491-5496 (DOI: 10.1021/acs.orglett.2c02331)

10. Turco S. -D., Sartini S., Sentieri C., Saponaro C., Navarra T., Dario B., Settimo F. -D., Motta C. -L., Basta G. (2014), A novel 2,3-diphenyl-4*H*-pyrido[1,2-*a*]pyrimidin-4-one derivative inhibits endothelial cell dysfunction and smooth muscle cell proliferation/activation, *Eur. J. Med. Chem.* 72, 102-109 (DOI: 10.1016/j.ejmech.2013.11.021)
11. Turco S.-D., Sartini S., Cigni G., Sentieri C., Sbrana S., Battaglia D., Papa A., Settimo F. -D., La Motta C., Basta G. (2015), Synthetic analogues of flavonoids with improved activity against platelet activation and aggregation as novel prototypes of food supplements, *Food Chem.* 175, 494-499 (DOI: 10.1016/j.foodchem.2014.12.005)
12. Jadhav S. B., Fatema S., Patil R. B., Sangshetti J. N., Farooqui M. (2017, Pyrido [1, 2-*a*] pyrimidin-4-ones: Ligand-based Design, Synthesis, and Evaluation as an Anti-inflammatory Agent, *J Heterocycl Chem.* 54, 3299-3313 (DOI: 10.1002/jhet.2950)
13. Jadhav S. B., Fatema S., Sanap G., Farooqui M. (2018), Antitubercular activity and synergistic study of novel pyrazole derivatives, *J Heterocycl Chem.* 55, 1634-1644 (DOI: 10.1002/jhet.3198)
14. Li A.-R., Johnson M. G., Liu J., Chen X., Du X., Mihalic J. T., Deignan J., Gustin D. J., Duquette J., Fu Z., Zhu L., Marcus A. P., Bergeron P., McGee L. R., Danao J., Lemon B., Carabeo T., Sullivan T., Ma J., Tang L., Tonn, G., Collin T. L., Medina J. C. (2018), Optimization of the heterocyclic core of the quinazolinone-derived CXCR3 antagonists, *Bioorg. Med. Chem.* 18, 688-693 (DOI: 10.1016/j.bmcl.2007.11.060)
15. Shulman D. G., Amdahl L., Washington C., Graves A. (2003), A combined analysis of two studies assessing the ocular comfort of antiallergy ophthalmic agents, *Clin Ther* 25, 1096-1106 (DOI: 10.1016/S0149-2918(03)80069-3)

16. Nakayama K., Ishida Y., Ohtsuka M., Kawato H., Yoshida K.-i., Yokomizo Y., Ohta T., Hoshino K., Otani T., Kurosaka Y., Yoshida K., Ishida H., Lee V. J., Renau T. E., Watkins W. J. (2003), MexAB-OprM specific efflux pump inhibitors in *Pseudomonas aeruginosa*, Part 2: achieving activity in vivo through the use of alternative scaffolds, *Bioorg. Med. Chem.* *13*, 4205-4208 (DOI: 10.1016/j.bmcl.2003.07.027)
17. Sadashiva C., Chandra J. N. S., Ponnappa K., Gowda T. V., Rangappa K. S. (2006), Synthesis and efficacy of 1-[bis(4-fluorophenyl)-methyl] piperazine derivatives for acetylcholinesterase inhibition, as a stimulant of central cholinergic neurotransmission in Alzheimer's disease, *Bioorg. Med. Chem.* *16*, 3932-3936 (DOI: 10.1016/j.bmcl.2006.05.030)
18. Motta C. -L., Sartini S., Mugnaini L., Simorini F., Taliani S., Salerno S., Marini A. M., Settimo F. -D., Lavecchia A., Novellino E., Cantore M., Failli P., Ciuffi M. (2007), Pyrido[1,2-*a*]pyrimidin-4-one Derivatives as a Novel Class of Selective Aldose Reductase Inhibitors Exhibiting Antioxidant Activity, *J. Med. Chem.* *50*, 4917-4927 (DOI: 10.1021/jm070398a)
19. Fenton C., Scott L. J. (2005), Risperidone: a review of its use in the treatment of bipolar mania, *CNS drugs* *19*, 429-444 (DOI: 10.2165/00023210-200519050-00005)
20. Kabri Y., Crozet M. D., Primas N., Vanelle P. (2012), One-Pot Chemoselective Bis (Suzuki–Miyaura Cross-Coupling): Efficient Access to 3, 9-Bis [(hetero) aryl]-4*H*-pyrido [1, 2-*a*]pyrimidin-4-one Derivatives Under Microwave Irradiation, *Eur. J. Org. Chem.* 5595-5604 (DOI: 10.1002/ejoc.201200748)
21. La Motta C., Da Settimo F., Dario B., Sartini S., Basta G., Del Turco S., Saponaro C. (2013), Therapeutic agent for treatment of blood vessels, PCT Int. Appl. WO2013144860
22. Guchhait S. K., Priyadarshani G. (2015), Pd-Catalyzed Ag (I)-promoted C3-arylation of pyrido[1,2-*a*]pyrimidin-4-ones with

- bromo/iodo-arenes, *J. Org. Chem.* **80**, 8482-8488 (DOI: 10.1021/acs.joc.5b01573)
23. Wang L., Bao P., Lui W., Liu S., Hu C., Yue H., Daoshan Y., Wei W. (2018), Direct C–H 3-Arylation of Quinoxalin-2(H) ones with Aryl Diazonium Salts under Visible Light Irradiation, *Chinese J. Org. Chem.* **38**, 3189-3196 (DOI: 10.6023/cjoc201807014)
 24. Ghosh I., Marzo L., Das A., Shaikh R., König B. (2016), Visible light mediated photo-redox catalytic arylation reactions, *Acc. Chem. Res.* **49**, 1566-1577 (DOI: 10.1021/acs.accounts.6b00229)
 25. Hermecz I., Mészáros Z., Vasvári-Debreczy L., Horváth Á., Horváth G., Pongor-Csákvári M. (1977), Nitrogen bridgehead compounds. Part 4. 1→3 N→C-acyl migration. Part 2, *J. Chem. Soc., Perkin trans. 1* 1977, 789-795 (DOI: 10.1039/P19770000789)
 26. Schober B. D., Kappe T. (1988), Rearrangement reactions of heterocycles. 12. Rearrangement of 6-substituted pyrido [1, 2-*a*] pyrimidines to isomeric 1, 8-naphthyridines and some of their further reactions, *J. Heterocycl. Chem.* **25**, 1231-1236 (DOI: 10.1002/jhet.5570250436)
 27. Náray-Szabó G., Hermecz I., Mészáros Z. (1974), Reactivity of the pyrido [1, 2-*a*] pyrimidin-4-one ring system, *J. Chem. Soc., Perkin trans.* 1753-1756 (DOI: 10.1039/P19740001753)
 28. Hari D. P., Schroll P., König B. (2012), Metal-free, visible-light-mediated direct C–H arylation of heteroarenes with aryl diazonium salts, *J. Am. Chem. Soc.* **134**, 2958-2961 (DOI: 10.1021/ja212099r)
 29. Zhang J., Chen J., Zhang X., Lei X. (2014), Total syntheses of menisporphine and daurioxoisoporphine C enabled by photo-redox-catalyzed direct C–H arylation of isoquinoline with aryldiazonium salt, *J. Org. Chem.* **79**, 10682-10688 (DOI: 10.1021/jo5020432)

30. Wang C.-S., Dixneuf P. H., Soulé J.-F. (2018), Photo-redox catalysis for building C–C bonds from C (sp²)–H bonds, *Chem. Rev.* **118**, 7532-7585 (DOI: 10.1021/acs.chemrev.8b00077)
31. Babu S. S., Muthuraja P., Yadav P., Gopinath P. (2021), Aryldiazonium salts in photo-redox catalysis—recent trends, *Adv. Synth. Catal.* **363**, 1782-1809 (DOI: 10.1002/adsc.202100136)
32. Bhawale R. T., Kshirsagar U. A. (2023), Visible Light Assisted Direct C3–H Arylation of Pyrido[1,2-*a*]pyrimidin-4-ones and Thiazolo[3,2-*a*]pyrimidin-5-ones, *J. Org. Chem.* **88**, 9537-9542 (DOI: 10.1021/acs.joc.3c00780)
33. Single crystal of product **3s** was grown and structure of it was confirmed with the single crystal x-ray (CCDC No. 2225945).
34. Ravi M., Chauhan P., Kant R., Shukla S. K., Yadav P. P. (2015), Transition-metal-free C-3 arylation of quinoline-4-ones with arylhydrazines, *J. Org. Chem.* **80**, 5369-5376 (DOI: 10.1021/acs.joc.5b00739)
35. Roslan I. I., Lim Q.-X., Han A., Chuah G.-K., Jaenicke S. (2015), Solvent-Free Synthesis of 4*H*-Pyrido[1,2-*a*]pyrimidin-4-ones Catalyzed by BiCl₃: A Green Route to a Privileged Backbone, *Eur. J. Org. Chem.* **2015**, 2351-2355 (DOI: 10.1002/ejoc.201500227)
36. Heinrich M. R., Blank O., Ullrich D., Kirschstein M. (2007), Allylation and vinylation of aryl radicals generated from diazonium salts, *J. Org. Chem.* **72**, 9609-9616 (DOI: 10.1021/jo701717k)



*Synergistic Approach for
Decarboxylative Ortho C–H
Aroylation of 2-Aryl-pyrido[1,2-
a]pyrimidin-4-ones and
Thiazolopyrimidinones*

Chapter 3

Synergistic Approach for Decarboxylative Ortho C–H Aroylation of 2-Aryl-pyrido[1,2-*a*]pyrimidin-4-ones and Thiazolopyrimidinones

3.1 Introduction

The nitrogen-fused heterocyclic motifs are significant to lead molecules because of their wide range of biological activities and applications in pharma, material sciences, and agrochemicals.^[1-4] Amongst them, pyrido[1,2-*a*]pyrimidin-4-one is an intriguing scaffold because of its prevalence in various bioactive molecules, drugs, and natural products (**Figure 3.1**).^[5-8] The derivatives of pyrido[1,2-*a*]pyrimidin-4-one display a wide array of bioactivities, such as acetylcholinesterase inhibition, MexAB-OprM specific efflux pump inhibition, CXCR3 antagonism, anti-ulcer, antipsychotic, anti-allergic, antioxidant, and antihypertensive seganserin.^[9-12] Diaryl ketone motifs are not only found in pharmaceuticals, and natural products but also crucial precursors

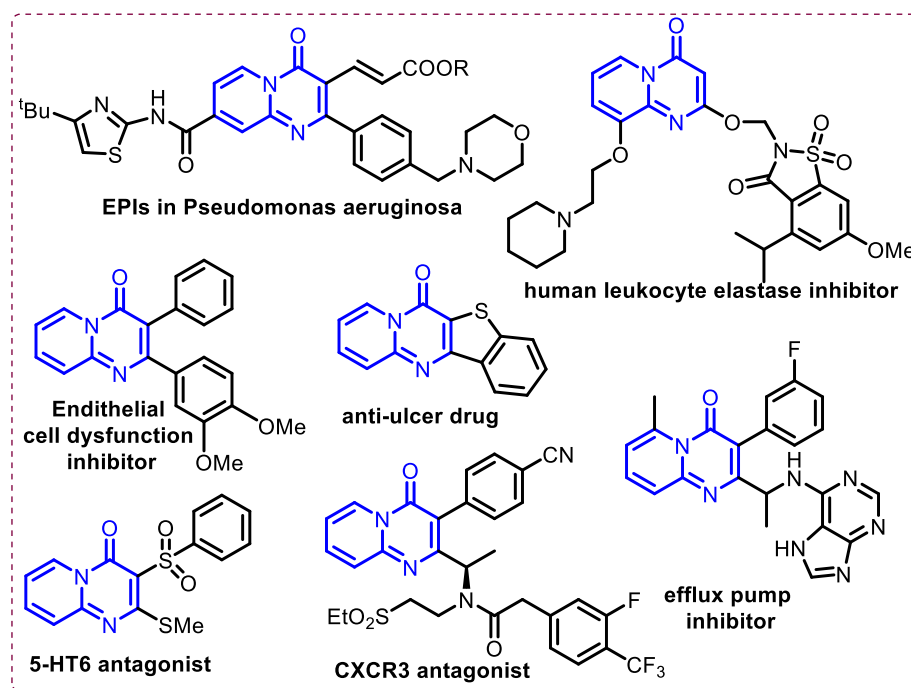
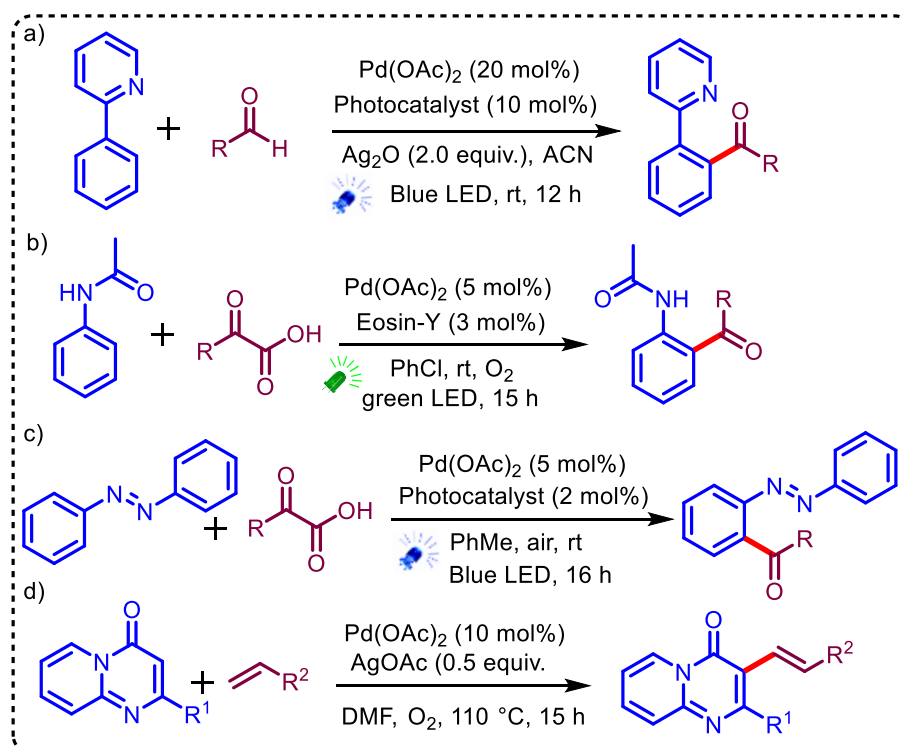


Figure 3.1 Biologically active pyrido[1,2-*a*]pyrimidin-4-ones.

of a wide range of bioactive natural products and bioactive compounds.^[13-15] Friedal-Craft acylation of aromatic rings is the classical, effective, and frequently employed protocol for aryl ketones, which suffers from certain limitations such as stoichiometric use of Lewis acid catalysts, weak regioselectivity, poor functional group tolerance, and harsh reaction conditions.^[16-17] Consequently, alternative approaches and protocols are desirable. In the past few decades, direct C–H functionalization catalyzed by transition metal catalysts has been considerably developed to provide distinctive opportunities for various C–H functionalization reactions including carbonylative derivatization.^[18-20] This invaluable process has a remarkable capacity for the rapid construction of a large number of organic molecules. Still, it has some limitations such as requiring excess stoichiometric amounts of toxic and expensive oxidant and high temperature reactions. Recently, visible light-mediated photo-redox catalysis has emerged as an important and attractive tool for the activation of substrate, generation, and utilization of radical intermediates for a diverse range of organic transformations under extremely mild conditions.^[21-23] Of late, the merger of transition-metal catalysis with photo-redox catalysis has appeared as a very powerful synthetic platform and attracted prominent interest.^[24-25] Exploration of this synergistic blend of ubiquitous catalysis has not only allowed the expansion of potent synthetic conversion which is difficult to access but has also the ability to overcome the disadvantages of the use of one catalyst system.^[26] In this dual catalysis, photocatalysis gives access to the reactive radical intermediates from simple and easily available functional groups and on blend with transition metal catalysis offers unique pathways of direct coupling of non-traditional nucleophilic partners. Successful installation of specific functional groups has been achieved using dual catalysis by merging transition metal catalysis and photocatalysis by different research groups.^[27-29]

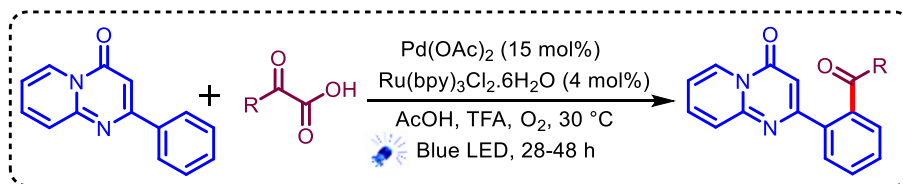
3.2 Previous Reports

A few examples are known for arylation/acylation functionalization by merging transition metal catalysis with photo-redox catalysis.^[13,26,30,31] Palladium-catalyzed C–H acylation of 2-phenyl pyridine with aldehydes has been reported by Xia et al. by merging with photo-redox catalysis (**Scheme 3.1a**).^[13] Because of being the versatile and greener alternative to an acylating agent, α -keto acid performed a crucial role in radical acylation. Ortho-acylation of acetanilids has been developed by Wang et. al. by merging palladium catalysis with a photo-redox catalysis (**Scheme 3.1b**).^[26] Whereas, C–H acylation of azo- and azoxybenzenes was reported with α -keto acid by dual catalysis protocol (**Scheme 3.1c**).^[30] Wang and Cao et. al. developed a palladium-catalyzed dehydrogenative coupling approach for the C3 alkenylation of pyrido[1,2-*a*]pyrimidin-4-ones (**Scheme 3.1d**).^[31]



Scheme 3.1 C–H functionalization of N-containing heterocycles.

3.3 Objective

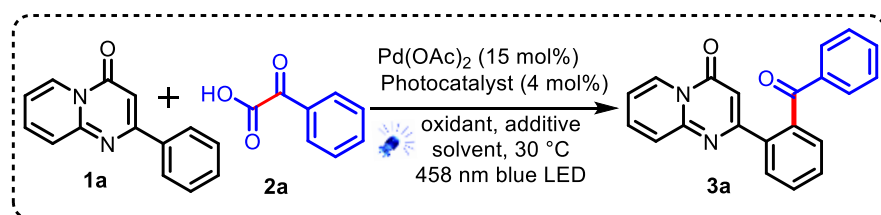


Scheme 3.2 Photoinduced ortho C-H acylation of pyrido[1,2-*a*]pyrimidin-4-one

We have developed a synergistic approach for the acylation of pyrido[1,2-*a*]pyrimidin-4-one using the greener acylating agent α -keto carboxylic acid. In this protocol, we have combined transition metal catalysis with photo-redox catalysis under visible light irradiation. Utilizing oxygen as a green oxidant and acetic acid as the solvent, the reaction proceeds under mild conditions at room temperature for 28-48 hours. (**Scheme 3.2**).^[32]

3.4 Result and Discussion

Our initial investigation commenced with the reaction of 2-phenyl-4*H*-pyrido[1,2-*a*]pyrimidin-4-one (**1a**) with phenyl glyoxylic acid (**2a**) in presence of $\text{Pd}(\text{OAc})_2$ (15 mol%) as transition metal catalyst, $[\text{Ru}(\text{bpy})_3]\text{Cl}_2 \cdot 6\text{H}_2\text{O}$ (4 mol%) as photo-redox catalyst and $\text{K}_2\text{S}_2\text{O}_8$ as oxidant in toluene as solvent at room temperature under the irradiation of 458 nm blue LED. After 48 h expected product **3a** was isolated in 22% yield. (**Table 3.1**; entry 1). The structure of **3a** was characterized and confirmed by NMR spectroscopy, HRMS, and single-crystal X-ray analysis (CCDC no. 2130006). An improved result of product **3a** was obtained when the reaction was carried out in the presence of trifluoroacetic acid (TFA, 0.1 mL) as an additive (61%, entry 2). The use of $\text{Pd}(\text{OTf})_2$ as a catalyst, with and without additive was unable to provide prominent results (entries 3 and 4). With these initial results, the reaction was studied for further optimization of reaction condition first by varying the photocatalyst such as $[\text{Ir}(\text{ppy})_2(\text{dtbbpy})]\text{PF}_6$, rose bengal, and Eosin-Y but change in the photo-redox catalyst provided inferior

Table 3.1 Optimization table^[a]

entry	catalyst	oxidant	solvent	Time	Yield ^[b]
1 ^[c]	[Ru(bpy) ₃]Cl ₂ ·6H ₂ O	K ₂ S ₂ O ₈	Toluene	48	22
2	[Ru(bpy) ₃]Cl ₂ ·6H ₂ O	K ₂ S ₂ O ₈	Toluene	48	61
3 ^[c,d]	[Ru(bpy) ₃]Cl ₂ ·6H ₂ O	K ₂ S ₂ O ₈	Toluene	48	36
4 ^[d]	[Ru(bpy) ₃]Cl ₂ ·6H ₂ O	K ₂ S ₂ O ₈	Toluene	48	53
5	[Ir(ppy) ₂ (dtbbpy)]PF ₆	K ₂ S ₂ O ₈	Toluene	48	54
6	Rose Bengal	K ₂ S ₂ O ₈	Toluene	48	52
7	Eosin Y	K ₂ S ₂ O ₈	Toluene	48	55
8	[Ru(bpy) ₃]Cl ₂ ·6H ₂ O	K ₂ S ₂ O ₈	DCE	48	30
9	[Ru(bpy) ₃]Cl ₂ ·6H ₂ O	K ₂ S ₂ O ₈	ACN	48	22
10	[Ru(bpy) ₃]Cl ₂ ·6H ₂ O	K ₂ S ₂ O ₈	DMSO	48	trace
11	[Ru(bpy) ₃]Cl ₂ ·6H ₂ O	K ₂ S ₂ O ₈	MeOH	48	68
12	[Ru(bpy) ₃]Cl ₂ ·6H ₂ O	K ₂ S ₂ O ₈	Toluene:MeOH	48	65
13	[Ru(bpy) ₃]Cl ₂ ·6H ₂ O	K ₂ S ₂ O ₈	Toluene:H ₂ O	48	40
14	[Ru(bpy) ₃]Cl ₂ ·6H ₂ O	K ₂ S ₂ O ₈	AcOH	28	78
15	[Ru(bpy) ₃]Cl ₂ ·6H ₂ O	Na ₂ S ₂ O ₈	AcOH	28	84
16	[Ru(bpy) ₃]Cl ₂ ·6H ₂ O	(NH ₄) ₂ S ₂ O ₈	AcOH	28	67
17	[Ru(bpy) ₃]Cl ₂ ·6H ₂ O	TBHP	AcOH	28	64
18	[Ru(bpy) ₃]Cl ₂ ·6H ₂ O	DTPB	AcOH	28	60
19	[Ru(bpy) ₃]Cl ₂ ·6H ₂ O	O ₂	AcOH	28	91
20 ^[e]	[Ru(bpy) ₃]Cl ₂ ·6H ₂ O	O ₂	AcOH	28	70
21 ^[f]	[Ru(bpy) ₃]Cl ₂ ·6H ₂ O	O ₂	AcOH	28	42
22	[Ru(bpy) ₃]Cl ₂ ·6H ₂ O	air	AcOH	28	56
23 ^[g]	[Ru(bpy) ₃]Cl ₂ ·6H ₂ O	O ₂	AcOH	28	32
24 ^[h]	[Ru(bpy) ₃]Cl ₂ ·6H ₂ O	O ₂	AcOH	28	53
25 ^[i]	[Ru(bpy) ₃]Cl ₂ ·6H ₂ O	O ₂	AcOH	28	62

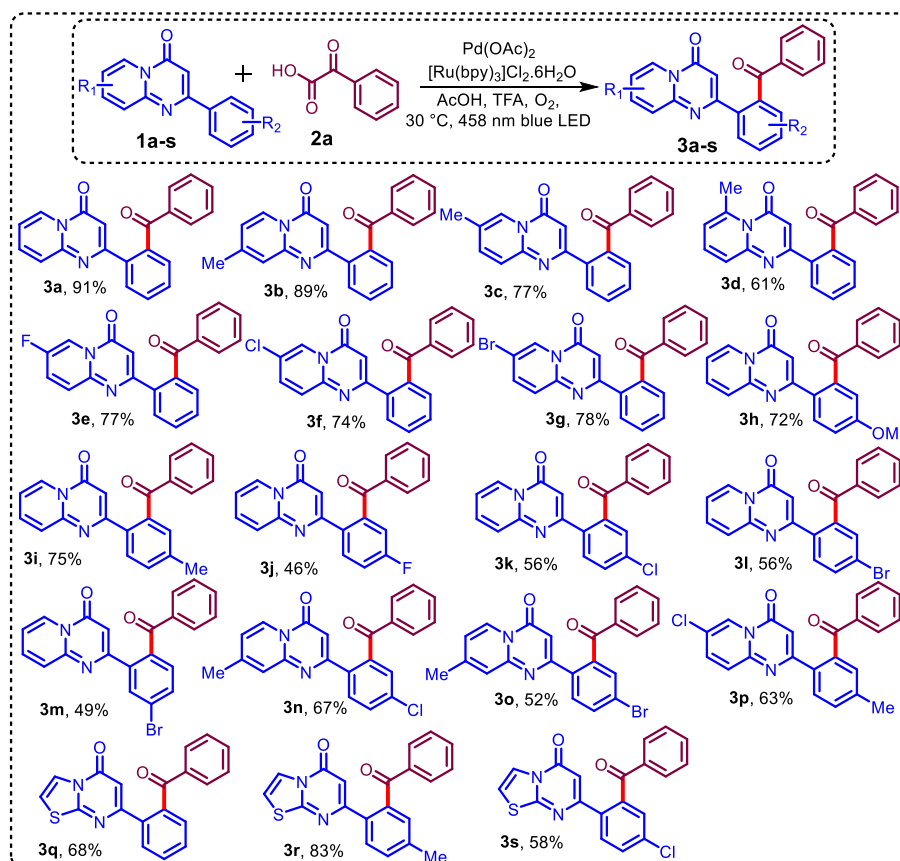
^[a]Reaction conditions: **1a** (0.1 mmol), **2a** (0.3 mmol), Pd(OAc)₂ (15 mol%), photocatalyst (4 mol%), oxidant (4 equiv.), additive (0.1 mL TFA), solvent (2.0 mL), 458 nm blue LED, rt. ^[b]isolated yields. ^[c]without additive. ^[d]Pd(OTf)₂ was used instead of Pd(OAc)₂. ^[e]10 mol% of Pd(OAc)₂ was used. ^[f]5 mol % of Pd(OAc)₂ was used.

[g]without light. [h]0.1 mmol of **2a** was used. [i]0.2 mmol of **2a** was used. TBHP = *tert*-butyl hydroperoxide, DTBP = di-*tert*-butyl peroxide.

results (54%, 52%, 55% respectively, entries 5-7). When the reaction was performed in various solvents of different polarity and combinations of solvents (entries 8-13), only polar protic solvents such as methanol (68% and 65%, entries 11 and 12) offered improved yields. When the reaction was performed in acetic acid, quantitative conversion of starting material was observed in only 28 h to provide a 78% yield of **3a** (entry 14). Upon replacement of oxidant with Na₂S₂O₈ gave desired product **3a** in 84% (entry 15) whereas, a decrease in the yield of **3a** was observed on using other oxidants such as (NH₄)₂S₂O₈, TBHP, DTPB (60-67%; entries 16-18). Gratifyingly, when the reaction was carried out in the presence of eco-friendly and very economical O₂ as a green oxidant, TLC results confirmed a clean reaction within 28 h with complete consumption of starting material **1a** and provided motivating isolated yield of **3a** in 91% (entry 19). Notably, when loading of the Pd(OAc)₂ catalyst was reduced from 15 mol% to 10 and 5 mol%, a decrease in the yield was observed (entries 20-21); whereas the use of ambient air as an oxidant instead of O₂ also afforded **3a** in decreased yield (56%; entry 22). When the reaction was performed in the absence of light, a drastic diminishing in the yield was observed (32%; entry 23). Formation of product **3a** was observed in lower yield when phenyl glyoxylic acid was used in lower equivalents (53 and 62%, entries 24 and 25).

To explore the further substrate scope of this optimized synergistic reaction approach, diverse 2-phenyl-4*H*-pyrido[1,2-*a*]pyrimidin-4-one (**1a-s**) reacted with phenyl glyoxylic acid (**2a**) (Scheme 3.3). When the reaction was performed with methyl substitution at various positions of the pyrido-pyrimidin-4-one ring (**1b-d**), it provided resultant aroylated product **3b-d** (89%, 77%, and 61% respectively). Reaction with halogen-substituted pyrido-pyrimidin-4-ones **1e-g** with phenyl glyoxylic acid (**2a**) under optimized reaction conditions, provided expected product **3e-g** in very good yield (77%, 74%, and 78%

Scheme 3.3 Substrate scope for arylation of pyrido[1,2-*a*]pyrimidin-4-ones^[a]



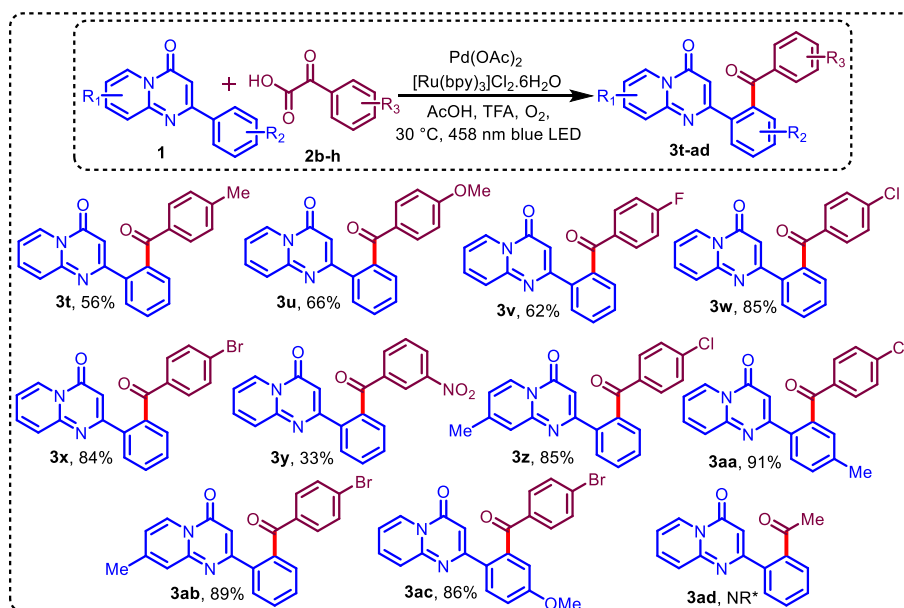
^[a]Reaction conditions: **1** (0.2 mmol), **2** (0.6 mmol), Pd(OAc)₂ (15 mol %), [Ru(bpy)₃]Cl₂·6H₂O (4 mol %), AcOH (4.0 mL), TFA (0.2 mL), O₂, rt, 28–48 h, 458 nm blue LED.

respectively). Electron-releasing groups such as methoxy and methyl on 2-phenyl ring gave the desired product in 72% and 75% yield respectively. Whereas reaction with 2-phenyl-4*H*-pyrido[1,2-*a*]pyrimidin-4-one having electron-withdrawing halogen groups on the 2-phenyl ring as well as on pyrido ring provided expected products (**3j–p**) in moderate yields (46–67%). When 7-phenyl-5*H*-thiazolo[3,2-*a*]pyrimidin-5-one (**1q–s**) was subjected under synergistic arylation conditions, delightfully it provided corresponding expected products (**3q–s**) in good to excellent yields (58–83%).

Further, the influence of substituted phenyl glyoxylic acid on the reactivity of dual catalytic arylation was investigated (**Scheme 3.4**). When 4-methylphenyl glyoxylic acid was treated with 2-phenyl-4*H*-pyrido[1,2-*a*]pyrimidin-4-one under optimized reactions, it provided an expected product in 56% yield. Whereas,

4-methoxy phenyl glyoxylic acid under similar conditions provided an expected product in 66% yield. Phenyl glyoxylic acid having moderated electron-withdrawing groups such as F, Cl, and Br provided desired products **3v-x** in very good yields (62-85%) under optimized reaction conditions. Whereas very strong electron-withdrawing groups on phenyl glyoxylic acid such as the nitro group also provided a desired product in only 33% yield. Substitution of halogen on phenyl glyoxylic acid and methyl/methoxy group on 2-phenyl-4*H*-pyrido[1,2-*a*]pyrimidin-4-one under optimized conditions provided desired products in excellent yields (85-91%). When 2-oxo propanoic acid was treated with 2-phenyl-4*H*-pyrido-[1,2-*a*]pyrimidin-4-one under this dual catalytic reaction condition, no desired product (**3ad**) was observed.

Scheme 3.4 Substrate scope of α -oxo carboxylic acids^[a]

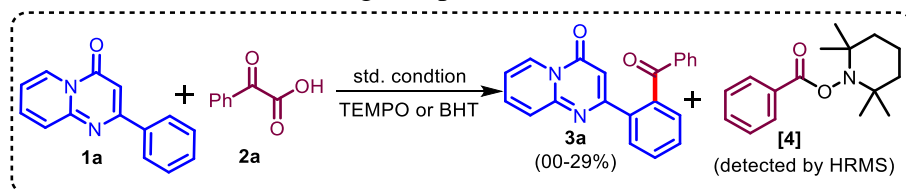


^[a]Reaction conditions: **1** (0.2 mmol), **2** (0.6 mmol), $\text{Pd}(\text{OAc})_2$ (15 mol %), $[\text{Ru}(\text{bpy})_3]\text{Cl}_2 \cdot 6\text{H}_2\text{O}$ (4 mol %), AcOH (4.0 mL), TFA (0.2 mL), O_2 , rt, 28-48 h, 458 nm blue LED.

To gain insights into the mechanistic pathway, a control experiments were carried out. Decarboxylative acylation was tried under standard reaction conditions in the presence of different equivalents of TEMPO as a radical quencher. Only 29% and 16% of the desired product were

formed when 2 and 3 equivalents of TEMPO were present in the reaction respectively (**Scheme 3.5**). The formation of the desired

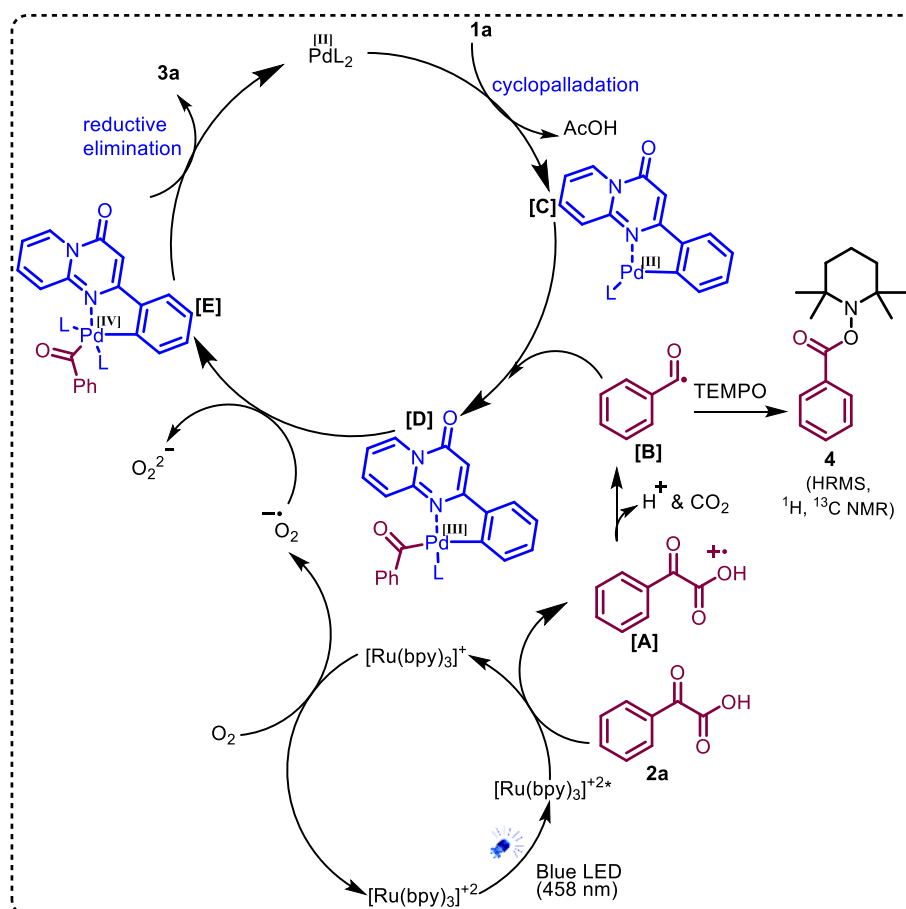
Scheme 3.5 Radical scavenger experiment



product was not observed in the presence of 4 and 5 equivalent of TEPMO, but the formation of acyl-trapped intermediate **4** was observed. Moreover, complete inhibition of the formation of desired product **3a** was observed when the reaction was performed in the presence of 3 and 4 equivalent of 3,5-di-*tert*-butyl-4-hydroxytoluene (BHT) respectively.

A plausible synergistic catalytic mechanism is proposed as shown in **scheme 3.6** based on literature study and controlled experiments^[13, 33-34]

Scheme 3.6 Proposed mechanism for synergistic arylation



.Photoexcitation of photo-catalyst $[\text{Ru}(\text{bpy})_3]^{2+}$ by visible light generates its excited state $[\text{Ru}(\text{bpy})_3]^{2+*}$. $[\text{Ru}(\text{bpy})_3]^{2+*}$ oxidizes phenyl glyoxylic acid (**2a**) to intermediate **A** and undergoes reduction to $[\text{Ru}(\text{bpy})_3]^+$. Intermediate **A** generates acyl radical intermediate (**B**) via decarboxylation. Molecular oxygen regenerates $[\text{Ru}(\text{bpy})_3]^{2+}$ by oxidizing $[\text{Ru}(\text{bpy})_3]^+$. Whereas, the palladium catalytic cycle can be commenced with C–H activation of 2-phenyl-pyrido[1,2-*a*]pyrimidin-4-one (**1a**) to generate palladacycle intermediate (**C**). This intermediate (**C**) would undergo oxidative coupling with radical intermediate (**B**), to furnish the putative Pd(III) intermediate (**D**) and then Pd(IV) intermediate (**E**) under oxidative conditions. Reductive elimination from the intermediate (**E**) would lead to the desired acylated product **3a** alongside Pd(II) species for the next catalytic cycle.

3.5 Summary

In this chapter, we developed a very mild and efficient synergistic aroylation of 2-aryl-pyrido[1,2-*a*]pyrimidin-4-ones by merging with a palladium-catalyst with a ruthenium photocatalyst under visible light irradiation in the presence of greener oxygen as oxidant using extremely mild conditions for C–H functionalization with good functional group tolerance. Having said that, the significant therapeutic of pyrido[1,2-*a*]pyrimidin-4-one and aryl ketones, this blend of the mild catalytic process of decarboxylative aroylation and aroylated products would be very attractive for applications and further synthetic modification for drug design and SAR.

3.6 Experimental section

The General procedure for synthesis of substituted pyrido[1,2-*a*]pyrimidin-4-ones (**1**)

All the starting material **1** were prepared using the reported procedure.^[35] A mixture of substituted 2-aminopyridine (1.0 mmol) and the substituted β -keto ester (1.5 mmol) in

polyphosphoric acid (2.00 g) was heated at 100 °C temperature with vigorous stirring under a nitrogen atmosphere. After 3.0 h, the mixture was cooled in an ice bath and neutralized with 5% aqueous sodium hydroxide. The solid precipitate was collected by filtration and washed with water. The crude products were purified by recrystallization from ethanol to give the corresponding products.

General procedure for decarboxylative arylation of pyrido[1,2-*a*]pyrimidin-4-one derivatives (3a-ac)

2-phenyl-4*H*-pyrido[1,2-*a*]pyrimidin-4-one (**1**, 0.2 mmol), 2-oxo-2-phenylacetic acid (**2**, 0.6 mmol), Pd(OAc)₂ (15 mol%), [Ru(bpy)₃]Cl₂·6H₂O (4 mol%), TFA (0.2 mL), AcOH (4 mL) were added to an oven dried reaction vessel equipped with magnetic stirring bar and reaction mixture was irradiated using 458 nm blue LED under O₂ atmosphere (O₂ balloon) for 28-48 h. Reaction progress was monitored by TLC. After completion of reaction, the reaction mixture was quenched by adding 10% NaHCO₃ (10 mL), and the resulting reaction mixture was extracted with EtOAc (3 × 25 mL) and was washed with brine solution and dried over Na₂SO₄. The combined organic layer was concentrated under reduced pressure to yield crude product and was purified by silica gel column chromatography (ethyl acetate: petroleum ether/Hexane 3:10) to give the desired product **3a-ac**. The ortho-arylated products were successfully characterized and confirmed through multiple analytical techniques, including ¹H NMR, ¹³C NMR spectroscopy, high-resolution mass spectrometry (HRMS), and infrared (IR) spectroscopy in the solid state (KBr). These complementary methods provided robust evidence for the structural integrity and purity of the synthesized compounds.

3.7 Characterization data of 3a-ac

2-(2-Benzoylphenyl)-4*H*-pyrido[1,2-*a*] pyrimidin-4-one (3a):
Reaction time: 28 h; white solid; 91% (59 mg); m.p.166-168 °C; ¹H NMR (500 MHz, CDCl₃): δ 8.92 (d, *J* = 5.3 Hz, 1H), 7.84 (d, *J* = 7.5

Hz, 1H), 7.75 (d, $J = 8.1$ Hz, 2H), 7.64 – 7.57 (m, 3H), 7.54 (d, $J = 7.3$ Hz, 1H), 7.38 (t, $J = 8.7$ Hz, 1H), 7.28 (t, $J = 7.7$ Hz, 2H), 7.21 (d, $J = 8.9$ Hz, 1H), 7.04 (t, $J = 6.9$ Hz, 1H), 6.76 (s, 1H); **^{13}C NMR** (126 MHz, CDCl_3): $\delta = 197.7, 161.9, 158.3, 150.0, 140.3, 138.2, 137.5, 136.4, 132.5, 130.3, 130.1, 129.2, 129.1, 128.7, 128.2, 127.2, 126.1, 115.6, 101.9$; **IR** (neat, KBr): 1689, 1627, 1444, 1274, 929, 777, 611 cm^{-1} ; **HRMS** (ESI, m/z): calculated for $\text{C}_{21}\text{H}_{14}\text{N}_2\text{O}_2\text{Na}^+ [\text{M}+\text{Na}]^+$: 349.0947, found: 349.0947.

2-(2-Benzoylphenyl)-8-methyl-4H-pyrido[1,2-*a*]pyrimidin-4-one

(3b): Reaction time: 32 h; white solid; 89% (61mg), m.p.176-178 $^{\circ}\text{C}$; **^1H NMR** (500 MHz, CDCl_3): δ 8.73 (d, $J = 7.1$ Hz, 1H), 7.75 (d, $J = 7.3$ Hz, 1H), 7.66 (d, $J = 7.5$ Hz, 2H), 7.56 - 7.42 (m, 3H), 7.31 (t, $J = 7.2$ Hz, 1H), 7.21 (t, $J = 7.5$ Hz, 2H), 6.92 (s, 1H), 6.80 (d, $J = 6.9$ Hz, 1H), 6.61 (s, 1H), 2.30 (s, 3H); **^{13}C NMR** (126 MHz, CDCl_3): $\delta = 197.6, 162.0, 158.3, 149.9, 148.6, 140.1, 138.1, 137.6, 132.3, 130.1, 129.9, 129.0, 128.9, 128.5, 128.0, 126.4, 124.0, 118.2, 100.9, 21.4$; **IR** (neat, KBr): 1693, 1577, 1496, 1460, 1180, 759, 621 cm^{-1} ; **HRMS** (ESI, m/z): calculated for $\text{C}_{22}\text{H}_{17}\text{N}_2\text{O}_2 [\text{M}+\text{H}]^+$: 341.1285, found: 341.1294

2-(2-Benzoylphenyl)-7-methyl-4H-pyrido[1,2-*a*]pyrimidin-4-one

(3c): Reaction time: 32 h; white solid; 77% (53mg), m.p.178-180 $^{\circ}\text{C}$; **^1H NMR** (500 MHz, CDCl_3): δ 8.72 (s, 1H), 7.82 (d, $J = 7.5$ Hz, 1H), 7.72 (d, $J = 7.7$ Hz, 2H), 7.62-7.52 (m, 3H), 7.46 (d, $J = 9.0$ Hz, 1H), 7.36 (t, $J = 7.4$ Hz, 1H), 7.26 (t, $J = 7.6$ Hz, 2H), 7.16 (d, $J = 9.0$ Hz, 1H), 6.73 (s, 1H), 2.35 (s, 3H); **^{13}C NMR** (126 MHz, CDCl_3): $\delta = 197.7, 161.4, 158.2, 148.9, 140.2, 139.4, 138.2, 137.5, 132.4, 130.3, 130.0, 129.0, 129.0, 128.5, 128.2, 126.0, 125.5, 124.7, 101.6, 18.4$; **IR** (neat, KBr): 1677, 1527, 1454, 1386, 1118, 773, 619 cm^{-1} ; **HRMS** (ESI, m/z): calculated for $\text{C}_{22}\text{H}_{17}\text{N}_2\text{O}_2 [\text{M}+\text{H}]^+$: 341.1285, found: 341.1291.

2-(2-Benzoylphenyl)-6-methyl-4H-pyrido[1,2-*a*]pyrimidin-4-one

(3d): Reaction time: 48 h; grey white solid; 61% (42mg), m.p.168-170 $^{\circ}\text{C}$; **^1H NMR** (500 MHz, CDCl_3): δ 7.82 (d, $J = 7.1$ Hz, 1H), 7.75 (d, $J = 7.5$ Hz, 2H), 7.60-7.50 (m, 3H), 7.41 (t, $J = 7.2$ Hz, 1H), 7.33 - 7.27

(m, 3H), 6.93 (d, $J = 8.8$ Hz, 1H), 6.58-6.54 (m, 2H), 2.98 (s, 3H); ^{13}C NMR (126 MHz, CDCl_3): $\delta = 197.6, 162.6, 160.0, 152.5, 144.0, 140.2, 138.3, 136.9, 135.4, 132.4, 130.2, 130.0, 129.1, 128.9, 128.4, 128.2, 124.9, 118.4, 104.0, 24.7$; IR (neat, KBr): 1689, 1498, 1458, 1284, 1116, 769, 621 cm^{-1} ; HRMS (ESI, m/z): calculated for $\text{C}_{22}\text{H}_{17}\text{N}_2\text{O}_2$ $[\text{M}+\text{H}]^+$: 341.1285, found: 341.1285.

2-(2-Benzoylphenyl)-7-flouro-4H-pyrido[1,2-a]pyrimidin-4-one

(3e): Reaction time: 48 h; matte brown solid; 77% (53mg), m.p.176-178 °C; ^1H NMR (500 MHz, CDCl_3): δ 8.82 (s, 1H), 7.82 (d, $J = 7.5$ Hz, 1H), 7.73 (d, $J = 7.7$ Hz, 2H), 7.63 - 7.57 (m, 2H), 7.53 - 7.49 (m, 2H), 7.40 (t, $J = 7.5$ Hz, 1H), 7.29 (t, $J = 7.6$ Hz, 2H), 7.23 - 7.20 (m, 1H), 6.77 (s, 1H); ^{13}C NMR (126 MHz, CDCl_3): $\delta = 197.6, 161.6, 157.8, 155.1$ (d, $J_{\text{CF}} = 246.3$ Hz), 148.0, 140.3, 138.0, 137.2, 132.6, 130.3, 130.2, 129.2, 129.1, 129.0 (d, $J_{\text{CF}} = 25.3$ Hz), 128.7, 128.3, 128.0 (d, $J_{\text{CF}} = 7.3$ Hz), 113.6 (d, $J_{\text{CF}} = 41.2$ Hz), 101.7; IR (neat, KBr): 1703, 1589, 1531, 1452, 1284, 1114, 842, 619 cm^{-1} ; HRMS (ESI, m/z): calculated for $\text{C}_{21}\text{H}_{14}\text{FN}_2\text{O}_2$ $[\text{M}+\text{H}]^+$: 345.1034, found: 345.1037.

2-(2-Benzoylphenyl)-7-chloro-4H-pyrido[1,2-a]pyrimidin-4-one

(3f): Reaction time: 32 h; pale yellow solid; 74% (53mg), m.p.166-168 °C; ^1H NMR (500 MHz, CDCl_3): δ 8.93 (s, 1H), 7.82 (d, $J = 7.4$ Hz, 1H), 7.73 (d, $J = 7.7$ Hz, 2H), 7.63 - 7.57 (m, 2H), 7.53 - 7.50 (m, 2H), 7.40 (t, $J = 7.4$ Hz, 1H), 7.30 (t, $J = 7.6$ Hz, 2H), 7.15 (d, $J = 9.4$ Hz, 1H), 6.77 (s, 1H); ^{13}C NMR (126 MHz, CDCl_3): $\delta = 197.5, 161.8, 157.3, 148.4, 140.3, 138.0, 137.7, 137.0, 132.6, 130.4, 130.3, 129.1$ (2C), 128.7, 128.3, 127.0, 125.0, 124.3, 102.4; IR (neat, KBr): 1688, 1622, 1450, 1386, 1124, 767, 617 cm^{-1} ; HRMS (ESI, m/z): calculated for $\text{C}_{21}\text{H}_{14}\text{ClN}_2\text{O}_2$ $[\text{M}+\text{H}]^+$: 361.0738, found: 361.0739.

2-(2-Benzoylphenyl)-7-bromo-4H-pyrido[1,2-a]pyrimidin-4-one

(3g): Reaction time: 32 h; pale yellow solid; 78% (63mg), m.p.170-172 °C; ^1H NMR (500 MHz, CDCl_3): δ 9.04 (s, 1H), 7.82 (d, $J = 7.4$ Hz, 1H), 7.73 (d, $J = 7.7$ Hz, 2H), 7.63 - 7.57 (m, 3H), 7.54 (d, $J = 7.1$ Hz, 1H), 7.41 (t, $J = 7.4$ Hz, 1H), 7.30 (t, $J = 7.6$ Hz, 2H), 7.08 (d, $J = 9.4$

Hz, 1H), 6.78 (s, 1H); **¹³C NMR** (126 MHz, CDCl₃): δ = 197.5, 161.9, 157.2, 148.5, 140.3, 139.8, 138.0, 137.1, 132.6, 130.3, 130.3, 129.1(2C), 128.7, 128.3, 127.4, 127.0, 110.9, 102.5; **IR** (neat, KBr): 1679, 1620, 1446, 1384, 1116, 767, 617 cm⁻¹; **HRMS** (ESI, m/z): calculated for C₂₁H₁₄BrN₂O₂ [M+H]⁺: 405.0233, found: 405.0236.

2-(2-Benzoyl-4-methoxyphenyl)-4H-pyrido[1,2-a]pyrimidin-4-one

(3h): Reaction time: 28 h; white solid; 72% (51mg), m.p.148-150 °C; **¹H NMR** (500 MHz, CDCl₃): δ 8.89 (d, *J* = 6.9 Hz, 1H), 7.80 (d, *J* = 8.6 Hz, 1H), 7.75 (d, *J* = 7.7 Hz, 2H), 7.55 (t, *J* = 7.7 Hz, 1H), 7.37 (t, *J* = 7.4 Hz, 1H), 7.30 (t, *J* = 7.6 Hz, 2H), 7.11 (t, *J* = 8.7 Hz, 2H), 7.01 - 6.98 (m, 2H), 6.71 (s, 1H), 3.88 (s, 3H); **¹³C NMR** (126 MHz, CDCl₃): δ = 197.2, 161.3, 161.1, 158.3, 149.8, 142.1, 138.1, 136.3, 132.4, 130.0, 129.3, 129.0, 128.2, 127.2, 125.8, 115.8, 115.3, 114.2, 100.6, 55.7; **HRMS** (ESI, m/z): calculated for C₂₂H₁₇N₂O₃ [M+H]⁺: 357.1234, found: 357.1234.

2-(2-Benzoyl-4-methylphenyl)-4H-pyrido[1,2-a]pyrimidin-4-one

(3i): Reaction time: 28 h; light brown solid; 75% (51mg), m.p.172-174 °C; **¹H NMR** (500 MHz, CDCl₃): δ 8.90 (d, *J* = 7.2 Hz, 1H), 7.74 (d, *J* = 7.8 Hz, 3H), 7.57 (t, *J* = 7.9 Hz, 1H), 7.42 - 7.36 (m, 2H), 7.33 (s, 1H), 7.29 (d, *J* = 7.7 Hz, 2H), 7.18 (d, *J* = 8.9 Hz, 1H), 7.01 (t, *J* = 6.9 Hz, 1H), 6.74 (s, 1H), 2.45 (s, 3H); **¹³C NMR** (126 MHz, CDCl₃): δ = 197.9, 161.7, 158.3, 149.9, 140.7, 140.3, 138.3, 136.3, 134.5, 132.3, 130.9, 129.6, 129.0, 128.5, 128.2, 127.2, 126.0, 115.4, 101.3, 21.4; **HRMS** (ESI, m/z): calculated for C₂₂H₁₇N₂O₂ [M+H]⁺: 341.1285, found: 341.1285.

2-(2-Benzoyl-4-fluorophenyl)-4H-pyrido[1,2-a]pyrimidin-4-one

(3j): Reaction time: 48 h; light brown solid; 46% (32mg), m.p.154-156 °C; **¹H NMR** (500 MHz, CDCl₃): δ 8.91 (d, *J* = 7.2 Hz, 1H), 7.85 - 7.82 (m, 1H), 7.74 (d, *J* = 7.7 Hz, 2H), 7.59 (t, *J* = 7.9 Hz, 1H), 7.41 (t, *J* = 7.4 Hz, 1H), 7.30 (t, *J* = 7.7 Hz, 3H), 7.24 - 7.22 (m, 1H), 7.16 (d, *J* = 8.9 Hz, 1H), 7.04 (t, *J* = 6.9 Hz, 1H), 6.71 (s, 1H); **¹³C NMR** (126 MHz, CDCl₃): δ = 196.0, 164.6 (d, *J*_{CF} = 253.4 Hz), 160.7, 158.2, 150.0, 142.7,

(d, J_{CF} = 6.8 Hz), 137.6, 136.6, 133.5 (d, J_{CF} = 3.3 Hz), 132.8, 130.8 (d, J_{CF} = 8.5 Hz), 129.1, 128.4, 127.3, 126.0, 117.3, (d, J_{CF} = 21.6 Hz), 116.4 (d, J_{CF} = 23.2 Hz), 115.6, 101.5; **IR** (neat, KBr): 1685, 1589, 1454, 1390, 1114, 835, 621 cm^{-1} ; **HRMS** (ESI, m/z): calculated for $\text{C}_{21}\text{H}_{14}\text{FN}_2\text{O}_2$ $[\text{M}+\text{H}]^+$: 345.1034, found: 345.1034.

2-(2-Benzoyl-4-chlorophenyl)-4H-pyrido[1,2-a]pyrimidin-4-one

(3k): Reaction time: 28 h; white solid; 56% (40mg), m.p.160-162 °C; **^1H NMR** (500 MHz, CDCl_3): δ 8.92 (d, J = 7.1 Hz, 1H), 7.79 (d, J = 8.3 Hz, 1H), 7.74 (d, J = 7.7 Hz, 2H), 7.62 - 7.57 (m, 2H), 7.50 (d, J = 2.2 Hz, 1H), 7.41 (t, J = 7.4 Hz, 1H), 7.31 (t, J = 7.6 Hz, 2H), 7.16 (d, J = 8.8 Hz, 1H), 7.05 (t, J = 6.9 Hz, 1H), 6.73 (s, 1H); **^{13}C NMR** (126 MHz, CDCl_3): δ = 196.0, 160.6, 158.2, 150.0, 141.9, 137.7, 136.6, 136.5, 135.8, 132.8, 130.3, 129.9, 129.1, 129.0, 128.4, 127.3, 126.0, 115.7, 101.6; **IR** (neat, KBr): 1687, 1631, 1454, 1388, 1110, 777, 617 cm^{-1} ; **HRMS** (ESI, m/z): calculated for $\text{C}_{21}\text{H}_{14}\text{ClN}_2\text{O}_2$ $[\text{M}+\text{H}]^+$: 361.0738, found: 361.0738.

2-(2-Benzoyl-4-bromophenyl)-4H-pyrido[1,2-a]pyrimidin-4-one

(3l): Reaction time: 32 h; pale yellow solid; 56% (45mg), m.p.166-168 °C; **^1H NMR** (500 MHz, CDCl_3): δ 8.92 (d, J = 8.9 Hz, 1H), 7.75 – 7.70 (m, 4H), 7.65 (d, J = 2.0 Hz, 1H), 7.61 – 7.58 (m, 1H), 7.41 (t, J = 7.4 Hz, 1H), 7.31 (t, J = 7.7 Hz, 2H), 7.16 (d, J = 8.9 Hz, 1H), 7.05 (t, J = 6.2 Hz, 1H), 6.73 (s, 1H); **^{13}C NMR** (126 MHz, CDCl_3): δ = 195.9, 160.7, 158.2, 150.0, 142.0, 137.6, 136.6, 136.2, 133.2, 132.8, 131.9, 130.0, 129.1, 128.4, 127.3, 126.0, 124.7, 115.7, 101.6; **HRMS** (ESI, m/z): calculated for $\text{C}_{21}\text{H}_{14}\text{BrN}_2\text{O}_2$ $[\text{M}+\text{H}]^+$: 405.0233, found: 405.0231.

2-(2-Benzoyl-5-bromophenyl)-4H-pyrido[1,2-a]pyrimidin-4-one

(3m): Reaction time: 48 h; pale yellow solid; 49% (40mg), m.p.172-174 °C; **^1H NMR** (500 MHz, CDCl_3): δ 8.92 (d, J = 7.2 Hz, 1H), 7.97 (d, J = 1.9 Hz, 1H), 7.72 (d, J = 7.9 Hz, 3H), 7.64 - 7.60 (m, 1H), 7.42 - 7.38 (m, 2H), 7.29 (t, J = 7.7 Hz, 2H), 7.23 (d, J = 8.9 Hz, 1H), 7.06 (t, J = 6.9 Hz, 1H), 6.69 (s, 1H); **^{13}C NMR** (126 MHz, CDCl_3): δ = 196.7, 160.5, 158.0, 150.2, 139.5, 138.9, 137.8, 136.7, 133.0, 132.7, 131.6,

130.6, 129.1, 128.3, 127.3, 126.1, 124.4, 115.8, 102.2; **HRMS** (ESI, m/z): calculated for $C_{21}H_{14}BrN_2O_2$ $[M+H]^+$: 405.0233, found: 405.0231.

2-(2-Benzoyl-4-chlorophenyl)-8-methyl-4H-pyrido[1,2-

a]pyrimidin-4-one (3n): Reaction time: 48 h; light green solid; 67% (50mg), m.p.176-178 °C; **1H NMR** (500 MHz, $CDCl_3$): δ 8.79 (d, J = 7.3 Hz, 1H), 7.77 (d, J = 8.4 Hz, 1H) 7.73 (d, J = 7.7 Hz, 2H), 7.57 (d, J = 8.4 Hz, 1H), 7.48 (d, J = 1.8 Hz, 1H), 7.40 (t, J = 7.4 Hz, 1H), 7.30 (t, J = 7.6 Hz, 2H), 6.93 (s, 1H), 6.87 (d, J = 7.2 Hz, 1H), 6.64 (s, 1H), 2.36 (s, 3H); **^{13}C NMR** (126 MHz, $CDCl_3$): δ = 196.0, 160.8, 158.3, 150.0, 148.9, 141.8, 137.7, 136.4, 136.0, 132.7, 130.2, 129.8, 129.1, 129.0, 128.3, 126.5, 124.0, 118.4, 100.7, 21.5; **IR** (neat, KBr): 1689, 1583, 1496, 1386, 1105, 829, 615 cm^{-1} ; **HRMS** (ESI, m/z): calculated for $C_{22}H_{16}ClN_2O_2$ $[M+H]^+$: 375.0895, found: 375.0895.

2-(2-Benzoyl-4-bromophenyl)-8-methyl-4H-pyrido[1,2-

a]pyrimidin-4-one (3o): Reaction time: 48 h; white solid; 52% (43mg), m.p.172-174 °C; **1H NMR** (500 MHz, $CDCl_3$): δ 8.80 (d, J = 7.2 Hz, 1H), 7.74 - 7.69 (m, 4H), 7.64 (d, J = 2.0 Hz, 1H), 7.41 (t, J = 7.4 Hz, 1H), 7.31 (t, J = 7.6 Hz, 2H), 6.94 (s, 1H), 6.88 (d, J = 7.3 Hz, 1H), 6.65 (s, 1H), 2.37 (s, 3H); **^{13}C NMR** (126 MHz, $CDCl_3$): δ = 195.9, 160.9, 158.3, 150.0, 148.9, 141.9, 137.7, 136.5, 133.2, 132.7, 131.9, 130.0, 129.1, 128.4, 126.6, 124.6, 124.0, 118.4, 100.8, 21.5; **HRMS** (ESI, m/z): calculated for $C_{22}H_{16}BrN_2O_2$ $[M+H]^+$: 419.0390, found: 419.0388.

2-(2-Benzoyl-4-methylphenyl)-7-chloro-4H-pyrido[1,2-

a]pyrimidin-4-one (3p): Reaction time: 48 h; white solid; 63% (47mg), m.p.176-178 °C; **1H NMR** (500 MHz, $CDCl_3$): δ 8.91 (d, J = 2.4 Hz, 1H), 7.72 - 7.70 (m, 3H), 7.50 (dd, J = 9.5, 2.4 Hz, 1H), 7.42 - 7.37 (m, 2H), 7.32 (d, J = 1.7 Hz, 1H), 7.28 (t, J = 7.6 Hz, 2H), 7.11 (d, J = 9.4 Hz, 1H), 6.75 (s, 1H), 2.45 (s, 3H); **^{13}C NMR** (126 MHz, $CDCl_3$): δ = 197.7, 161.7, 157.4, 148.3, 141.0, 140.4, 138.2, 137.5, 134.1, 132.5, 131.0, 129.7, 129.1, 128.5, 128.3, 126.9, 125.1, 124.1, 101.9, 21.4; **HRMS** (ESI, m/z): calculated for $C_{22}H_{16}ClN_2O_2$ $[M+H]^+$: 375.0895, found: 375.0890.

7-(2-Benzoylphenyl)-5*H*-thiazolo[3,2-*a*]pyrimidin-5-one (3q):

Reaction time: 48 h; pale yellow solid; 68% (45mg), m.p.166-168 °C; **¹H NMR** (500 MHz, CDCl₃): δ 7.85 (d, *J* = 4.9 Hz, 1H), 7.74 (d, *J* = 7.3 Hz, 1H), 7.69 (d, *J* = 7.2 Hz, 1H), 7.61 - 7.53 (m, 3H), 7.39 (t, *J* = 7.3 Hz, 1H), 7.29 (t, *J* = 7.6 Hz, 2H), 6.90 (d, *J* = 4.9 Hz, 1H), 6.53 (s, 1H); **¹³C NMR** (126 MHz, CDCl₃): δ = 197.5, 161.8, 161.5, 158.6, 139.8, 138.0, 137.0, 132.6, 130.5, 130.1, 129.4, 129.0, 128.7, 128.3, 121.8, 111.8, 103.4; **IR** (neat, KBr): 1677, 1595, 1461, 1384, 1118, 783, 619 cm⁻¹; **HRMS** (ESI, *m/z*): calculated for C₁₉H₁₃N₂O₂S[M+H]⁺: 333.0692, found: 333.0685.

7-(2-Benzoyl-4-methylphenyl)-5*H*-thiazolo[3,2-*a*]pyrimidin-5-one

(3r): Reaction time: 48 h; brown solid; 83% (57mg), m.p.164-166 °C; **¹H NMR** (500 MHz, CDCl₃): δ 7.84 (d, *J* = 4.9 Hz, 1H), 7.69 (d, *J* = 7.9 Hz, 2H), 7.65 (d, *J* = 7.9 Hz, 1H), 7.41 - 7.34 (m, 3H), 7.29 (t, *J* = 7.6 Hz, 2H), 6.88 (d, *J* = 4.9 Hz, 1H), 6.52 (s, 1H), 2.45 (s, 3H); **¹³C NMR** (126 MHz, CDCl₃): δ = 197.8, 161.7, 161.4, 158.3, 140.8, 139.8, 138.1, 134.0, 132.5, 131.1, 129.9, 128.9, 128.5, 128.3, 121.8, 111.6, 102.8, 21.4; **IR** (neat, KBr): 1693, 1598, 1506, 1382, 1122, 833, 617 cm⁻¹; **HRMS** (ESI, *m/z*): calculated for C₂₀H₁₅N₂O₂S[M+H]⁺: 347.0849, found: 347.0849.

7-(2-Benzoyl-4-chlorophenyl)-5*H*-thiazolo[3,2-*a*]pyrimidin-5-one

(3s): Reaction time: 48 h; yellow solid; 58% (42mg), m.p.162-164 °C; **¹H NMR** (500 MHz, CDCl₃): δ 7.87 (d, *J* = 4.9 Hz, 1H), 7.71 - 7.68 (m, 3H), 7.58 (d, *J* = 8.3 Hz, 1H), 7.52 (s, 1H), 7.43 (t, *J* = 7.4 Hz, 1H), 7.32 (t, *J* = 7.6 Hz, 2H), 6.91 (d, *J* = 4.8 Hz, 1H), 6.51 (s, 1H); **¹³C NMR** (126 MHz, CDCl₃): δ = 195.9, 161.9, 160.3, 158.5, 141.3, 137.4, 136.6, 135.3, 132.9, 130.5, 129.9, 129.4, 129.0, 128.4, 121.9, 111.9, 103.3; **HRMS** (ESI, *m/z*): calculated for C₁₉H₁₂ClN₂O₂SN⁺ [M+Na]⁺: 389.0122, found: 389.0122.

2-(2-(4-Methylbenzoyl)phenyl)-4*H*-pyrido[1,2-*a*]pyrimidin-4-one

(3t): Reaction time: 48 h; white solid; 56% (38mg), m.p.160-162 °C; **¹H NMR** (500 MHz, CDCl₃): δ 8.93 (d, *J* = 7.2 Hz, 1H), 7.83 (d, *J* = 7.5

Hz, 1H), 7.65 - 7.55 (m, 5H), 7.51 (d, $J = 7.2$ Hz, 1H), 7.24 (d, $J = 8.9$ Hz, 1H), 7.10 (d, $J = 7.9$ Hz, 2H), 7.04 (t, $J = 6.9$ Hz, 1H), 6.75 (s, 1H), 2.31 (s, 3H); ^{13}C NMR (126 MHz, CDCl_3): $\delta = 197.5, 162.0, 158.4, 150.0, 143.3, 140.6, 137.4, 136.4, 135.7, 130.1, 130.0, 129.4, 129.0, 129.0, 128.7, 127.2, 126.2, 115.5, 102.0, 21.7$; HRMS (ESI, m/z): calculated for $\text{C}_{22}\text{H}_{17}\text{N}_2\text{O}_2$ $[\text{M}+\text{H}]^+$: 341.1285, found: 341.1281.

2-(2-(4-Methoxybenzoyl)phenyl)-4H-pyrido[1,2-*a*]pyrimidin-4-one

(**3u**): Reaction time: 48 h; white solid; 66% (47mg), m.p.152-154 °C; ^1H NMR (500 MHz, CDCl_3): δ 8.94 (d, $J = 7.1$ Hz, 1H), 7.82 (d, $J = 7.6$ Hz, 1H), 7.74 (d, $J = 8.5$ Hz, 2H), 7.61 - 7.54 (m, 3H), 7.50 (d, $J = 7.3$ Hz, 1H), 7.24 (d, $J = 9.0$ Hz, 1H), 7.04 (t, $J = 6.9$ Hz, 1H), 6.80 (d, $J = 8.5$ Hz, 2H), 6.74 (s, 1H), 3.78 (s, 3H); ^{13}C NMR (126 MHz, CDCl_3): $\delta = 196.5, 163.1, 162.2, 158.4, 150.1, 140.6, 137.4, 136.4, 131.6, 131.2, 130.0, 129.9, 128.9, 128.8, 127.2, 126.2, 115.5, 113.7, 102.1, 55.5$; HRMS (ESI, m/z): calculated for $\text{C}_{22}\text{H}_{17}\text{N}_2\text{O}_3$ $[\text{M}+\text{H}]^+$: 357.1234, found: 357.1230.

2-(2-(4-Fluorobenzoyl)phenyl)-4H-pyrido[1,2-*a*]pyrimidin-4-one

(**3v**): Reaction time: 48 h; pale yellow solid; 62% (43mg), m.p.152-154 °C; ^1H NMR (500 MHz, CDCl_3): δ 8.94 (d, $J = 7.1$ Hz, 1H), 7.84 (d, $J = 7.6$ Hz, 1H), 7.78 - 7.75 (m, 2H), 7.63 - 7.56 (m, 3H), 7.50 (d, $J = 7.2$ Hz, 1H), 7.18 (d, $J = 9.0$ Hz, 1H), 7.05 (t, $J = 6.9$ Hz, 1H), 6.97 (t, $J = 8.4$ Hz, 2H), 6.76 (s, 1H); ^{13}C NMR (126 MHz, CDCl_3): $\delta = 196.1, 166.3$ (d, $J_{\text{CF}} = 254.2$ Hz), 161.7, 158.3, 150.0, 140.0, 137.4, 136.6, 134.7 (d, $J_{\text{CF}} = 3.1$ Hz), 131.7 (d, $J_{\text{CF}} = 9.2$ Hz), 130.4, 130.2, 128.9, 128.7, 127.3, 126.0, 115.6 (d, $J_{\text{CF}} = 15.2$ Hz), 115.3, 101.9; HRMS (ESI, m/z): calculated for $\text{C}_{21}\text{H}_{14}\text{FN}_2\text{O}_2$ $[\text{M}+\text{H}]^+$: 345.1034, found: 345.1034.

2-(2-(4-Chlorobenzoyl)phenyl)-4H-pyrido[1,2-*a*]pyrimidin-4-one

(**3w**): Reaction time: 48 h; pale yellow solid; 85% (61mg), m.p.162-164 °C; ^1H NMR (500 MHz, CDCl_3): δ 8.94 (d, $J = 7.1$ Hz, 1H), 7.84 (d, $J = 7.6$ Hz, 1H), 7.69 (d, $J = 8.2$ Hz, 2H), 7.63 - 7.56 (m, 3H), 7.49 (d, $J = 7.3$ Hz, 1H), 7.28 (d, $J = 8.4$ Hz, 2H), 7.18 (d, $J = 8.9$ Hz, 1H), 7.06 (t, $J = 6.9$ Hz, 1H), 6.77 (s, 1H); ^{13}C NMR (126 MHz, CDCl_3): $\delta =$

196.4, 161.5, 158.3, 150.0, 139.8, 138.8, 137.3, 136.6, 136.6, 130.4, 130.4, 130.2, 128.9, 128.7, 128.6, 127.3, 125.9, 115.7, 101.7; HRMS (ESI, m/z): calculated for C₂₁H₁₄ClN₂O₂ [M+H]⁺: 361.0738, found: 361.0734.

2-(2-(4-Bromobenzoyl) phenyl)-4H-pyrido[1,2-*a*]pyrimidin-4-one (3x): Reaction time: 48 h; white solid; 84% (67mg), m.p.164-166 °C; ¹H NMR (500 MHz, CDCl₃): δ 8.95 (d, *J* = 7.1 Hz, 1H), 7.85 (d, *J* = 7.1 Hz, 1H), 7.64 - 7.56 (m, 5H), 7.49 (d, *J* = 7.5 Hz, 1H), 7.44 (d, *J* = 8.5 Hz, 2H), 7.19 (d, *J* = 8.9 Hz, 1H), 7.06 (t, *J* = 6.9 Hz, 1H), 6.78 (s, 1H); ¹³C NMR (126 MHz, CDCl₃): δ = 196.6, 161.5, 158.3, 150.0, 139.8, 137.3, 137.0, 136.7, 131.6, 130.6, 130.5, 130.3, 128.9, 128.7, 127.6, 127.3, 125.9, 115.7, 101.7; HRMS (ESI, m/z): calculated for C₂₁H₁₄BrN₂O₂ [M+H]⁺: 405.0233, found: 405.0234.

2-(2-(3-Nitrobenzoyl)-4H-pyrido[1,2-*a*]pyrimidin-4-one (3y): Reaction time: 48 h; pale yellow solid; 33% (40mg), m.p.174-176 °C; ¹H NMR (500 MHz, CDCl₃): δ 8.93 (d, *J* = 7.1 Hz, 1H), 8.61 (s, 1H), 8.23 (d, *J* = 8.1 Hz, 1H), 7.99 (d, *J* = 7.7 Hz, 1H), 7.89 (d, *J* = 7.6 Hz, 1H), 7.70 - 7.61 (m, 3H), 7.56 (d, *J* = 7.5 Hz, 1H), 7.48 (t, *J* = 7.9 Hz, 1H), 7.15 (d, *J* = 8.9 Hz, 1H), 7.07 (t, *J* = 6.9 Hz, 1H), 6.81 (s, 1H); ¹³C NMR (126 MHz, CDCl₃): δ = 195.2, 160.9, 158.2, 149.9, 148.3, 140.0, 138.9, 137.3, 137.0, 134.2, 131.0, 130.7, 129.5, 129.0, 128.8, 127.5, 126.5, 125.6, 123.5, 115.9, 101.5; HRMS (ESI, m/z): calculated for C₂₁H₁₃N₃O₄Na⁺ [M+Na]⁺: 394.0798, found: 394.0794.

2-(2-(4-Chlorobenzoyl)phenyl)-8-methyl-4H-pyrido[1,2-*a*]pyrimidin-4-one (3z): Reaction time: 48 h; white solid; 85% (64mg), m.p.176-178 °C; ¹H NMR (500 MHz, CDCl₃): δ 8.83 (d, *J* = 7.2 Hz, 1H), 7.83 (d, *J* = 9.0 Hz, 1H), 7.68 (d, *J* = 8.6 Hz, 2H), 7.63 - 7.55 (m, 2H), 7.49 (d, *J* = 7.3 Hz 1H), 7.27 (d, *J* = 8.7 Hz, 2H), 6.97 (s, 1H) 6.90 (dd, *J* = 7.3, 2.0 Hz 1H), 6.69 (s, 1H), 2.39 (s, 3H); ¹³C NMR (126 MHz, CDCl₃): δ = 196.5, 161.7, 158.4, 150.0, 149.0, 139.7, 138.7, 137.5, 136.7, 130.4 (2C), 130.2, 128.9, 128.6, 128.6, 126.6, 124.0, 118.4,

100.9, 21.5; **HRMS** (ESI, m/z): calculated for C₂₂H₁₆ClN₂O₂ [M+H]⁺: 375.0895, found: 375.0890.

2-(2-(4-Chlorobenzoyl)-4-methylphenyl)-4H-pyrido[1,2-

a]pyrimidin-4-one (3aa): Reaction time: 32 h; pale yellow solid; 91% (68mg), m.p.178-180 °C; ¹H NMR (500 MHz, CDCl₃): δ 8.94 (d, *J* = 7.1 Hz, 1H), 7.76 (d, *J* = 8.0 Hz, 1H), 7.70 (d, *J* = 8.2 Hz, 2H), 7.60 (t, *J* = 7.9 Hz, 1H), 7.43 (d, *J* = 8.0 Hz, 1H), 7.29 - 7.26 (m, 3H), 7.17 (d, *J* = 9.1 Hz, 1H), 7.05 (t, *J* = 6.9 Hz, 1H), 6.76 (s, 1H) 2.46 (s, 3H); ¹³C NMR (126 MHz, CDCl₃): δ = 196.6, 161.3, 158.3, 149.9, 140.9, 139.9, 138.7, 136.8, 136.5, 134.3, 131.0, 130.4, 129.4, 128.6, 128.6, 127.3, 125.8, 115.5, 101.2, 21.4; **HRMS** (ESI, m/z): calculated for C₂₂H₁₆ClN₂O₂ [M+H]⁺: 375.0895, found: 375.0890.

2-(2-(4-Bromobenzoyl)phenyl)-8-methyl-4H-pyrido[1,2-

a]pyrimidin-4-one (3ab): Reaction time: 32 h; pale yellow solid; 89% (74mg), m.p.174-176 °C; ¹H NMR (500 MHz, CDCl₃): δ 8.84 (d, *J* = 7.3 Hz, 1H), 7.83 (d, *J* = 6.6 Hz, 1H), 7.63 - 7.55 (m, 4H), 7.49 (d, *J* = 7.3 Hz, 1H), 7.44 (d, *J* = 8.4 Hz, 2H), 6.98 (s, 1H), 6.91 (dd, *J* = 7.3, 1.9 Hz, 1H), 6.70 (s, 1H) 2.39 (s, 3H); ¹³C NMR (126 MHz, CDCl₃): δ = 196.7, 161.8, 158.4, 150.0, 149.0, 139.7, 137.5, 137.0, 131.6, 130.6, 130.5, 130.2, 129.0, 128.7, 127.5, 126.6, 124.0, 118.5, 100.9, 21.5. **HRMS** (ESI, m/z): calculated for C₂₂H₁₆BrN₂O₂ [M+H]⁺: 419.0390, found: 419.0393.

2-(2-(4-Bromobenzoyl)-4-methoxyphenyl)-4H-pyrido[1,2-

a]pyrimidin-4-one (3ac): Reaction time: 32 h; pale yellow solid; 86% (75mg), m.p.166-168 °C; ¹H NMR (500 MHz, CDCl₃): δ 8.93 (d, *J* = 7.1 Hz, 1H), 7.82 (d, *J* = 8.6 Hz, 1H), 7.63 - 7.58 (m, 3H), 7.45 (d, *J* = 8.2 Hz, 2H), 7.13 (d, *J* = 9.0 Hz, 2H), 7.04 (t, *J* = 6.9 Hz, 1H), 6.98 (d, *J* = 2.7 Hz, 1H), 6.74 (s, 1H) 3.88 (s, 3H); ¹³C NMR (126 MHz, CDCl₃): δ = 196.2, 161.4, 160.8, 158.4, 149.8, 141.6, 137.0, 136.6, 131.7, 130.5, 130.1, 129.0, 127.5, 127.4, 125.7, 116.0, 115.5, 114.1, 100.4, 55.8; **HRMS** (ESI, m/z): calculated for C₂₂H₁₆BrN₂O₃ [M+H]⁺: 435.0339, found: 435.0338.

2,2,6,6-tetramethylpiperidin-1-yl benzoate (4): ^1H NMR (500MHz, CDCl_3): δ 8.29 (d, $J = 7.0$ Hz, 2H), 7.79 - 7.76 (m, 1H), 7.68 - 7.65 (m, 2H), 2.02 - 1.89 (m, 3H), 1.82 - 1.78 (m, 2H), 1.68 - 1.65 (m, 1H), 1.49 (s, 6H), 1.33 (s, 6H); ^{13}C NMR (126 MHz, CDCl_3): $\delta = 165.3, 132.0, 128.7, 128.6, 127.6, 59.3, 38.0, 31.0, 19.9, 16.0$; **HRMS** (ESI, m/z): calculated for $\text{C}_{16}\text{H}_{24}\text{NO}_2$ $[\text{M}+\text{H}]^+$: 262.1802, found: 262.1798.

3.8 ^1H and ^{13}C NMR spectra of selected compounds

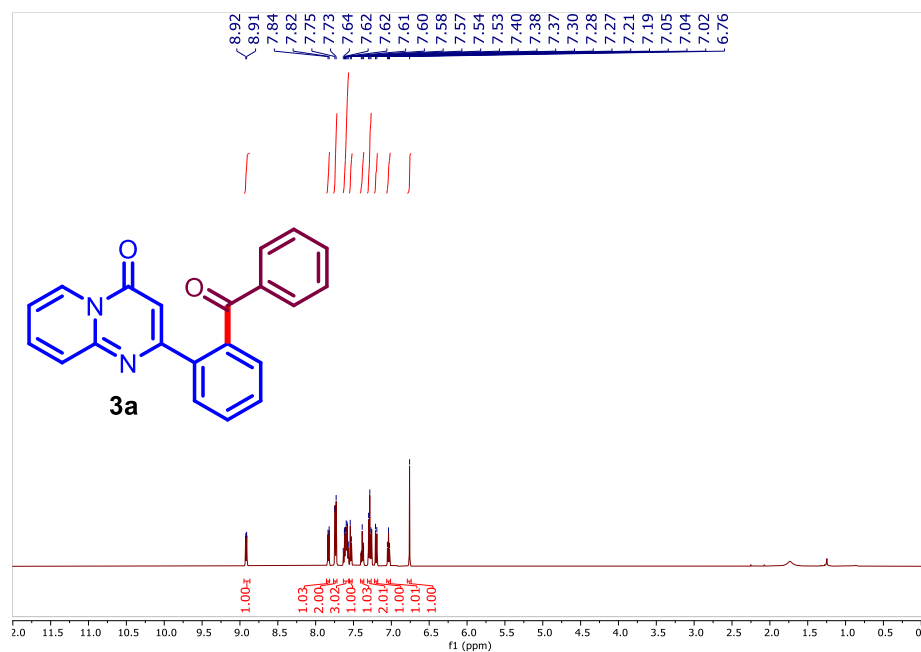


Figure 3.2 ^1H NMR spectrum of compound **3a** (500 MHz, CDCl_3)

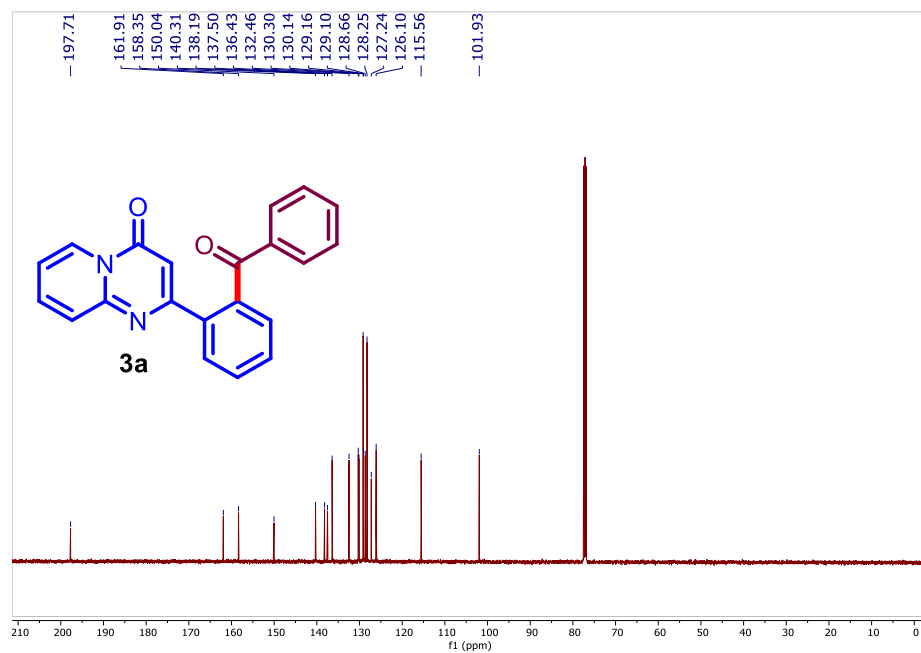


Figure 3.3 ^{13}C NMR spectrum of compound **3a** (126 MHz, CDCl_3)

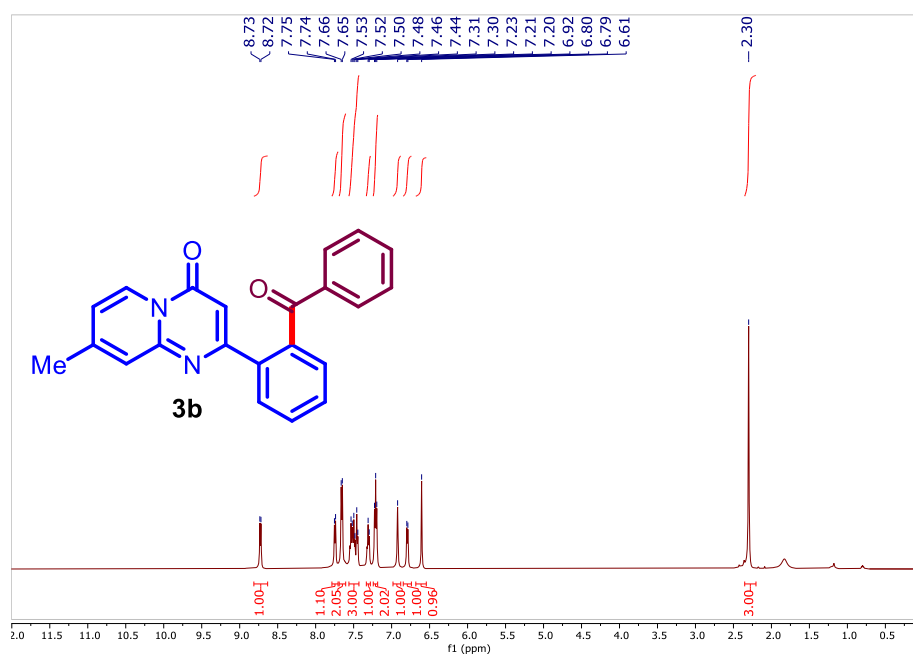


Figure 3.4 ¹H NMR spectrum of compound **3b** (500 MHz, CDCl₃)

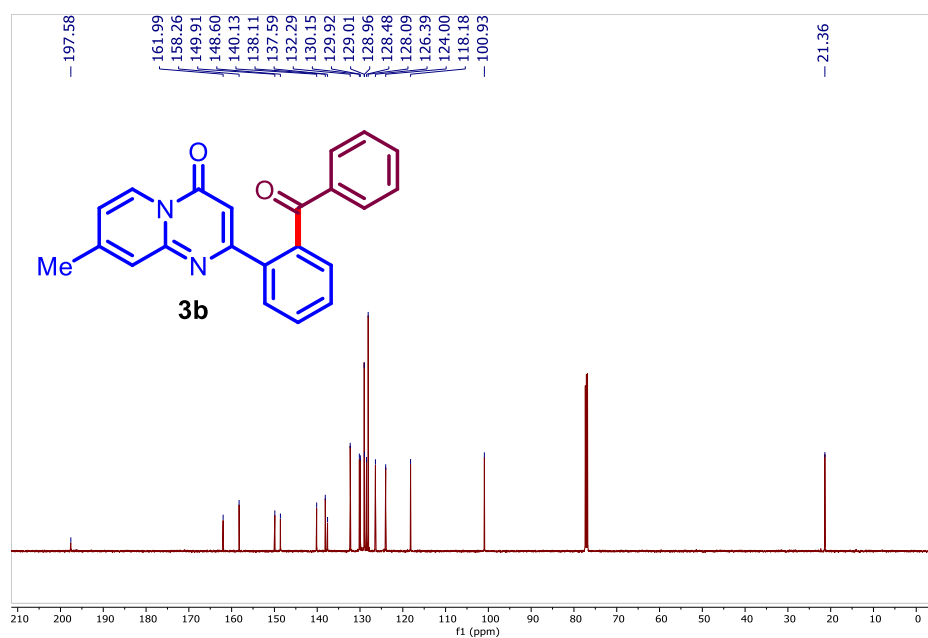


Figure 3.5 ¹³C NMR spectrum of compound **3b** (126 MHz, CDCl₃)

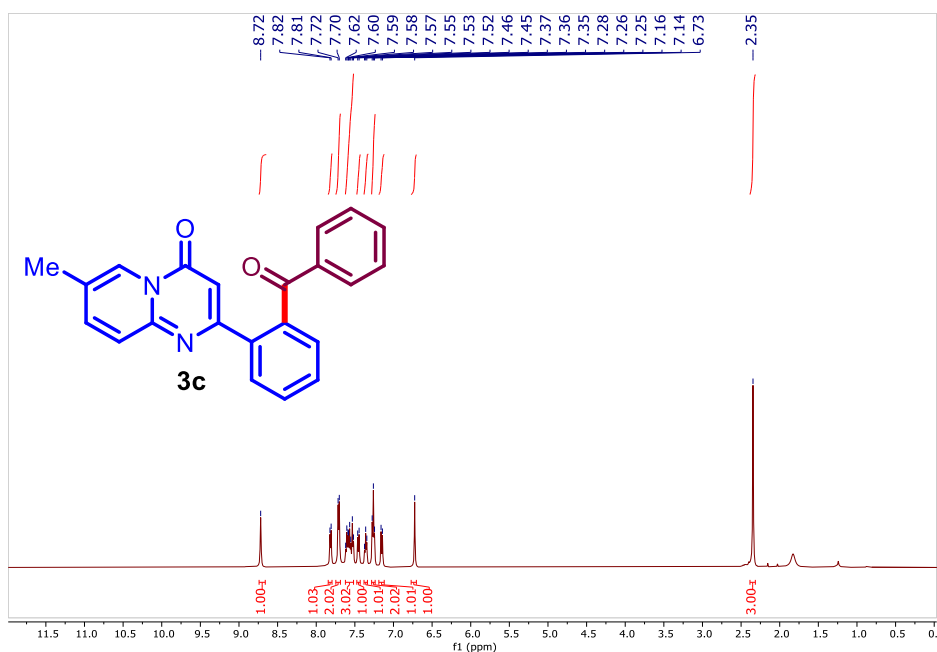


Figure 3.6 ¹H NMR spectrum of compound **3c** (500 MHz, CDCl₃)

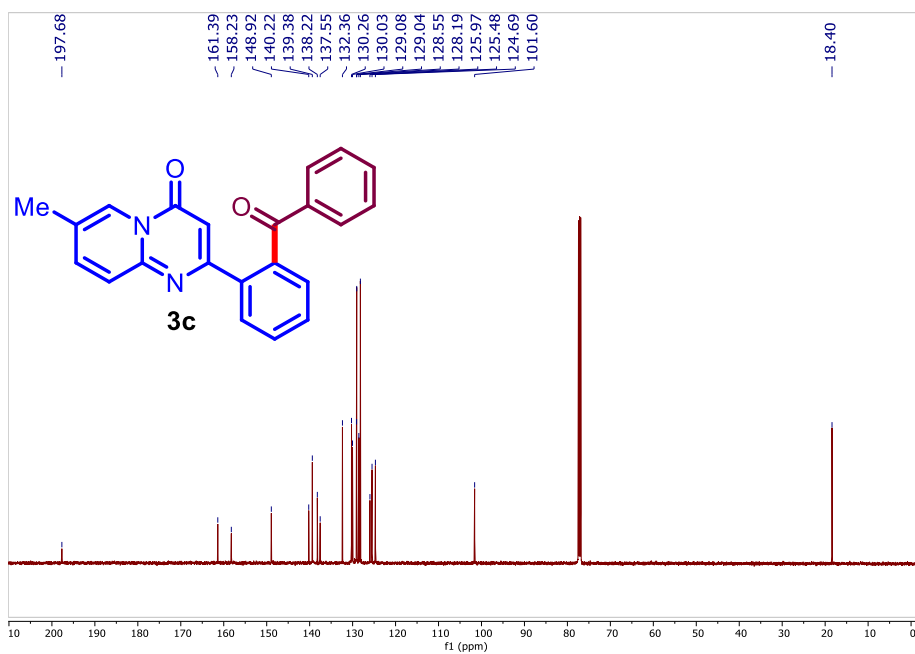


Figure 3.7 ¹³C NMR spectrum of compound **3c** (126 MHz, CDCl₃)

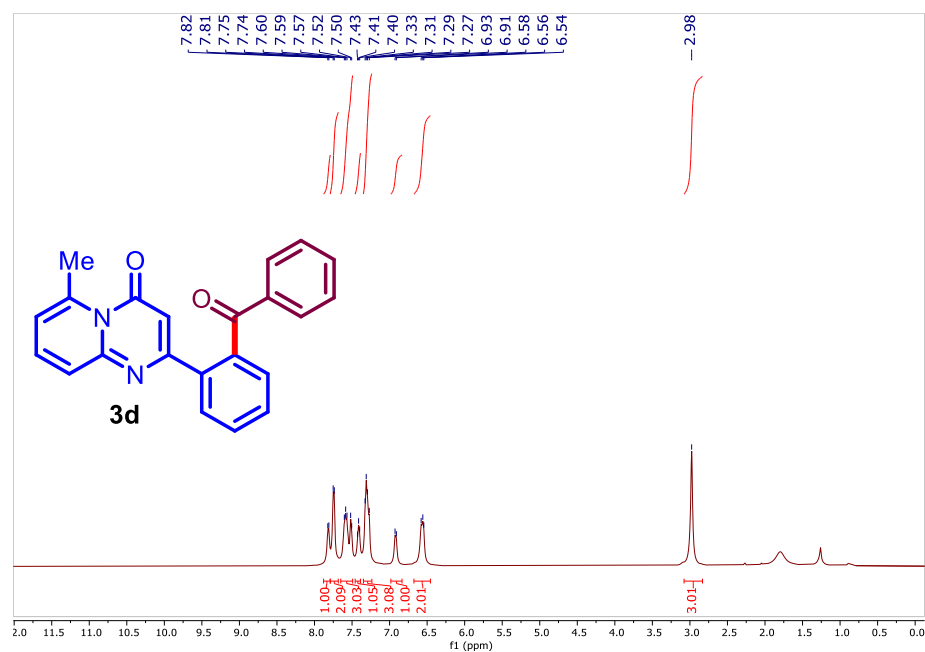


Figure 3.8 ¹H NMR spectrum of compound **3d** (500 MHz, CDCl₃)

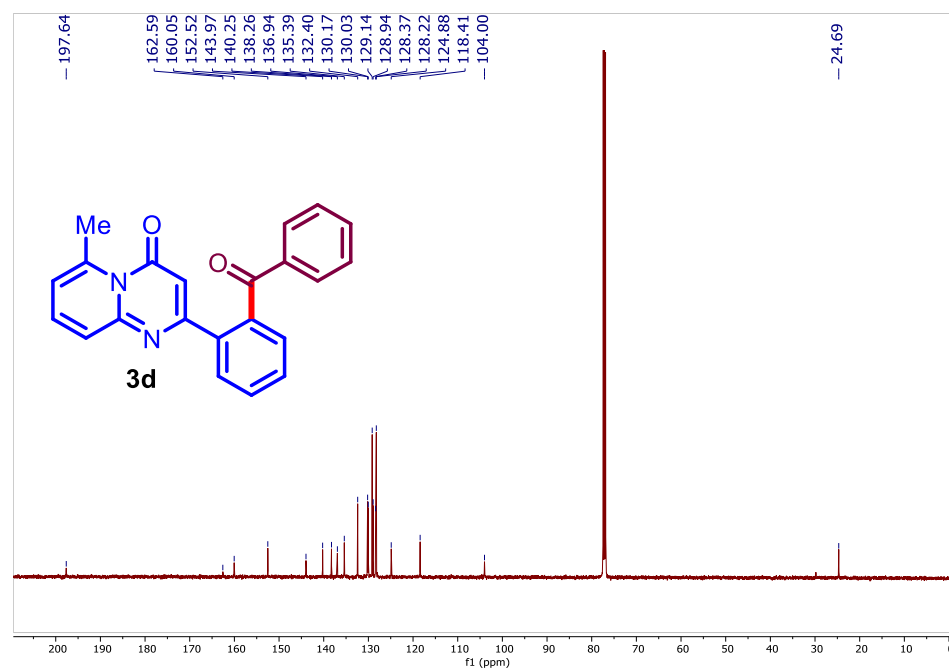


Figure 3.9 ¹³C NMR spectrum of compound **3d** (126 MHz, CDCl₃)

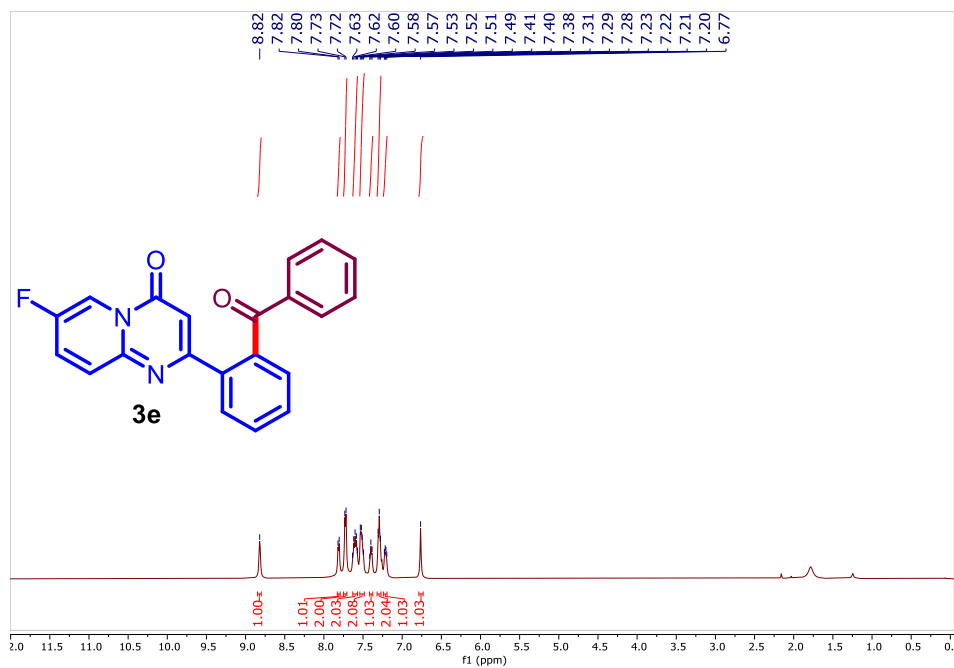


Figure 3.10 ¹H NMR spectrum of compound **3e** (500 MHz, CDCl₃)

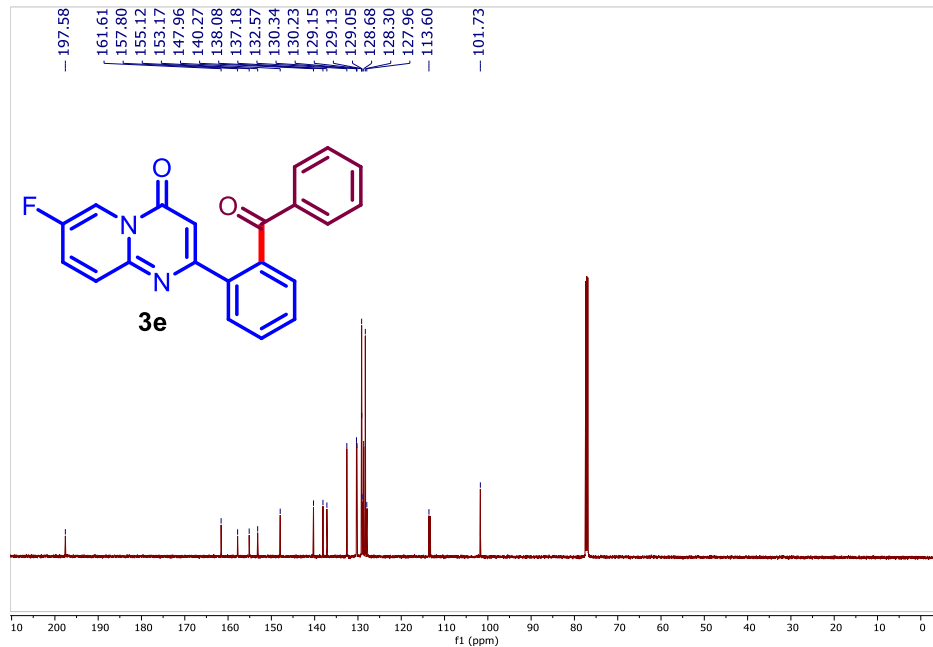


Figure 3.11 ¹³C NMR spectrum of compound **3e** (126 MHz, CDCl₃)

3.9 The single-crystal X-ray diffraction data

The single-crystal X-ray diffraction study of **3a**. The compound **3a** was readily crystallized from mixtures of acetonitrile and dichloromethane.

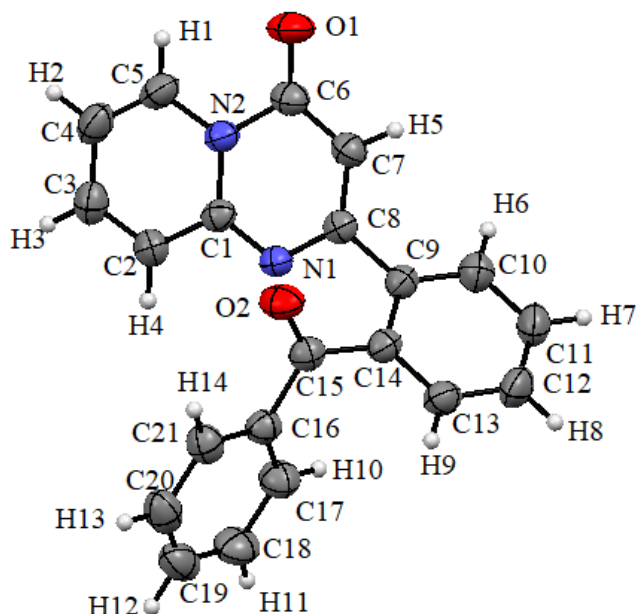


Table 3.2 Crystal data and structure refinement for 3a.

Compound	3a
Empirical formula	C ₂₁ H ₁₄ N ₂ O ₂
Formula weight	326.1055
Temperature/K	293(2)
Wavelength (Å)	0.71073 Å
Crystal system	orthorhombic
Space group	Pna2 ₁
a/Å	12.7445(3)
b/Å	16.2952(5)
c/Å	7.8165(2)
α/°	90
β/°	90
γ/°	90
Volume/Å ³	1623.29(8)
Z	8

$\rho_{\text{calc}}/\text{cm}^3$	2.671
μ/mm^{-1}	0.175
F (000)	1360.0
Radiation	MoK α ($\lambda = 0.71073$)
2 Θ range for data collection/ $^\circ$	5.934 to 58.64
Index ranges	$-15 \leq h \leq 17$, $-20 \leq k \leq 21$, $-10 \leq l \leq 10$
Reflections collected	17337
Independent reflections	3962 [$R_{\text{int}} = 0.0567$, $R_{\text{sigma}} = 0.0441$]
Data/restraints/parameters	3962/1/226
Goodness-of-fit on F^2	1.098
Final R indexes [$I \geq 2\sigma(I)$]	$R_1 = 0.0522$, $wR_2 = 0.1139$
Final R indexes [all data]	$R_1 = 0.0729$, $wR_2 = 0.1349$
Largest diff. peak/hole / e \AA^{-3}	0.24/-0.17
Flack parameter	0.0(8)

3.10 References

- [1] Matveeva M. D., R Purgatorio., Voskressensky L. G., Altomare C. D. (2019), Pyrrolo[2,1-*a*]isoquinoline Scaffold in Drug Discovery: Advances in Synthesis and Medicinal Chemistry, *Future Med Chem* 11, 2735-2755 (DOI: 10.4155/fmc-2019-0136)
- [2] Jean D. J. St., Fotsch C. (2012), Mitigating Heterocycle Metabolism in Drug Discovery, *J. Med. Chem.* 55, 6002-6020 (DOI: 10.1021/jm300343m)
- [3] Shiri M. (2012), Indoles in Multicomponent Processes (MCPs), *Chem. Rev.* 112, 3508-3549 (DOI: 10.1021/cr2003954)
- [4] Baviskar A. T., Madaan C., Preet R., Mohapatra P., Jain V., Agarwal A., Guchhait S. K., Kundu C. N., Banerjee U. C.,

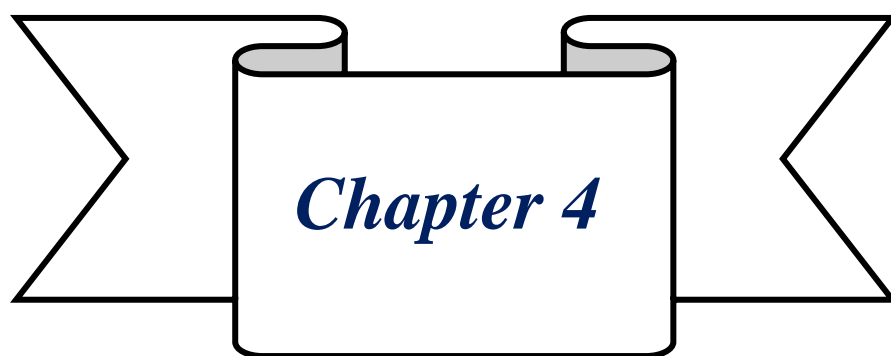
- Bharatam P. V. (2011), N-Fused Imidazoles As Novel Anticancer Agents That Inhibit Catalytic Activity of Topoisomerase II α and Induce Apoptosis in G1/S Phase, *J. Med. Chem.* 54, 5013-5030 (DOI: 10.1021/jm200235u)
- [5] Hu S., Huang Y., Wu Y.-J., He H., Grant-Young K. A., Bertekap R. L., Whiterock V., Brassil P., Lentz K., Sivaprakasam P., Langley D. R., Westphal R. S., Scola P. M. (2014), *Bioorg. Med. Chem.* 22, 1782-1790 (DOI: 10.1016/j.bmc.2014.01.003)
- [6] Peng L., Gao X., Duan L., Ren X., Wu D., Ding K. (2011), Identification of pyrido [1, 2- α] pyrimidine-4-ones as new molecules improving the transcriptional functions of estrogen-related receptor α , *J. Med. Chem.* 54, 7729-7733 (DOI: 10.1021/jm200976s)
- [7] Li A.-R., Johnson M. G., Liu J., Chen X., Du X., Mihalic J. T., Deignan J., Gustin D. J., Duquette J., Fu Z. et al. (2008), Optimization of the heterocyclic core of the quinazolinone-derived CXCR₃ antagonists, *Bioorganic Med. Chem. Lett.* 18, 688-693 (DOI: 10.1016/j.bmcl.2007.11.060)
- [8] Hermecz I., Mészáros Z. (1988), Pyrido[1,2-*a*]pyrimidines; New chemical entities in medicinal chemistry, *Med Res Rev* 8, 203-230 (DOI: 10.1002/med.2610080204)
- [9] Motta C. -L., Sartini S., Mugnaini L., Simorini F., Taliani S., Salerno S., Marini A. M., Settimo F. -D., Lavecchia A., Novellino E., Cantore M., Failli P., Ciuffi M. (2007), Pyrido[1,2-*a*]pyrimidin-4-one Derivatives as a Novel Class of Selective Aldose Reductase Inhibitors Exhibiting Antioxidant Activity, *J. Med. Chem.* 50, 4917-4927 (DOI: 10.1021/jm070398a)
- [10] Sadashiva C., Chandra J. N. S., Ponnappa K., Gowda T. V., Rangappa K. S. (2006), Synthesis and efficacy of 1-[bis(4-fluorophenyl)-methyl]piperazine derivatives for

- acetylcholinesterase inhibition, as a stimulant of central cholinergic neurotransmission in Alzheimer's disease, *Bioorganic Med. Chem. Lett.* **16**, 3932-3936 (DOI: 10.1016/j.bmcl.2006.05.030)
- [11] Nakayama K., Ishida Y., Ohtsuka M., Kawato H., Yoshida K.-i., Yokomizo Y., Ohta T., Hoshino K., Otani T., Kurosaka Y., Yoshida K., Ishida H., Lee V. J., Renau T. E., Watkins W. J. (2003), MexAB-OprM specific efflux pump inhibitors in *Pseudomonas aeruginosa*, Part 2: achieving activity in vivo through the use of alternative scaffolds, *Bioorg. Med. Chem.* **13**, 4205-4208 (DOI: 10.1016/j.bmcl.2003.07.027)
- [12] Shulman D. G., Amdahl L., Washington C., Graves A. (2003), A combined analysis of two studies assessing the ocular comfort of antiallergy ophthalmic agents, *Clin Ther* **25**, 1096-1106 (DOI: 10.1016/S0149-2918(03)80069-3)
- [13] Wang H., Li T., Hu D., Tong X., Zheng L., Xia C. (2021), Acylation of Arenes with Aldehydes through Dual C–H Activations by Merging Photocatalysis and Palladium Catalysis, *Org. Lett.* **23**, 3772-3776 (DOI: 10.1021/acs.orglett.1c01184)
- [14] Penteado F., Lopes E. F., Alves D., Perin G., Jacob R. G., Lenardão E. J. (2019), α -Keto Acids: Acylating Agents in Organic Synthesis, *Chem. Rev.* **119**, 7113-7278 (DOI: 10.1021/acs.chemrev.8b00782)
- [15] Deng Y., Chin Y.-W., Chai H., Keller W. J., Kinghorn A. D. (2007), Anthraquinones with Quinone Reductase-Inducing Activity and Benzophenones from *Morinda citrifolia* (Noni) Roots, *J. Nat. Prod.* **70**, 2049-2052 (DOI: 10.1021/np070501z)
- [16] Sartori G., Maggi R. (2006), Use of Solid Catalysts in Friedel–Crafts Acylation Reactions, *Chem. Rev.* **106**, 1077-1104 (DOI: 10.1021/cr040695c)

- [17] Olah G. A., Prakash G. S. (2003), *Across Conventional Lines: Selected Papers Of George A Olah (In 2 Volumes)*, World scientific, 2003.
- [18] Gandeepan P., Müller T., Zell D., Cera G., Warratz S., Ackermann L. (2018), 3d Transition Metals for C–H Activation, *Chem. Rev.*, *119*, 2192-2452 (DOI: 10.1021/acs.chemrev.8b00507)
- [19] Newhouse T., Baran P. S. (2011), If C–H Bonds Could Talk: Selective C–H Bond Oxidation, *Angew. Chem. Int. Ed.* *50*, 3362-3374 (DOI: 10.1002/anie.201006368)
- [20] Wencel-Delord J., Dröge T., Liu F., Glorius F. (2011), Towards mild metal-catalyzed C–H bond activation, *Chem. Soc. Rev.* *40*, 4740-4761 (DOI: 10.1039/C1CS15083A)
- [21] Nielsen M. K., Shields B. J., Liu J., Williams M. J., Zacuto M. J., Doyle A. G. (2017), Mild, Redox-Neutral Formylation of Aryl Chlorides through the Photocatalytic Generation of Chlorine Radicals, *Angew. Chem. Int. Ed.* *56*, 7191-7194 (DOI: 10.1002/anie.201702079)
- [22] Prier C. K., Rankic D. A., MacMillan D. W. (2013), Visible Light Photo-redox Catalysis with Transition Metal Complexes: Applications in Organic Synthesis, *Chem. Rev.* *113*, 5322-5363 (DOI: 10.1021/cr300503r)
- [23] Creutz S. E., Lotito K. J., Fu G. C., Peters J. C. (2012), Photoinduced Ullmann C–N Coupling: Demonstrating the Viability of a Radical Pathway, *Science*, *338*, 647-651 (DOI: 10.1126/science.1226458)
- [24] Oderinde M. S., Frenette M., Robbins D. W., Aquila B., Johannes J. W. (2016), Photo-redox Mediated Nickel Catalyzed Cross-Coupling of Thiols with Aryl and Heteroaryl Iodides via Thiyl Radicals, *J. Am. Chem. Soc.* *138*, 1760-1763 (DOI: 10.1021/jacs.5b11244)

- [25] Hopkinson M. N., Sahoo B., Li J. L., Glorius F. (2014), Dual Catalysis Sees the Light: Combining Photo-redox with Organo-, Acid, and Transition-Metal Catalysis, *Chem. Eur. J.* **20**, 3874-3886 (DOI: 10.1002/chem.201304823)
- [26] Zhou C., Li P., Zhu X., Wang L. (2015), Merging Photo-redox with Palladium Catalysis: Decarboxylative ortho-Acylation of Acetanilides with α -Oxocarboxylic Acids under Mild Reaction Conditions, *Org. Lett.* **17**, 6198-6201 (DOI: 10.1021/acs.orglett.5b03192)
- [27] Wang L., Wang T., Cheng G.-J., Li X., Wei J.-J., Guo B., Zheng C., Chen G., Ran C., Zheng C. (2020), Direct C–H Arylation of Aldehydes by Merging Photocatalyzed Hydrogen Atom Transfer with Palladium Catalysis, *ACS Catal.* **10**, 7543-7551 (DOI: 10.1021/acscatal.0c02105)
- [28] Fabry D. C., Ronge M. A., Zoller J., Rueping M. (2015), C–H Functionalization of Phenols Using Combined Ruthenium and Photo-redox Catalysis: In Situ Generation of the Oxidant, *Angew. Chem. Int. Ed.* **54**, 2801-2805 (DOI: 10.1002/anie.201408891)
- [29] Noble A., McCarver S. J., MacMillan D. W. (2015), Merging Photo-redox and Nickel Catalysis: Decarboxylative Cross-Coupling of Carboxylic Acids with Vinyl Halides, *J. Am. Chem. Soc.* **137**, 624-627 (DOI: 10.1021/ja511913h)
- [30] Xu N., Li P., Xie Z., Wang L. (2016), Merging Visible-Light Photocatalysis and Palladium Catalysis for C–H Acylation of Azo- and Azoxybenzenes with α -Keto Acids, *Chem. Eur. J.* **22**, 2236-2242 (DOI: 10.1002/chem.201504530)
- [31] Liu W., Wang S., Zhang Q., Yu J., Li J., Xie Z., Cao H., (2014), Regioselective C3 Alkenylation of 4*H*-pyrido[1,2-*a*]pyrimidin-4-ones via Palladium-Catalyzed C–H Activation, *Chem Asian J.* **9**, 2436-2439 (DOI: 10.1002/asia.201402455)

- [32] Bhawale R. T., Sarothiya D., Kshirsagar U. A. (2022), Synergistic Approach for Decarboxylative Ortho C–H Aroylation of 2-Aryl-pyrido[1,2-*a*]pyrimidin-4-ones and Thiazolopyrimidinones by Merging Palladium Catalysis with Photocatalysis, *Asian J. Org. Chem.* 11, e202200134 (DOI: 10.1002/ajoc.202200134)
- [33] Hu X.-Q., Liu Z.-K., Xiao W.-J. (2020), Radical Carbonylative Synthesis of Heterocycles by Visible Light Photo-redox Catalysis, *Catalysts*, 10, 1054 (DOI: 10.3390/catal10091054)
- [34] Waghmare D. S., Tambe S. D., Kshirsagar U. A. (2020), Pd-Catalyzed Decarboxylative Ortho-Aroylation of 2-Aryl-quinazolinone Comprising Intrinsic Directing Group with α -Oxocarboxylic Acids, *Asian J. Org. Chem.* 9, 2095-2098 (DOI: 10.1002/ajoc.202000487)
- [35] Peng L., Gao X., Duan L., Ren X., Wu D., Ding K. (2011), Identification of Pyrido[1,2- α]pyrimidine-4-ones as New Molecules Improving the Transcriptional Functions of Estrogen-Related Receptor α , *J. Med. Chem.* 54, 7729-7733 (DOI: doi.org/10.1021/jm200976s)



*Visible-Light Induced Ag-
Palladacycle-complex Mediated
Regioselective C–H Arylation*

Chapter 4

Visible-Light Induced Ag-Palladacycle-complex Mediated Regioselective C–H Arylation

4.1 Introduction

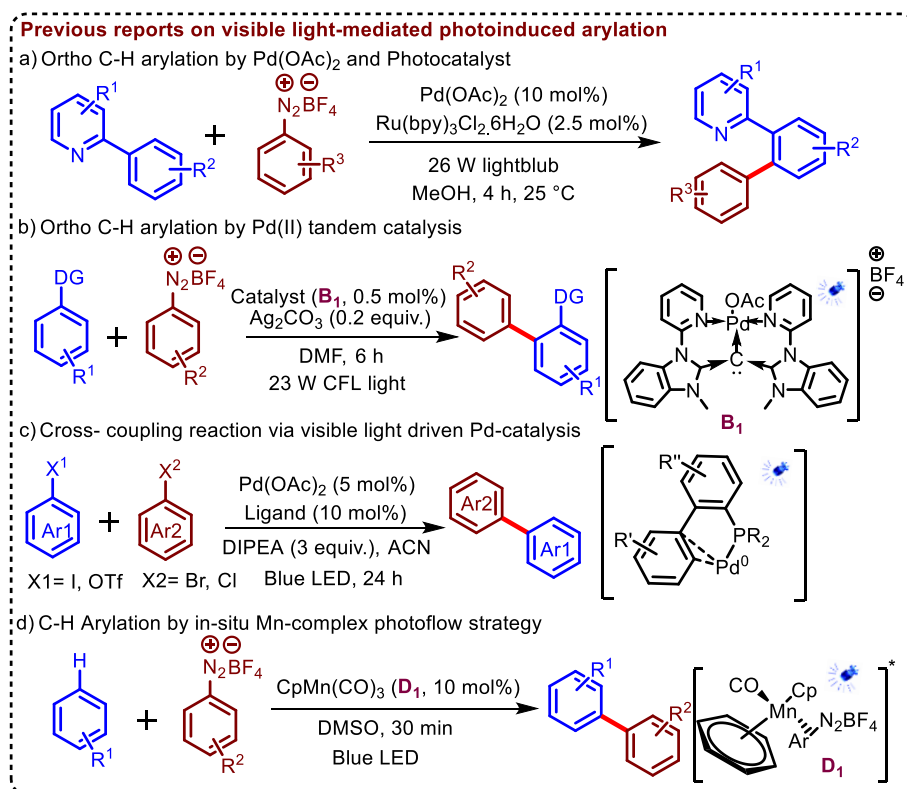
The heterocyclic biaryl motifs constitute highly significant structural elements in a wide array of pharmaceuticals, natural products, and organic materials.^[1-4] Consequently, it has been demonstrated that the direct regioselective arylation via the activation of C–H bonds through transition metal catalysis, leading to the synthesis of biaryl compounds, is a crucial aspect of ongoing research efforts in the realm of aryl-aryl (C–C) bond formation.^[5-9] This is due to the multitude of benefits it offers, including regioselectivity, broad substrate applicability, and excellent tolerance to various functional groups.^[10-12] In spite of these developments, regioselective C–H arylation reactions through C–H activation still require harsh reaction conditions, including elevated temperatures, strong oxidizing agents, ligands, etc.^[13-15] Recently, researchers have embraced visible light-mediated photocatalysis as a profoundly influential and practical approach, leveraging its tools to propel advancements in organic synthesis.^[16-17] These transformations mainly rely on the external photo-catalyst based on transition metal complexes or organic dyes.^[18-22] Apart from this, recently, it has been observed that these reactions can be performed under external photocatalyst-free conditions, such as through electron donor-acceptor (EDA) complexes.^[23-26]

Traditionally, the aryl radical generation under photo-catalytic conditions entails the use of diverse sources, including aryl halides, aryl carboxylic acids, Ar-DBT⁺ salts, and aryl boronic acids, which are often dependent on external stoichiometric reagents.^[27-30] Aryl diazonium salts are crucial arylating agents in synthetic organic chemistry

employing visible light-mediated photocatalysis,^[31-32] and this significance arises from their readily available aniline precursors and heightened reactivity, attributed to their low reduction potential (-0.16V vs SCE).^[33]

4.2 Previous Reports

In 2011, the Sanford group innovated regioselective C–H arylation of 2-aryl heterocyclic substrates by amalgamating transition metal catalysis (Pd) with photo-redox catalysis (Ru), under the visible light source at room temperature. The procedure entailed the initial generation of an aryl radical from an aryl diazonium salt using a Ru-based photocatalyst (**Scheme 4.1a**).^[34] Furthermore, similar approaches were developed by various groups.^[18, 19, 35] In 2018, Wang and colleagues employed tandem catalysis for regio-selective C–H arylation under photo-catalytic

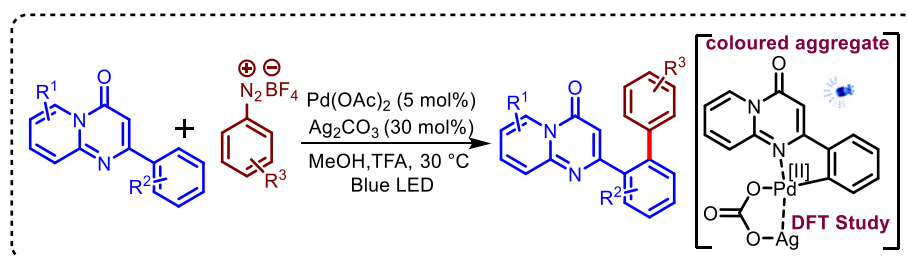


Scheme 4.1 Previous reports on visible light-mediated photoinduced arylation

conditions using palladium complex (**B1**) as a tandem catalyst performing the dual role of C–H activation and photo-catalysis (**Scheme 4.1b**).^[36] Very recently, the Maiti group devised a ligand-controlled, external photocatalyst-free visible light-induced cross-electrophile

coupling reaction for biaryl synthesis using a Pd-catalyst (**Scheme 4.1c**).^[37-40] These processes allow arylation reactions to be carried out at room temperature in the presence of a photocatalyst or Pd catalyst and ligand. Ackermann's group demonstrated the in-situ generation of an arene-Mn-diazo complex (**D1**) capable of photoexcitation under visible light irradiation for the aryl radical generation and subsequent arylation (**Scheme 4.1d**).^[41]

4.3 Objective

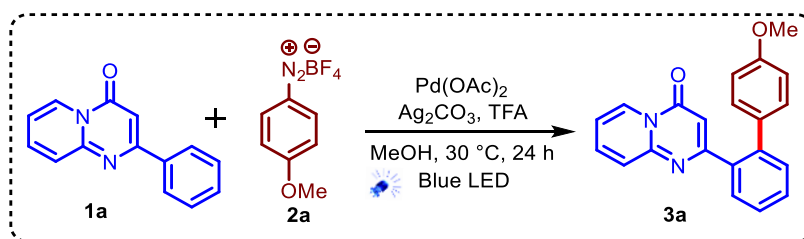


Scheme 4.2 Light-mediated photoinduced arylation of pyrido[1,2-*a*]pyrimidin-4-one.

We have developed an external photocatalyst-free, visible light-mediated regio-selective ortho C–H arylations of pyrido[1,2-*a*]pyrimidin-4-ones as well as of other heteroarenes at ambient temperature using a simple palladium (II) catalyst under ligand-free conditions. Observations of colored aggregates, DFT study, and UV-visible analysis suggest the in-situ generated silver-palladacycle complexes of 2-aryl heteroarenes could absorb visible light and play a crucial role in generating aryl radicals from aryldiazonium salts, leading to the regioselective ortho C–H arylated products (**Scheme 4.2**).^[42]

4.4 Result and Discussion

We investigated the reaction parameters using 2-phenyl-4*H*-pyrido[1,2-*a*]pyrimidin-4-ones (**1a**) and 4-methoxy benzenediazonium tetrafluoroborate (**2a**) employing Pd(OAc)₂ (5 mol%), Ag₂CO₃ (30 mol%), trifluoroacetic acid (TFA, 0.1 mL),^[43-45] and methanol as the solvent under blue LED irradiation at 30 °C for 24 hours which yielded the regioselective ortho C–H arylated product, 2-(4'-methoxy-[1,1'-biphenyl]-2-yl)-4*H*-pyrido[1,2-*a*]pyrimidin-4-one (**3a**), in 88% yield

Table 4.1 Optimization of the reaction conditions^[a]

Entry	Variation from the above conditions	Yield ^[b]
1	Std. conditions	88%
2	EtOH instead of MeOH	47%
3	DMF instead of MeOH	15%
4	DCE/ACN/DMSO/Toluene as solvent	n.d.
5	AgNO ₃ /AgBF ₄ /AgPF ₆ /CF ₃ COOAg instead of Ag ₂ CO ₃	53/52/39/50%
6	2a used as 1.2 equiv.	68%
7	No TFA	64%
8	No Palladium catalyst	n.d.
9	No Ag ₂ CO ₃	n.d.
10	No light	n.d.
11	green LED instead of blue LED	15%
12	CFL blub instead of blue LED	41%
13	Std. conditions with N ₂	77%
14	Eosin Y as Photocatalyst (3%), no Ag ₂ CO ₃	5%

^[a]Reaction conditions: **1a** (0.2 mmol), **2a** (0.3 mmol), Pd(OAc)₂ (5 mol%), Ag₂CO₃ (30 mol%), TFA 0.1 mL, MeOH 2.0 mL, blue LED, 30 °C, 24 h.

^[b]isolated yields. n.d.-not detected.

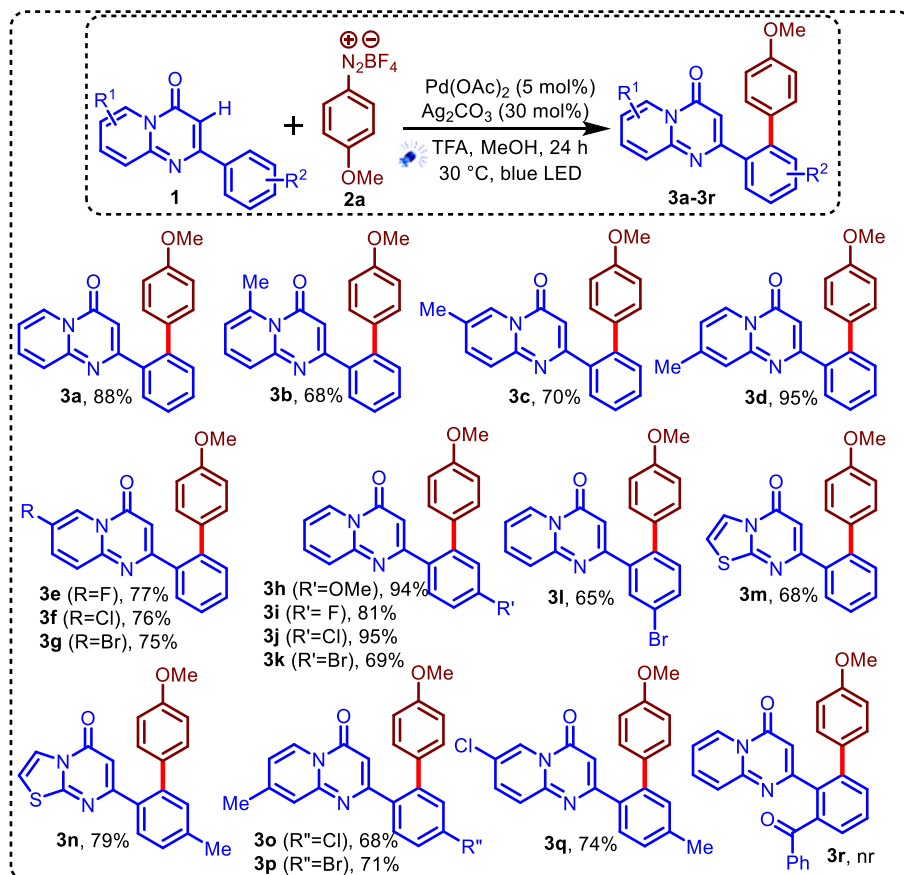
(**Table 4.1**, entry 1). The structure of the ortho-arylated product **3a** was confirmed by the NMR spectroscopy, HRMS analysis, and single-crystal X-ray analysis (CCDC:2287203 of **3w**).^[46] Using ethanol as a solvent instead of methanol provided a decreased yield of **3a** (47%, entry 2), whereas DMF gave a much lower amount (15%, entry 3). Subsequently, alternative solvents such as DCE, ACN, DMSO, and toluene were explored. Unfortunately, these solvents proved unsuitable for generating the desired products (entry 4). When the reaction was conducted using other silver salts instead of silver carbonate, a lowered

yield of desired product **3a** was observed (39-53%, entry 5). A reduction in yield for the formation of product **3a** was also noted when the aryl diazonium salt was employed in a 1.2 equivalent (68%, entry 6). In the absence of TFA, the yield **3a** decreased to 64% (entry 7). It is noteworthy that the presence of palladium catalyst, silver salt, and blue light (422-490) was very crucial to the formation of the desired product, as the formation of **3a** was not observed in the absence of a palladium catalyst (entry 8), or silver salt (entry 9), or light (entry 10), and the starting material was found to be unreacted. Notably, when the reaction was performed under green light (470-566), a meagre yield of **3a** was obtained (15%, entry 11), whereas, under irradiation of white light (white CFL), the desired product was obtained in 41% yield (entry 12). When the reaction was performed under a nitrogen atmosphere, the yield of the desired product was lowered (77%, entry 13), suggesting no involvement of oxygen in the reaction. When the reaction was carried out using Eosin-Y (3 mol%) as a photocatalyst under standard conditions but in the absence of silver salt, desired product **3a** was obtained in only 5% yield, indicating the potential importance of silver salt in the reaction (entry 14).

After optimizing the reaction conditions, we investigated the substrate scope of ortho C–H arylation with substituted 2-aryl-pyrido[1,2-*a*]pyrimidin-4-ones (**1**) and 4-methoxybenzenediazonium tetrafluoroborate (**2a**) (Scheme 4.3). A methyl group substituted on different positions of 2-aryl-pyrido[1,2-*a*]pyrimidin-4-ones underwent smooth ortho C–H arylation reaction under optimized conditions and yielded corresponding products **3b-d** in good to excellent yields (68-95%). Electron-withdrawing halogens (-F, -Cl, -Br) on 2-aryl-pyrido[1,2-*a*]pyrimidin-4-ones successfully delivered the desired products **3e-g** with favourable outcomes (75-77%). Altering the substitution patterns on ortho and meta positions of the 2-aryl ring of 2-aryl-pyrido[1,2-*a*]pyrimidin-4-ones by strong donating methoxy group and halogens, produced the corresponding products **3h-3l** in 65-95%

yield. Further, the ortho arylation approach was applied to structurally diverse 7-phenyl-5*H*-thiazolo[3,2-*a*]pyrimidin-5-ones, forming **3m** and

Scheme 4.3 Substrate scope arylation of pyrido[1,2-*a*]pyrimidin-4-ones^[a]



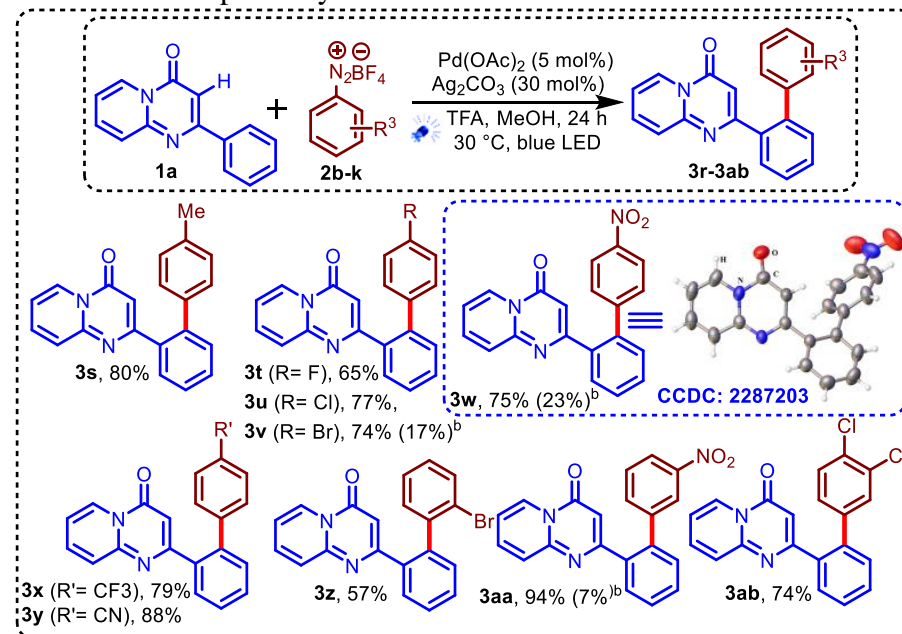
^[a]Reaction conditions: **1a** (0.2 mmol), **2a** (0.3 mmol), Pd(OAc)₂ (5 mol%), Ag₂CO₃(30 mol%), TFA 0.1 mL, MeOH 2.0 mL, blue LED, 30 °C, 24 h.; nr = no reaction.

3n in 68% and 79%, respectively. Having methyl and halogens at various positions on 2-aryl-4*H*-pyrido[1,2-*a*]pyrimidin-4-one yielded the desired products **3o**, **3p**, and **3q** in good yields of 68%, 71%, and 74%, respectively. The reaction with 2-(2-benzoyl phenyl)-4*H*-pyrido[1,2-*a*]pyrimidin-4-one did not produce the desired product **3r**, and the starting material was found to be unreacted.

Subsequently, the substrate scope of substituted aryl diazonium salts was also investigated (**Scheme 4.4**). Para-substituted (-Me, -F, -Cl, -Br) aryl diazonium salts were reacted with 2-phenyl-4*H*-pyrido[1,2-*a*]pyrimidin-4-one to give the corresponding C-H arylated products **3s-v** in good yields (65-80%). Notably, para-substituted aryl diazonium

salts having strong withdrawing groups (-NO₂, -CF₃, -CN) produced desired products **3w-3y** in excellent yields (75-88%). Whereas ortho bromo-benzene diazonium tetrafluoroborate delivered the desired

Scheme 4.4 Scope of aryl diazonium tetrafluoroborate^[a]



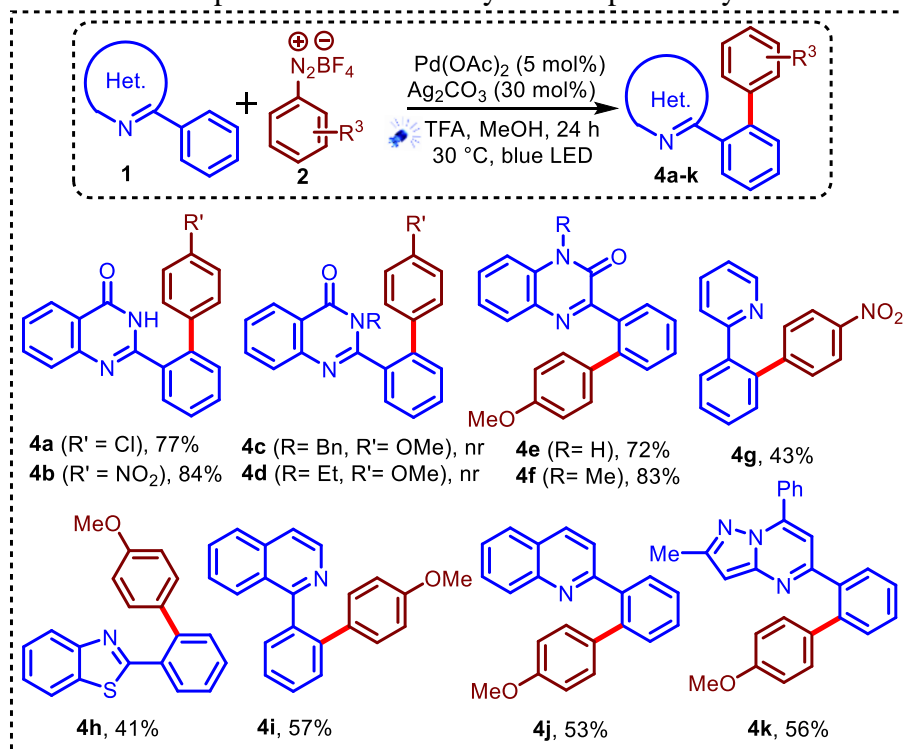
^[a]Reaction conditions: **1a** (0.2 mmol), **2a** (0.3 mmol), Pd(OAc)₂ (5 mol%), Ag₂CO₃(30 mol%), TFA 0.1 mL, MeOH 2.0 mL, blue LED, 30 °C, 24 h, ^[b]without Ag₂CO₃.

-product **3z** in moderate yield (57%). Importantly, meta-nitrobenzene diazonium tetrafluoroborate gave an excellent yield of the desired product **3aa** (94%). 3,4-Dichlorobenzenediazonium tetrafluoroborate with **1a**, produced ortho arylated product **3ab** in 74% yield.

Next, the generality of the optimized external photocatalyst-free, light-induced reaction condition for ortho C–H arylation was explored on a diverse range of 2-aryl heterocycles (**Scheme 4.5**). At the outset, the reaction between 2-phenylquinazolin-4(3H)-one and 4-substituted benzene-diazonium tetrafluoroborate (-Cl, -NO₂) led to the formation of the targeted products **4a** and **4b**, with impressive yields of 77% and 84%, respectively. Whereas the reaction failed to produce desired products **4c-4d** when 3-benzyl and 3-ethyl-2-phenylquinazolin-4(3H)-one was reacted with **2a**. Further, 3-phenylquinoxalin-2(1H)-one and 1-methyl-

3-phenyl-quinoxalin-2(1*H*)-one was both reacted with 4-methoxybenzenediazonium tetrafluoroborate to give **4e** and **4f** in 72% and 83% yield, respectively. 2-Phenylpyridine, 2-phenylbenzo-*[d]*thiazole, 1-phenylisoquinoline, 2-phenylquinoline, and 2-methyl-

Scheme 4.5 Scope of various heterocyclic compound arylation^[a]

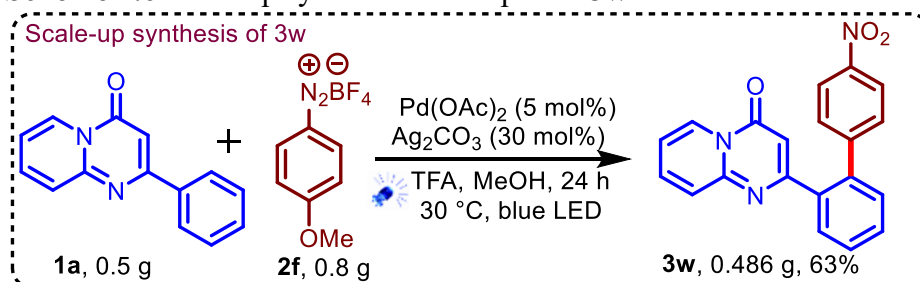


^[a]Reaction conditions: **1a** (0.2 mmol), **2a** (0.3 mmol), Pd(OAc)₂ (5 mol%), Ag₂CO₃ (30 mol%), TFA 0.1 mL, MeOH 2.0 mL, blue LED, 30 °C, 24 h.; nr = no reaction.

5,7-diphenylpyrazolo[1,5-*a*]pyrimidine were successfully underwent the regioselective C–H arylation under the optimized reaction conditions to deliver desired products **4g-4k** in moderate yields (41-57%).

In addition, scale-up synthesis of compound **3w** was performed under optimized reaction conditions to deliver the desired product **3w** in 63% yield (Scheme 4.6).

Scheme 4.6 Scale-up synthesis of compound **3w**



To gain insight into the mechanism of the photocatalyst-free, ortho C–H arylation reaction, a series of control experiments were conducted (**Scheme 4.7**). The investigation commenced by examining radical scavengers to elucidate the nature of the reaction pathway, precisely whether it followed an ionic or radical mechanism. A light-mediated reaction was executed in the presence of the radical scavenger TEMPO in varying equivalents under the standard conditions (**Scheme 4.7a**). The yield of the ortho-arylated desired product significantly decreased to 18%, accompanied by the formation of TEMPO adduct **5a**, as confirmed through high-resolution mass spectrometry (HRMS) analysis. In addition to the light dependency of the reaction-

Scheme 4.7 Control experiments, light On/Off, color observation and UV-visible study

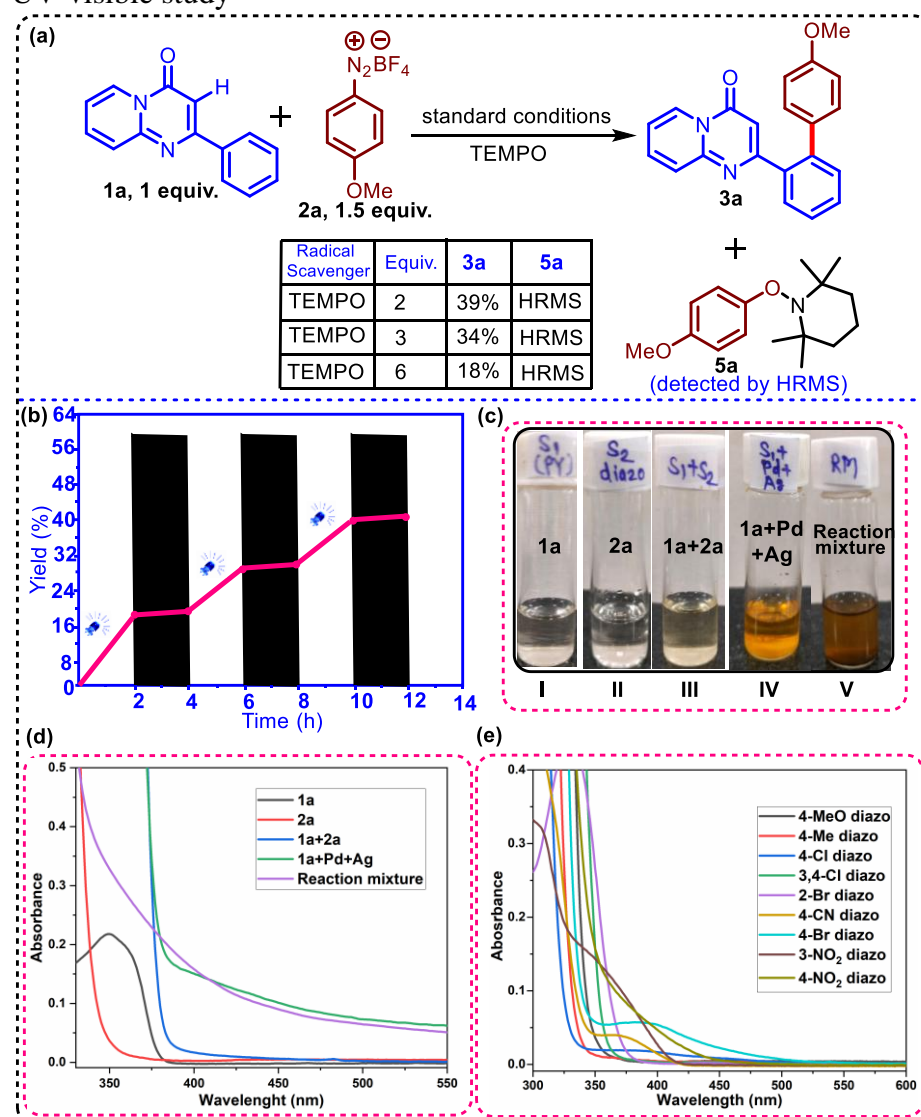


(Table 4.1, entry 10), the light-on-off experiment was performed (Scheme 4.7b), which further established the necessity of the continuous irradiation of the blue light for the anticipated reaction. The quantum yield of the reaction was measured to be $\Phi = 0.185$. Each reaction component and their diverse combinations (I-V) in methanol as solvent were observed visually (Scheme 4.7c). It was observed that individual components **1a** (I), **2a** (II), and the mixture of **1a+2a** (III) were almost colorless, whereas visual coloration emerged notably for the combination of **1a** with Pd(II) catalyst and Ag₂CO₃, i.e., IV, and reaction mixture (V). The UV-visible spectroscopic study of these individual components and their combinations (I-V) revealed that individual components such as pyrido[1,2-*a*]pyrimidin-4-one (**1a**), 4-methoxy benzene diazonium tetrafluoroborate (**2a**), or a mixture of **1a+2a** did not exhibit absorption above 400 nm. However, the combination of **1a** with Pd(II) catalyst and Ag₂CO₃ i.e. IV and reaction mixture (V), absorption gradually increased, surpassing 400 nm (Scheme 4.7d). Further, UV-visible spectroscopic analysis was conducted on various aryl-diazonium tetrafluoroborate using methanol as solvent. The findings indicated that the absorption for most aryl-diazonium tetrafluoroborate occurred below 390 nm. Exceptions were observed in the cases of 4-bromo, 4-nitro, and 3-nitro aryl-diazonium tetrafluoroborate, where a subtle increase in absorption beyond 400 nm was observed (Scheme 4.7e). Further, H/D exchange experiments were conducted using CD₃OD under standard reaction conditions, both in the absence and presence of 4-methoxy benzene diazonium tetrafluoroborate (**2a**). Additionally, Kinetic Isotope Effect experiments were performed using **1a** and [**D5**]-**1a** under standard reaction conditions.

Further, time-dependent density functional theory (TDDFT) calculations of possible intermediates were performed. Based on the results and observations of the above control experiments, DFT studies, and previous literature reports,^[23-26, 47-51] plausible reaction mechanism paths for the reaction are proposed (Scheme 4.8). The mechanism initiates with the formation of palladacycle intermediate [A]. Time-

dependent density functional theory (TDDFT) calculations show that the EDA complex **[B]** is supposed to absorb light ~488 nm. This excitation is an intermolecular charge transfer excitation (**Figure 4.1**).

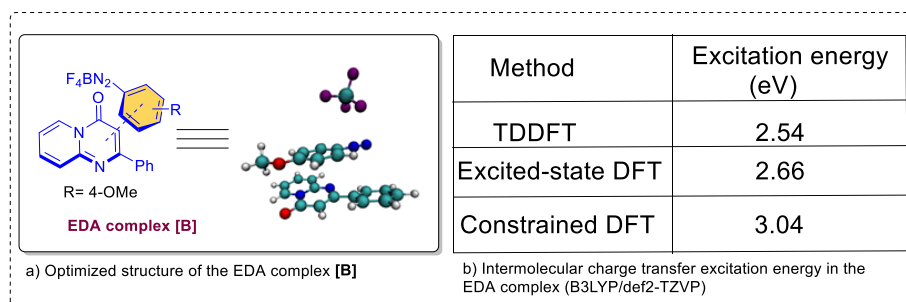
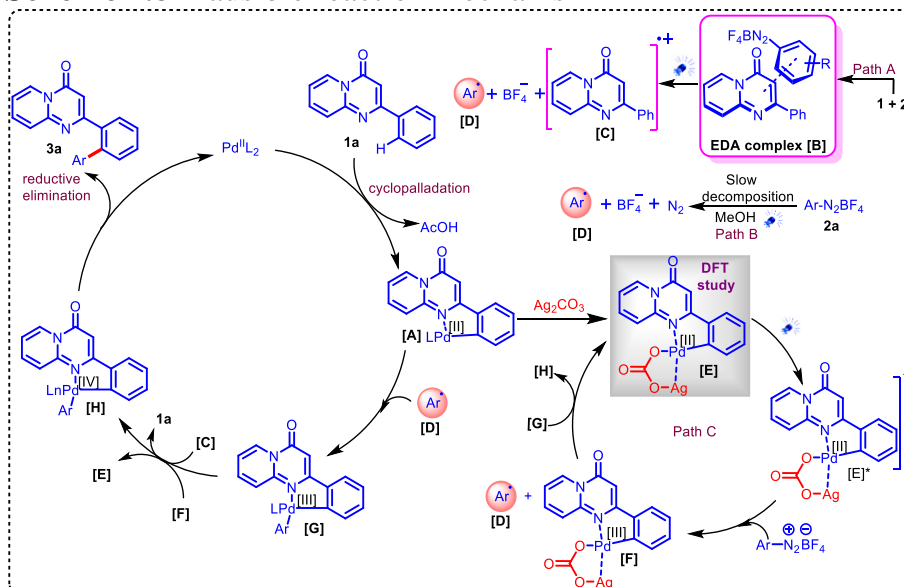


Figure 4.1 a) Optimized structure of the EDA complex **[B]** and b) Table of intermolecular charge transfer excitation energy in the EDA complex (B3LYP/def2-TZVP)

As TDDFT is known to underestimate such excitations, we have employed other approaches in (**Figure 4.1b**) to provide a possible energy range of ~408-488 nm where this excitation may occur for the EDA complex. Previous studies^[23-26] have suggested that heterocycles, when combined with aryl diazonium salt, form EDA complexes, which may play a role in light absorption and generation of aryl radicals for subsequent arylation. Oliveira's group has shown that the formation of the EDA complex is solvent-dependent.^[23] Aprotic solvents like DMSO facilitate the formation of the EDA complex, but in the presence of protic solvents, the formation of the EDA complex has not been observed.^[23] The color observation (**Scheme 4.7c**) and UV-visible study (**Scheme 4.7d**) of the mixture of **1a** with **2a** do not prominently suggest the formation of an EDA complex between them. It may be possible that a weak EDA complex between **1a** and **2a** may generate aryl radical under visible light irradiation (**Scheme 4.8**, Path A) and combine with palladacycle intermediate **[A]** to form an intermediate **[G]**. Although the possibility of generation of aryl radicals through a slow decomposition of aryl diazonium salt under visible light may not be completely ruled out (**Scheme 4.8**, Path B), aryl diazonium salts did not show prominent UV-visible absorption in the visible range (**Scheme 4.7e**).^[49] The combination of palladacycle intermediate **[A]** with silver carbonate

Scheme 4.8 Plausible reaction mechanism



forms a silver-palladacycle complex **[E]** which can further undergo excitation upon absorption of blue light to generate an excited intermediate **[E]^{*}**. The computed optimized structure of the Ag-Palladacycle complex **[E]** is presented in **scheme 4.9**.

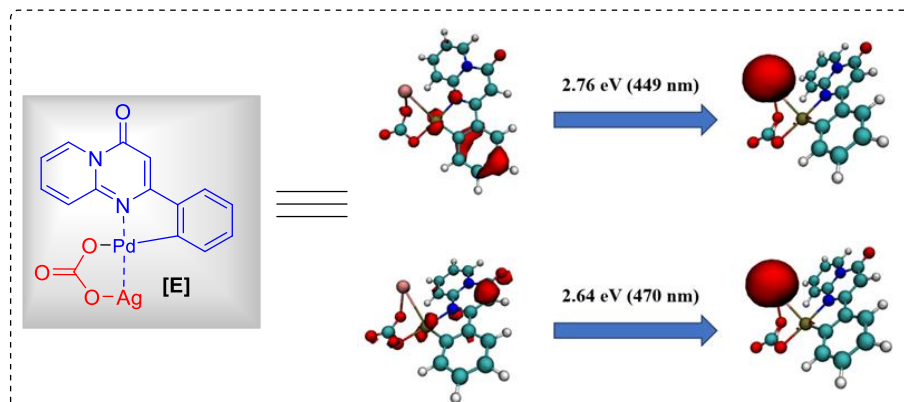
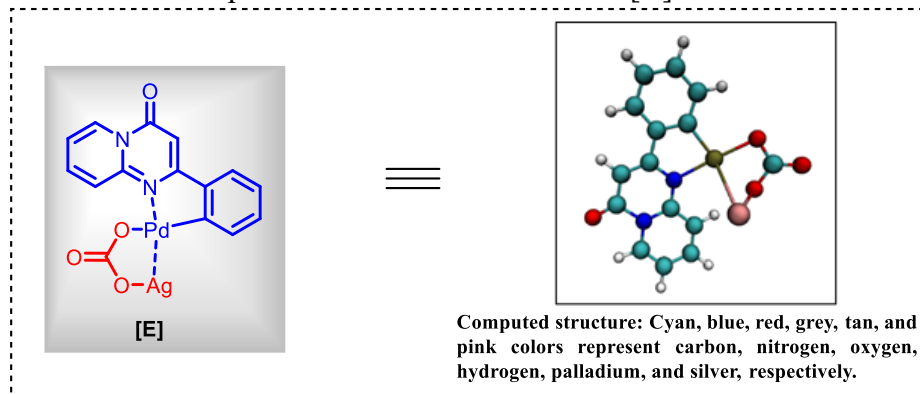


Figure 4.2 Orbitals involved in the low-lying excited states in intermediate **[E]**.

TDDFT calculation shows that complex **[E]** has two excitations, 2.64 eV (470 nm) and 2.76 eV (449 nm), that come in the blue region (**Figure 4.2**). Both these excitations correspond to electronic transitions from Pd 4d orbitals to Ag 5s orbital. Hence, computation suggests that metal-to-metal electronic excitations play an essential role in the photocatalysis process.

Scheme 4.9 Computed structure of intermediate [E]



This justifies the fact that the reaction does not occur without a palladium catalyst or silver carbonate (**Table 4.1**, entries 8 & 9). Further, excited intermediate [E]^{*} generates radical intermediate [D] from aryl diazonium salt **2** and Palladium (III) intermediate [F]. Palladacycle intermediate [A] undergoes oxidative coupling with aryl radical [D], providing the Pd(III) intermediate [G]. Pd(III) intermediate [G] is oxidized to the Pd(IV) intermediate [H] by the reduction of [F] to [E]. Finally, reductive elimination occurs, producing the ortho-arylated product **3a** and Pd(II) for the subsequent cycle. The fact that the necessity of the silver salt and Pd(II), as well as the formation of colored aggregate between **1a**, Pd(II), and Ag (**Scheme 4.7c**) and their UV-visible absorption above 400 nm (**Scheme 4.7d**) underscores the potential involvement of silver-Pd-complex [E] in this process. DFT study of the complex [E] further supports this.

4.5 Summary

An extrinsic photocatalyst-free and ligand-free approach is developed, featuring an in situ formed Ag-Pd complex-mediated regioselective C–H arylation of 4H-pyrido[1,2-a]pyrimidin-4-ones under visible-light irradiation. This method yields ortho-arylated products with 41-95% efficiency at room temperature. To support the possible mechanistic paths, various controlled experiments, UV-visible spectroscopic analysis, observation of colored complexes, and their DFT studies have been carried out. Apart from 4H-pyrido[1,2-a]pyrimidin-4-ones, the range of 2-aryl heterocycles successfully underwent regioselective ortho

C–H arylation by a photocatalyst-free visible light-induced approach. The current method for ortho C–H arylation has proven to be applicable to the scalable synthesis process.

4.6 Experimental section

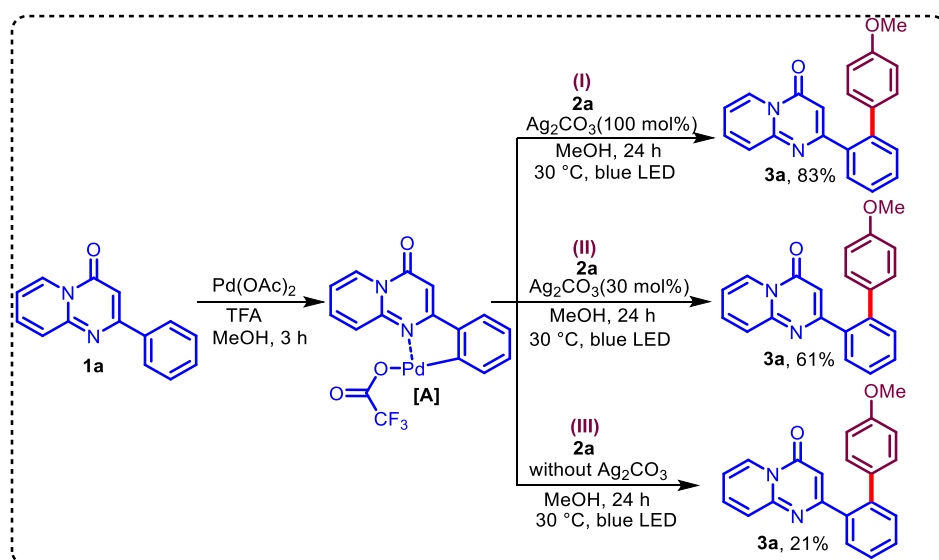
Procedure for synthesis of 2-(4'-methoxy-[1,1'-biphenyl]-2-yl)-4H-pyrido[1,2-*a*]pyrimidin-4-one (3a):

A mixture of 2-phenyl-4H-pyrido[1,2-*a*]pyrimidin-4-one (**1a**) (1.0 equiv., 0.2 mmol, 45 mg), 4-methoxybenzenediazonium tetrafluoroborate (**2a**) (1.5 equiv., 0.3 mmol, 67 mg), Pd(OAc)₂ (5 mol%), Ag₂CO₃ (30 mol%) were added in oven-dried reaction vessel equipped with magnetic stirring bar, followed by addition of methanol (2.0 mL) and TFA (0.1 mL). The reaction mixture was stirred at room temperature (30 °C) under blue LED irradiation for 24 h. The resulting reaction mixture was quenched with water (2.0 mL), extracted with ethyl acetate (3 × 10 mL), and washed with brine solution. The combined organic layer was separated and dried over Na₂SO₄. After filtration and evaporation under reduced pressure to yield the crude product, which was further subjected to silica gel column chromatography using pet ether: ethyl acetate as eluent to give product 2-(4'-methoxy-[1,1'-biphenyl]-2-yl)-4H-pyrido[1,2-*a*]pyrimidin-4-one (**3a**) in 88% (57 mg). The above procedure was used to synthesize all ortho-arylated 2-phenyl-pyrido[1,2-*a*]pyrimidin-4-ones (**3a-3ab**) and (**4a-4k**).

4.7 Mechanistic insights into product formation (3a)

A mixture of 2-phenyl-4H-pyrido[1,2-*a*]pyrimidin-4-one (**1a**) (1.0 equiv., 0.4 mmol) and Pd(OAc)₂ (1.0 equiv.) was placed in an oven-dried reaction vessel equipped with a magnetic stirring bar. Methanol (4.0 mL) and TFA (0.2 mL) were added, and the mixture was stirred at room temperature (30 °C) under blue LED irradiation for 3 hours. The mixture was then filtered, producing the intermediate compound [A], which was light yellow in color. Further, the reaction of intermediate [A] was performed with aryl diazonium salt under standard conditions

with and without Ag_2CO_3 . The formation of the desired ortho-arylated product **3a** was observed in an 83% yield in the presence of Ag_2CO_3 (100 mol%), in a 61% yield in the presence of Ag_2CO_3 (30 mol%), whereas in the absence of Ag_2CO_3 , it delivered the desired product **3a** in 21% yield, which further highlights the role of Ag_2CO_3 in arylation reaction.



Scheme 4.10: Mechanistic insights into product formation (**3a**)

4.8 Characterization data of **3a-3ab** and **4a-4k**

2-(4'-Methoxy-[1,1'-biphenyl]-2-yl)-4H-pyrido[1,2-a]pyrimidin-4-one (3a**):** Brown solid; yield: 88% (57 mg); m.p.168-170 °C; ^1H NMR (500 MHz, CDCl_3): δ 9.02 (d, J = 7.2 Hz, 1H), 7.71 (t, J = 8.2 Hz, 2H), 7.64 (d, J = 9.0 Hz, 1H), 7.50 - 7.42 (m, 3H), 7.19 (d, J = 8.1 Hz, 2H), 7.12 (t, J = 7.0 Hz, 1H), 6.80 (d, J = 8.2 Hz, 2H), 6.22 (s, 1H), 3.77 (s, 3H); ^{13}C NMR (126 MHz, CDCl_3): δ = 165.1, 158.9, 157.8, 151.0, 140.7, 137.7, 136.2, 133.3, 131.0, 130.5, 130.0, 129.6, 127.4, 127.3, 126.7, 115.4, 113.9, 105.7, 55.3; **IR** (ATR): 1672, 1514, 1471, 1243, 1033, 836, 760 cm^{-1} ; **HRMS** (ESI, m/z): calcd for $\text{C}_{21}\text{H}_{17}\text{N}_2\text{O}_2[\text{M}+\text{H}]^+$: 329.1285, found: 329.1290.

2-(4'-Methoxy-[1,1'-biphenyl]-2-yl)-6-methyl-4H-pyrido[1,2-a]pyrimidin-4-one (3b**):** Golden solid; yield: 68% (46 mg); m.p.160-162 °C; ^1H NMR (500 MHz, CDCl_3): δ 7.70 (d, J = 7.3 Hz, 1H), 7.45 -

7.34 (m, 5H), 7.21 (d, $J = 8.7$ Hz, 2H), 6.82 (d, $J = 8.8$ Hz, 2H), 6.62 (d, 6.5 Hz, 1H), 6.03 (s, 1H), 3.78 (s, 3H), 3.02 (s, 3H); ^{13}C NMR (126 MHz, CDCl_3): $\delta = 163.2, 162.0, 158.8, 153.4, 143.9, 140.6, 137.2, 135.0, 133.4, 130.9, 130.4, 129.8, 129.4, 127.3, 125.6, 118.2, 113.8, 107.7, 55.3, 24.8$; IR (ATR): 1668, 1475, 1438, 1236, 1027, 799, 756 cm^{-1} ; HRMS (ESI, m/z): calcd for $\text{C}_{22}\text{H}_{19}\text{N}_2\text{O}_2[\text{M}+\text{H}]^+$: 343.1441, found: 343.1454.

2-(4'-Methoxy-[1,1'-biphenyl]-2-yl)-7-methyl-4H-pyrido[1,2-

a]pyrimidin-4-one (3c): Grey solid; yield: 70% (48 mg); m.p.186-188 °C; ^1H NMR (500 MHz, CDCl_3): δ 8.82 (s, 1H), 7.69 (d, $J = 7.5$ Hz, 1H), 7.56 (s, 2H), 7.48 - 7.40 (m, 3H), 7.18 (d, $J = 8.6$ Hz, 2H), 6.78 (d, $J = 8.5$ Hz, 2H), 6.19 (s, 1H), 3.76 (s, 3H), 2.41 (s, 3H); ^{13}C NMR (126 MHz, CDCl_3): $\delta = 164.7, 158.9, 157.7, 150.0, 140.7, 139.2, 137.8, 133.4, 130.9, 130.5, 130.0, 129.5, 127.4, 126.2, 125.8, 124.8, 113.9, 105.4, 55.3, 18.5$; IR (ATR): 1670, 1524, 1473, 1243, 1033, 819, 758 cm^{-1} ; HRMS (ESI, m/z): calcd for $\text{C}_{22}\text{H}_{19}\text{N}_2\text{O}_2[\text{M}+\text{H}]^+$: 343.1441, found: 343.1446.

2-(4'-Methoxy-[1,1'-biphenyl]-2-yl)-8-methyl-4H-pyrido[1,2-

a]pyrimidin-4-one (3d): White solid; yield: 95% (64 mg); m.p.170-172 °C; ^1H NMR (500 MHz, CDCl_3): δ 8.90 (d, $J = 7.3$ Hz, 1H), 7.67 (d, $J = 7.6$ Hz, 1H), 7.47 - 7.40 (m, 4H), 7.18 (d, $J = 8.7$ Hz, 2H), 6.95 - 6.93 (dd, $J = 7.3, 1.9$ Hz, 1H), 6.79 (d, $J = 8.7$ Hz, 2H), 6.13 (s, 1H), 3.76 (s, 3H), 2.46 (s, 3H); ^{13}C NMR (126 MHz, CDCl_3): $\delta = 165.4, 158.8, 157.8, 151.0, 148.3, 140.6, 137.9, 133.3, 130.9, 130.5, 129.9, 129.4, 127.3, 126.6, 124.8, 118.2, 113.9, 104.8, 55.3, 21.6$; IR (ATR): 1674, 1516, 1469, 1243, 1177, 830, 762 cm^{-1} ; HRMS (ESI, m/z): calcd for $\text{C}_{22}\text{H}_{19}\text{N}_2\text{O}_2[\text{M}+\text{H}]^+$: 343.1441, found: 343.1444.

7-Fluoro-2-(4'-methoxy-[1,1'-biphenyl]-2-yl)-4H-pyrido[1,2-

a]pyrimidin-4-one (3e): Light yellow solid; yield: 77% (52 mg); m.p.168-170 °C; ^1H NMR (500 MHz, CDCl_3): δ 8.92 (d, $J = 4.9$ Hz, 1H), 7.69 (d, $J = 7.3$ Hz, 1H), 7.64 - 7.62 (m, 2H), 7.51 - 7.42 (m, 3H),

7.17 (d, $J = 8.6$ Hz, 2H), 6.80 (d, $J = 8.6$ Hz, 2H), 6.24 (s, 1H), 3.78 (s, 3H); ^{13}C NMR (126 MHz, CDCl_3): $\delta = 164.7, 158.9, 157.3$ (d, $J_{\text{CF}} = 2.1$ Hz), 155.2 (d, $J_{\text{CF}} = 245.8$ Hz), 149.0, 140.7, 137.4, 133.2, 131.0, 130.5, 130.0, 129.7, 128.8 (d, $J_{\text{CF}} = 22.7$ Hz), 128.6 (d, $J_{\text{CF}} = 4.9$ Hz), 127.4, 113.9, 113.7 (d, $J_{\text{CF}} = 41.1$ Hz), 105.4, 55.3; ^{19}F NMR (471 MHz, CDCl_3): $\delta = -132.9$ (s, 1F); HRMS (ESI, m/z): calcd for $\text{C}_{21}\text{H}_{16}\text{FN}_2\text{O}_2[\text{M}+\text{H}]^+$: 347.1190, found: 347.1210.

7-Chloro-2-(4'-methoxy-[1,1'-biphenyl]-2-yl)-4H-pyrido[1,2-*a*]pyrimidin-4-one (3f): Light green solid; yield: 76% (55 mg); m.p. 164-166 °C; ^1H NMR (500 MHz, CDCl_3): δ 9.02 (d, $J = 2.4$ Hz, 1H), 7.69 (d, $J = 7.6$ Hz, 1H), 7.64 (dd, $J = 9.5, 2.4$ Hz, 1H), 7.57 (d, $J = 9.5$ Hz, 1H), 7.50 - 7.41 (m, 3H), 7.17 (d, $J = 8.6$ Hz, 2H), 6.80 (d, $J = 8.6$ Hz, 2H), 6.24 (s, 1H), 3.77 (s, 3H); ^{13}C NMR (126 MHz, CDCl_3): $\delta = 164.9, 158.9, 156.8, 149.4, 140.7, 137.4, 137.3, 133.1, 131.0, 130.5, 129.9, 129.7, 127.7, 127.4, 125.1, 124.1, 113.9, 106.1, 55.3$; IR (ATR): 1682, 1623, 1518, 1464, 1241, 1031, 830, 762 cm^{-1} ; HRMS (ESI, m/z): calcd for $\text{C}_{21}\text{H}_{16}\text{ClN}_2\text{O}_2[\text{M}+\text{H}]^+$: 363.0895, found: 363.0906.

7-Bromo-2-(4'-methoxy-[1,1'-biphenyl]-2-yl)-4H-pyrido[1,2-*a*]pyrimidin-4-one (3g): White solid; yield: 75% (60 mg); m.p. 186-188 °C; ^1H NMR (500 MHz, CDCl_3): δ 9.13 (d, $J = 2.3$ Hz, 1H), 7.73 (dd, $J = 9.4, 7.5$ Hz, 2H), 7.50 - 7.41 (m, 4H), 7.16 (d, $J = 8.3$ Hz, 2H), 6.80 (d, $J = 8.3$ Hz, 2H), 6.24 (s, 1H), 3.78 (s, 3H); ^{13}C NMR (126 MHz, CDCl_3): $\delta = 165.0, 158.9, 156.7, 149.4, 140.7, 139.5, 137.3, 133.1, 131.0, 130.5, 129.9, 129.8, 127.7, 127.5, 127.4, 113.9, 110.8, 106.2, 55.3$; IR (ATR): 1678, 1512, 1464, 1243, 1035, 828, 760 cm^{-1} ; HRMS (ESI, m/z): calcd for $\text{C}_{21}\text{H}_{16}\text{BrN}_2\text{O}_2[\text{M}+\text{H}]^+$: 407.0390, found: 407.0399.

2-(4',5'-Dimethoxy-[1,1'-biphenyl]-2-yl)-4H-pyrido[1,2-*a*]pyrimidin-4-one (3h): Brown solid; yield: 94% (66 mg); m.p. 174-176 °C; ^1H NMR (500 MHz, CDCl_3): δ 8.98 (d, $J = 7.2$ Hz, 1H), 7.72 - 7.67 (m, 2H), 7.62 (d, $J = 8.9$ Hz, 1H), 7.19 (d, $J = 8.3$ Hz, 2H), 7.08 (t, $J = 6.9$ Hz, 1H), 6.98 (d, $J = 8.5$ Hz, 1H), 6.92 (s, 1H), 6.81 (d, $J = 8.2$

Hz, 2H), 6.13 (s, 1H), 3.87 (s, 3H), 3.77 (s, 3H); **¹³C NMR** (126 MHz, CDCl₃): δ = 164.3, 160.2, 158.8, 157.5, 150.7, 142.2, 135.7, 133.1, 131.4, 130.2, 130.0, 127.1, 126.4, 116.0, 114.9, 113.7, 112.8, 105.1, 55.3, 55.0; **HRMS** (ESI, *m/z*): calcd for C₂₂H₁₉N₂O₃[M+H]⁺: 359.1390, found: 359.1398.

2-(5-Fluoro-4'-methoxy-[1,1'-biphenyl]-2-yl)-4H-pyrido[1,2-

a]pyrimidin-4-one (3i): White solid; yield: 81% (56 mg); m.p.162-164 °C; **¹H NMR** (500 MHz, CDCl₃): δ 9.01 (d, *J* = 6.3 Hz, 1H), 7.73 - 7.69 (m, 2H), 7.62 (d, *J* = 9.0 Hz, 1H), 7.17 - 7.11 (m, 5H), 6.81 (d, *J* = 8.7 Hz, 2H), 6.15 (s, 1H), 3.77 (s, 3H); **¹³C NMR** (126 MHz, CDCl₃): δ = 164.2 (d, *J*_{CF} = 20.7 Hz), 162.2, 159.2, 157.7, 151.0, 143.1 (d, *J*_{CF} = 8.3 Hz), 136.3 133.8 (d, *J*_{CF} = 3.2 Hz), 132.2 (d, *J*_{CF} = 1.7 Hz), 132.1 (d, *J*_{CF} = 8.8 Hz), 130.4, 127.4, 126.6, 117.7 (d, *J*_{CF} = 21.6 Hz), 115.5, 114.3 (d, *J*_{CF} = 21.5 Hz), 114.0, 105.6, 55.3; **¹⁹F NMR** (471 MHz, CDCl₃): δ = -112.0 (s, 1F); **IR (ATR):** 1670, 1464, 1440, 1243, 1175, 1023, 819, 766 cm⁻¹; **HRMS** (ESI, *m/z*): calcd for C₂₁H₁₆FN₂O₂[M+H]⁺: 347.1190, found: 347.1202.

2-(5-Chloro-4'-methoxy-[1,1'-biphenyl]-2-yl)-4H-pyrido[1,2-

a]pyrimidin-4-one (3j): Brown solid; yield: 95% (68 mg); m.p.178-180 °C; **¹H NMR** (500 MHz, CDCl₃): δ 9.01 (d, *J* = 7.1 Hz, 1H), 7.72 (t, *J* = 7.8 Hz, 1H), 7.67 (dd, *J* = 8.2, 8.9 Hz, 2H), 7.39 (t, *J* = 7.3 Hz, 2H), 7.17 - 7.12 (m, 3H), 6.80 (d, *J* = 8.3 Hz, 2H), 6.15 (s, 1H), 3.77 (s, 3H); **¹³C NMR** (126 MHz, CDCl₃): δ = 163.9, 159.3, 157.7, 151.1, 142.4, 136.4, 136.1, 135.5, 132.0, 131.5, 130.9, 130.4, 127.4, 127.4, 126.7, 115.6, 114.1, 105.6, 55.3; **HRMS** (ESI, *m/z*): calcd for C₂₁H₁₆ClN₂O₂[M+H]⁺: 363.0895, found: 363.0898.

2-(5-Bromo-4'-methoxy-[1,1'-biphenyl]-2-yl)-4H-pyrido[1,2-

a]pyrimidin-4-one (3k): Light yellow solid; yield: 69% (55 mg); m.p.192-194 °C; **¹H NMR** (500 MHz, CDCl₃): δ 9.01 (d, *J* = 7.0 Hz, 1H), 7.73 (t, *J* = 7.7 Hz, 1H), 7.65 (d, *J* = 8.7 Hz, 1H), 7.60 - 7.56 (m, 3H), 7.15 (t, *J* = 7.7 Hz, 1H), 6.81 (d, *J* = 8.1 Hz, 2H), 6.16 (s, 1H), 3.78

(s, 3H); **¹³C NMR** (126 MHz, CDCl₃): δ = 163.9, 159.3, 157.7, 151.1, 142.6, 136.5, 136.4, 133.7, 131.8, 131.6, 130.4, 130.3, 127.4, 126.6, 123.8, 115.6, 114.0, 105.5, 55.3; **IR (ATR)**: 1678, 1514, 1438, 1245, 1015, 817, 768 cm⁻¹; **HRMS** (ESI, *m/z*): calcd for C₂₁H₁₆BrN₂O₂[M+H]⁺: 407.0390, found: 407.0399.

2-(4-Bromo-4'-methoxy-[1,1'-biphenyl]-2-yl)-4*H*-pyrido[1,2-*a*]pyrimidin-4-one (3l): Light green solid; yield: 65% (44 mg); m.p.186-188 °C; **¹H NMR** (500 MHz, CDCl₃): δ 9.01 (d, *J* = 7.1 Hz, 1H), 7.87 (d, *J* = 2.2 Hz, 1H), 7.77 - 7.73 (m, 1H), 7.68 (d, *J* = 8.9 Hz, 1H), 7.60 (dd, *J* = 8.3, 2.2 Hz, 1H), 7.29 (d, *J* = 8.2 Hz, 1H), 7.16 - 7.13 (m, 3H), 6.80 (d, *J* = 8.7 Hz, 2H), 6.14 (s, 1H), 3.77 (s, 3H); **¹³C NMR** (126 MHz, CDCl₃): δ = 163.4, 159.2, 157.6, 151.2, 139.6, 139.3, 136.4, 132.8, 132.5, 132.5, 132.0, 130.4, 127.4, 126.7, 121.3, 115.7, 114.0, 105.7, 55.3; **HRMS** (ESI, *m/z*): calcd for C₂₁H₁₆BrN₂O₂[M+H]⁺: 407.0390, found: 407.0392.

7-(4'-Methoxy-[1,1'-biphenyl]-2-yl)-5*H*-thiazolo[3,2-*a*]pyrimidin-5-one (3m): Light yellow solid; yield: 68% (46 mg); m.p.168-170 °C; **¹H NMR** (500 MHz, CDCl₃): δ 7.96 (d, *J* = 4.8 Hz, 1H), 7.66 (d, *J* = 7.7 Hz, 1H), 7.48 - 7.45 (m, 1H), 7.43 - 7.39 (m, 2H), 7.18 (d, *J* = 8.7 Hz, 2H), 6.98 (d, *J* = 4.8 Hz, 1H), 6.84 (d, *J* = 8.6 Hz, 2H), 6.07 (s, 1H), 3.79 (s, 3H); **¹³C NMR** (126 MHz, CDCl₃): δ = 164.1, 162.5, 158.9, 158.5, 140.7, 136.9, 133.2, 131.0, 130.4, 129.8, 129.7, 127.3, 122.0, 114.0, 111.5, 106.5, 55.3; **HRMS** (ESI, *m/z*): calcd for C₁₉H₁₅N₂O₂S[M+H]⁺: 335.0849, found: 335.0854.

7-(4'-Methoxy-5-methyl-[1,1'-biphenyl]-2-yl)-5*H*-thiazolo[3,2-*a*]pyrimidin-5-one(3n): Brownish solid; yield: 79% (54 mg); m.p.164-166 °C; **¹H NMR** (500 MHz, CDCl₃): δ 7.94 (d, *J* = 4.9 Hz, 1H), 7.59 (d, *J* = 7.8 Hz, 1H), 7.24 - 7.21 (m, 2H), 7.17 (d, *J* = 8.5 Hz, 2H), 6.97 (d, *J* = 4.9 Hz, 1H), 6.83 (d, *J* = 8.2 Hz, 2H), 6.03 (s, 1H), 3.79 (s, 3H), 2.42 (s, 3H); **¹³C NMR** (126 MHz, CDCl₃): δ = 164.0, 162.4, 158.9, 158.5, 140.6, 139.8, 134.0, 133.3, 131.8, 130.4, 129.9, 128.0, 121.9,

113.9, 111.4, 106.3, 55.3, 21.4; **HRMS** (ESI, m/z): calcd for $C_{20}H_{17}N_2O_2S[M+H]^+$: 349.1005, found: 349.1015.

2-(5-Chloro-4'-methoxy-[1,1'-biphenyl]-2-yl)-8-methyl-4H-

pyrido[1,2-*a*]pyrimidin-4-one (3o): Brown solid; yield: 68% (51 mg); m.p.158-160 °C; **¹H NMR** (500 MHz, $CDCl_3$): δ 8.90 (d, J = 7.1 Hz, 1H), 7.65 (d, J = 8.1 Hz, 1H), 7.45 (s, 1H), 7.40 - 7.38 (m, 2H), 7.17 (d, J = 8.6 Hz, 2H), 6.97 (d, J = 7.2 Hz, 1H), 6.80 (d, J = 8.3 Hz, 2H), 6.07 (s, 1H), 3.77 (s, 3H), 2.47 (s, 3H); **¹³C NMR** (126 MHz, $CDCl_3$): δ = 164.1, 159.2, 157.7, 151.0, 148.5, 142.3, 136.3, 135.3, 132.0, 131.4, 130.7, 130.4, 127.3, 126.7, 124.7, 118.3, 114.0, 104.7, 55.3, 21.6; **IR (ATR)**: 1670, 1514, 1458, 1241, 1019, 914, 821 cm^{-1} ; **HRMS** (ESI, m/z): calcd for $C_{22}H_{18}ClN_2O_2[M+H]^+$: 377.1051, found: 377.1060

2-(5-Bromo-4'-methoxy-[1,1'-biphenyl]-2-yl)-8-methyl-4H-

pyrido[1,2-*a*]pyrimidin-4-one (3p): Golden solid; yield: 71% (58 mg); m.p.170-172 °C; **¹H NMR** (500 MHz, $CDCl_3$): δ 8.90 (d, J = 7.3 Hz, 1H), 7.57 - 7.55 (m, 3H), 7.41 (s, 1H), 7.16 (d, J = 8.7 Hz, 2H), 6.97 (d, J = 7.3 Hz, 1H), 6.80 (d, J = 8.7 Hz, 2H), 6.08 (s, 1H), 3.77 (s, 3H), 2.47 (s, 3H); **¹³C NMR** (126 MHz, $CDCl_3$): δ = 164.2, 159.2, 157.7, 151.1, 148.6, 142.5, 136.8, 133.6, 131.9, 131.5, 130.4, 130.3, 126.7, 124.7, 123.6, 118.3, 114.0, 104.7, 55.3, 21.6; **HRMS** (ESI, m/z): calcd for $C_{22}H_{18}BrN_2O_2[M+H]^+$: 421.0546, found: 421.0555.

7-Chloro-2-(4'-methoxy-5-methyl-[1,1'-biphenyl]-2-yl)-4H-

pyrido[1,2-*a*]pyrimidin-4-one (3q): White solid; yield: 74% (55 mg); m.p.164-166 °C; **¹H NMR** (500 MHz, $CDCl_3$): δ 9.01 (d, J = 2.6 Hz, 1H), 7.62 (d, J = 7.9 Hz, 2H), 7.56 (d, J = 9.5 Hz, 1H), 7.24 (d, J = 5.3 Hz, 2H), 7.16 (d, J = 8.7 Hz, 2H), 6.80 (d, J = 8.7 Hz, 2H), 6.21 (s, 1H), 3.78 (s, 3H), 2.43 (s, 3H); **¹³C NMR** (126 MHz, $CDCl_3$): δ = 164.9, 158.9, 156.8, 149.3, 140.7, 139.9, 137.2, 134.5, 133.3, 131.8, 130.5, 130.0, 128.1, 127.6, 125.1, 124.0, 113.9, 106.0, 55.3, 21.4; **HRMS** (ESI, m/z): calcd for $C_{22}H_{18}ClN_2O_2[M+H]^+$: 377.1051, found: 377.1065.

2-(4'-Methyl-[1,1'-biphenyl]-2-yl)-4H-pyrido[1,2-a]pyrimidin-4-one (3s): White solid; yield: 80% (49 mg); m.p.194-196 °C; ¹H NMR (500 MHz, CDCl₃): δ 9.02 (d, *J* = 7.1 Hz, 1H), 7.72 (t, *J* = 7.8 Hz, 2H), 7.65 (d, *J* = 8.9 Hz, 1H), 7.49 - 7.42 (m, 3H), 7.16 - 7.11 (m, 3H), 7.07 (d, *J* = 7.8 Hz, 2H), 6.19 (s, 1H), 2.31 (s, 3H); ¹³C NMR (126 MHz, CDCl₃): δ = 165.0, 157.8, 151.0, 141.1, 138.0, 137.8, 136.9, 136.1, 131.0, 130.0, 129.6, 129.3, 129.2, 127.5, 127.4, 126.7, 115.4, 105.8, 21.3; **IR (ATR):** 1674, 1518, 1464, 1257, 1017, 795, 760 cm⁻¹; **HRMS** (ESI, *m/z*): calcd for C₂₁H₁₇N₂O[M+H]⁺: 313.1335, found: 313.1339.

2-(4'-Fluoro-[1,1'-biphenyl]-2-yl)-4H-pyrido[1,2-a]pyrimidin-4-one (3t): Brown solid; yield: 65% (40 mg); m.p.182-184 °C; ¹H NMR (500 MHz, CDCl₃): δ 9.02 (d, *J* = 7.1 Hz, 1H), 7.71 (t, *J* = 7.4 Hz, 2H), 7.59 (d, *J* = 8.9 Hz, 1H), 7.51 - 7.45 (m, 2H), 7.42 (d, *J* = 7.3 Hz, 1H), 7.24 - 7.21 (m, 2H), 7.12 (t, *J* = 6.9 Hz, 1H), 6.95 (t, *J* = 6.9 Hz, 2H), 6.23 (s, 1H); ¹³C NMR (126 MHz, CDCl₃): δ = 164.8, 163.1 (d, *J*_{CF} = 246.4 Hz), 157.7, 151.0, 140.0, 137.8, 137.0 (d, *J*_{CF} = 3.4 Hz), 136.3, 131.0, 130.9, 130.0, 129.6, 127.8, 127.3, 126.6, 115.5 (d, *J*_{CF} = 16.4 Hz), 115.2, 105.5; ¹⁹F NMR (471 MHz, CDCl₃): δ = -115.5 (s, 1F); **IR (ATR):** 1668, 1520, 1471, 1411, 1012, 830, 758 cm⁻¹; **HRMS** (ESI, *m/z*): calcd for C₂₀H₁₄FN₂O[M+H]⁺: 317.1086, found: 317.1085.

2-(4'-Chloro-[1,1'-biphenyl]-2-yl)-4H-pyrido[1,2-a]pyrimidin-4-one (3u): White solid; yield: 77% (50 mg); m.p.190-192 °C; ¹H NMR (500 MHz, CDCl₃): δ 9.03 (d, *J* = 6.6 Hz, 1H), 7.74 - 7.69 (m, 2H), 7.59 (d, *J* = 9.0 Hz, 1H), 7.51 - 7.48 (m, 2H), 7.42 - 7.40 (m, 1H), 7.24 - 7.19 (m, 4H), 7.15 - 7.12 (m, 1H), 6.26 (s, 1H); ¹³C NMR (126 MHz, CDCl₃): δ = 163.6, 156.6, 149.8, 138.6, 138.4, 136.7, 135.2, 132.1, 129.7, 129.5, 128.9, 128.6, 127.4, 126.9, 126.2, 125.5, 114.4, 104.3; **IR (ATR):** 1668, 1625, 1469, 1411, 920, 832, 760 cm⁻¹; **HRMS** (ESI, *m/z*): calcd for C₂₀H₁₄ClN₂O[M+H]⁺: 333.0789, found: 333.0804.

2-(4'-Bromo-[1,1'-biphenyl]-2-yl)-4H-pyrido[1,2-a]pyrimidin-4-one (3v): White solid; yield: 74% (55 mg); m.p.196-198 °C; ¹H NMR (500

MHz, CDCl₃): δ 9.02 (d, J = 7.1 Hz, 1H), 7.73 - 7.68 (m, 2H), 7.58 (d, J = 9.0 Hz, 1H), 7.50 - 7.47 (m, 2H), 7.41 - 7.37 (m, 3H), 7.14 - 7.11 (m, 3H), 6.25 (s, 1H); ¹³C NMR (126 MHz, CDCl₃): δ = 164.6, 157.7, 150.9, 140.0, 139.7, 137.7, 136.4, 131.5, 131.0, 130.8, 130.1, 129.7, 128.0, 127.3, 126.6, 121.5, 115.6, 105.4; IR (ATR): 1670, 1522, 1462, 1411, 1066, 825, 762 cm⁻¹; HRMS (ESI, m/z): calcd for C₂₀H₁₄BrN₂O[M+H]⁺: 377.0284, found: 377.0294.

2-(4'-Nitro-[1,1'-biphenyl]-2-yl)-4H-pyrido[1,2-*a*]pyrimidin-4-one

(**3w**): Light yellow solid; yield: 75% (50 mg); m.p.196-198 °C; ¹H NMR (500 MHz, CDCl₃): δ 9.02 (d, J = 7.2 Hz, 1H), 8.12 (d, J = 8.8 Hz, 2H), 7.73 - 7.69 (m, 2H), 7.55 - 7.54 (m, 2H), 7.47 - 7.42 (m, 4H), 7.14 (t, J = 6.9 Hz, 1H), 6.31 (s, 1H); ¹³C NMR (126 MHz, CDCl₃): δ = 164.2, 157.7, 150.9, 148.2, 146.8, 138.8, 138.0, 136.7, 130.7, 130.3, 130.2, 129.9, 129.0, 127.4, 126.5, 123.5, 115.8, 105.1; HRMS (ESI, m/z): calcd for C₂₀H₁₄N₃O₃[M+H]⁺: 344.1030, found: 344.1036.

2-(4'-(Trifluoromethyl)-[1,1'-biphenyl]-2-yl)-4H-pyrido[1,2-

***a*]pyrimidin-4-one (**3x**):** Brown white solid; yield: 79% (57 mg); m.p.168-170 °C; ¹H NMR (500 MHz, CDCl₃): δ 9.03 (d, J = 7.1 Hz, 1H), 7.73 - 7.70 (m, 2H), 7.55 - 7.51 (m, 5H), 7.44 (d, J = 8.1 Hz, 1H), 7.40 (d, J = 8.0 Hz, 2H), 7.14 (t, J = 6.9 Hz, 1H), 6.29 (s, 1H); ¹³C NMR (126 MHz, CDCl₃): δ = 164.5, 157.8, 151.0, 144.9, 139.6, 137.9, 136.5, 130.9, 130.2, 129.8, 129.7, 128.5, 127.4, 126.6, 125.3, 125.29, 125.26(d, J_{CF} = 3.9 Hz), 115.7, 105.3; ¹⁹F NMR (471 MHz, CDCl₃): δ = -62.4 (s, 3F); IR (ATR): 1680, 1524, 1471, 1321, 1066, 836, 762 cm⁻¹; HRMS (ESI, m/z): calcd for C₂₁H₁₃F₃N₂ONa[M+Na]⁺: 389.0872, found: 389.0854.

2'-(4-Oxo-4H-pyrido[1,2-*a*]pyrimidin-2-yl)-[1,1'-biphenyl]-4-

carbonitrile (3y**):** Light yellow solid; yield: 88% (56 mg); m.p.182-184 °C; ¹H NMR (500 MHz, CDCl₃): δ 9.02 (d, J = 7.2 Hz, 1H), 7.75 - 7.71 (m, 2H), 7.55 - 7.50 (m, 5H), 7.42 (d, J = 6.9 Hz, 1H), 7.38 (d, J = 8.2 Hz, 2H), 7.16 (t, J = 6.9 Hz, 1H), 6.29 (s, 1H); ¹³C NMR (126 MHz,

CDCl₃): δ = 164.0, 157.6, 150.8, 146.0, 139.2, 137.6, 136.9, 132.1, 130.7, 130.2, 130.0, 129.9, 128.8, 127.4, 126.3, 118.9, 115.9, 110.8, 105.1; **HRMS** (ESI, m/z): calcd for C₂₁H₁₄N₃O[M+H]⁺: 324.1131, found: 324.1139.

2-(3'-Bromo-[1,1'-biphenyl]-2-yl)-4H-pyrido[1,2-*a*]pyrimidin-4-one (3z): Brown solid; yield: 57% (42 mg); m.p.188-190 °C; **¹H NMR** (500 MHz, CDCl₃): δ 8.97 (d, J = 7.0 Hz, 1H), 7.85 (d, J = 7.1 Hz, 1H), 7.67 (t, J = 7.0 Hz, 1H), 7.57 - 7.50 (m, 4H), 7.36 (d, J = 8.9 Hz, 1H), 7.25 (d, J = 4.6 Hz, 2H), 7.15 - 7.11 (m, 1H), 7.08 (t, J = 7.1 Hz, 1H), 6.23 (s, 1H); **¹³C NMR** (126 MHz, CDCl₃): δ = 163.7, 157.9, 150.8, 141.9, 140.1, 137.9, 136.0, 132.8, 131.6, 131.3, 129.6, 129.3, 129.0, 128.5, 127.3, 127.3, 126.7, 123.6, 115.3, 104.7; **HRMS** (ESI, m/z): calcd for C₂₀H₁₄BrN₂O[M+H]⁺: 377.0284, found: 377.0289.

2-(3'-Nitro-[1,1'-biphenyl]-2-yl)-4H-pyrido[1,2-*a*]pyrimidin-4-one (3aa): Light yellow solid; yield: 94% (63 mg); m.p.184-186 °C; **¹H NMR** (500 MHz, CDCl₃): δ 9.02 (d, J = 7.2 Hz, 1H), 8.23 (s, 1H), 8.10 (d, J = 8.0 Hz, 1H), 7.76 - 7.73 (m, 2H), 7.59 - 7.54 (m, 4H), 7.47 (d, J = 8.6 Hz, 1H), 7.41 (t, J = 7.9 Hz, 1H), 7.16 (t, J = 6.9 Hz, 1H), 6.28 (s, 1H); **¹³C NMR** (126 MHz, CDCl₃): δ = 163.9, 157.6, 150.8, 148.2, 142.8, 138.5, 137.6, 137.0, 135.5, 130.8, 130.3, 130.1, 129.1, 128.8, 127.4, 126.3, 124.3, 122.1, 116.0, 105.1; **HRMS** (ESI, m/z): calcd for C₂₀H₁₄N₃O₃[M+H]⁺: 344.1030, found: 344.1034.

2-(3',4'-Dichloro-[1,1'-biphenyl]-2-yl)-4H-pyrido[1,2-*a*]pyrimidin-4-one (3ab): White solid; yield: 74% (53 mg); m.p.136-138 °C; **¹H NMR** (500 MHz, CDCl₃): δ 9.04 (d, J = 6.5 Hz, 1H), 7.76 - 7.73 (m, 1H), 7.71 - 7.69 (m, 1H), 7.61 (d, J = 9.0 Hz, 1H), 7.52 - 7.49 (m, 2H), 7.44 (d, J = 2.1 Hz, 2H), 7.40 - 7.38 (m, 1H), 7.29 (d, J = 8.2 Hz, 1H), 7.16 (t, J = 6.9 Hz, 1H), 7.05 (dd, J = 8.3, 2.1 Hz, 1H), 6.29 (s, 1H); **¹³C NMR** (126 MHz, CDCl₃): δ = 164.2, 157.7, 150.9, 141.1, 138.5, 137.6, 136.7, 132.4, 131.4, 131.1, 130.8, 130.2, 130.2, 129.8, 128.9, 128.5,

127.4, 126.5, 115.8, 105.2; **HRMS** (ESI, m/z): calcd for $C_{20}H_{13}ClN_2O[M+H]^+$: 367.0399, found: 367.0403.

2-(4'-Chloro-[1,1'-biphenyl]-2-yl)quinazolin-4(3H)-one (4a): Cream solid; yield: 77% (50 mg); m.p.164-166 °C; **1H NMR** (500 MHz, $CDCl_3$): δ 10.33 (s, 1H), 8.16 (d, $J = 7.9$ Hz, 1H), 7.81 - 7.75 (m, 3H), 7.56 (t, $J = 7.6$ Hz, 1H), 7.52 - 7.41 (m, 3H), 7.23 (d, $J = 8.6$ Hz, 2H), 7.17 (d, $J = 8.5$ Hz, 2H); **^{13}C NMR** (126 MHz, $CDCl_3$): $\delta = 162.5, 153.7, 149.0, 139.6, 137.9, 135.0, 134.1, 132.7, 131.2, 130.9, 130.5, 130.4, 128.8, 128.3, 127.9, 127.3, 126.5, 120.6$; **HRMS** (ESI, m/z): calcd for $C_{20}H_{14}ClN_2O[M+H]^+$: 333.0789, found: 333.0791.

2-(4'-Nitro-[1,1'-biphenyl]-2-yl)quinazolin-4(3H)-one (4b): Cream solid; yield: 84% (56 mg); m.p.238-240 °C; **1H NMR** (500 MHz, $CDCl_3$): δ 11.14 (s, 1H), 8.13 (d, $J = 7.9$ Hz, 1H), 8.05 (d, $J = 8.6$ Hz, 2H), 7.81 - 7.76 (m, 2H), 7.65 (d, $J = 7.9$ Hz, 2H), 7.58 (t, $J = 6.9$ Hz, 1H), 7.51 - 7.45 (m, 4H); **^{13}C NMR** (126 MHz, $CDCl_3$): $\delta = 163.2, 153.0, 148.9, 147.2, 146.8, 139.0, 135.3, 132.9, 131.3, 130.8, 130.3, 130.1, 129.2, 128.0, 127.5, 126.3, 123.6, 120.4$; **HRMS** (ESI, m/z): calcd for $C_{20}H_{14}N_2O_3[M+H]^+$: 344.1030, found: 344.1028.

3-(4'-Methoxy-[1,1'-biphenyl]-2-yl)quinoxalin-2(1H)-one (4e): Pale yellow solid; yield: 72% (47 mg); m.p.162-164 °C; **1H NMR** (500 MHz, $DMSO-d_6$): δ 12.65 (s, 1H), 7.76 (d, $J = 8.0$ Hz, 1H), 7.55 - 7.49 (m, 3H), 7.46 - 7.41 (m, 2H), 7.30 - 7.24 (m, 2H), 7.12 (d, $J = 8.2$ Hz, 2H), 6.82 (d, $J = 8.2$ Hz, 2H), 3.68 (s, 3H); **^{13}C NMR** (126 MHz, $DMSO-d_6$): $\delta = 160.2, 158.3, 153.7, 140.8, 135.4, 133.4, 132.2, 131.9, 130.2, 129.9, 129.5, 129.3$ (2C), 128.7, 126.5, 123.2, 115.2, 113.6, 55.0; **HRMS** (ESI, m/z): calcd for $C_{21}H_{17}N_2O_2[M+H]^+$: 329.1285, found: 329.1284.

3-(4'-Methoxy-[1,1'-biphenyl]-2-yl)-1-methylquinoxalin-2(1H)-one (4f): Brown solid; yield: 83% (56 mg); m.p.156-158 °C; **1H NMR** (500 MHz, $CDCl_3$): δ 7.88 (d, $J = 7.9$ Hz, 1H), 7.56 - 7.48 (m, 3H), 7.44 - 7.40 (m, 2H), 7.33 (t, $J = 7.7$ Hz, 1H), 7.24 (d, $J = 8.4$ Hz, 1H), 7.20 (d,

$J = 8.6$ Hz, 2H), 6.75 (d, $J = 8.7$ Hz, 2H), 3.72 (s, 3H), 3.49 (s, 3H); ^{13}C NMR (126 MHz, CDCl_3): $\delta = 159.4, 158.7, 154.1, 141.5, 135.6, 134.2, 133.7, 133.0, 130.44, 130.39, 129.97, 129.95, 129.8, 129.7, 127.1, 123.7, 113.76, 113.72, 55.3, 29.4$; HRMS (ESI, m/z): calcd for $\text{C}_{22}\text{H}_{19}\text{N}_2\text{O}_2[\text{M}+\text{H}]^+$: 343.1441, found: 343.1441.

2-(4'-Nitro-[1,1'-biphenyl]-2-yl)pyridine (4g): Light yellow solid; yield: 43% (23 mg); m.p. 128-130 °C; ^1H NMR (500 MHz, CDCl_3): δ 8.58 (d, $J = 4.9$ Hz, 1H), 8.09 (d, $J = 8.7$ Hz, 2H), 7.70 - 7.68 (m, 1H), 7.56 - 7.50 (m, 3H), 7.45 - 7.43 (m, 1H), 7.31 (d, $J = 8.7$ Hz, 2H), 7.19 - 7.16 (m, 1H), 7.02 (d, $J = 7.7$ Hz, 1H); ^{13}C NMR (126 MHz, CDCl_3): $\delta = 158.5, 149.5, 148.4, 146.7, 139.5, 138.6, 136.3, 130.9, 130.5, 130.4, 129.1, 129.0, 125.2, 123.4, 122.1$; HRMS (ESI, m/z): calcd for $\text{C}_{17}\text{H}_{13}\text{N}_2\text{O}_2[\text{M}+\text{H}]^+$: 277.0972, found: 277.0961.

2-(4'-Methoxy-[1,1'-biphenyl]-2-yl)benzo[d]thiazole (4h): Light yellow solid; yield: 41% (26 mg); m.p. 172-174 °C; ^1H NMR (500 MHz, CDCl_3): δ 8.04 (t, $J = 7.6$ Hz, 2H), 7.69 (d, $J = 7.9$ Hz, 1H), 7.47 - 7.40 (m, 3H), 7.37 (d, $J = 7.4$ Hz, 1H), 7.29 (d, $J = 7.7$ Hz, 1H), 7.22 (d, $J = 8.5$ Hz, 2H), 6.85 (d, $J = 8.7$ Hz, 2H), 3.78 (s, 3H); ^{13}C NMR (126 MHz, CDCl_3): $\delta = 168.2, 159.5, 152.8, 141.5, 136.8, 132.8, 132.6, 131.3, 131.1, 130.5, 130.2, 127.6, 126.0, 125.0, 123.3, 121.5, 113.9, 55.3$; HRMS (ESI, m/z): calcd for $\text{C}_{20}\text{H}_{15}\text{NOSNa}[\text{M}+\text{Na}]^+$: 340.0767, found: 340.0754.

1-(4'-Methoxy-[1,1'-biphenyl]-2-yl)isoquinoline (4i): Brown solid; yield: 57% (35 mg); m.p. 144-146 °C; ^1H NMR (500 MHz, CDCl_3): δ 8.54 (d, $J = 5.7$ Hz, 1H), 7.74 (d, $J = 8.2$ Hz, 1H), 7.59 - 7.50 (m, 6H), 7.47 (t, $J = 7.5$ Hz, 1H), 7.31 (t, $J = 7.7$ Hz, 1H), 7.00 (d, $J = 8.5$ Hz, 2H), 6.55 (d, $J = 8.5$ Hz, 2H), 3.62 (s, 3H); ^{13}C NMR (126 MHz, CDCl_3): $\delta = 161.6, 158.3, 141.9, 141.3, 138.1, 136.2, 133.6, 130.8, 130.2, 130.0, 129.97, 128.9, 127.6, 127.4, 127.0, 126.97, 126.7, 120.0, 113.0, 55.1$; HRMS (ESI, m/z): calcd for $\text{C}_{22}\text{H}_{18}\text{NO}[\text{M}+\text{H}]^+$: 312.1383, found: 312.1377.

2-(4'-Methoxy-[1,1'-biphenyl]-2-yl)quinoline (4j): Brown solid; yield: 53% (33 mg); m.p.158-160 °C; ¹H NMR (500 MHz, CDCl₃): δ 8.40 (d, *J* = 8.5 Hz, 1H), 8.01 (d, *J* = 8.6 Hz, 1H), 7.87 - 7.81 (m, 3H), 7.63 (t, *J* = 7.6 Hz, 1H), 7.57 - 7.49 (m, 3H), 7.14 (d, *J* = 8.2 Hz, 2H), 7.04 (d, *J* = 8.5 Hz, 1H), 6.77 (d, *J* = 8.2 Hz, 2H), 3.75 (s, 3H); ¹³C NMR (126 MHz, CDCl₃): δ = 159.3, 159.1, 144.8, 141.0, 137.8, 136.0, 132.9, 131.4, 131.3, 131.1, 130.8, 130.4, 127.8, 127.75, 127.74, 126.8, 126.6, 124.3, 114.0, 55.3; HRMS (ESI, *m/z*): calcd for C₂₂H₁₈NO[M+H]⁺: 312.1383, found: 312.1381.

5-(4'-Methoxy-[1,1'-biphenyl]-2-yl)-2-methyl-7-

phenylpyrazolo[1,5-*a*]pyrimidine (4k) Pale yellow solid; yield: 56% (44 mg); m.p.150-152 °C; ¹H NMR (500 MHz, CDCl₃): δ 7.91 (d, *J* = 9.1 Hz, 1H), 7.58 (d, *J* = 6.5 Hz, 2H), 7.51 - 7.40 (m, 6H), 7.22 (d, *J* = 8.7 Hz, 2H), 6.90 (d, *J* = 8.8 Hz, 2H), 6.59 (s, 1H), 6.30 (s, 1H), 3.81 (s, 3H), 2.53 (s, 3H); ¹³C NMR (126 MHz, CDCl₃): δ = 159.3, 158.5, 155.0, 150.8, 144.3, 140.7, 137.9, 133.6, 131.4, 131.1, 130.7, 130.6, 130.3, 129.7, 129.3, 128.5, 127.8, 114.2, 109.6, 96.6, 55.5, 15.0; HRMS (ESI, *m/z*): calcd for C₂₆H₂₁N₃O[M+H]⁺: 392.1757, found: 392.1758.

4.9 ^1H and ^{13}C NMR spectra of selected compounds

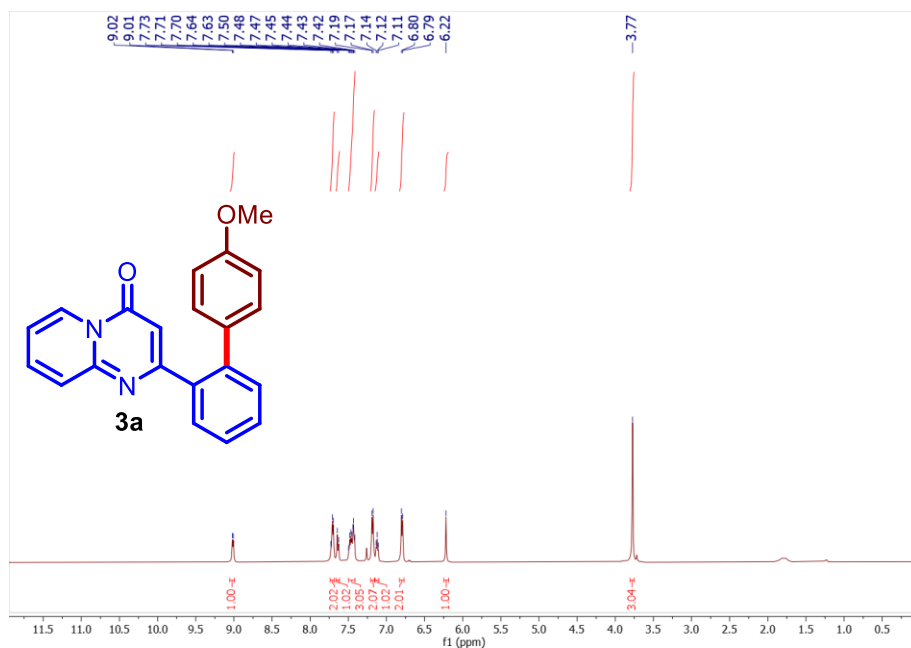


Figure 4.3 ^1H NMR spectrum of compound **3a** (500 MHz, CDCl_3)

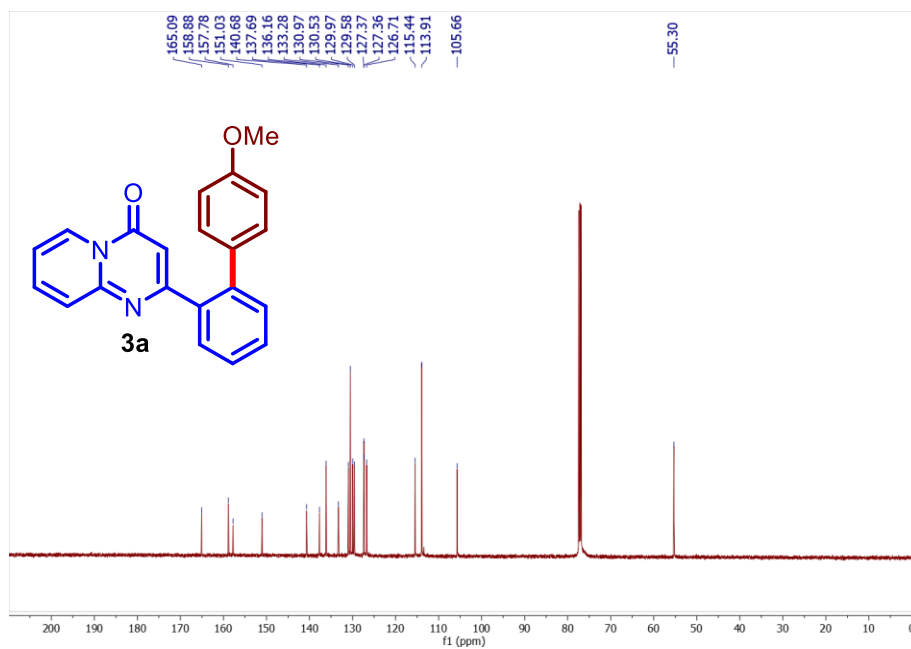


Figure 4.4 ^{13}C NMR spectrum of compound **3a** (126 MHz, CDCl_3)

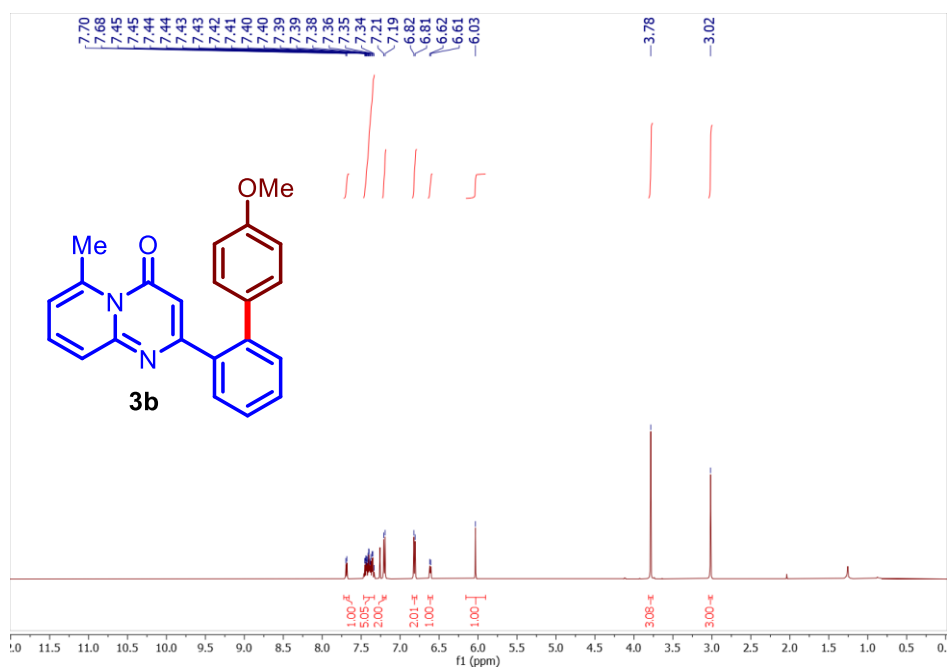


Figure 4.5 ¹H NMR spectrum of compound **3b** (500 MHz, CDCl₃)

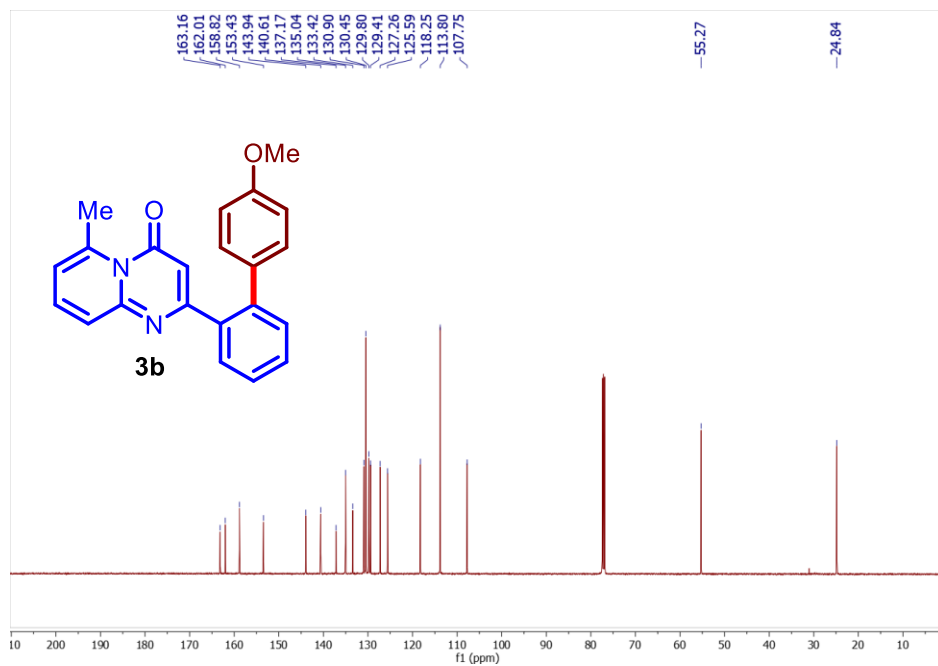


Figure 4.6 ¹³C NMR spectrum of compound **3b** (126 MHz, CDCl₃)

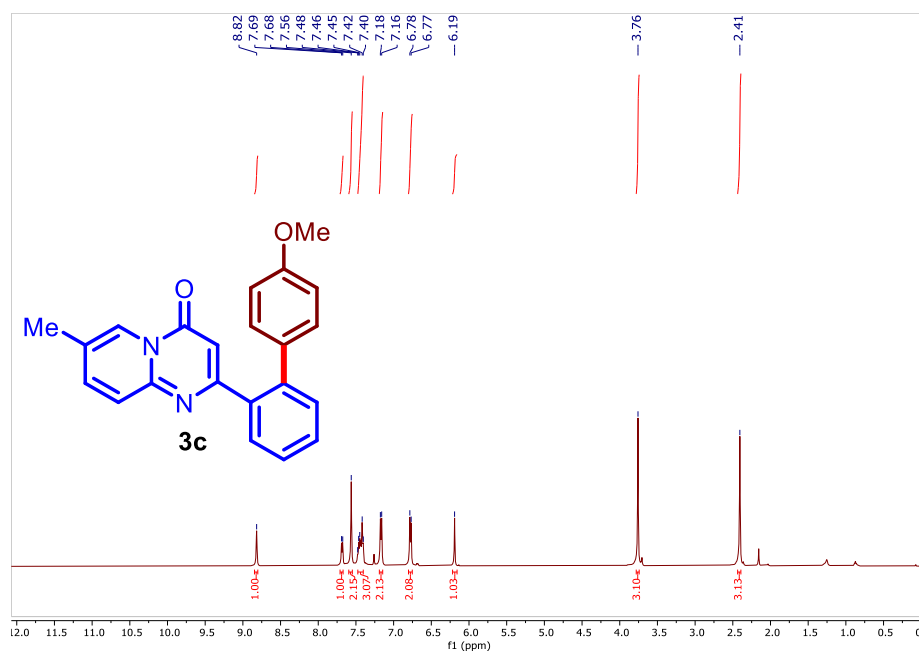


Figure 4.7 ^1H NMR spectrum of compound **3c** (500 MHz, CDCl_3)

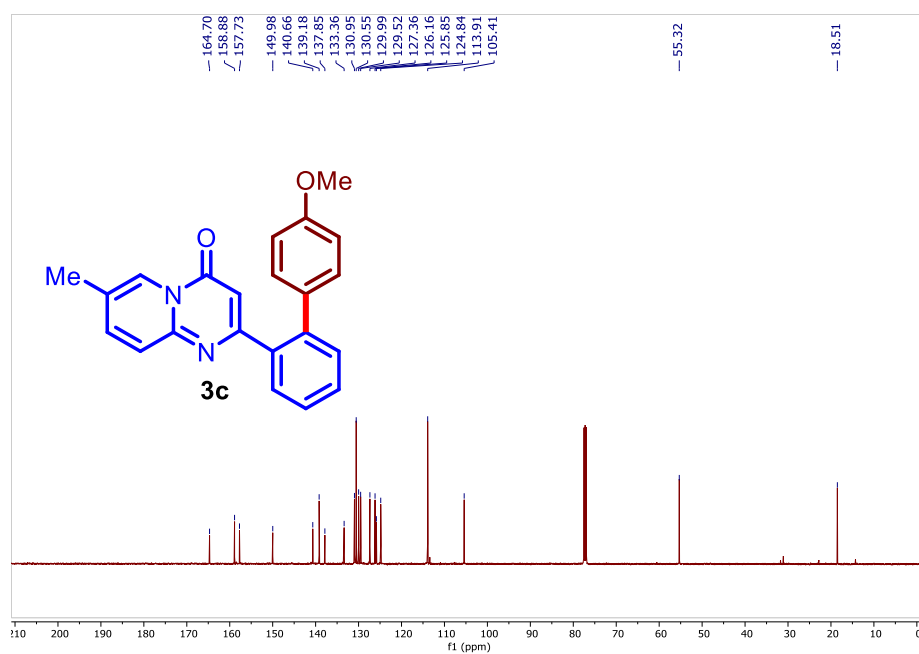


Figure 4.8 ^{13}C NMR spectrum of compound **3c** (126 MHz, CDCl_3)

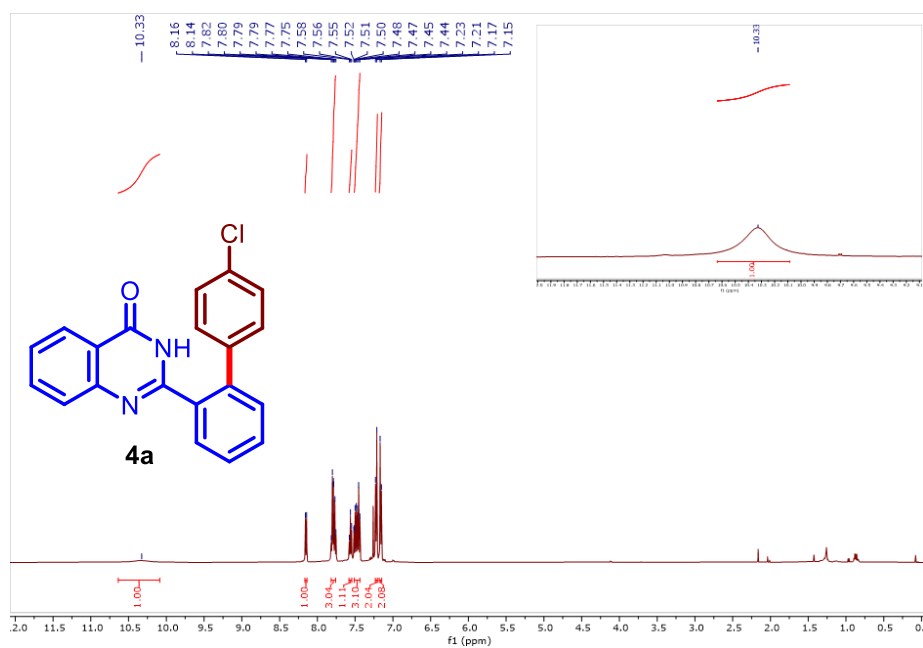


Figure 4.9 ¹H NMR spectrum of compound **4a** (500 MHz, CDCl₃)

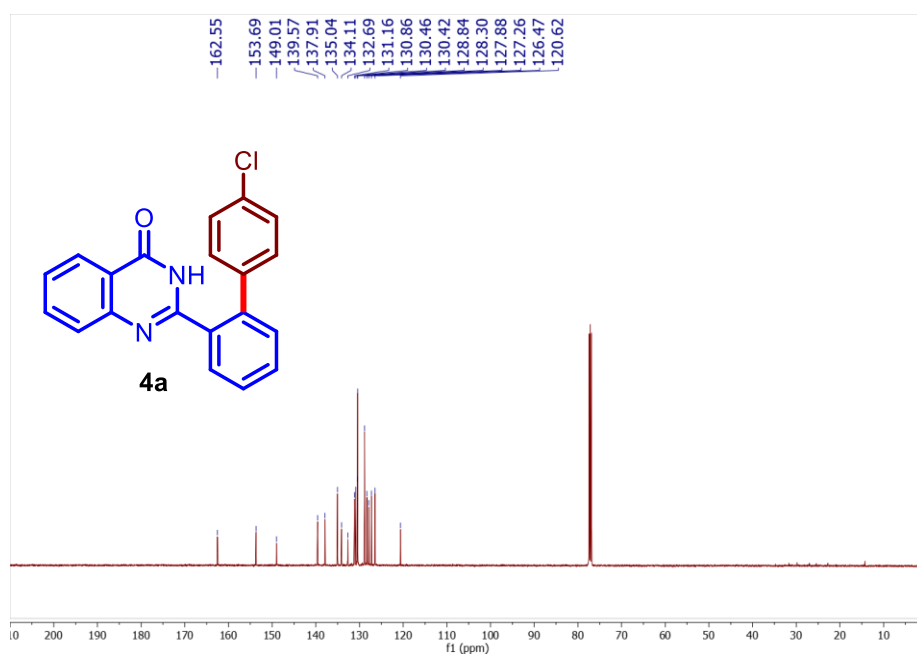


Figure 4.10 ¹³C NMR spectrum of compound **4a** (126 MHz, CDCl₃)

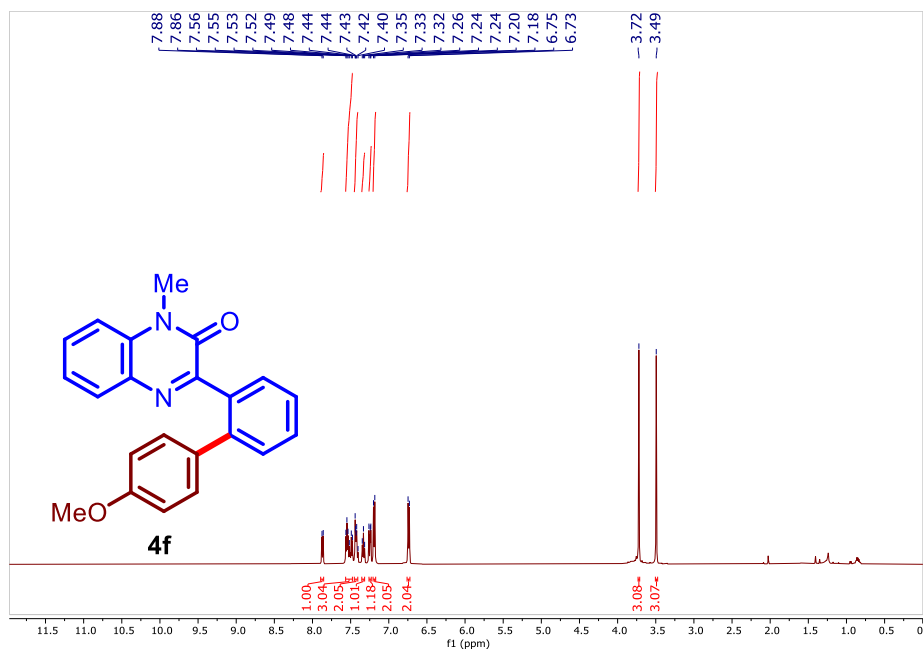


Figure 4.11 ¹H NMR spectrum of compound **4f** (500 MHz, CDCl₃)

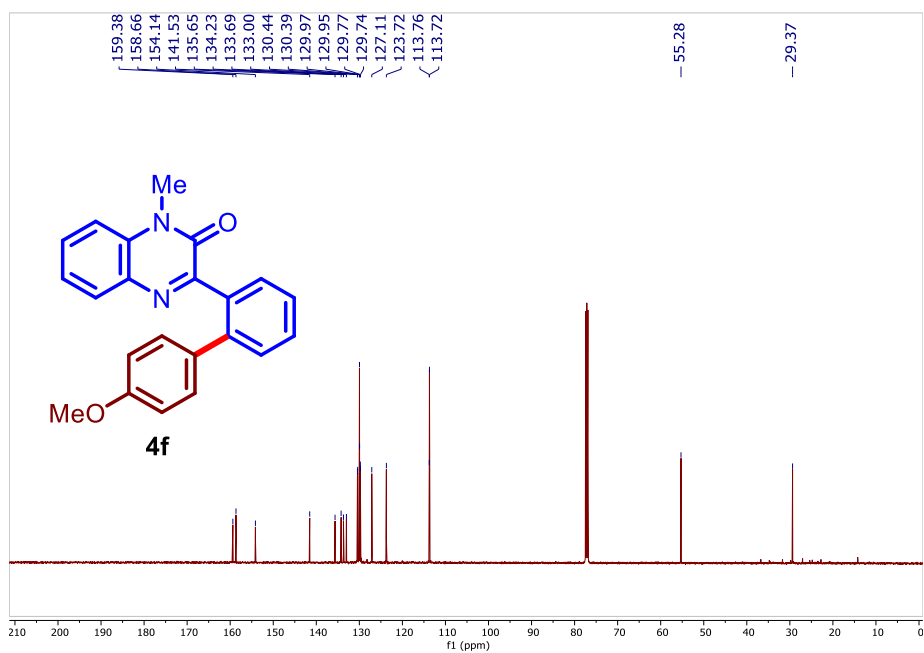


Figure 4.12 ¹³C NMR spectrum of compound **4f** (126 MHz, CDCl₃):

4.10 Computational studies

It is well known that TDDFT with several local and global hybrid exchange-correlation functionals underestimate intermolecular charge transfer excitations. Constrained DFT can eliminate that error. Here, this EDA complex has an intermolecular charge transfer excited state with excitation energy between 2.54 eV to 3.04 eV.

Computational Details^[52-53] All molecular geometries were optimized at the Kohn-Sham density functional theory level with B3LYP exchange-correlation functional and def2-TZVP basis set. Grimme's D3 dispersion correction was used with Beck-Johnson damping factor. TDDFT calculations were also performed at the same level of theory. Solvent effects were modeled via the conductor-like screening model (COSMO). All calculations were performed using NWChem computational chemistry software.

4.11 The Single Crystal X-ray Diffraction data

Sample Preparation: 2-(4'-Nitro-[1,1'-biphenyl]-2-yl)-4*H*-pyrido[1,2-*a*]pyrimidin-4-one (**3w**) was dissolved in 5.0 mL of acetonitrile. The solution was stored at room temperature for seven days, followed by further storage in a -20 °C freezer for another five days, forming yellowish crystals. The single crystal X-ray diffraction data for **3w** were obtained with a 50% ellipsoid probability.

The single crystal X-ray diffraction data were collected using MoK α ($\lambda = 0.71073$) radiation on a SCXRD dual core Agilent Technologies (Oxford Diffraction) Supernova CCD System. Structure refinements were carried out using SELEX and OLEX2. Direct method was used to solve this structure, and routine refinement was used to refine the solution. These data can be obtained free of charge from The Cambridge Crystallographic Data Centre via www.ccdc.cam.ac.uk/request/cif. (or from the Cambridge Crystallographic Data Centre, 12 Union Road, Cambridge CB21 3EZ, UK; Fax: (+44) 1223-336-033; or deposit@ccdc.cam.ac.uk).

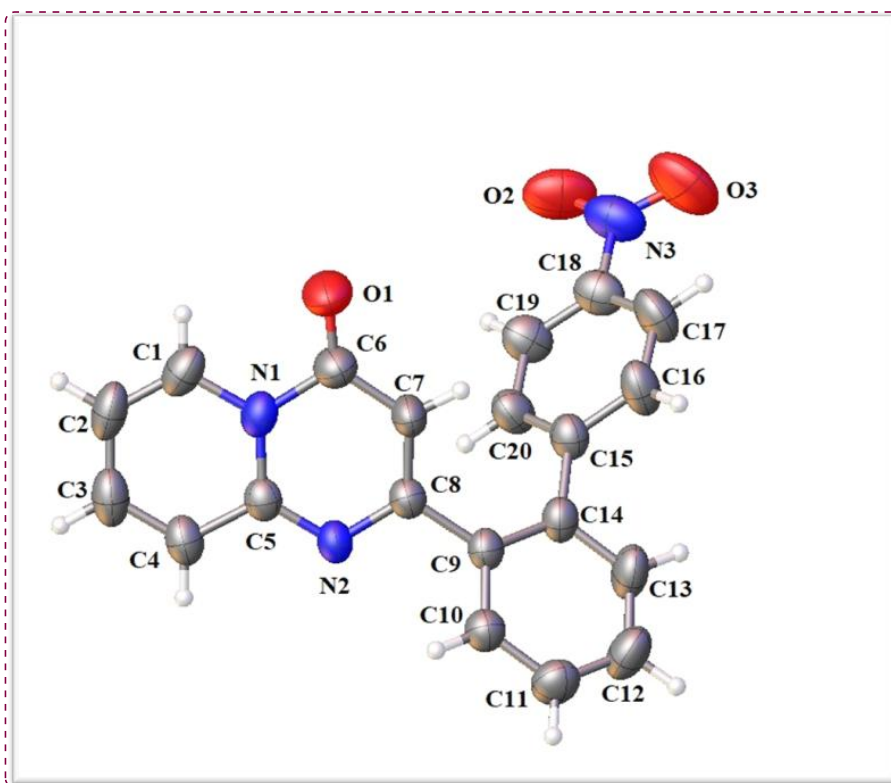


Figure 4.13. The ORTEP plot of sample **3w** (CCDC 2287203) with 50% ellipsoid probability.

Table 4.2 The crystallographic data for compound **3w**:

Compound name	2-(4'-Nitro-[1,1'-biphenyl]-2-yl)-4 <i>H</i> -pyrido[1,2- <i>a</i>]pyrimidin-4-one
Empirical formula	C ₂₀ H ₁₃ N ₃ O ₃
Formula weight	343.33
Temperature/K	293(2)
Wavelength (Å)	0.71073 Å
Crystal system	triclinic
Space group	P-1
<i>a</i> /Å	7.2670(6)
<i>b</i> /Å	13.4090(12)
<i>c</i> /Å	17.3897(14)
α /°	94.103(7)
β /°	90.679(7)
γ /°	100.511(7)

Volume/Å ³	1661.3(2)
Z	7
ρ _{calc} /g/cm ³	1.373
μ/mm ⁻¹	0.095
F (000)	712.0
Radiation	MoKα (λ = 0.71073)
2Θ range for data collection/°	5.82 to 58.242
Index ranges	-9 ≤ h ≤ 9, -17 ≤ k ≤ 18, -23 ≤ l ≤ 23
Reflections collected	17876
Independent reflections	7836 [R _{int} = 0.0525, R _{sigma} = 0.0650]
Data/restraints/parameters	7836/0/469
Goodness-of-fit on F ²	1.058
Final R indexes [I ≥ 2σ (I)]	R1 = 0.0651, wR2 = 0.1606
Final R indexes [all data]	R1 = 0.1131, wR2 = 0.1970
Largest diff. peak/hole / e Å ⁻³	0.33/-0.34

4.12 References

1. Yamaguchi J., Yamaguchi A. D., Itami K. (2012), C–H Bond Functionalization: Emerging Synthetic Tools for Natural Products and Pharmaceuticals, *Angew. Chem. Int. Ed.* **51**, 8960-9009 (DOI: 10.1002/anie.201201666)
2. Bringmann G., Gulder T., Gulder T. A., Breuning M. (2011), Atroposelective Total Synthesis of Axially Chiral Biaryl Natural Products, *Chem. Rev.* **111**, 563-639 (DOI: 10.1021/cr100155e)
3. Han Z., Pinkner J. S., Ford B., Chorell E., Crowley J. M., Cusumano C. K., Campbell S., Henderson J. P., Hultgren S. J., Janetka J. W. (2012), Lead Optimization Studies on FimH Antagonists: Discovery of Potent and Orally Bioavailable Ortho-Substituted Biphenyl Mannosides, *J. Med. Chem.* **55**, 3945-3959 (DOI: 10.1021/jm300165m)

4. Kozlowski M. C., Morgan B. J., Linton E. C. (2009), Total synthesis of chiral biaryl natural products by asymmetric biaryl coupling, *Chem. Soc. Rev.* **38**, 3193-3207 (DOI: 10.1039/B821092F)
5. Kuhl N., Hopkinson M. N., Wencel-Delord J., Glorius F. (2012), Beyond Directing Groups: Transition-Metal-Catalyzed C–H Activation of Simple Arenes, *Angew. Chem. Int. Ed.* **51**, 10236-10254 (DOI: 10.1002/anie.201203269)
6. Alberico D., Scott M. E., Lautens M. (2007), Aryl–Aryl Bond Formation by Transition-Metal-Catalyzed Direct Arylation, *Chem. Rev.* **107**, 174-238 (DOI: 10.1021/cr0509760)
7. McGlacken G. P., Bateman L. M. (2009), Recent advances in aryl–aryl bond formation by direct arylation, *Chem. Soc. Rev.* **38**, 2447-2464 (DOI: 10.1039/B805701J)
8. Yuan Y.-C., Bruneau C., Roisnel T., Gramage-Doria R. (2009), Site-Selective Ruthenium-Catalyzed C–H Bond Arylations with Boronic Acids: Exploiting Isoindolinones as a Weak Directing Group, *J. Org. Chem.* **84**, 12893-12903 (DOI: 10.1021/acs.joc.9b01563)
9. Chiusoli G. P., Catellani M., Costa M., Motti E., Della Ca N., Maestri G. (2010), Catalytic C–C coupling through C–H arylation of arenes or heteroarenes, *Coord Chem Rev* **254**, 456-469 (DOI: 10.1016/j.ccr.2009.07.023)
10. Jaiswal Y., Kumar Y., Thakur R., Pal J., Subramanian R., Kumar A. (2016), Primary Amide Directed Regioselective ortho-C–H Arylation of (Aryl)Acetamides, *J. Org. Chem.* **81**, 12499-12505 (DOI: 10.1021/acs.joc.6b02353)
11. Huang L., Hackenberger D., Gooßen L. J. (2015), Iridium-katalysierte ortho-Arylierung von Benzoessäuren mit Aryldiazoniumsalzen, *Angew. Chem. Int. Ed.* **127**, 12798-12802 (DOI: 10.1002/ange.201505769)
12. Chinnagolla R. K., Jeganmohan M. (2012), Regioselective Ortho-Arylation and Alkenylation of N-Alkyl Benzamides with Boronic Acids via Ruthenium-Catalyzed C–H Bond Activation:

- An Easy Route to Fluorenones Synthesis, *Org. Lett.* **14**, 5246-5249 (DOI: 10.1021/ol3024067)
13. Albano G., Punzi A., Capozzi M. A. M., Farinola G. M. (2022), Sustainable protocols for direct C–H bond arylation of (hetero)arenes, *Green Chem.* **24**, 1809-1894 (DOI: 10.1039/D1GC03168F)
14. Lee S., Mah S., Hong S. (2015), Catalyst Controlled Divergent C4/C8 Site-Selective C–H Arylation of Isoquinolones, *Org. Lett.* **17**, 3864-3867 (DOI: 10.1021/acs.orglett.5b01840)
15. Wencel-Delord J., Dröge T., Liu F., Glorius F. (2011), Towards mild metal-catalyzed C–H bond activation, *Chem. Soc. Rev.* **40**, 4740-4761 (DOI: 10.1039/C1CS15083A)
16. Babu S. S., Muthuraja P., Yadav P., Gopinath P. (2021), Aryldiazonium Salts in Photo-redox Catalysis – Recent Trends, *Adv. Synth. Catal.* **363**, 1782-1809 (DOI: 10.1002/adsc.202100136)
17. Wang C.-S., Dixneuf P. H., Soulé J.-F. (2018), Photo-redox Catalysis for Building C–C Bonds from C(sp²)–H Bonds, *Chem. Rev.* **118**, 7532-7585 (DOI: 10.1021/acs.chemrev.8b00077)
18. Babu S. S., Shahid M., Gopinath P. (2020), Dual palladium–photo-redox catalyzed chemoselective C–H arylation of phenylureas, *ChemComm* **56**, 5985-5988 (DOI: 10.1039/D0CC01443E)
19. Liang L., Xie M.-S., Wang H.-X., Niu H.-Y., Qu G.-R., Guo H.-M. (2017), Visible-Light-Mediated Monoselective Ortho C–H Arylation of 6-Arylpurine Nucleosides with Diazonium Salts, *J. Org. Chem.* **82**, 5966-5973 (DOI: 10.1021/acs.joc.7b00659)
20. Khan R., Boonseng S., Kemmitt P. D., Felix R., Coles S. J., Tizzard G. J., Williams G., Simmonds O., Harvey J. L., Atack J., Cox H., Spencer J. (2017), Combining Sanford Arylations on Benzodiazepines with the Nuisance Effect, *Adv. Synth. Catal.* **359**, 3261-3269 (DOI: 10.1002/adsc.201700626)

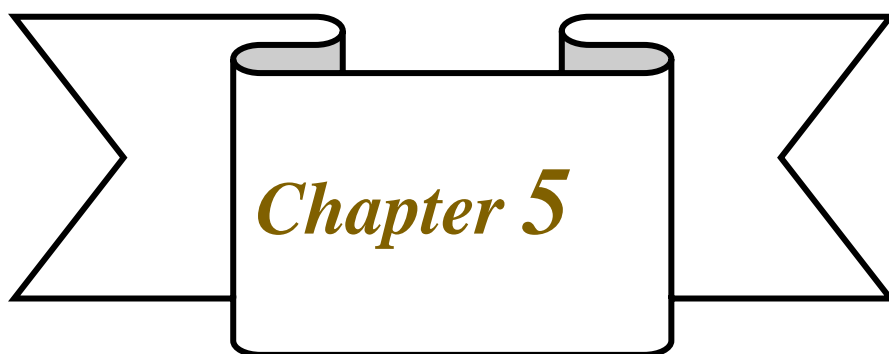
21. Rajat, Jain N. (2023), Photo-redox/Palladium Dual Catalysis for Site-Selective C–H Arylation and Acylation of N-Protected Carbazoles in Visible Light, *J. Org. Chem.* 88, 8600-8608 (DOI: 10.1021/acs.joc.3c00511)
22. Hari D. P., König B. (2014), Synthetic applications of eosin Y in photo-redox catalysis, *ChemComm* 50, 6688-6699 (DOI: 10.1039/C4CC00751D)
23. Silva R. C., Villela L. F., Brocksom T. J., de Oliveira K. T. (2020), Direct C–H photoarylation of diazines using aryldiazonium salts and visible-light, *RSC Adv.* 10, 31115-31122 (DOI: 10.1039/D0RA06876D)
24. Bartolomeu A. d. A., Silva R. C., Brocksom T. J., Noël T., de Oliveira K. T. (2019), Photoarylation of Pyridines Using Aryldiazonium Salts and Visible Light: An EDA Approach, *J. Org. Chem* 84, 10459-10471 (DOI: 10.1021/acs.joc.9b01879)
25. Aganda K. C. C., Kim J., Lee A. (2019), Visible-light-mediated direct C3-arylation of 2*H*-indazoles enabled by an electron-donor–acceptor complex, *Org. Biomol. Chem.* 17, 9698-9702 (DOI: 10.1039/C9OB02074H)
26. Marzo L., Wang S., König B. (2017), Visible-Light-Mediated Radical Arylation of Anilines with Acceptor-Substituted (Hetero)aryl Halides, *Org. Lett.* 19, 5976-5979 (DOI: 10.1021/acs.orglett.7b03001)
27. Meyer A. U., Slanina T., Yao C.-J., König B. (2016), Metal-Free Perfluoroarylation by Visible Light Photo-redox Catalysis, *ACS Catal.* 6, 369-375 (DOI: 10.1021/acscatal.5b02410)
28. Candish L., Freitag M., Gensch T., Glorius F. (2017), Mild, visible light-mediated decarboxylation of aryl carboxylic acids to access aryl radicals, *Chem. Sci.* 8, 3618-3622 (DOI: 10.1039/C6SC05533H)

29. Wang X., Xun X., Song H., Liu Y., Wang Q. (2012), Palladium Metallaphotoredox-Catalyzed 2-Arylation of Indole Derivatives, *Org. Lett.* **24**, 4580-4585 (DOI: 10.1021/acs.orglett.2c01674)
30. Chilamari M., Immel J. R., Bloom S., (2020), General Access to C-Centered Radicals: Combining a Bioinspired Photocatalyst with Boronic Acids in Aqueous Media, *ACS Catal.* **10**, 12727-12737 (DOI: 10.1021/acscatal.0c03422)
31. Wang C.-S., Dixneuf P. H., Soulé J.-F. (2018), Photo-redox Catalysis for Building C–C Bonds from C(sp²)–H Bonds, *Chem. Rev.* **118**, 7532-7585 (DOI: 10.1021/acs.chemrev.8b00077)
32. Babu S. S., Muthuraja P., Yadav P., Gopinath P. (2021), Aryldiazonium Salts in Photo-redox Catalysis – Recent Trends, *Adv. Synth. Catal.* **363**, 1782-1809 (DOI: 10.1002/adsc.202100136)
33. Kvasovs N., Gevorgyan V. (2021), Contemporary methods for generation of aryl radicals, *Chem. Soc. Rev.* **50**, 2244-2259 (DOI: 10.1039/D0CS00589D)
34. Kalyani D., McMurtrey K. B., Neufeldt S. R., Sanford M. S. (2011), Room-Temperature C–H Arylation: Merger of Pd-Catalyzed C–H Functionalization and Visible-Light Photocatalysis, *J. Am. Chem. Soc.* **133**, 18566-18569 (DOI: 10.1021/ja208068w)
35. Jiang J., Zhang W.-M., Dai J.-J., Xu J., Xu H.-J. (2017), Visible-Light-Promoted C–H Arylation by Merging Palladium Catalysis with Organic Photo-redox Catalysis, *J. Org. Chem.* **82**, 3622-3630 (DOI: 10.1021/acs.joc.7b00140)
36. Hsu Y. C., Wang V. C. C., Au-Yeung K. C., Tsai C. Y., Chang C. C., Lin B. C., Chan Y. T., Hsu C. P., Yap G. P., Jurca T., Ong T.-G. (2018), One-Pot Tandem Photo-redox and Cross-Coupling Catalysis with a Single Palladium Carbodicarbene Complex, *Angew. Chem. Int. Ed.* **57**, 4622-4626 (DOI: 10.1002/anie.201800951)

37. Maiti S., Ghosh P., Raja D., Ghosh S., Chatterje S., Sankar V., Roy S., Lahiri G. K., Maiti D. (2024), Light-induced Pd catalyst enables C(sp²)–C(sp²) cross-electrophile coupling bypassing the demand for transmetalation, *Nat. Catal.* 7, 285-294 (DOI: 10.1038/s41929-024-01109-4)
38. Parasram M., Chuentragool P., Sarkar D., Gevorgyan V., (2016), Photoinduced Formation of Hybrid Aryl Pd-Radical Species Capable of 1,5-HAT: Selective Catalytic Oxidation of Silyl Ethers into Silyl Enol Ethers, *J. Am. Chem. Soc.* 138, 6340-6343 (DOI: 10.1021/jacs.6b01628)
39. Torres G. M., Liu Y., Arndtsen B. A. (2020), A dual light-driven palladium catalyst: Breaking the barriers in carbonylation reactions, *Science* 368, 318-323 (DOI: 10.1126/science.aba590)
40. Cheung K. -P. -S., Fang J., Mukherjee K., Mihranyan A., Gevorgyan V. (2022), Asymmetric intermolecular allylic C–H amination of alkenes with aliphatic amines, *Science* 378, 1207-1213 (DOI: 10.1126/science.abq1274)
41. Liang Y. F., Steinbock R., Yang L., Ackermann L. (2018), Continuous Visible-Light Photoflow Approach for a Manganese-Catalyzed (Het)Arene C–H Arylation, *Angew. Chem. Int. Ed.* 130, 10785-10789 (DOI: 10.1002/ange.201805644)
42. Bhawale R. T., Chillal A. S., Ghosh S., Kshirsagar U. A. (2024), Visible-Light Induced Ag-Palladacycle-Complex-Mediated Regioselective C–H Arylation, *Adv. Synth. Catal.* 366, 3603-3609 (DOI: 10.1002/adsc.202400466)
43. Zhao X., Yeung C. S., Dong V. M. (2010), Palladium-Catalyzed Ortho-Arylation of O-Phenylcarbamates with Simple Arenes and Sodium Persulfate, *J. Am. Chem. Soc.* 132, 5837-5844 (DOI: 10.1021/ja100783c)
44. Váňa J., Lang J., Šoltésová M., Hanusek J., Růžička A., Sedlák M., Roithová J. (2017), The role of trinuclear species in a

- palladium acetate/trifluoroacetic acid catalytic system, *Dalton Trans.* **46**, 16269-16275 (DOI: 10.1039/C7DT03832A)
45. Lee P.-Y., Liang P., Yu W.-Y. (2017), Pd(II)-Catalyzed Direct ortho-C–H Acylation of Aromatic Ketones by Oxidative Decarboxylation of α -Oxocarboxylic Acids, *Org. Lett.* **19**, 2082-2085 (DOI: 10.1021/acs.orglett.7b00677)
 46. CCDC: 2287203 for (**3w**) contains the supplementary crystallographic data for this paper. The crystallographic data can be obtained from The Cambridge Crystallographic Data Centre via www.ccdc.cam.uk/request/cif.
 47. Witzel S., Hoffmann M., Rudolph M., Kerscher M., Comba P., Dreuw A., Hashmi A. S. K. (2021), Excitation of aryl cations as the key to catalyst-free radical arylations, *Cell. Rep. Phys. Sci.* **2**, 100325 (DOI: 10.1016/j.xcrp.2021.100325)
 48. Zhang J., Han L., Bi S., Liu T. (2020), Distinct Roles of Ag(I) and Cu(II) as Cocatalysts in Achieving Positional-Selective C–H Alkenylation of Isoxazoles: A Theoretical Investigation, *J. Org. Chem.* **2020**, **85**, 8387-8396 (DOI: 10.1021/acs.joc.0c00721)
 49. Yamamoto Y., Jiang J., Yasui T. (2020), Palladium-Catalyzed [3+2] and [2+2+2] Annulations of 4-Iodo-2-quinolones with Activated Alkynes through Selective C–H Activation, *Chem. Eur. J.* **26**, 3749-3757 (DOI: 10.1002/chem.201904558)
 50. Anand M., Sunoj R. B., Schaefer H. F. (2014), Non-innocent Additives in a Palladium(II)-Catalyzed C–H Bond Activation Reaction: Insights into Multimetallic Active Catalysts, *J. Am. Chem. Soc.* **136**, 5535-5538 (DOI: 10.1021/ja412770h)
 51. Bhattacharya T., Dutta S., Maiti D. (2021), Deciphering the Role of Silver in Palladium-Catalyzed C–H Functionalizations, *ACS Catal.* **11**, 9702-9714 (DOI: 10.1021/acscatal.1c02552)

52. Becke A. D. (1993), Density-Functional Thermochemistry. III. The Role of Exact Exchange, *J. Chem. Phys.* 98, 5648–5652 (DOI: 10.1063/1.464913)
53. Weigend F., Ahlrichs R. (2005), Balanced basis sets of split valence, triple zeta valence and quadruple zeta valence quality for H to Rn: Design and Assessment of Accuracy, *Phys. Chem. Chem. Phys.* 7, 3297-3305 (DOI: 10.1039/b508541a)



*Visible-Light-Enabled
Regioselective C–H alkylation and
alkenylation of 2-Aryl
Heterocycles using Dual Catalysis*

Chapter 5

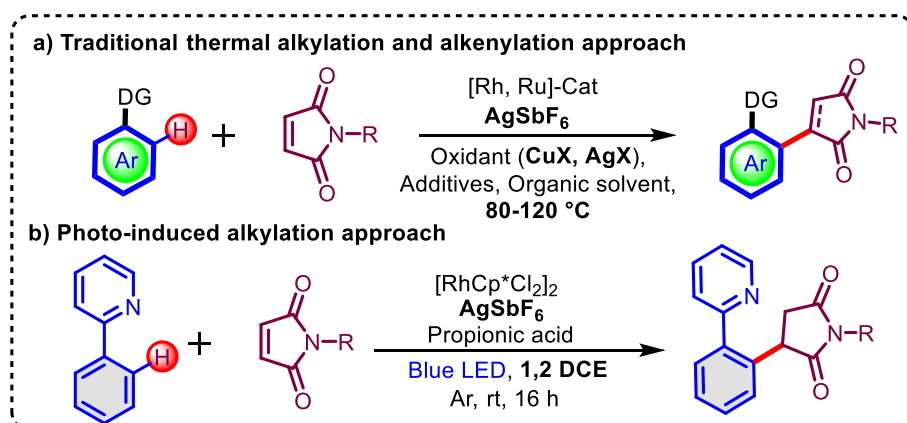
Visible-Light-Enabled Regioselective C–H alkylation and alkenylation of 2-Aryl Heterocycles using Dual Catalysis

5.1 Introduction

Heterocyclic scaffolds containing nitrogen are extensively utilized due to their biological activity in numerous therapeutic molecules.^[1-4] The site-selective functionalization of various heterocyclic compounds, particularly at the ortho-position via alkylation and alkenylation strategies, is well-regarded for its practical feasibility and high effectiveness.^[5-7] The maleimide and succinimide scaffolds, either aryl or heterocyclic, are frequently found in natural products and pharmaceutical ingredients, demonstrating a diverse array of biological activities.^[8-9]

5.2 Previous Reports

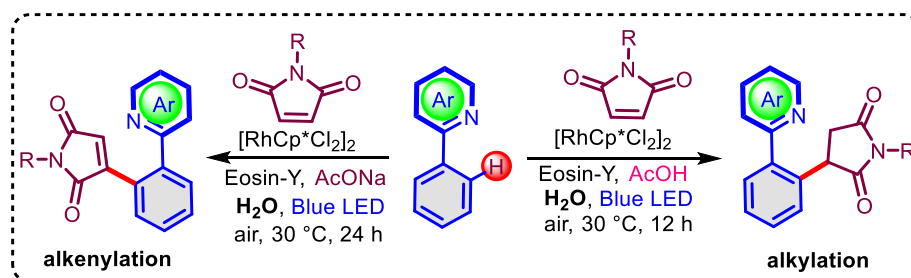
In previous studies, several reports have demonstrated the achievement of directing group-assisted transition metal-catalyzed C–H alkylation or alkenylation with maleimides under thermal reaction conditions. However, the majority of rhodium and ruthenium-catalyzed C–H alkylation and alkenylation strategies necessitate silver additives, stoichiometric amounts of oxidants ($\text{Cu}(\text{OAc})_2$, Ag_2CO_3 , AgOAc , TBHP etc.), and elevated temperatures (80-120 °C) in organic solvents as reaction media (**Scheme 5.1a**).^[10-16] Recently, Koenigs and co-workers developed a rhodium-catalyzed alkylation of 2-phenyl pyridine with maleimides via external photocatalyst-free visible light and propionic acid-induced protodemetalation reaction (**Scheme 5.1b**).^[17]



Scheme 5.1 Previous reports for alkylation and alkenylation of heterocycles with maleimides

However, limitations of this approach include the need for silver salts, the use of organic solvents, and its applicability being restricted to 2-phenyl pyridine and quinoline derivatives. Additionally, due to the necessity of acid, this approach is limited to alkylation only. Consequently, developing a mild, environmentally friendly, and operationally simple reaction condition method for achieving the desired C–H alkylation and alkenylation with maleimides would be highly advantageous. In recent times, there has been a growing interest in visible-light photo-redox catalysis in organic synthesis due to its relevance in sustainable chemistry as an increasingly attractive technique for substrate activation and functionalization.^[18-20] Under mild reaction conditions, this catalytic method allows the formation of a variety of substrates, often without the need for stoichiometric oxidants or additives.^[21-23] Recently, synthetic chemists have discovered significant benefits from dual catalysis, which combines photocatalysis with transition metal catalysis particularly when it comes to selectively accessing and activating specific functional groups or bonds to produce C–C bonds under mild and simple conditions under mild and simple conditions.^[24-25]

5.3 Objective

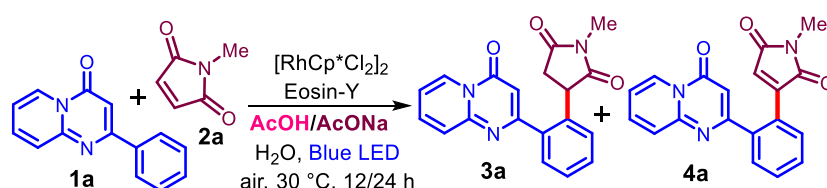


Scheme 5.2 Current approach for photoinduced alkylation and alkenylation of 2-aryl heterocycles.

In this chapter we developed a dual catalytic, silver/copper-free, external oxidant-free, mild, and simple strategy for site-selective alkylation as well as alkenylation of 4*H*-pyrido[1,2-*a*]pyrimidin-4-ones and other related 2-aryl heterocycles with maleimides by merging of organic dyes with rhodium-catalyst, in the presence of acid or base under visible light irradiation at room temperature in an aqueous reaction condition (Scheme 5.2).^[26]

5.4 Result and Discussion

Optimization of reaction conditions was performed on 2-phenyl-4*H*-pyrido[1,2-*a*]pyrimidin-4-one (**1a**) as 4*H*-pyrido[1,2-*a*]pyrimidin-4-ones stand out as an intriguing scaffold due to their incorporation in various pharmacological compounds exhibiting a range of bioactivities.^[27-28] We began our study by reacting 2-phenyl-4*H*-pyrido[1,2-*a*]pyrimidin-4-one (**1a**) with 1-methyl-1*H*-pyrrole-2,5-dione (**2a**), using [RhCp*Cl₂]₂ (5 mol%) as a catalyst, Eosin Y (3 mol%) as a photocatalyst, and AcOH (0.5 mL) as an additive in water as solvents. After illuminating the reaction mixture to blue LED at room temperature (30 °C) for 12 hours, the formation of alkylated product **3a** was selectively observed in 91% yield (Table 5.1, entry 1). When the reaction was carried out without acetic acid, the desired product **3a** was not detected (entry 2). Subsequently, other acid additives were screened, which were unsuitable for better results (entries 3-4). When the reaction was performed in an O₂ atmosphere (entry 5), it produced the desired

Table 5.1. Selected optimization of reaction conditions^[a,b]


entry	Variation from the above conditions	Yield (%) ^[c]	
		3a	4a
1 ^[a]	No any change	91	n.d.
2 ^[a]	without AcOH	n.d.	n.d.
3 ^[a]	TFA instead of AcOH	n.d.	n.d.
4 ^[a]	PivOH instead of AcOH	39	n.d.
5 ^[a]	O ₂ balloon	90	n.d.
6 ^[a]	N ₂ balloon	35	n.d.
7 ^[a]	without Rh cat.	n.d.	n.d.
8 ^[a]	[Ru(<i>p</i> -cymene)Cl ₂] ₂ instead of Rh cat.	48	n.d.
9 ^[a]	without Eosin-Y	72	n.d.
10 ^[a]	without light & Eosin-Y	32	n.d.
11 ^[a]	AcONa instead of AcOH	08	59
12 ^[b]	No any change	11	82
13 ^[b]	without AcONa	n.d.	n.d.
14 ^[b]	AcOK instead of AcONa	10	34
15 ^[b]	AcONH ₄ instead of AcONa	08	26
16 ^[b]	O ₂ balloon	12	79
17 ^[b]	N ₂ balloon	trace	trace
18 ^[b]	without Rh cat.	n.d.	n.d.
19 ^[b]	[Ru(<i>p</i> -cymene)Cl ₂] ₂ instead of Rh cat.	n.d.	n.d.
20 ^[b]	without Eosin-Y	trace	18
21 ^[b]	without light & Eosin-Y	trace	12

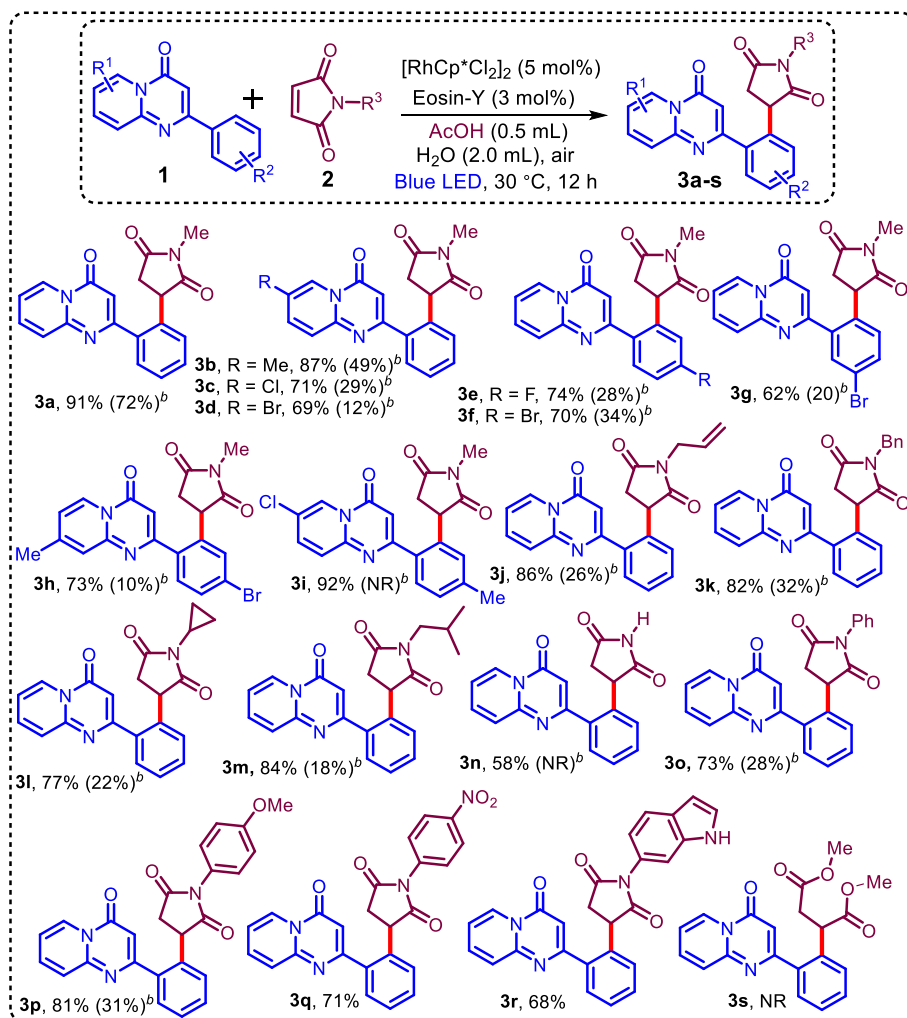
^[a]Reaction conditions: **1a** (0.2 mmol), **2a** (0.4 mmol), [RhCp*Cl₂]₂ (5 mol%), Eosin-Y (3 mol%), AcOH (0.5 mL), H₂O (2.0 mL), air, blue LED, 30 °C, 12 h. ^[b]Reaction conditions: **1a** (0.2 mmol), **2a** (0.4 mmol), [RhCp*Cl₂]₂ (10 mol%), Eosin-Y (3 mol%), AcONa (0.2 mmol), H₂O (2.0 mL), air, blue LED, rt (30 °C), 24 h. ^[c]isolated yields. n.d.- not detected.

product in comparable yield (90%) as in open-air. Whereas reaction in N₂ atmosphere, produced the desired product in a very low yield (35%, entry 6). Furthermore, the Rh catalyst was essential, as the reaction was not initiated in its absence (entry 7). Whereas, replacing Rh-catalyst with a Ru-based catalyst led to a significantly reduced yield of desired product **3a** (48%, entry 8). When the reaction was performed in the visible light but without the eosin-Y, the yield of desired product was

lowered to 72% (entry 9). Notably, when the reaction was carried out in the absence of both light and eosin-Y, the product yield was drastically decreased to 32%, indicating the critical role of visible light photocatalysis (entry 10). Significantly, when the reaction was conducted in the presence of AcONa instead of AcOH, it produced alkylated product **3a** in only 8%, while 59% of alkenylated product **4a** was formed (entry 11). Fortunately, a brief optimization of the reaction condition resulted in 82% of the alkenylated product **4a** and 11% of the **3a** in 24 hours reaction duration (entry 12). In the absence of AcONa, the desired product **4a** was not observed (entry 13). Subsequently, other bases, such as AcOK and AcONH₄ were investigated, but it resulted in lower yields of **4a** (entries 14-15). In the meantime, the reaction using an O₂ balloon yielded a slightly lower yield of 79% (entry 16), and an N₂ atmosphere resulted in only a trace amount of **4a** (entry 17). In the absence of the Rh-catalyst or replacing the Rh-catalyst with other catalysts, such as Ru-catalyst, the desired alkenylated product **4a** was not detected (entries 18-19). When the reaction was performed in the visible light but without the eosin-Y, the desired product **4a** was observed in only 18% yield (entry 20). Whereas in the dark and without eosin-Y, the reaction yielded 12% of **4a** (entry 21).

With these optimizations of the reaction conditions, further substrate scope for the alkylation of 2-aryl-pyrido[1,2-*a*]pyrimidin-4-ones with various maleimides was explored (**Scheme 5.3**). Alkylation of substituted 2-phenyl-4*H*-pyrido[1,2-*a*]pyrimidin-4-ones (-Me, -Cl, -Br) produced the desired products (**3b-d**) with good yields of 87%, 71%, and 69%, respectively. 2-Aryl-pyrido[1,2-*a*]pyrimidin-4-ones having substituents on 2-aryl ring (*p*-F, *p*-Br, *m*-Br) resulted in the desired products (**3e-g**) in acceptable yields of 74%, 70%, and 62%, respectively. Substrates having disubstituent, produced the desired products (**3h** and **3i**) in 73% and 92% yield, respectively. Other maleimides such as *N*-allyl, -Bn, -cyclopropyl, and -isobutyl maleimides were reacted with **1a** to produce the desired alkylated products (**3j-m**) in good yields (77-86%). The reaction of the maleimides with free N-H

Scheme 5.3 Substrate scope for alkylation of pyrido[1,2-*a*]pyrimidin-4-ones with maleimides^[a]



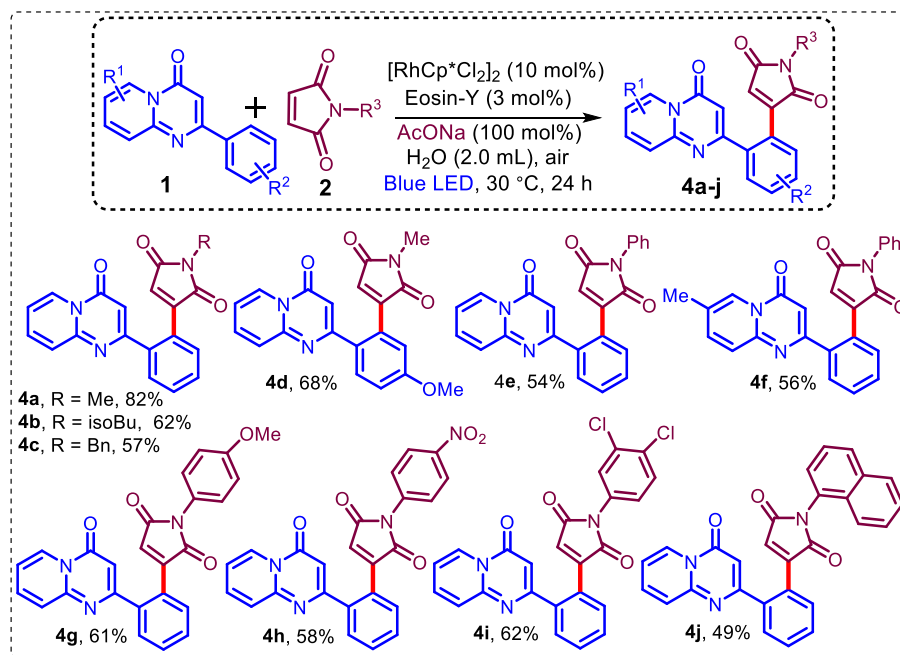
^[a]Reaction conditions: **1** (0.2 mmol), **2** (0.4 mmol), [RhCp*Cl₂]₂ (5 mol%), Eosin-Y (3 mol%), AcOH (0.5 mL), H₂O (2.0 mL), air, blue LED, 30 °C, 12 h. ^[b]Reaction conditions: **1** (0.2 mmol), **2** (0.4 mmol), [RhCp*Cl₂]₂ (5 mol%), AcOH (0.5 mL), H₂O (2.0 mL), air, blue LED, rt (30 °C), 12 h. NR- no reaction.

group with **1a** under optimized reaction conditions produced the product **3n** with a moderate yield of 58%. Similarly, the reaction of *N*-phenyl, strong donating substituted *N*-(4-methoxyphenyl) maleimides, and strong withdrawing substituted *N*-(4-nitrophenyl) maleimides proceeded smoothly with 2-phenyl-pyrido[1,2-*a*]pyrimidin-4-ones, yielding the expected products **3o**, **3p**, and **3q** in 73%, 81%, and 71%, respectively. Alkylation on all these substrates was also performed under optimized conditions, but in the absence of Eosin Y to substantiate the importance of the photocatalyst (**3b-p**, Table 2, condition b). Most

of the substrates provided a very poor yield of alkylated product under photocatalyst-free conditions. Heterocyclic-ring substituted indole-maleimide underwent the alkylation reaction smoothly, yielding 68% of the intended product **3r**. Dimethyl maleate was found unreactive coupling partner in the alkylation reaction, as the desired product **3s** was not detected.

To further assess the adaptability of the visible light-mediated photocatalyzed alkenylation reaction, the reaction was performed on various 2-aryl-pyrido[1,2-*a*]pyrimidin-4-ones (**Scheme 5.4**). Maleimides with different *N*-substituents (-Me, -isobutyl, -Bn) reacted smoothly with various 2-aryl-pyrido[1,2-*a*]pyrimidin-4-ones, producing the desired alkenylated products (**4a-d**) in moderate to good yields (57-82%). Subsequently, the reaction of *N*-aryl maleimides with 2-aryl-pyrido[1,2-*a*]pyrimidin-4-ones yielded the respective alkenylated products **4e-i** in 54-62% yields. Maleimides with *N*-naphthyl substituent yielded the desired alkenylated product **4j** in moderate yield (49%).

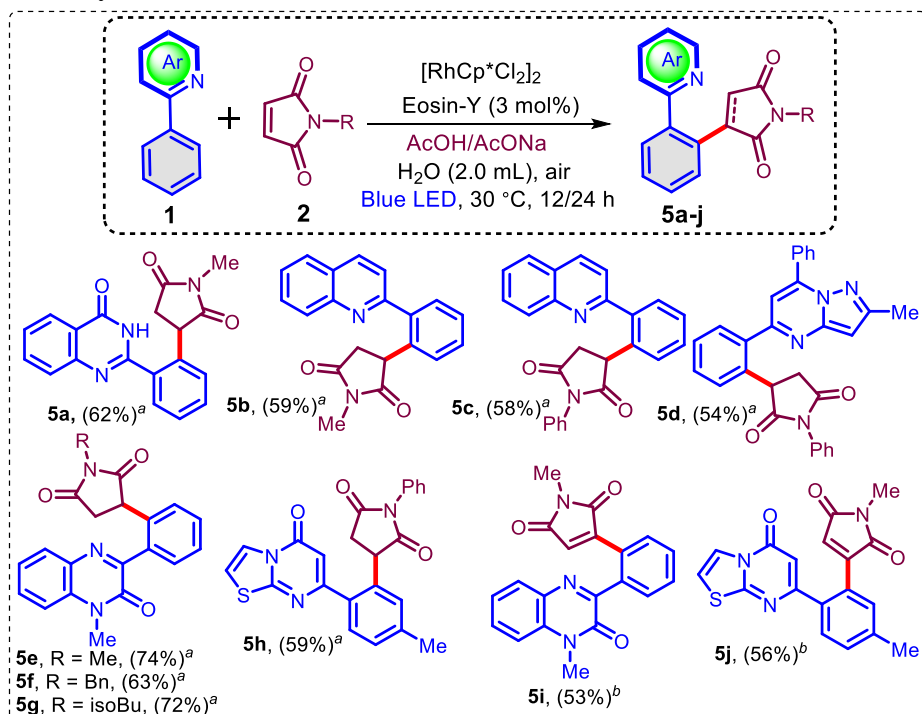
Scheme 5.4 Substrate scope for alkenylation of pyrido[1,2-*a*]pyrimidin-4-ones with maleimides^[a]



^[a]Reaction conditions: **1** (0.2 mmol), **2** (0.4 mmol), $[\text{RhCp}^*\text{Cl}_2]_2$ (10 mol%), Eosin-Y (3 mol%), AcONa (0.2 mmol), H_2O (2.0 mL), air, blue LED, rt (30 °C), 24 h.

Next, the visible light-enabled ortho alkylation and alkenylation protocol was evaluated on other 2-aryl heterocycles using *N*-alkyl/aryl maleimides (**Scheme 5.5**). 2-Phenylquinazolin-4(3*H*)-one with 1-methyl-1*H*-pyrrole-2,5-dione under optimized reaction conditions for alkylation reaction delivered corresponding alkylated product (**5a**) in 62% yield. Further, 2-phenylquinoline, 2-methyl-5,7-diphenylpyrazolo[1,5-*a*]pyrimidine, 1-methyl-3-phenylquinoxalin-2(1*H*)-one and 7-(*p*-tolyl)-5*H*-thiazolo[3,2-*a*]pyrimidin-5-one were reacted successfully with *N*-alkyl/aryl maleimides under alkylation reaction conditions, yielding the desired alkylated products (**5b-h**) in good to moderate yields (54-74%). Further attempts were made for the alkenylation on 1-methyl-3-phenylquinoxalin-2(1*H*)-one and 7-(*p*-tolyl)-5*H*-thiazolo[3,2-*a*]pyrimidin-5-one with maleimides under visible light photo-redox alkenylation reaction conditions. Resulting alkenylated products **5i**, and **5j** were isolated in 53%, and 56% yield, respectively.

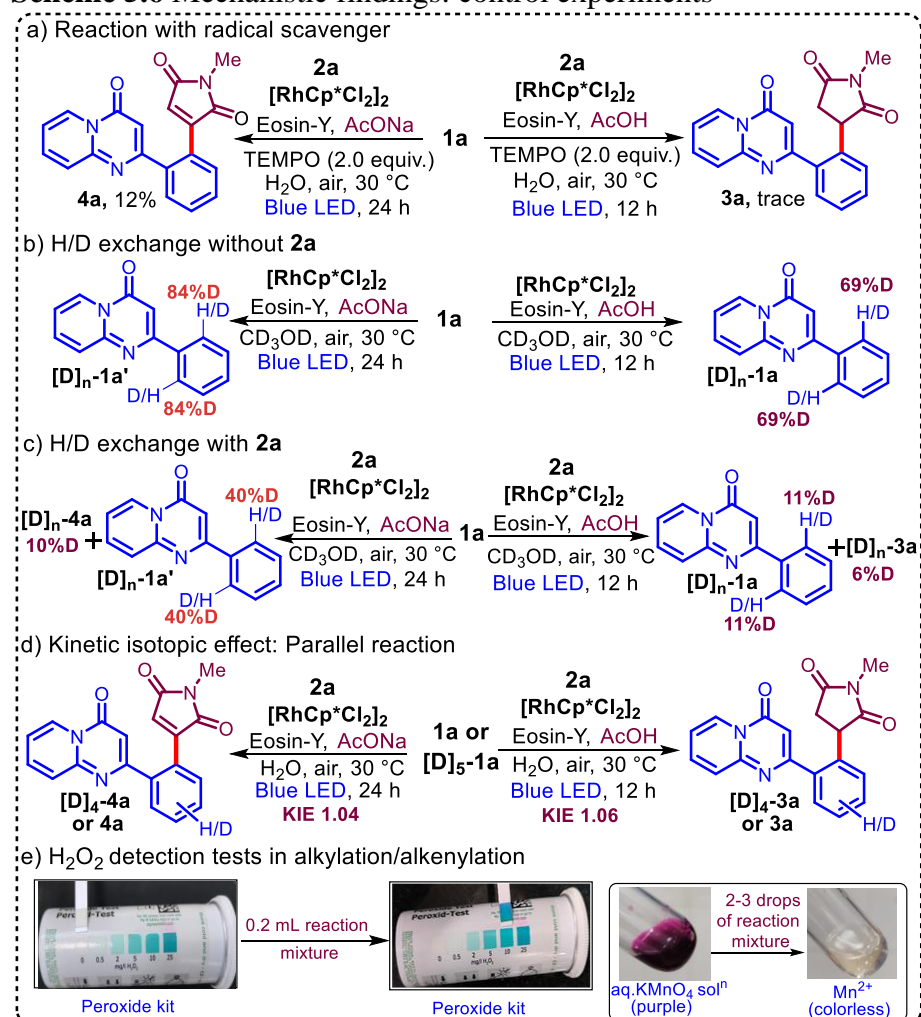
Scheme 5.5 Substrate scope for alkylation and alkenylation of other heterocycles with maleimides^[a,b]



^[a]Reaction conditions: **1** (0.2 mmol), **2** (0.4 mmol), [RhCp*Cl₂]₂ (5 mol%), Eosin-Y (3 mol%), AcOH (0.5 mL), H₂O (2.0 mL), air, blue LED, 30 °C, 12 h. ^[b]Reaction conditions: **1** (0.2 mmol), **2** (0.4 mmol), [RhCp*Cl₂]₂ (10 mol%), Eosin-Y (3 mol%), AcONa (0.2 mmol), H₂O (2.0 mL), air, blue LED, rt (30 °C), 24 h.

To gain insight into the dual catalytic alkylation and alkenylation reaction mechanisms, a series of control experiments were conducted (**Scheme 5.6**). First, the reaction was carried out in the presence of radical scavenger TEMPO (2,2,6,6-tetramethylpiperidin-1-yl)oxyl), which completely or significantly inhibited the formation of products **3a** and **4a** (**Scheme 5.6a**). Next, H/D exchange experiments were performed using CD₃OD (0.5 mL), revealing significant deuterium incorporation. In the absence of **2a** under alkenylation reaction conditions, [D]_n-**1a'** exhibited 84% deuterium incorporation. Similarly, under alkylation reaction conditions with **1a** and in the absence of **2a**, [D]_n-**1a** showed 69% deuterium incorporation (**Scheme 5.6b**). Additionally, H/D exchange experiments were conducted with **1a** in the presence of **2a** under alkenylation reaction conditions, where [D]_n-**1a'** showed 40% and [D]_n-**4a** showed 10% deuterium incorporation. Under

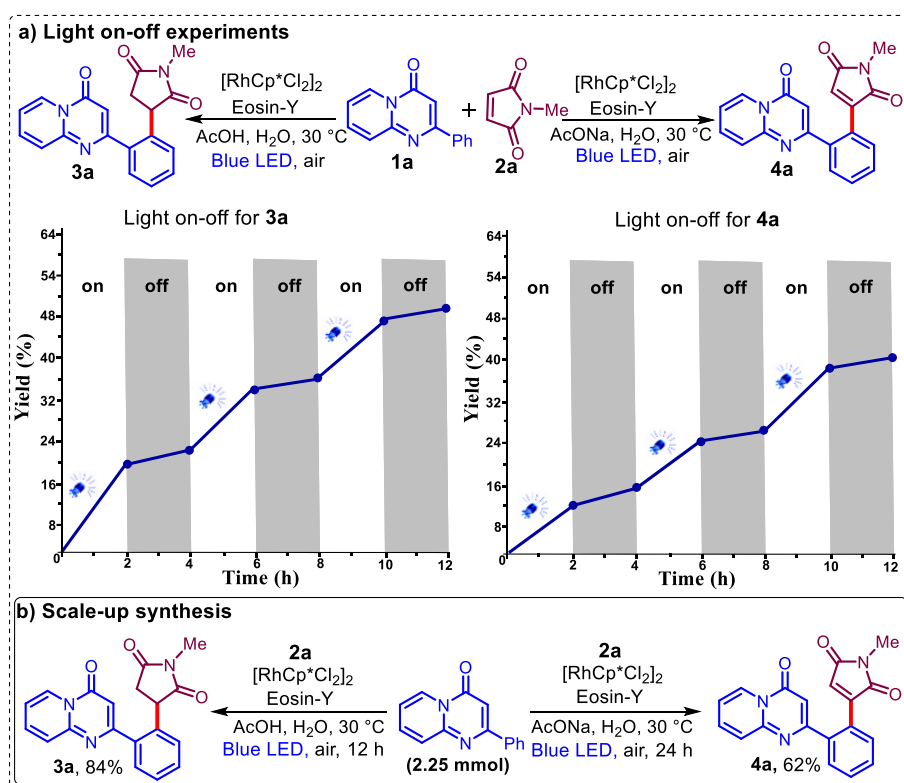
Scheme 5.6 Mechanistic findings: control experiments



alkylation reaction conditions with **1a** in the presence of **2a**, **[D]_n-1a** exhibited 11% and **[D]_n-3a** exhibited 6% deuterium incorporation (**Scheme 5.6c**). These findings indicate that, in both the alkenylation and alkylation reactions the C–H bond activation is reversible^[29]. Next, a kinetic isotope effect experiment was performed using **1a** or **1a-D₅** with 1-methyl-1*H*-pyrrole-2,5-dione (**2a**) in parallel reactions. The k_H/k_D values were Calculated using ¹H NMR spectroscopy, 1.04 for the alkenylation reaction **[D]₄-4a** and 1.06 for the alkylation reaction **[D]₄-3a** (**Scheme 5.6d**). These results suggest that C–H bond cleavage is not involved in the rate-determining step.^[30] The generation of H₂O₂ was confirmed by using both a peroxide kit and a KMnO₄ test (**Scheme 5.6e**).

Next, light-on-off experiments suggest the requirement of continuous light for the reaction (**Scheme 5.7a**). Quantum yield calculations were performed for both alkylation ($\Phi = 0.197$) and alkenylation ($\Phi = 0.157$) reactions. Further, to assess the scalability of the dual catalytic alkylation and alkenylation methodology, a scale-up synthesis was performed with 2.25 mmol of 2-phenyl-pyrido[1,2-*a*]pyrimidin-4-ones

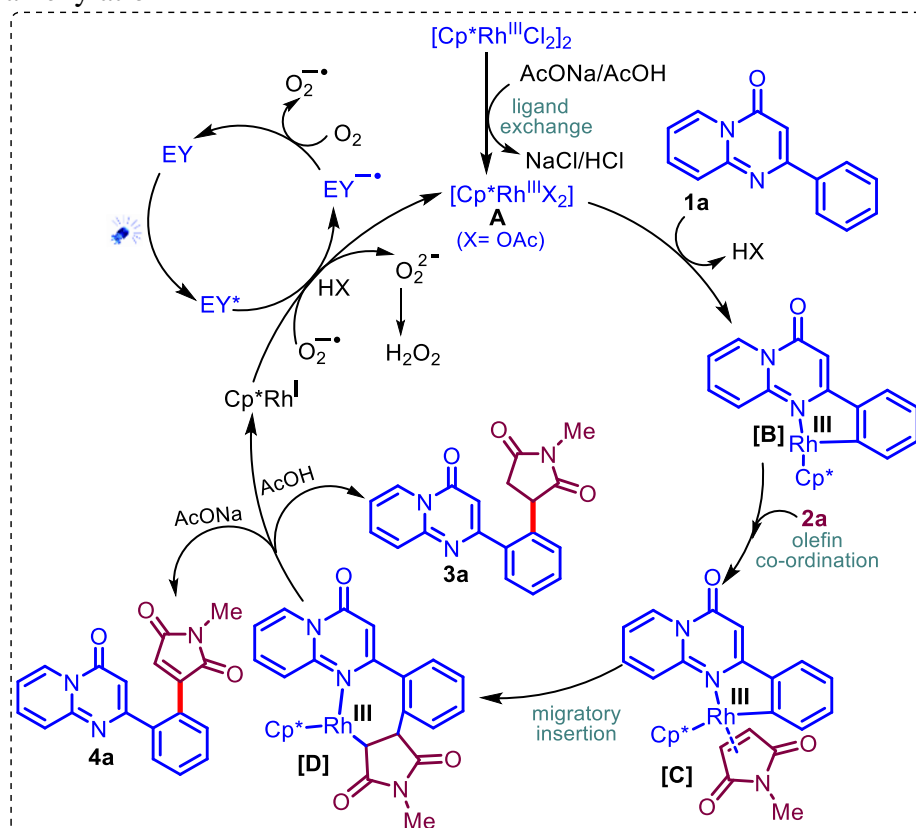
Scheme 5.7 Light on-off experiments



under standard reaction conditions. This resulted in yields of 84% of alkylated product **3a** and 62% of alkenylated product **4a** (Scheme 5.7b).

Based on the analysis of control experiments and the literature^[17,31-33] study, plausible mechanistic pathways for the alkylation and alkenylation of 2-phenyl-4*H*-pyrido[1,2-*a*]pyrimidin-4-one with maleimide were proposed (Scheme 5.8). First, the Rh(III) undergoes ligand exchange with an acid or base to generate intermediate **A**. Intermediate **A** undergoes C–H activation with **1a** to the rhodacycle **B**. Further, coordination with maleimide **2a** generates intermediate **C**, which subsequently undergoes migratory insertion to afford Rh(III) intermediate **D**. In the presence of sodium acetate, the intermediate **D** undergoes β -hydrogen elimination, resulting in the alkenylated product **4a** and Rh(I) species. Conversely, protonation in an acidic medium leads to the generation of the alkylated product **3a** along with the Rh(I)

Scheme 5.8 Proposed reaction mechanism for alkylation and alkenylation



species. The Rh(I) species gets converted to Rh(III) through a visible-light-induced photocatalyzed oxidation.

5.5 Summary

In summary, we developed mild, facile, and operationally simple dual catalysis conditions for visible light-induced rhodium-catalyzed, site-selective alkylation and alkenylation of 2-aryl heteroaryl compounds with maleimide in the presence of water as a solvent at room temperature. Merger of organic photo-redox catalyst with rhodium-catalyst enables the synthesis of alkylation and alkenylation products, incorporating a diverse range of H/alkyl/arylated and N-heteroaryl maleimides with good substrate scope and up to 92%. Control experiments, H/D labeling, KIE studies, and light on-off experiments were conducted to substantiate the proposed mechanistic pathways. Additionally, present conditions were found adequate for scale-up synthesis.

5.6 Experimental section

General procedure for the synthesis of H/alkyl/aryl maleimides^[34]

All 1-H/alkyl/aryl-1H-pyrrole-2,5-dione compounds (**2**) were prepared according to the literature. To a solution of substituted maleic anhydride (2.0 g, 20.4 mmol) in acetic acid (15 mL), the corresponding amine (H/alkyl/aryl, 40.8 mmol) was added in a 100 mL round-bottom flask. The reaction mixture was heated in an oil bath at 110 °C for 8 hours. Afterward, the mixture was cooled, and the acetic acid was removed under vacuum. The reaction mixture was then neutralized to pH 6-7 using aqueous NaHCO₃. The resulting mixture was extracted with ethyl acetate (3 × 25 mL), followed by washing with 1N HCl and a brine solution. The combined organic layers were separated, dried over Na₂SO₄, and filtered. Evaporation under reduced pressure yielded the crude product, which was purified using silica gel column chromatography with petroleum ether and ethyl acetate as the eluent to afford the desired product **2** in good yield.

Procedure for synthesis of 1-methyl-3-(2-(4-oxo-4*H*-pyrido[1,2-*a*]pyrimidin-2-yl)phenyl)pyrrolidine-2,5-dione (3a): In an oven-dried reaction vessel equipped with a magnetic stirring bar, 2-phenyl-4*H*-pyrido[1,2-*a*]pyrimidin-4-one (**1a**) (1.0 equiv., 0.2 mmol, 45 mg), 1-methyl-1*H*-pyrrole-2,5-dione (**2a**) (2.0 equiv., 0.4 mmol, 45 mg), [RhCp*Cl₂]₂ (5 mol%), and Eosin Y (3 mol%) were added, followed by H₂O (2.0 mL) and AcOH (0.5 mL). The reaction mixture was stirred at room temperature (30 °C) under blue LED irradiation for 12 hours. After completion, the reaction mixture was extracted with ethyl acetate (3 × 10 mL) and washed with a brine solution. The combined organic layers were dried over Na₂SO₄, filtered, and concentrated under reduced pressure to yield the crude product, which was further purified by silica gel column chromatography using petroleum ether and ethyl acetate as eluents, affording the solid product 1-methyl-3-(2-(4-oxo-4*H*-pyrido[1,2-*a*]pyrimidin-2-yl)phenyl)pyrrolidine-2,5-dione (**3a**) in 91% yield (61 mg). This procedure was used to synthesize all ortho-alkylated 2-phenyl-pyrido[1,2-*a*]pyrimidin-4-one derivatives (**3a-r**) and (**5a-h**).

Procedure for synthesis of 1-methyl-3-(2-(4-oxo-4*H*-pyrido[1,2-*a*]pyrimidin-2-yl)phenyl)-1*H*-pyrrole-2,5-dione (4a): In an oven-dried reaction vessel equipped with a magnetic stirring bar, 2-phenyl-4*H*-pyrido[1,2-*a*]pyrimidin-4-one (**1a**) (1.0 equiv., 0.2 mmol, 45 mg), 1-methyl-1*H*-pyrrole-2,5-dione (**2a**) (2.0 equiv., 0.4 mmol, 45 mg), [RhCp*Cl₂]₂ (10 mol%), Eosin Y (3 mol%), and NaOAc (1.0 equiv., 0.2 mmol, 17 mg) were added, followed by H₂O (2.0 mL). The reaction mixture was stirred at room temperature (30 °C) under blue LED irradiation for 24 hours. Afterward, the reaction mixture was extracted with ethyl acetate (3 × 10 mL) and washed with a brine solution. The combined organic layers were dried over Na₂SO₄, filtered, and concentrated under reduced pressure to obtain the crude product. This was then purified by silica gel column chromatography using petroleum ether and ethyl acetate as eluents, yielding the solid product 1-methyl-3-(2-(4-oxo-4*H*-pyrido[1,2-*a*]pyrimidin-2-yl)phenyl)-1*H*-pyrrole-2,5-dione (**4a**) in 82% yield (55 mg) and **3a** in 11% yield. This procedure

was used for the synthesis of all ortho-alkenylated 2-phenyl-pyrido[1,2-*a*]pyrimidin-4-one derivatives (**4a-j**) and (**5i-j**).

5.7 Characterization data of **3a-r**, **4a-j** and **5a-j**

1-Methyl-3-(2-(4-oxo-4H-pyrido[1,2-*a*]pyrimidin-2-

yl)phenyl)pyrrolidine-2,5-dione (3a): Light pink solid; yield: 91% (61 mg); m.p.196-198 °C; ¹H NMR (500 MHz, CDCl₃): δ 9.10 (d, *J* = 7.2 Hz, 1H), 7.82 – 7.78 (m, 1H), 7.59 – 7.54 (m, 2H), 7.47 – 7.40 (m, 2H), 7.23 – 7.19 (m, 2H), 6.69 (s, 1H), 4.50 (dd, *J* = 9.5 Hz, 5.7 Hz, 1H), 3.26 (dd, *J* = 18.3 Hz, 9.5 Hz, 1H), 3.05 (dd, *J* = 18.3 Hz, 5.8 Hz, 1H), 2.89 (s, 3H); ¹³C NMR (126 MHz, CDCl₃): δ 178.3, 176.7, 164.3, 157.9, 150.4, 138.4, 137.2, 135.7, 130.6, 130.5, 129.5, 128.3, 127.6, 126.2, 116.0, 104.2, 44.8, 39.0, 25.1; IR (ATR): 1690, 1625, 1430, 1280, 1121, 777, 675 cm⁻¹; HRMS (ESI, *m/z*): calcd for C₁₉H₁₆N₃O₃[M+H]⁺: 334.1186, found: 334.1181.

1-Methyl-3-(2-(7-methyl-4-oxo-4H-pyrido[1,2-*a*]pyrimidin-2-

yl)phenyl)pyrrolidine-2,5-dione (3b): Yellow solid; yield: 87% (60 mg); m.p.252-254 °C; ¹H NMR (500 MHz, CDCl₃): δ 8.91 (s, 1H), 7.66 (d, *J* = 9.0 Hz, 1H), 7.55 (d, *J* = 7.4 Hz, 1H), 7.51 (d, *J* = 9.0 Hz, 1H), 7.46 – 7.39 (m, 2H), 7.22 (d, *J* = 7.5 Hz, 1H), 6.66 (s, 1H), 4.49 (dd, *J* = 9.5 Hz, 5.7 Hz, 1H), 3.27 (dd, *J* = 18.2 Hz, 9.5 Hz, 1H), 3.07 (dd, *J* = 18.3 Hz, 5.8 Hz, 1H), 2.89 (s, 3H), 2.45 (s, 3H); ¹³C NMR (126 MHz, CDCl₃): δ 178.2, 176.8, 164.0, 157.9, 149.3, 140.0, 138.6, 135.6, 130.6, 130.3, 129.6, 128.3, 126.4, 125.7, 125.1, 103.9, 45.0, 39.0, 25.1, 18.5; IR (ATR): 1683, 1634, 1436, 1283, 1121, 71, 664 cm⁻¹; HRMS (ESI, *m/z*): calcd for C₂₀H₁₈N₃O₃[M+H]⁺: 348.1343, found: 348.1340.

3-(2-(7-Chloro-4-oxo-4H-pyrido[1,2-*a*]pyrimidin-2-yl)phenyl)-1-

methylpyrrolidine-2,5-dione (3c): Brown solid; yield: 71% (52 mg); m.p. 220-222 °C; ¹H NMR (500 MHz, CDCl₃): δ 9.11 (s, 1H), 7.71 (dd, *J* = 9.4 Hz, 2.4 Hz, 1H), 7.54 – 7.50 (m, 2H), 7.47 – 7.40 (m, 2H), 7.23 (d, *J* = 7.6 Hz, 1H), 6.72 (s, 1H), 4.48 (dd, *J* = 9.5 Hz, 5.7 Hz, 1H), 3.27 (dd, *J* = 18.2 Hz, 9.5 Hz, 1H), 3.05 (dd, *J* = 18.3 Hz, 5.8 Hz, 1H), 2.90

(s, 3H); **¹³C NMR** (126 MHz, CDCl₃): δ 178.1, 176.7, 164.5, 157.0, 148.9, 138.2, 138.2, 135.7, 130.7, 130.6, 129.6, 128.4, 127.4, 125.4, 124.6, 104.8, 44.8, 39.0, 25.2; **IR (ATR)**: 1685, 1498, 1437, 1284, 1120, 953, 762 cm⁻¹; **HRMS** (ESI, m/z): calcd for C₁₉H₁₅ClN₃O₃[M+H]⁺: 368.0796, found: 368.0781.

3-(2-(7-Bromo-4-oxo-4H-pyrido[1,2-a]pyrimidin-2-yl)phenyl)-1-methylpyrrolidine-2,5-dione (3d): Light green solid; yield: 69% (56 mg); m.p.198-200 °C; **¹H NMR** (500 MHz, CDCl₃): δ 9.22 (s, 1H), 7.81 (d, J = 9.3 Hz, 1H), 7.55 (d, J = 7.5 Hz, 1H), 7.48 – 7.41 (m, 3H), 7.23 (d, J = 7.5 Hz, 1H), 6.73 (s, 1H), 4.49 (dd, J = 9.5 Hz, 5.7 Hz, 1H), 3.27 (dd, J = 18.2 Hz, 9.5 Hz, 1H), 3.06 (dd, J = 18.3 Hz, 5.6 Hz, 1H), 2.91 (s, 3H); **¹³C NMR** (126 MHz, CDCl₃): δ 178.1, 176.7, 164.5, 157.0, 148.9, 138.2, 138.2, 135.7, 130.7, 130.6, 129.6, 128.4, 127.4, 125.4, 124.6, 104.8, 44.8, 39.0, 25.2; **HRMS** (ESI, m/z): calcd for C₁₉H₁₅BrN₃O₃[M+H]⁺: 412.0291, found: 412.0294.

3-(5-Fluoro-2-(4-oxo-4H-pyrido[1,2-a]pyrimidin-2-yl)phenyl)-1-methylpyrrolidine-2,5-dione (3e): Light yellow solid; yield: 74% (52 mg); m.p.230-232 °C; **¹H NMR** (500 MHz, CDCl₃): δ 9.11 (d, J = 7.2 Hz, 1H), 7.82 (t, J = 7.9 Hz, 1H), 7.59 – 7.54 (m, 2H), 7.22 (t, J = 6.9 Hz, 1H), 7.14 – 7.11 (m, 1H), 6.97 (d, J = 9.3 Hz, 1H), 6.66 (s, 1H), 4.51 (dd, J = 9.5, 5.6 Hz, 1H), 3.30 (dd, J = 18.3, 9.6 Hz, 1H), 3.06 (dd, J = 18.3, 5.8 Hz, 1H), 2.91 (s, 3H); **¹³C NMR** (126 MHz, CDCl₃): δ 177.7, 176.3, 164.6, 163.2 (d, J_{CF} = 69.9 Hz), 157.8, 150.4, 138.2 (d, J_{CF} = 7.4 Hz), 137.5, 134.6, 132.8 (d, J_{CF} = 8.7 Hz), 127.7, 126.1, 116.6 (d, J_{CF} = 22.5 Hz), 116.2, 115.6 (d, J_{CF} = 21.1 Hz), 104.2, 44.5, 38.7, 25.3; **¹⁹F NMR** (471 MHz, CDCl₃): δ = -112.0 (s, 1F; **HRMS** (ESI, m/z): calcd for C₁₉H₁₅FN₃O₃[M+H]⁺: 352.1092, found: 352.1092.

3-(5-Bromo-2-(4-oxo-4H-pyrido[1,2-a]pyrimidin-2-yl)phenyl)-1-methylpyrrolidine-2,5-dione (3f): White solid; yield: 70% (57 mg); m.p.236-238 °C; **¹H NMR** (500 MHz, CDCl₃): δ 9.11 (d, J = 7.0 Hz, 1H), 7.85 (t, J = 7.8 Hz, 1H), 7.58 (t, J = 9.8 Hz, 2H), 7.44 (d, J = 8.2

Hz, 1H), 7.38 (s, 1H), 7.26 – 7.23 (m, 1H), 6.66 (s, 1H), 4.48 – 4.45 (m, 1H), 3.29 (dd, $J = 18.2, 9.4$ Hz, 1H), 3.08 (dd, $J = 17.5, 4.9$ Hz, 1H), 2.90 (s, 3H); ^{13}C NMR (126 MHz, CDCl_3): δ 177.8, 176.3, 162.8, 157.7, 150.3, 137.8, 137.6, 137.2, 132.5, 132.2, 131.6, 127.8, 126.0, 124.8, 116.4, 104.1, 44.6, 38.7, 25.3; HRMS (ESI, m/z): calcd for $\text{C}_{19}\text{H}_{14}\text{BrN}_3\text{O}_3\text{Na}[\text{M}+\text{Na}]^+$: 434.0111, found: 434.0102.

3-(4-Bromo-2-(4-oxo-4H-pyrido[1,2-a]pyrimidin-2-yl)phenyl)-1-

methylpyrrolidine-2,5-dione (3g): Orange solid; yield: 62% (51 mg); m.p.226-228 °C; ^1H NMR (500 MHz, CDCl_3): δ 9.12 (d, $J = 7.2$ Hz, 1H), 7.85 (t, $J = 7.9$ Hz, 1H), 7.70 (d, $J = 2.1$ Hz, 1H), 7.62 – 7.57 (m, 2H), 7.26 – 7.24 (m, 1H), 7.12 (d, $J = 8.2$ Hz, 1H), 6.67 (s, 1H), 4.45 (dd, $J = 9.6, 5.6$ Hz, 1H), 3.27 (dd, $J = 18.2, 9.3$ Hz, 1H), 3.02 (dd, $J = 18.5, 5.6$ Hz, 1H), 2.90 (s, 3H); ^{13}C NMR (126 MHz, CDCl_3): δ 177.9, 176.3, 162.3, 157.6, 150.4, 140.2, 137.8, 134.6, 133.4, 133.4, 130.9, 127.8, 126.0, 122.1, 116.5, 104.3, 44.3, 38.6, 25.3; HRMS (ESI, m/z): calcd for $\text{C}_{19}\text{H}_{14}\text{BrN}_3\text{O}_3\text{Na}[\text{M}+\text{Na}]^+$: 434.0111, found: 434.0122.

3-(5-Bromo-2-(8-methyl-4-oxo-4H-pyrido[1,2-a]pyrimidin-2-

yl)phenyl)-1-methylpyrrolidine-2,5-dione (3h): Brown solid; yield: 73% (61 mg); m.p.218-220 °C; ^1H NMR (500 MHz, CDCl_3): δ 9.0 (d, $J = 7.3$ Hz, 1H), 7.57 (dd, $J = 8.3, 2.1$ Hz, 1H), 7.43 – 7.37 (m, 3H), 7.11 (d, $J = 7.3$ Hz, 1H), 6.57 (s, 1H), 4.49 (dd, $J = 9.5, 5.6$ Hz, 1H), 3.32 (dd, $J = 18.5, 9.5$ Hz, 1H), 3.04 (dd, $J = 18.4, 5.6$ Hz, 1H), 2.94 (s, 3H), 2.53 (s, 3H); ^{13}C NMR (126 MHz, CDCl_3): δ 178.0, 176.2, 157.4, 149.8, 137.5, 136.9, 132.1, 132.0, 131.5, 129.9, 127.0, 124.8, 123.6, 123.6, 119.3, 103.1, 44.2, 38.4, 25.2, 21.7; HRMS (ESI, m/z): calcd for $\text{C}_{20}\text{H}_{16}\text{BrN}_3\text{O}_3\text{Na}[\text{M}+\text{Na}]^+$: 448.0267, found: 448.0257.

3-(2-(7-Chloro-4-oxo-4H-pyrido[1,2-a]pyrimidin-2-yl)-5-

methylphenyl)-1-methylpyrrolidine-2,5-dione (3i): Ash-brown solid; yield: 92% (69 mg); m.p.228-230 °C; ^1H NMR (500 MHz, CDCl_3): δ 9.10 (s, 1H), 7.71 (d, $J = 9.5$ Hz, 1H), 7.52 (d, $J = 9.3$ Hz, 1H), 7.45 (d, $J = 7.9$ Hz, 1H), 7.23 (d, $J = 8.1$ Hz, 1H), 7.01 (s, 1H), 6.71

(s, 1H), 4.48 (dd, $J = 9.5, 5.7$ Hz, 1H), 3.27 (dd, $J = 18.3, 9.5$ Hz, 1H), 3.05 (dd, $J = 18.3, 5.8$ Hz, 1H), 2.92 (s, 3H), 2.39 (s, 3H); ^{13}C NMR (126 MHz, CDCl_3): δ 178.3, 176.8, 164.4, 157.0, 148.8, 141.0, 138.2, 135.6, 135.3, 130.8, 130.3, 129.2, 127.2, 125.4, 124.6, 104.5, 44.8, 39.0, 25.2, 21.4; **IR (ATR)**: 1686, 1631, 1437, 1280, 1121, 830, 757 cm^{-1} ; **HRMS** (ESI, m/z): calcd for $\text{C}_{20}\text{H}_{17}\text{ClN}_3\text{O}_3[\text{M}+\text{H}]^+$: 382.0953, found: 382.0959.

1-Allyl-3-(2-(4-oxo-4H-pyrido[1,2-a]pyrimidin-2-yl)phenyl)pyrrolidine-2,5-dione (3j): Brunette solid; yield: 86% (61 mg); m.p. 192-194 $^{\circ}\text{C}$; ^1H NMR (500 MHz, CDCl_3): δ 9.10 (d, $J = 7.2$ Hz, 1H), 7.71 (t, $J = 7.9$ Hz, 1H), 7.59 (d, $J = 9.0$ Hz, 1H), 7.54 (d, $J = 7.5$ Hz, 1H), 7.45 – 7.41 (m, 2H), 7.21 – 7.17 (m, 2H), 6.68 (s, 1H), 5.70 – 5.62 (m, 1H), 5.19 (d, $J = 17.2$ Hz, 1H), 5.09 (d, $J = 10.1$ Hz, 1H), 4.52 (dd, $J = 9.6, 5.8$ Hz, 1H), 4.03 – 3.99 (m, 2H), 3.30 (dd, $J = 18.4, 9.5$ Hz, 1H), 3.11 (dd, $J = 18.3, 5.8$ Hz, 1H); ^{13}C NMR (126 MHz, CDCl_3): δ 177.6, 176.1, 164.6, 158.0, 150.5, 138.8, 136.9, 135.8, 130.6 (2C), 130.4, 129.2, 128.3, 127.5, 126.5, 118.8, 115.9, 104.3, 44.7, 41.2, 39.1; **HRMS** (ESI, m/z): calcd for $\text{C}_{21}\text{H}_{17}\text{N}_3\text{O}_3\text{Na}[\text{M}+\text{Na}]^+$: 382.1162, found: 382.1162.

1-Benzyl-3-(2-(4-oxo-4H-pyrido[1,2-a]pyrimidin-2-yl)phenyl)pyrrolidine-2,5-dione (3k): Dull-brown solid; yield: 82% (66 mg); m.p. 206-208 $^{\circ}\text{C}$; ^1H NMR (500 MHz, CDCl_3): δ 9.08 (d, $J = 7.2$ Hz, 1H), 7.82 (t, $J = 7.9$ Hz, 1H), 7.62 (d, $J = 8.9$ Hz, 1H), 7.54 (d, $J = 8.4$ Hz, 1H), 7.44 – 7.38 (m, 2H), 7.33 (d, $J = 8.4$ Hz, 2H), 7.26 – 7.22 (m, 4H), 7.13 (d, $J = 7.6$ Hz, 1H), 6.68 (s, 1H), 4.65 (d, $J = 14.0$ Hz, 1H), 4.56 (d, $J = 14.0$ Hz, 1H), 4.51 (dd, $J = 9.5, 5.4$ Hz, 1H), 3.29 (dd, $J = 18.5, 9.5$ Hz, 1H), 3.03 (dd, $J = 18.4, 5.4$ Hz, 1H); ^{13}C NMR (126 MHz, CDCl_3): δ 178.3, 176.2, 157.5, 149.9, 138.3, 137.7, 135.8, 135.7, 130.8, 130.6, 129.9, 128.8, 128.8, 128.7, 128.3, 128.0, 127.8, 125.3, 116.7, 104.2, 44.2, 42.7, 38.7; **HRMS** (ESI, m/z): calcd for $\text{C}_{25}\text{H}_{19}\text{N}_3\text{O}_3\text{Na}[\text{M}+\text{Na}]^+$: 432.1319, found: 432.1311.

1-Cyclopropyl-3-(2-(4-oxo-4*H*-pyrido[1,2-*a*]pyrimidin-2-

yl)phenyl)pyrrolidine-2,5-dione (3l): Light brown solid; yield: 77% (55 mg); m.p.204-206 °C; ¹H NMR (500 MHz, CDCl₃): δ 9.09 (d, *J* = 7.2 Hz, 1H), 7.78 (t, *J* = 7.9 Hz, 1H), 7.60 (d, *J* = 8.9 Hz, 1H), 7.54 (d, *J* = 7.6 Hz, 1H), 7.45 – 7.38 (m, 2H), 7.20 – 7.17 (m, 2H), 6.68 (s, 1H), 4.39 (dd, *J* = 9.8, 6.0 Hz, 1H), 3.20 (dd, *J* = 18.2, 9.7 Hz, 1H), 3.05 (dd, *J* = 18.3, 6.1 Hz, 1H), 2.48 – 2.44 (m, 1H), 0.87 – 0.80 (m, 4H); ¹³C NMR (126 MHz, CDCl₃): δ 178.5, 177.1, 164.5, 158.0, 150.4, 138.5, 137.1, 135.8, 130.6, 130.4, 129.5, 128.2, 127.5, 126.4, 115.9, 104.2, 44.5, 38.8, 22.6, 4.6 (2C); HRMS (ESI, *m/z*): calcd for C₂₁H₁₇N₃O₃Na[M+Na]⁺: 382.1162, found: 382.1165.

1-Isobutyl-3-(2-(4-oxo-4*H*-pyrido[1,2-*a*]pyrimidin-2-

yl)phenyl)pyrrolidine-2,5-dione (3m): Charcoal solid; yield: 84% (62 mg); m.p.220-222 °C; ¹H NMR (500 MHz, CDCl₃): δ 9.11 (d, *J* = 7.2 Hz, 1H), 7.81 (t, *J* = 7.9 Hz, 1H), 7.62 (d, *J* = 8.9 Hz, 1H), 7.55 (d, *J* = 7.6 Hz, 1H), 4.48 – 4.40 (m, 2H), 7.21 (d, *J* = 7.5 Hz, 2H), 6.70 (s, 1H), 4.54 (dd, *J* = 9.7, 5.6 Hz, 1H), 3.32 – 3.24 (m, 3H), 3.01 (dd, *J* = 18.5, 5.6 Hz, 1H), 2.04 – 1.99 (m, 1H), 0.87 (d, *J* = 6.7 Hz, 6H); ¹³C NMR (126 MHz, CDCl₃): δ 178.4, 176.8, 164.5, 158.0, 150.5, 138.8, 137.0, 136.1, 130.5, 130.5, 128.7, 128.2, 127.5, 126.4, 115.9, 104.4, 46.3, 44.2, 39.0, 27.2, 20.2 (2C); HRMS (ESI, *m/z*): calcd for C₂₂H₂₁N₃O₃Na[M+Na]⁺: 398.1475, found: 398.1476.

3-(2-(4-oxo-4*H*-pyrido[1,2-*a*]pyrimidin-2-yl)phenyl)pyrrolidine-

2,5-dione (3n): Off white solid; yield: 58% (37 mg); m.p.284-286 °C; ¹H NMR (500 MHz, DMSO-*d*₆): δ 11.20 (s, 1H), 9.02 (d, *J* = 7.2 Hz, 1H), 8.02 (t, *J* = 8.2 Hz, 1H), 7.65 (d, *J* = 8.9 Hz, 1H), 7.58 (d, *J* = 7.6 Hz, 1H), 7.49 (t, *J* = 7.6 Hz, 1H), 7.44 – 7.37 (m, 3H), 6.58 (s, 1H), 4.55 – 4.51 (m, 1H), 3.14 (dd, *J* = 17.9, 9.6 Hz, 1H), 2.83 (dd, *J* = 18.9, 5.0 Hz, 1H); ¹³C NMR (126 MHz, DMSO-*d*₆): δ 179.7, 177.9, 163.8, 157.2, 150.1, 138.7, 137.9, 136.3, 130.0, 129.9, 129.8, 127.5, 127, 126.1, 116.6, 102.8, 45.7, 39.8; IR (ATR): 1697, 1626, 1443, 1280, 1123, 830,

763 cm⁻¹; **HRMS** (ESI, *m/z*): calcd for C₁₈H₁₄N₃O₃[M+H]⁺: 320.1030, found: 320.1039.

3-(2-(4-oxo-4*H*-pyrido[1,2-*a*]pyrimidin-2-yl)phenyl)-1-

phenylpyrrolidine-2,5-dione (3o): Sandy brown solid; yield: 73% (57 mg); m.p.184-186 °C; ¹H NMR (500 MHz, CDCl₃): δ 9.11 (d, *J* = 7.3 Hz, 1H), 7.72 (t, *J* = 7.9 Hz, 1H), 7.60 – 7.58 (m, 2H), 7.52 – 7.45 (m, 2H), 7.38 – 7.31 (m, 4H), 7.17 (t, *J* = 7.0 Hz, 1H), 7.12 (d, *J* = 8.1 Hz, 2H), 6.74 (s, 1H), 4.68 (dd, *J* = 9.7, 5.9 Hz, 1H), 3.47 (dd, *J* = 18.4, 9.7 Hz, 1H), 3.32 (dd, *J* = 18.5, 6.1 Hz, 1H); ¹³C NMR (126 MHz, CDCl₃): δ 177.0, 175.6, 164.4, 157.9, 150.5, 138.5, 137.3, 135.7, 132.0, 130.8, 130.5, 129.7, 129.1, 128.5 (2C), 127.5, 126.4, 126.1, 116.1, 104.3, 45.0, 39.1; **IR (ATR)**: 1681, 1495, 1451, 1382, 1165, 755, 697 cm⁻¹; **HRMS** (ESI, *m/z*): calcd for C₂₄H₁₇N₃O₃Na[M+Na]⁺: 418.1162, found: 418.1152.

1-(4-Methoxyphenyl)-3-(2-(4-oxo-4*H*-pyrido[1,2-*a*]pyrimidin-2-

yl)phenyl)pyrrolidine-2,5-dione (3p): Orange-red solid; yield: 81% (68 mg); m.p.212-214 °C; ¹H NMR (500 MHz, CDCl₃): δ 9.10 (d, *J* = 7.2 Hz, 1H), 7.74 (t, *J* = 7.9 Hz, 1H), 7.60 – 7.56 (m, 2H), 7.51 – 7.42 (m, 2H), 7.34 (d, *J* = 7.6 Hz, 1H), 7.18 (t, *J* = 7.0 Hz, 1H), 7.03 (d, *J* = 8.4 Hz, 2H), 6.88 (d, *J* = 8.5 Hz, 2H), 6.72 (s, 1H), 4.66 (dd, *J* = 9.7, 5.8 Hz, 1H), 3.77 (s, 3H), 3.44 (dd, *J* = 18.4, 9.7 Hz, 1H), 3.27 (dd, *J* = 18.4, 5.8 Hz, 1H); ¹³C NMR (126 MHz, CDCl₃): δ 177.4, 175.9, 164.1, 159.4, 157.8, 150.4, 138.4, 137.5, 135.8, 130.8, 130.6, 129.5, 128.4, 127.5, 127.3, 126.2, 124.6, 116.2, 114.4, 104.2, 55.5, 44.8, 38.9; **HRMS** (ESI, *m/z*): calcd for C₂₅H₁₉N₃O₄Na[M+Na]⁺: 448.1268, found: 448.1256.

1-(4-Nitrophenyl)-3-(2-(4-oxo-4*H*-pyrido[1,2-*a*]pyrimidin-2-

yl)phenyl)pyrrolidine-2,5-dione (3q): Brown solid; yield: 71% (62 mg); m.p.180-182 °C; ¹H NMR (500 MHz, CDCl₃): δ 9.11 (d, *J* = 7.0 Hz, 1H), 8.20 (d, *J* = 7.9 Hz, 2H), 7.71 – 7.68 (m, 1H), 7.61 (d, *J* = 7.3 Hz, 1H), 7.54 – 7.46 (m, 3H), 7.39 (dd, *J* = 18.8, 7.8 Hz, 3H), 7.18 (t, *J* = 6.9 Hz, 1H), 6.74 (s, 1H), 4.70 (dd, *J* = 9.8, 6.3 Hz, 1H), 3.50 (dd, *J* =

18.4, 9.7 Hz, 1H), 3.42 (dd, $J = 18.5, 6.5$ Hz, 1H); ^{13}C NMR (126 MHz, CDCl_3): δ 176.1, 174.9, 164.5, 158.0, 150.5, 146.7, 138.4, 137.6, 137.3, 134.9, 131.0, 130.6, 130.2, 128.8, 127.6, 126.3, 124.5, 124.2, 116.2, 104.2, 45.4, 38.9; HRMS (ESI, m/z): calcd for $\text{C}_{24}\text{H}_{17}\text{N}_4\text{O}_5[\text{M}+\text{H}]^+$: 441.1193, found: 441.1193.

1-(1*H*-Indol-6-yl)-3-(2-(4-oxo-4*H*-pyrido[1,2-*a*]pyrimidin-2-

yl)phenyl)pyrrolidine-2,5-dione (3r): Latte brown solid; yield: 68% (59 mg); m.p. 174–176 °C; ^1H NMR (500 MHz, DMSO-d_6): δ 11.21 (s, 1H), 9.02 (d, $J = 7.2$ Hz, 1H), 7.95 (t, $J = 8.1$ Hz, 1H), 7.66 (d, $J = 9.0$ Hz, 1H), 7.57 (d, $J = 7.6$ Hz, 1H), 7.51 – 7.41 (m, 4H), 7.39 – 7.35 (m, 2H), 7.13 (s, 1H), 6.62 – 6.58 (m, 2H), 6.42 (s, 1H), 4.75 – 7.71 (m, 1H), 3.26 – 3.23 (m, 1H), 3.15 (dd, $J = 17.5, 6.7$ Hz, 1H); ^{13}C NMR (126 MHz, DMSO-d_6): δ 178.4, 176.5, 174.3, 172.5, 164.4, 157.7, 150.8, 139.5, 138.4, 137.0, 135.7, 130.4, 128.1, 127.7, 127.4, 127.3, 126.7, 126.3, 120.1, 118.2, 117.2, 110.8, 103.4, 101.6, 48.9, 30.6; HRMS (ESI, m/z): calcd for $\text{C}_{26}\text{H}_{19}\text{N}_4\text{O}_3[\text{M}+\text{H}]^+$: 435.1450, found: 435.1452.

1-Methyl-3-(2-(4-oxo-4*H*-pyrido[1,2-*a*]pyrimidin-2-yl)phenyl)-1*H*-

pyrrole-2,5-dione (4a): White solid; yield: 82% (55 mg); m.p. 238–240 °C; ^1H NMR (500 MHz, CDCl_3): δ 9.06 (d, $J = 7.2$ Hz, 1H), 7.80 (d, $J = 7.6$ Hz, 1H), 7.73 (t, $J = 7.9$ Hz, 1H), 7.60 – 7.46 (m, 4H), 7.16 (t, $J = 7.0$ Hz, 1H), 6.74 (s, 1H), 6.56 (s, 1H), 2.89 (s, 3H); ^{13}C NMR (126 MHz, CDCl_3): δ 170.8, 170.1, 163.3, 158.2, 150.5, 149.1, 137.9, 137.0, 131.0, 130.8, 130.2, 129.9, 128.2, 127.6, 125.9, 125.8, 115.8, 103.0, 24.0; HRMS (ESI, m/z): calcd for $\text{C}_{19}\text{H}_{14}\text{N}_3\text{O}_4[\text{M}+\text{H}]^+$: 332.1030, found: 332.1023.

1-Isobutyl-3-(2-(4-oxo-4*H*-pyrido[1,2-*a*]pyrimidin-2-yl)phenyl)-1*H*-

pyrrole-2,5-dione (4b): Yellow solid; yield: 62% (46 mg); m.p. 226–228 °C; ^1H NMR (500 MHz, CDCl_3): δ 9.06 (d, $J = 7.2$ Hz, 1H), 7.78 (d, $J = 7.6$ Hz, 1H), 7.72 – 7.69 (m, 1H), 7.60 – 7.48 (m, 4H), 7.14 (t, $J = 6.9$ Hz, 1H), 6.74 (s, 1H), 6.60 (s, 1H), 3.19 (d, $J = 7.2$ Hz, 2H), 1.78 – 1.73

(m, 1H), 0.72 (d, $J = 6.7$ Hz, 6H); ^{13}C NMR (126 MHz, CDCl_3): δ 171.1, 170.1, 163.8, 158.2, 150.6, 148.5, 138.3, 136.7, 131.1, 130.8, 130.1, 130.0, 128.2, 127.6, 126.2, 125.8, 115.7, 103.2, 45.3, 27.9, 20.0 (2C); **HRMS** (ESI, m/z): calcd for $\text{C}_{22}\text{H}_{20}\text{N}_3\text{O}_3[\text{M}+\text{H}]^+$: 374.1499, found: 374.1499.

1-Benzyl-3-(2-(4-oxo-4H-pyrido[1,2-a]pyrimidin-2-yl)phenyl)-1H-pyrrole-2,5-dione (4c): Off-white solid; yield: 57% (46 mg); m.p. 232–234 °C; ^1H NMR (500 MHz, CDCl_3): δ 9.02 (d, $J = 7.3$ Hz, 1H), 7.80 (d, $J = 7.6$ Hz, 1H), 7.58 – 7.52 (m, 2H), 7.48 – 7.42 (m, 2H), 7.22 – 7.15 (m, 5H), 7.08 (d, $J = 7.8$ Hz, 2H), 6.78 (s, 1H), 6.59 (s, 1H), 4.54 (s, 2H); ^{13}C NMR (126 MHz, CDCl_3): δ 170.5, 169.5, 163.2, 158.3, 150.3, 149.5, 138.0, 136.7, 136.5, 131.1, 130.8, 130.2, 129.8, 128.7, 128.6, 128.3, 127.7, 127.3, 125.7, 125.4, 115.6, 102.7, 41.6; **HRMS** (ESI, m/z): calcd for $\text{C}_{25}\text{H}_{18}\text{N}_3\text{O}_3[\text{M}+\text{H}]^+$: 408.1343, found: 408.1354.

3-(5-Methoxy-2-(4-oxo-4H-pyrido[1,2-a]pyrimidin-2-yl)phenyl)-1-methyl-1H-pyrrole-2,5-dione (4d): Orange solid; yield: 68% (48 mg); m.p. 210–212 °C; ^1H NMR (500 MHz, CDCl_3): δ 9.04 (d, $J = 6.9$ Hz, 1H), 7.78 (d, $J = 8.7$ Hz, 1H), 7.72 – 7.68 (m, 1H), 7.41 (d, $J = 8.9$ Hz, 1H), 7.14 – 7.08 (m, 2H), 6.98 (d, $J = 2.7$ Hz, 1H), 6.72 (s, 1H), 6.56 (s, 1H), 3.88 (s, 3H), 2.91 (s, 3H); ^{13}C NMR (126 MHz, CDCl_3): δ 170.8, 169.9, 162.7, 160.9, 158.1, 150.3, 149.6, 136.7, 131.4, 130.0, 129.8, 127.5, 125.6, 125.4, 116.6, 115.7, 115.5, 102.0, 55.7, 23.9; **IR (ATR)**: 1687, 1601, 1436, 1123, 1019, 770 cm^{-1} ; **HRMS** (ESI, m/z): calcd for $\text{C}_{20}\text{H}_{16}\text{N}_3\text{O}_3[\text{M}+\text{H}]^+$: 362.1135, found: 362.1142.

3-(2-(4-oxo-4H-pyrido[1,2-a]pyrimidin-2-yl)phenyl)-1-phenyl-1H-pyrrole-2,5-dione (4e): Light yellow solid; yield: 54% (42 mg); m.p. 218–220 °C; ^1H NMR (500 MHz, CDCl_3): δ 9.07 (d, $J = 5.8$ Hz, 1H), 7.86 (d, $J = 7.3$ Hz, 1H), 7.71 (t, $J = 7.8$ Hz, 1H), 7.64 – 7.57 (m, 2H), 7.53 (d, $J = 9.2$ Hz, 1H), 7.34 (t, $J = 7.8$ Hz, 2H), 7.29 – 7.25 (m, 2H), 7.16 – 7.11 (m, 3H), 6.84 (s, 1H), 6.74 (s, 1H); ^{13}C NMR (126 MHz, CDCl_3): δ 169.5, 168.6, 163.1, 158.2, 150.4, 149.5, 137.8, 136.9,

131.6, 131.2, 131.0, 130.3, 129.8, 129.1, 129.0, 128.1, 127.7, 127.6, 125.9, 125.4, 115.7, 102.9; **IR** (ATR): 1706, 1672, 1477, 1120, 753, 683 cm^{-1} ; **HRMS** (ESI, m/z): calcd for $\text{C}_{24}\text{H}_{16}\text{N}_3\text{O}_3[\text{M}+\text{H}]^+$: 394.1186, found: 394.1175.

3-(2-(7-Methyl-4-oxo-4H-pyrido[1,2-a]pyrimidin-2-yl)phenyl)-1-phenyl-1H-pyrrole-2,5-dione (4f): Orange solid; yield: 56% (46 mg); m.p. 226–228 °C; **^1H NMR** (500 MHz, CDCl_3): δ 8.87 (s, 1H), 7.85 (d, $J = 8.5$ Hz, 1H), 7.62 – 7.55 (m, 4H), 7.46 (d, $J = 9.0$ Hz, 1H), 7.34 (t, $J = 7.6$ Hz, 2H), 7.28 – 7.25 (m, 1H), 7.14 – 7.11 (m, 2H), 6.81 (s, 1H), 6.72 (s, 1H), 2.41 (s, 3H); **^{13}C NMR** (126 MHz, CDCl_3): δ 169.6, 168.6, 162.7, 158.2, 149.6, 149.4, 139.8, 138.0, 131.7, 131.2, 131.0, 130.2, 129.8, 129.0, 128.2, 127.7, 126.3, 125.9, 125.4 (2C), 125.1, 102.6, 18.4; **IR** (ATR): 1705, 1664, 1492, 1387, 1132, 754, 695 cm^{-1} ; **HRMS** (ESI, m/z): calcd for $\text{C}_{25}\text{H}_{18}\text{N}_3\text{O}_3[\text{M}+\text{H}]^+$: 408.1343, found: 408.1356.

1-(4-Methoxyphenyl)-3-(2-(4-oxo-4H-pyrido[1,2-a]pyrimidin-2-yl)phenyl)-1H-pyrrole-2,5-dione (4g): Brunt orange solid; yield: 61% (51 mg); m.p. 216–218 °C; **^1H NMR** (500 MHz, CDCl_3): δ 9.05 (d, $J = 6.6$ Hz, 1H), 7.84 (d, $J = 7.9$ Hz, 1H), 7.73 – 7.70 (m, 1H), 7.62 – 7.55 (m, 4H), 7.16 – 7.12 (m, 1H), 7.02 (d, $J = 9.0$ Hz, 2H), 6.86 – 6.82 (m, 3H), 6.73 (s, 1H), 3.74 (s, 3H); **^{13}C NMR** (126 MHz, CDCl_3): δ 169.9, 168.9, 163.2, 159.0, 158.2, 150.5, 149.4, 137.9, 136.9, 131.2, 131.0, 130.3, 129.9, 128.2, 127.7, 127.5, 126.0, 125.4, 124.2, 115.8, 114.4, 102.9, 55.5; **HRMS** (ESI, m/z): calcd for $\text{C}_{25}\text{H}_{18}\text{N}_3\text{O}_4[\text{M}+\text{H}]^+$: 424.1292, found: 424.1297.

1-(4-Nitrophenyl)-3-(2-(4-oxo-4H-pyrido[1,2-a]pyrimidin-2-yl)phenyl)-1H-pyrrole-2,5-dione (4h): Neon orange solid; yield: 58% (50 mg); m.p. 238–240 °C; **^1H NMR** (500 MHz, CDCl_3): δ 9.09 (d, $J = 7.2$ Hz, 1H), 8.21 (d, $J = 9.2$ Hz, 2H), 7.89 (d, $J = 7.6$ Hz, 1H), 7.71 – 7.57 (m, 4H), 7.44 (t, $J = 10.4$ Hz, 3H), 7.17 (t, $J = 6.9$ Hz, 1H), 6.85 (s, 1H), 6.79 (s, 1H); **^{13}C NMR** (126 MHz, CDCl_3): δ 168.6, 167.8, 162.9, 158.2, 150.5, 150.3, 146.0, 137.9, 137.5, 137.2, 131.4, 131.2, 130.5,

130.0, 127.8, 127.7, 125.7, 125.5, 125.3, 124.5, 116.0, 103.0; **HRMS** (ESI, m/z): calcd for $C_{24}H_{14}N_4O_5Na[M+Na]^+$: 461.0856, found: 461.0840.

1-(3,4-Dichlorophenyl)-3-(2-(4-oxo-4H-pyrido[1,2-a]pyrimidin-2-yl)phenyl)-1H-pyrrole-2,5-dione (4i): Yellow solid; yield: 62% (56 mg); m.p. 210–212 °C; **1H NMR** (500 MHz, DMSO- d_6): δ 9.00 (d, J = 7.2 Hz, 1H), 8.04 (d, J = 8.1 Hz, 1H), 7.97 (t, J = 7.9 Hz, 1H), 7.71 – 7.60 (m, 4H), 7.62 (d, J = 9.0 Hz, 1H), 7.39 (t, J = 6.9 Hz, 1H), 7.31 (s, 1H), 7.23 (s, 1H), 7.14 (d, J = 8.7 Hz, 1H), 6.90 (s, 1H); **^{13}C NMR** (126 MHz, DMSO- d_6): δ 168.7, 167.9, 162.0, 157.4, 149.9, 149.6, 138.4, 137.0, 131.5, 131.4, 131.1, 130.9, 130.8, 130.3, 130.1, 129.5, 128.0, 127.9, 127.1, 126.4, 125.5, 125.4, 116.8, 101.4; **HRMS** (ESI, m/z): calcd for $C_{24}H_{14}Cl_2N_3O_3[M+H]^+$: 462.0407, found: 462.0401.

1-(Naphthalen-1-yl)-3-(2-(4-oxo-4H-pyrido[1,2-a]pyrimidin-2-yl)phenyl)-1H-pyrrole-2,5-dione (4j): Red orange solid; yield: 49% (43 mg); m.p. 224–226 °C; **1H NMR** (500 MHz, $CDCl_3$): δ 9.04 (d, J = 7.2 Hz, 1H), 7.86 – 7.82 (m, 3H), 7.74 – 7.68 (m, 2H), 7.65 – 7.60 (m, 3H), 7.45 – 7.42 (m, 3H), 7.33 – 7.30 (m, 1H), 7.20 (d, J = 8.5 Hz, 1H), 7.12 – 7.09 (m, 1H), 6.92 (s, 1H), 6.81 (s, 1H); **^{13}C NMR** (126 MHz, $CDCl_3$): δ 170.0, 169.0, 163.7, 158.1, 150.7, 149.4, 138.4, 136.9, 134.4, 131.3, 131.1, 130.3, 130.2, 130.2, 129.9, 129.8, 128.6, 128.0, 127.7, 126.9, 126.8, 126.5, 126.3, 126.2, 125.3, 122.4, 115.7, 103.2; **IR (ATR)**: 1709, 1680, 1406, 1131, 762, 679 cm^{-1} ; **HRMS** (ESI, m/z): calcd for $C_{28}H_{17}N_3O_3Na[M+Na]^+$: 466.1162, found: 466.1178.

1-Methyl-3-(2-(4-oxo-3,4-dihydroquinazolin-2-yl)phenyl)pyrrolidine-2,5-dione (5a): Peach solid; yield: 62% (41 mg); m.p. 232–234 °C; **1H NMR** (500 MHz, $CDCl_3$): δ 11.18 (s, 1H), 8.25 (d, J = 7.9 Hz, 1H), 7.76 (d, J = 6.8 Hz, 2H), 7.60 (d, J = 8.2 Hz, 1H), 7.52 – 7.47 (m, 3H), 7.30 (d, J = 7.5 Hz, 1H), 4.38 (t, J = 7.6 Hz, 1H), 3.27 (d, J = 7.6 Hz, 2H), 2.71 (s, 3H); **^{13}C NMR** (126 MHz, $CDCl_3$): δ 178.8, 176.5, 162.8, 152.9, 148.3, 135.9, 135.0, 133.8, 131.4,

130.3, 130.1, 128.6, 127.6, 127.4, 126.7, 121.0, 45.1, 38.3, 25.2; **IR** (**ATR**): 1691, 1612, 1433, 1282, 1117, 953, 766 cm^{-1} ; **HRMS** (ESI, m/z): calcd for $\text{C}_{19}\text{H}_{15}\text{N}_3\text{O}_3\text{Na}[\text{M}+\text{Na}]^+$: 356.1006, found: 356.1000.

1-Methyl-3-(2-(quinolin-2-yl)phenyl)pyrrolidine-2,5-dione (5b):

Gray solid; yield: 59% (37 mg); m.p. 182–184 °C; **^1H NMR** (500 MHz, CDCl_3): δ 8.26 (d, J = 8.5 Hz, 1H), 8.01 (d, J = 8.7 Hz, 1H), 7.85 (d, J = 8.1 Hz, 1H), 7.74 – 7.68 (m, 2H), 7.60 – 7.54 (m, 2H), 7.46 – 7.44 (m, 2H), 7.30 – 7.28 (m, 1H), 4.36 (dd, J = 9.0, 6.4 Hz, 1H), 3.36 – 3.26 (m, 2H), 2.61 (s, 3H); **^{13}C NMR** (126 MHz, CDCl_3): δ 178.5, 176.9, 159.3, 147.0, 140.2, 137.3, 135.9, 131.0, 130.2, 130.2, 129.4, 129.2, 128.2, 127.7, 127.0, 126.8, 122.4, 45.5, 39.3, 24.9; **HRMS** (ESI, m/z): calcd for $\text{C}_{20}\text{H}_{16}\text{N}_2\text{O}_2\text{Na}[\text{M}+\text{Na}]^+$: 339.1104, found: 339.1109.

1-Phenyl-3-(2-(quinolin-2-yl)phenyl)pyrrolidine-2,5-dione (5c):

Light-yellow solid; yield: 58% (43 mg); m.p. 178–180 °C; **^1H NMR** (500 MHz, CDCl_3): δ 8.26 (d, J = 8.5 Hz, 1H), 8.03 (d, J = 8.5 Hz, 1H), 7.87 (d, J = 8.1 Hz, 1H), 7.71 – 7.67 (m, 2H), 7.62 (dd, J = 5.7, 3.5 Hz, 1H), 7.56 (t, J = 7.5 Hz, 1H), 7.50 (dd, J = 5.7, 3.4 Hz, 2H), 7.41 – 7.39 (m, 1H), 7.27 – 7.24 (m, 3H), 6.78 – 6.76 (m, 2H), 4.57 (dd, J = 9.7, 6.3 Hz, 1H), 3.68 (dd, J = 18.2, 6.3 Hz, 1H), 3.50 (dd, J = 18.2, 9.7 Hz, 1H); **^{13}C NMR** (126 MHz, CDCl_3): δ 177.3, 175.8, 159.6, 147.4, 140.7, 137.2, 135.8, 131.9, 131.1, 130.3, 130.2, 129.5, 129.4, 128.8, 128.3, 128.2, 127.7, 127.0, 126.9, 126.2, 122.4, 45.8, 39.5; **IR** (**ATR**): 1697, 1494, 1385, 1167, 831, 756, 696 cm^{-1} ; **HRMS** (ESI, m/z): calcd for $\text{C}_{25}\text{H}_{19}\text{N}_2\text{O}_2[\text{M}+\text{H}]^+$: 379.1441, found: 379.1442.

3-(2-(2-Methyl-7-phenylpyrazolo[1,5-*a*]pyrimidin-5-yl)phenyl)-1-

phenylpyrrolidine-2,5-dione (5d): Yellow solid; yield: 54% (49 mg); m.p. 184–186 °C; **^1H NMR** (500 MHz, CDCl_3): δ 8.12 – 8.10 (m, 2H), 7.68 (dd, J = 7.2, 2.1 Hz, 1H), 7.57 – 7.56 (m, 3H), 7.51 – 7.47 (m, 2H), 7.40 – 7.36 (m, 3H), 7.33 – 7.31 (m, 1H), 7.15 (s, 1H), 7.05 (d, J = 9.3 Hz, 2H), 6.44 (s, 1H), 4.64 (dd, J = 9.3, 6.4 Hz, 1H), 3.50 – 3.42 (m, 2H), 2.48 (s, 3H); **^{13}C NMR** (126 MHz, CDCl_3): δ 177.3, 175.7, 157.8,

155.8, 149.7, 146.6, 138.7, 135.9, 132.1, 131.3, 131.3, 130.7, 130.1, 129.5, 129.0, 128.8, 128.5, 128.4, 126.6, 126.3, 107.6, 97.1, 45.7, 39.1, 14.9; **HRMS** (ESI, m/z): calcd for $C_{29}H_{22}N_4O_2Na[M+Na]^+$: 481.1632, found: 481.1641.

1-Methyl-3-(2-(4-methyl-3-oxo-3,4-dihydroquinoxalin-2-

yl)phenyl)pyrrolidine-2,5-dione (5e): Orange peel solid; yield: 74% (51 mg); m.p.186-188 °C; **1H NMR** (500 MHz, $CDCl_3$): δ 7.75 (t, J = 8.9 Hz, 2H), 7.59 (t, J = 7.1 Hz, 1H), 7.46 – 7.40 (m, 2H), 7.36 (t, J = 7.1 Hz, 2H), 7.27 – 7.25 (m, 1H), 4.28 – 4.25 (m, 1H), 3.76 (s, 3H), 3.27 (dd, J = 18.3, 9.5 Hz, 1H), 3.15 (dd, J = 18.3, 6.0 Hz, 1H), 2.66 (s, 3H); **^{13}C NMR** (126 MHz, $CDCl_3$): δ 178.4, 176.6, 156.6, 154.6, 136.4, 135.4, 133.6, 132.3, 131.2, 131.1, 130.3 (2C), 129.5, 127.4, 124.0, 113.9, 45.1, 38.8, 29.7, 24.9; **HRMS** (ESI, m/z): calcd for $C_{20}H_{18}N_3O_3[M+H]^+$: 348.1345, found: 348.1343.

1-Benzyl-3-(2-(4-methyl-3-oxo-3,4-dihydroquinoxalin-2-

yl)phenyl)pyrrolidine-2,5-dione (5f): Orange solid; yield: 63% (53 mg); m.p.174-176 °C; **1H NMR** (500 MHz, $CDCl_3$): δ 7.82 (d, J = 7.9 Hz, 1H), 7.73 (d, J = 9.2 Hz, 1H), 7.60 (t, J = 7.9 Hz, 1H), 7.42 – 7.31 (m, 6H), 7.26 – 7.24 (m, 3H), 7.17 (d, J = 9.0 Hz, 1H), 4.48 (d, J = 14.0 Hz, 1H), 4.36 (d, J = 14.0 Hz, 1H), 4.27 (dd, J = 9.5, 5.6 Hz, 1H), 3.76 (s, 3H), 3.28 (dd, J = 18.5, 9.4 Hz, 1H), 3.07 (dd, J = 18.5, 5.6 Hz, 1H); **^{13}C NMR** (126 MHz, $CDCl_3$): δ 177.9, 176.2, 156.5, 154.6, 136.7, 135.9, 135.6, 133.6, 132.4, 131.1, 131.1, 130.4, 130.3, 128.9, 128.7(2C), 128.0, 127.4, 124.0, 113.9, 44.7, 42.4, 38.9, 29.7; **HRMS** (ESI, m/z): calcd for $C_{26}H_{22}N_3O_3[M+H]^+$: 424.1656, found: 424.1646.

1-Isobutyl-3-(2-(4-methyl-3-oxo-3,4-dihydroquinoxalin-2-

yl)phenyl)pyrrolidine-2,5-dione (5g): White solid; yield: 72% (55 mg); m.p.188-190 °C; **1H NMR** (500 MHz, $CDCl_3$): δ 7.81 (d, J = 7.9 Hz, 1H), 7.72 (d, J = 7.5 Hz, 1H), 7.60 (t, J = 7.9 Hz, 1H), 7.47 – 7.41 (m, 2H), 7.37 (d, J = 8.1 Hz, 2H), 7.24 (d, J = 7.3 Hz, 1H), 4.30 (dd, J = 9.6, 5.6 Hz, 1H), 3.76 (s, 3H), 3.26 (dd, J = 18.5, 9.5 Hz, 1H), 3.14 (dd, J = 13.1, 7.5 Hz, 1H), 3.07 – 3.01 (m, 2H), 1.99 – 1.93 (m, 1H), 0.83 (d,

$J = 3.4$ Hz, 6H); ^{13}C NMR (126 MHz, CDCl_3): δ 178.4, 176.8, 156.5, 154.6, 136.9, 135.7, 133.7, 132.5, 131.1, 131.1, 130.4, 130.3, 128.5, 127.4, 124.0, 113.9, 46.1, 44.5, 38.8, 29.7, 27.1, 20.2, 20.1.; HRMS (ESI, m/z): calcd for $\text{C}_{23}\text{H}_{23}\text{N}_3\text{O}_3\text{Na}[\text{M}+\text{Na}]^+$: 412.1632, found: 412.1632.

3-(5-Methyl-2-(5-oxo-5H-thiazolo[3,2-a]pyrimidin-7-yl)phenyl)-1-phenylpyrrolidine-2,5-dione (5h): Light brown solid; yield: 59% (48 mg); m.p.230-232 °C; ^1H NMR (500 MHz, CDCl_3): δ 8.04 (d, $J = 4.9$ Hz, 1H), 7.46 – 7.43 (m, 3H), 7.36 (t, $J = 7.1$ Hz, 1H), 7.27 – 7.24 (m, 3H), 7.12 (s, 1H), 7.02 (d, $J = 5.0$ Hz, 1H), 6.57 (s, 1H), 4.63 (dd, $J = 9.8, 5.7$ Hz, 1H), 3.42 (dd, $J = 18.6, 9.8$ Hz, 1H), 3.15 (dd, $J = 18.6, 5.8$ Hz, 1H), 2.41 (s, 3H); ^{13}C NMR (126 MHz, CDCl_3): δ 177.2, 175.6, 163.7, 162.5, 158.6, 141.1, 135.5, 135.0, 132.2, 130.8, 130.3, 129.3, 129.2, 128.6, 126.2, 122.1, 112.1, 105.2, 44.9, 38.7, 21.5; HRMS (ESI, m/z): calcd for $\text{C}_{23}\text{H}_{18}\text{N}_3\text{O}_3\text{S}[\text{M}+\text{H}]^+$: 416.1063, found: 416.1053.

1-Methyl-3-(2-(4-methyl-3-oxo-3,4-dihydroquinoxalin-2-yl)phenyl)-1H-pyrrole-2,5-dione (5i): Off-white solid; yield: 53% (36 mg); m.p.194-196 °C; ^1H NMR (500 MHz, CDCl_3): δ 8.01 (d, $J = 9.6$ Hz, 1H), 7.77 (d, $J = 8.2$ Hz, 1H), 7.61 – 7.56 (m, 4H), 7.35 – 7.33 (m, 2H), 6.52 (s, 1H), 3.73 (s, 3H), 2.85 (s, 3H); ^{13}C NMR (126 MHz, CDCl_3): δ 170.8, 170.4, 156.1, 154.6, 148.1, 135.9, 133.7, 132.8, 131.1, 130.9, 130.3, 130.3, 130.1, 130.0, 128.9, 125.7, 124.0, 114.0, 29.6, 23.8; HRMS (ESI, m/z): calcd for $\text{C}_{20}\text{H}_{16}\text{N}_3\text{O}_3[\text{M}+\text{H}]^+$: 346.1186, found: 346.1170.

1-Methyl-3-(5-methyl-2-(5-oxo-5H-thiazolo[3,2-a]pyrimidin-7-yl)phenyl)-1H-pyrrole-2,5-dione (5j): Orange solid; yield: 56% (38.5 mg); m.p.210-212 °C; ^1H NMR (500 MHz, CDCl_3): δ 8.01 (d, $J = 4.7$ Hz, 1H), 7.66 (d, $J = 7.9$ Hz, 1H), 7.39 (d, $J = 7.9$ Hz, 1H), 7.27 (d, $J = 5.2$ Hz, 2H), 7.01 (d, $J = 4.8$ Hz, 1H), 6.55 (d, $J = 9.2$ Hz, 1H), 2.98 (s, 3H), 2.44 (s, 3H); ^{13}C NMR (126 MHz, CDCl_3): δ 170.7, 170.1, 162.6, 158.7, 151.8, 148.9, 140.7, 134.3, 131.6, 131.4, 129.7, 128.0, 125.9,

122.2, 111.6, 103.7, 23.9, 21.2; **HRMS** (ESI, m/z): calcd for $\text{C}_{18}\text{H}_{14}\text{N}_3\text{O}_3\text{S}[\text{M}+\text{H}]^+$: 352.0750, found: 352.0757.

5.8 ^1H and ^{13}C NMR spectra of selected compounds

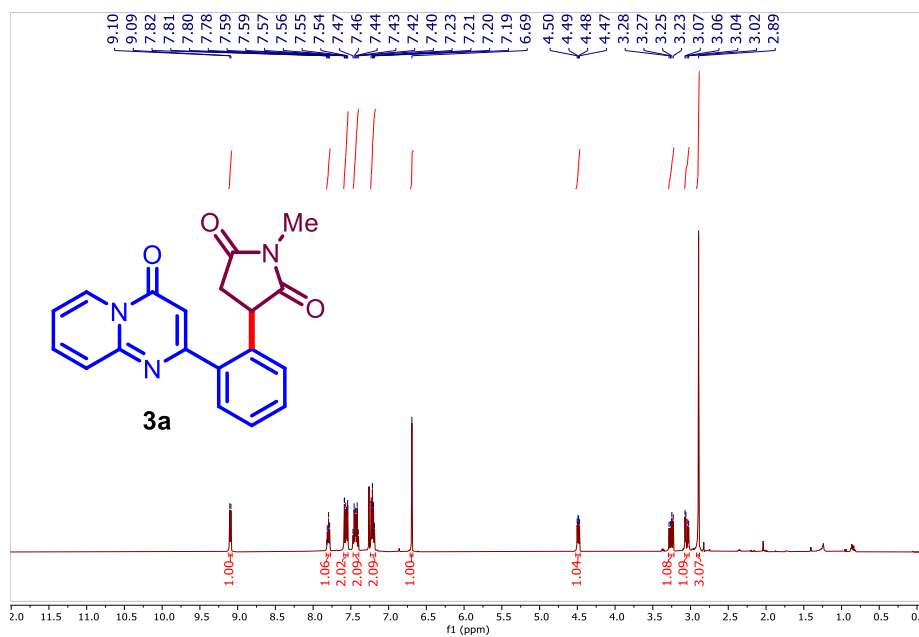


Figure 5.1 ^1H NMR spectrum of compound **3a** (500 MHz, CDCl_3)

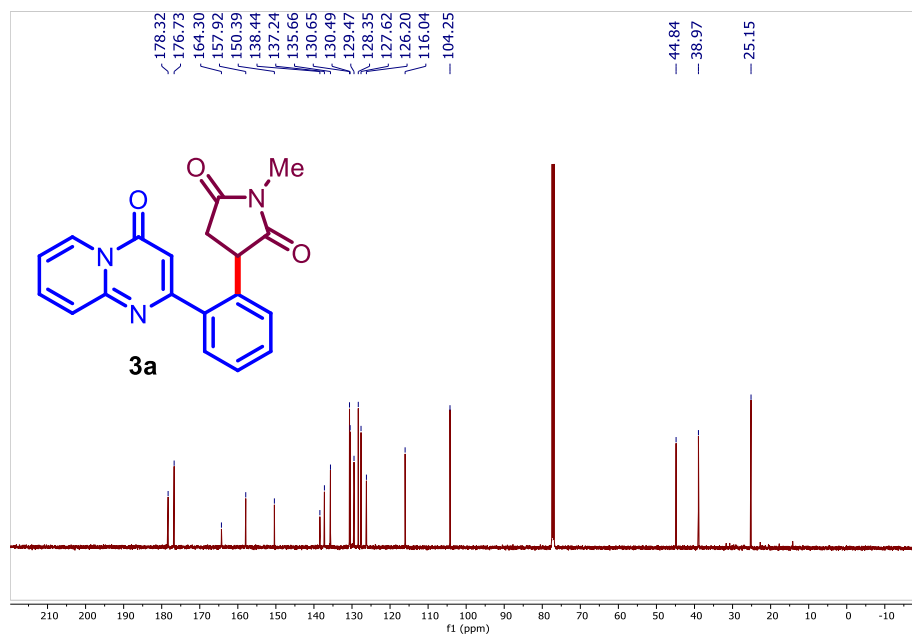


Figure 5.2 ^{13}C NMR spectrum of compound **3a** (126 MHz, CDCl_3)

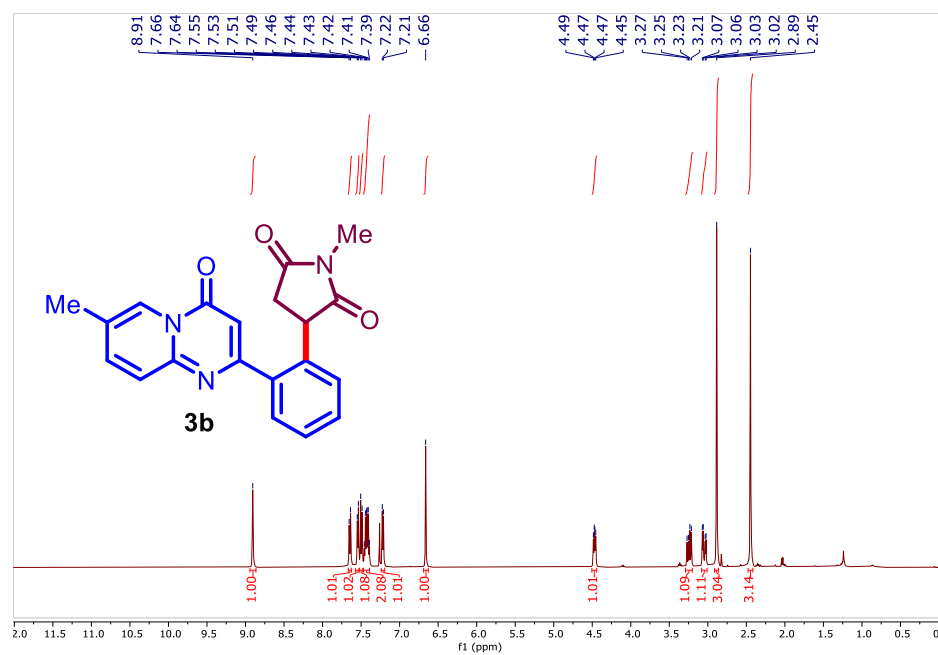


Figure 5.3 ¹H NMR spectrum of compound **3b** (500 MHz, CDCl₃)

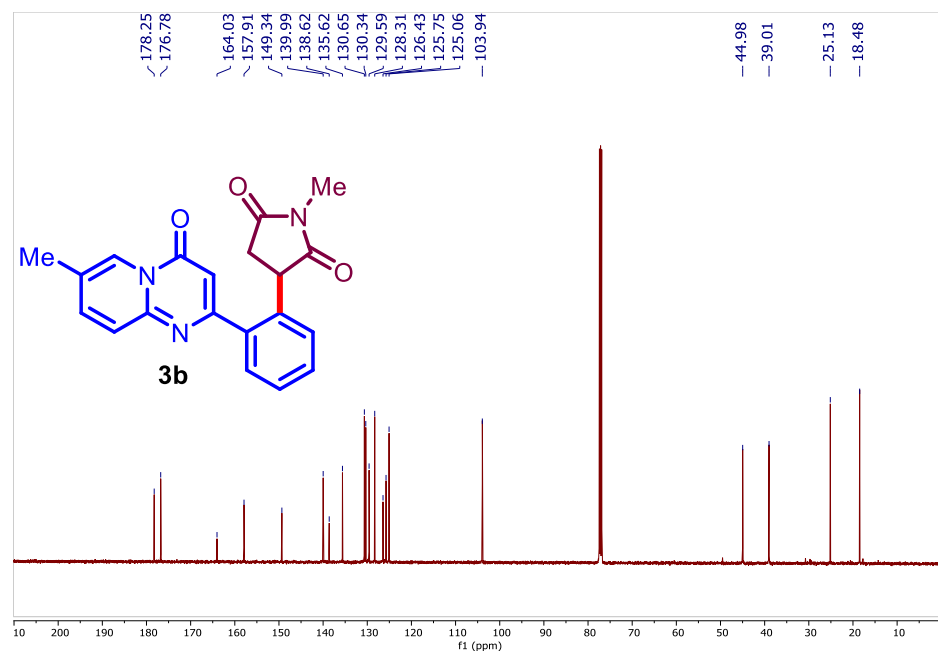


Figure 5.4 ¹³C NMR spectrum of compound **3b** (126 MHz, CDCl₃)

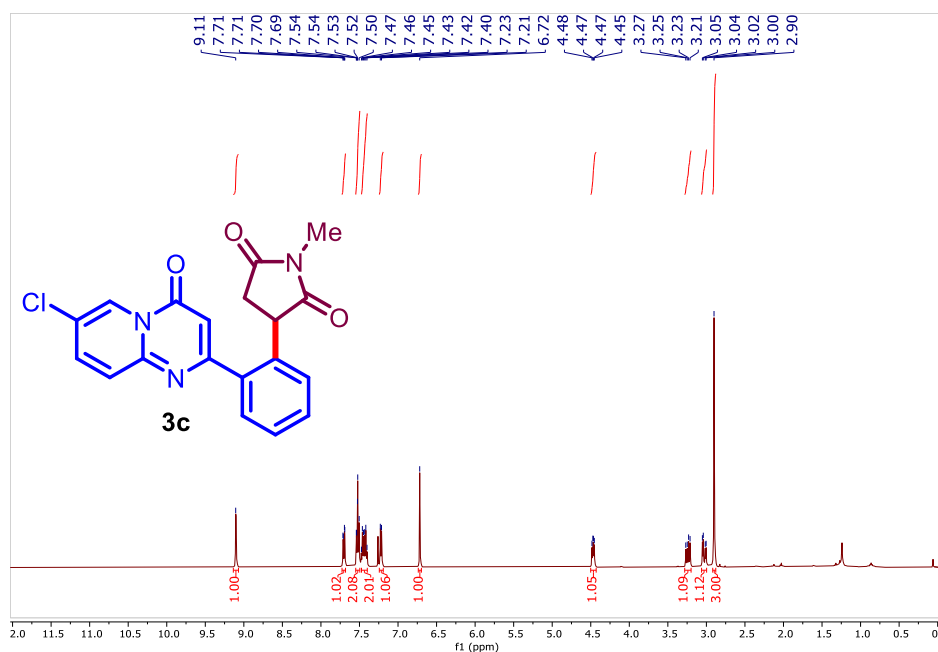


Figure 5.5 ¹H NMR spectrum of compound **3c** (500 MHz, CDCl₃)

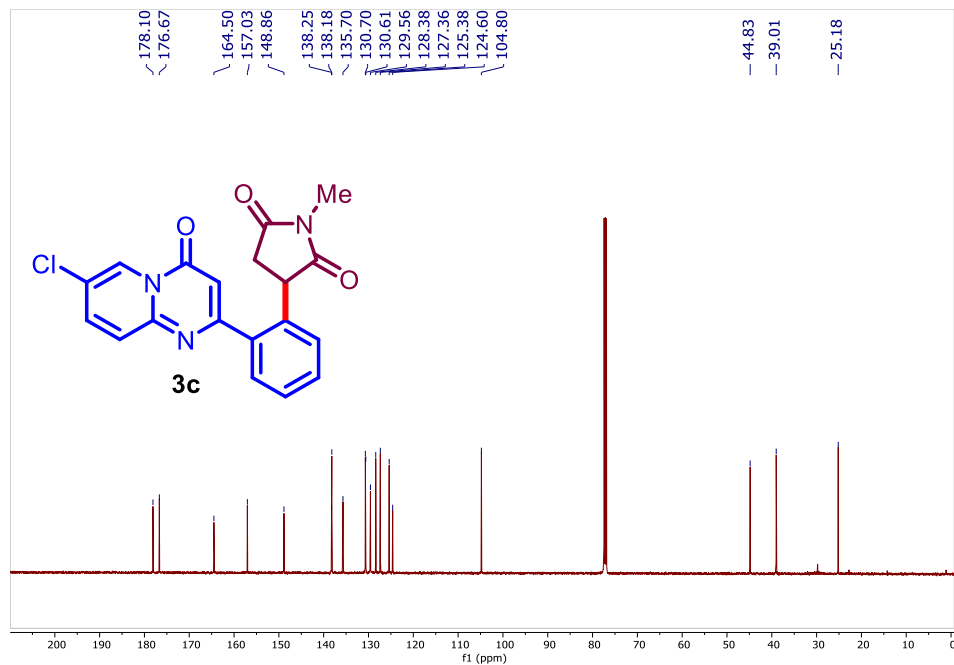


Figure 5.6 ¹³C NMR spectrum of compound **3c** (126 MHz, CDCl₃)

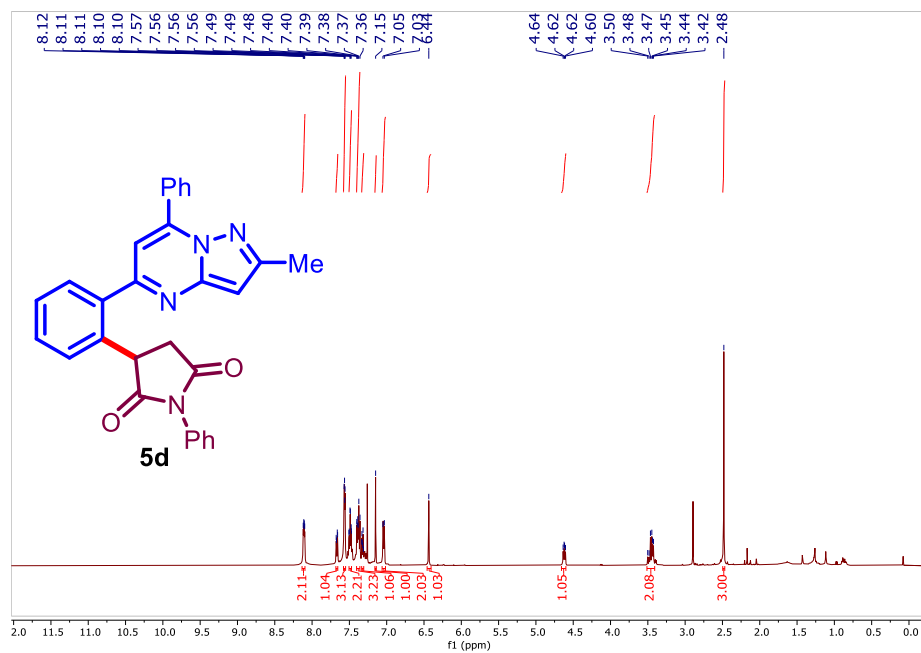


Figure 5.7 ¹H NMR spectrum of compound **5d** (500 MHz, CDCl₃)

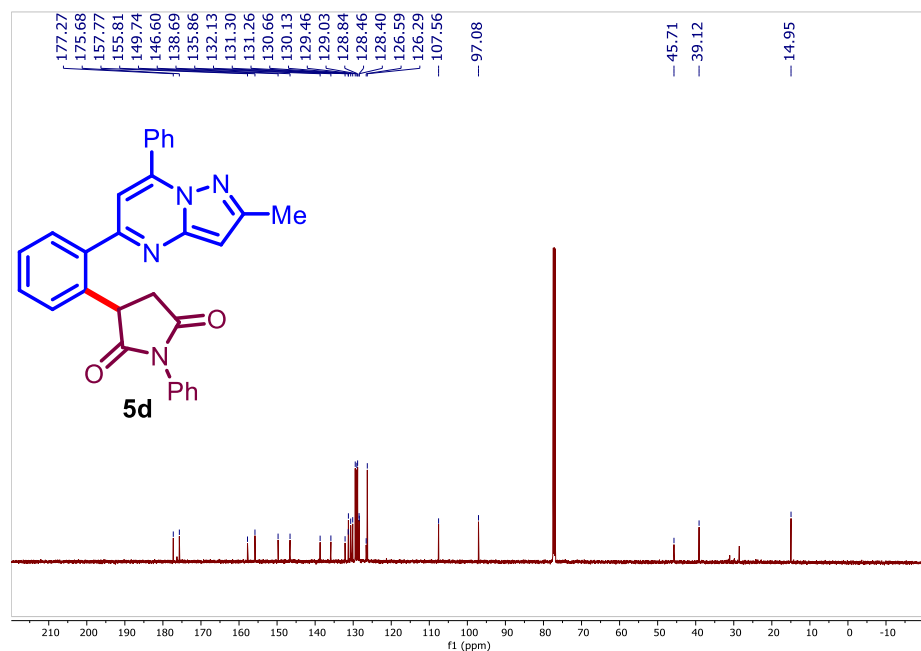


Figure 5.8 ¹³C NMR spectrum of compound **5d** (126 MHz, CDCl₃)

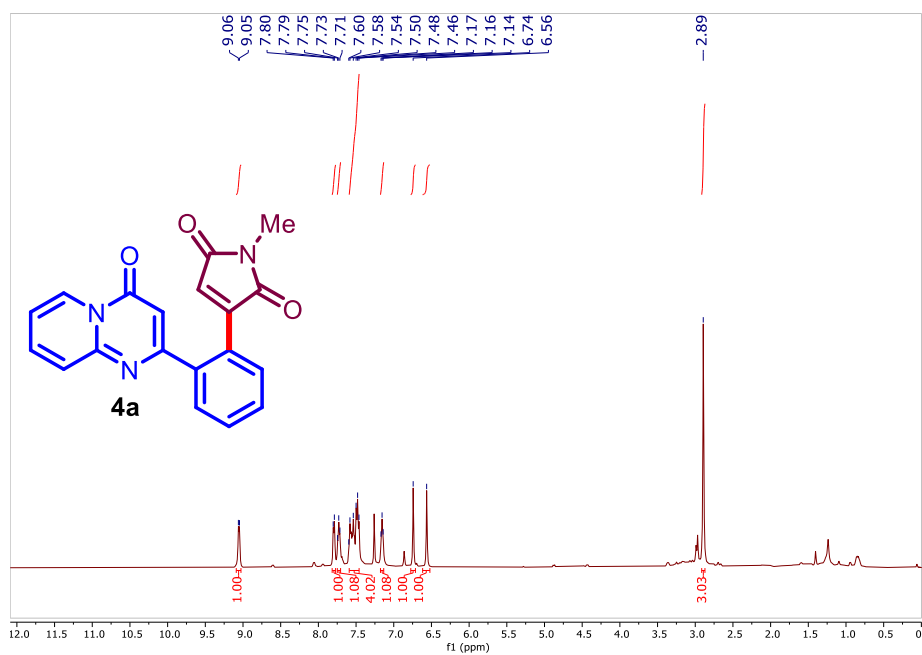


Figure 5.9 ¹H NMR spectrum of compound **4a** (500 MHz, CDCl₃)

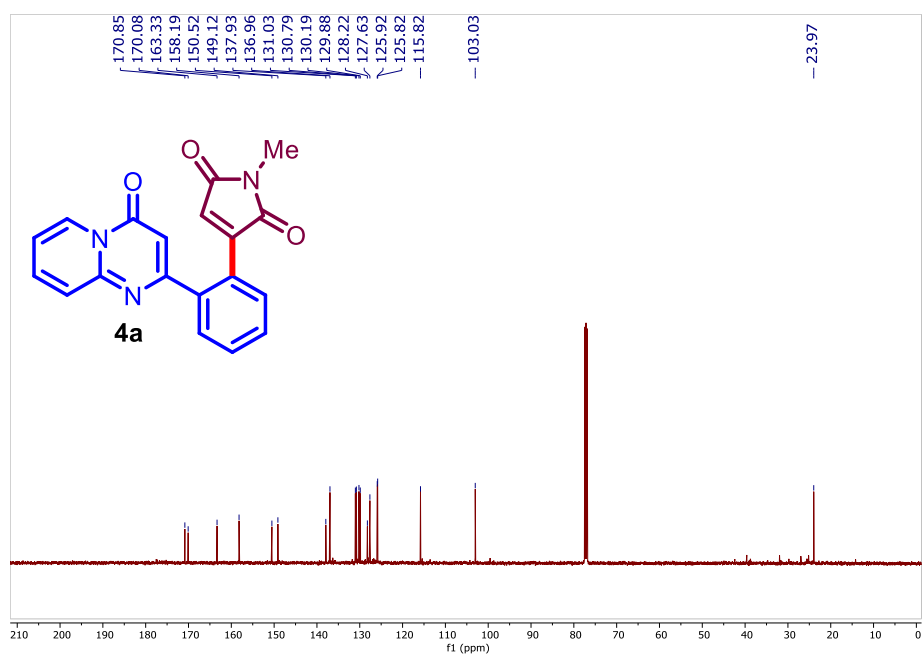


Figure 5.10 ¹³C NMR spectrum of compound **4a** (126 MHz, CDCl₃)

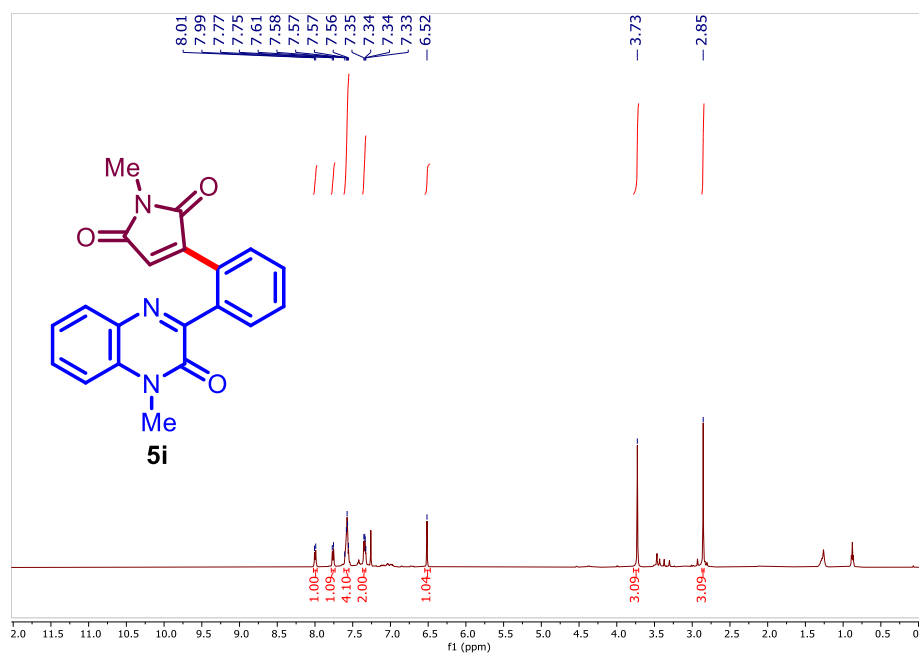


Figure 5.11 ^1H NMR spectrum of compound **5i** (500 MHz, CDCl_3)

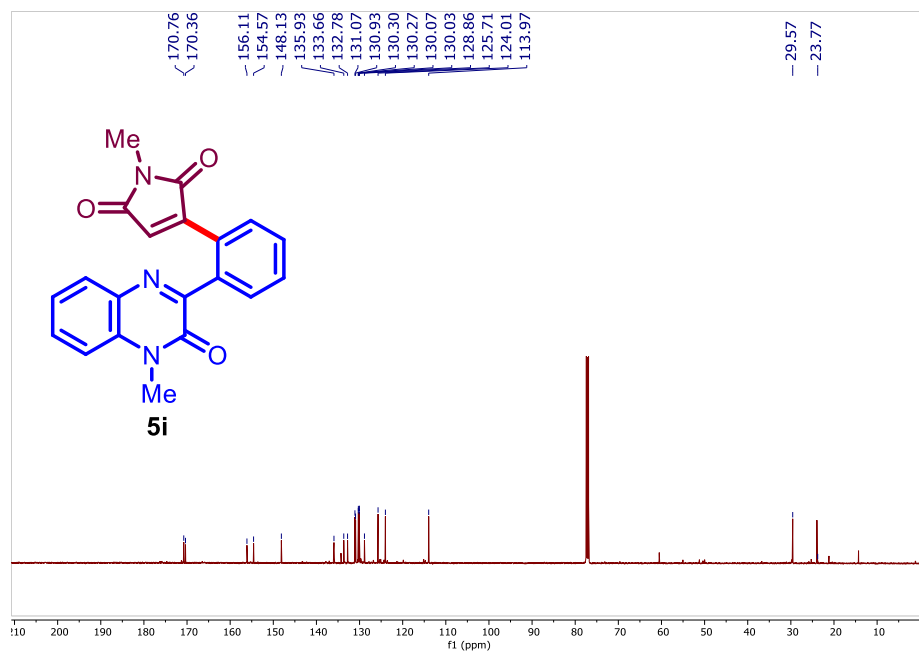


Figure 5.12 ^{13}C NMR spectrum of compound **5i** (126 MHz, CDCl_3)

5.9 References

1. De Angelis M., Stossi F., Carlson K. A., Katzenellenbogen B. S., Katzenellenbogen J. A. (2005), Indazole Estrogens: Highly Selective Ligands for the Estrogen Receptor β , *J. Med. Chem.*, **48**, 1132-1144 (DOI: 10.1021/jm049223g)
2. Larionov O. V., Stephens D., Mfuh A., Chavez G. (2014), Direct, Catalytic, and Regioselective Synthesis of 2-Alkyl-, Aryl-, and Alkenyl-Substituted N-Heterocycles from N-Oxides, *Org. Lett.* **16**, 864-867 (DOI: 10.1021/ol403631k)
3. Kalaria P. N., Karad S. C., Raval D. K. (2018), A review on diverse heterocyclic compounds as the privileged scaffolds in antimalarial drug discovery, *Eur. J. Med. Chem.* **158**, 917-936 (DOI: 10.1016/j.ejmech.2018.08.040)
4. Savelieff M. G., Nam G., Kang J., Lee H. J., Lee M., Lim M. H. (2018), Development of Multifunctional Molecules as Potential Therapeutic Candidates for Alzheimer's Disease, Parkinson's Disease, and Amyotrophic Lateral Sclerosis in the Last Decade, *Chem. Rev.* **119**, 1221-1322 (DOI: 10.1021/acs.chemrev.8b00138)
5. Lee D.-H., Kwon K.-H., Yi C. S. (2012), Dehydrative C–H Alkylation and Alkenylation of Phenols with Alcohols: Expedient Synthesis for Substituted Phenols and Benzofurans, *J. Am. Chem. Soc.* **134**, 7325-7328 (DOI: 10.1021/ja302710v)
6. Dong Z., Ren Z., Thompson S. J., Xu Y., Dong G. (2017), Transition-Metal-Catalyzed C–H Alkylation Using Alkenes, *Chem. Rev.* **117**, 9333-9403 (DOI: 10.1021/acs.chemrev.6b00574)
7. Mandal D., Roychowdhury S., Biswas J. P., Maiti S., Maiti D. (2022), Transition-metal-catalyzed C–H bond alkylation using olefins: recent advances and mechanistic aspects *Chem. Soc. Rev.* **51**, 7358-7426 (DOI: 10.1039/D1CS00923K)

8. Sato M., Dander J. E., Sato C., Hung Y.-S., Gao S.-S., Tang M.-C., Hang L., Winter J. M., Garg N. K., Watanabe K., Tang Y. (2017), Collaborative Biosynthesis of Maleimide- and Succinimide-Containing Natural Products by Fungal Polyketide Megasyntases, *J. Am. Chem. Soc.* *139*, 5317-5320 (DOI: 10.1021/jacs.7b02432)
9. Zhao Z., Yue J., Ji X., Nian M., Kang K., Qiao H., Zheng X. (2021), Research progress in biological activities of succinimide derivatives, *Bioorg Chem* *108*, 104557 (DOI: 10.1016/j.bioorg.2020.104557)
10. Yakkala P. A., Giri D., Chaudhary B., Auti P., Sharma S. (2019), Regioselective C–H alkylation and alkenylation at the C5 position of 2-amino-1,4-naphthoquinones with maleimides under Rh(III) catalysis, *Org. Chem. Front* *6*, 2441-2446 (DOI: 10.1039/C9QO00538B)
11. Thakur A., Dhiman A. K., Sumit, Kumar R., Sharma U., (2021), Rh(III)-Catalyzed Regioselective C8-Alkylation of Quinoline N-Oxides with Maleimides and Acrylates, *J. Org. Chem.* *86*, 6612-6621 (DOI: 10.1021/acs.joc.1c00393)
12. An W., Lee S. H., Kim D., Oh H., Kim S., Byun Y., Kim H. J., Mishra N. K., Kim I. S. (2021), Site-Selective C8-Alkylation of Quinoline N-Oxides with Maleimides under Rh(III) Catalysis, *J. Org. Chem.* *86*, 7579-7587 (DOI: 10.1021/acs.joc.1c00612)
13. Nale S. D., Thombal R. S., Lee Y. R. (2021), Ruthenium(II)-Catalyzed Direct Ortho Functionalization of 1-Arylpyrazoles with Maleimides: A Condition Controlled Installation of Succinimides and Maleimides on Arenes, *Asian J. Org. Chem.* *10*, 2374-2378 (DOI: 10.1002/ajoc.202100211)
14. Sheng Y., Gao Y., Duan B., Lv M., Chen Y., Yang M., Zhou J., Liang G., Song Z. (2022), Rhodium(III)-Catalyzed Direct C7-Selective Alkenylation and Alkylation of Indoles with

- Maleimides, *Adv. Synth. Catal.* **364**, 307-313 (DOI: 10.1002/adsc.202101055)
15. Ramkumar A., Sreedharan R., Rajeshwaran P., Gandhi T. (2023), Ruthenium(II)-catalyzed oxidative dehydrogenation and hydroarylation of maleimides with phthalazinones – insights into additive-controlled product selectivity, *Org. Biomol. Chem.* **21**, 2695-2699 (DOI: 10.1039/D3OB00297G)
 16. Manisha, Chandra D., Sharma U. (2023), Rhodium-Catalyzed C8-Alkenylation of Isoquinolones with Maleimides, *Eur. J. Org. Chem.* **26**, e202300411 (DOI: 10.1002/ejoc.202300411)
 17. Empel C., Jana S., Koodan A., Koenigs R. M. (2022), Unlocking C–H Functionalization at Room Temperature via a Light-Mediated Protodemetalation Reaction, *ACS Catal.* **12**, 8229-8236 (DOI: 10.1021/acscatal.2c01267)
 18. Revathi L., Ravindar L., Fang W. -Y, Rakesh K., Qin H. -L. (2018), Visible light-induced C–H bond functionalization: a critical review, *Adv. Synth. Catal.* **360**, 4652-4698 (DOI: 10.1002/adsc.201800736)
 19. Chen H., Yu S. (2020), Remote C–C bond formation via visible light photo-redox-catalyzed intramolecular hydrogen atom transfer, *Org. Biomol. Chem.* **18**, 4519-4532 (DOI: 10.1039/D0OB00854K)
 20. Yu X.-Y., Chen J.-R., Xiao W.-J. (2021), Visible light-driven radical-mediated C–C bond cleavage/functionalization in organic synthesis, *Chem. Rev.* **121**, 506-561 (DOI: 10.1021/acs.chemrev.0c00030)
 21. Tian W.-F., Hu C.-H., He K.-H., He X.-Y., Li Y. (2019), Visible-light photo-redox-catalyzed decarboxylative alkylation of heteroarenes using carboxylic acids with hydrogen release, *Org. Lett.* **21**, 6930-6935 (DOI: 10.1021/acs.orglett.9b02539)

22. Guo J.-Y., Zhang Z.-Y., Guan T., Mao L.-W., Ban Q., Zhao K., Loh T.-P. (2019), Photo-redox-catalyzed stereoselective alkylation of enamides with N-hydroxyphthalimide esters via decarboxylative cross-coupling reactions, *Chem. Sci.* **10**, 8792-8798 (DOI: 10.1039/C9SC03070K)
23. Mantry L., Parthasarathy G. (2024), Photochemical Direct Alkylation of Heteroarenes with Alkanes, Alcohols, Amides, and Ethers, *Org. Biomol. Chem.* **22**, 7643-7648 (DOI: 10.1039/D4OB01119H)
24. Prier C. K., Rankic D. A., MacMillan D. W. (2013), Visible Light Photo-redox Catalysis with Transition Metal Complexes: Applications in Organic Synthesis, *Chem. Rev.* **113**, 5322-5363 (DOI: 10.1021/cr300503r)
25. Fabry D. C., Rueping M. (2016), Merging Visible Light Photo-redox Catalysis with Metal Catalyzed C–H Activations: On the Role of Oxygen and Superoxide Ions as Oxidants, *Acc. Chem. Res.* **49**, 1969-1979 (DOI: 10.1021/acs.accounts.6b00275)
26. Bhawale R. T., Chillal A. S., Kshirsagar U. A. (2025), Visible-Light-Enabled Regioselective C–H alkylation and alkenylation of 2-Aryl Heterocycles using Dual Catalysis, *Adv. Synth. Catal.* **367**, e202401294 (DOI: 10.1002/adsc.202401294).
27. Peng L., Gao X., Duan L., Ren X., Wu D., Ding K. (2011), Identification of Pyrido[1,2-*a*]pyrimidine-4-ones as New Molecules Improving the Transcriptional Functions of Estrogen-Related Receptor α , *J. Med. Chem.* **54**, 7729-7733 (10.1021/jm200976s)
28. Bhawale R. T., Chillal A. S., Kshirsagar U. A. (2023), 4*H*-Pyrido[1,2-*a*]pyrimidin-4-one, biologically important fused heterocyclic scaffold: Synthesis and functionalization, *J. Heterocycl. Chem.* **60**, 1356-1373 (DOI: 10.1002/jhet.4637)
29. Song Q., Zhang L., Wang B., Chen Z., Jin W., Xia Y., Wu S., Liu C., Zhang Y. (2024), Pd-Catalyzed Direct C7

Trifluoromethylation of Indolines with Umemoto's Reagent, *Org. Lett.* 26, 3685-3690 (10.1021/acs.orglett.3c04123)

30. Sikari R., Chakraborty G., Guin A. K., Paul N. D. (2020), Nickel-Catalyzed [4 + 2] Annulation of Nitriles and Benzylamines by C–H/N–H Activation, *J. Org. Chem.* 86, 279-290 (10.1021/acs.joc.0c02069)
31. Kalsi D., Barsu N., Chakrabarti S., Dahiya P., Rueping M., Sundararaju B. (2019), C–H and N–H bond annulation of aryl amides with unactivated olefins by merging cobalt(III) and photo-redox catalysis, *Chem. Commun.* 55, 11626-11629 (DOI: 10.1039/C9CC05744G)
32. Sen C., Sarvaiya B., Sarkar S., Ghosh S. C. (2020), Room-Temperature Synthesis of Isoindolone Spirosuccinimides: Merger of Visible-Light Photocatalysis and Cobalt-Catalyzed C–H Activation, *J. Org. Chem.* 85, 15287-15304 (DOI: 10.1021/acs.joc.0c02120)
33. Liu S.-L., Ye C., Wang X. (2022), Recent advances in transition-metal-catalyzed directed C–H alkenylation with maleimides, *Org. Biomol. Chem.* 20, 4837-4845 (DOI: 10.1039/D2OB00604A)
34. Xiao L., Liu X.-G., Bao M.-Z., Song J.-L., Chen S.-Y., Zheng Y.-C., Liu Y.-Z., Zhang S.-S. (2023), Cp*Rh(III)-Catalyzed ortho-Alkylation/Alkenylation of Nitroarenes, *Org. Lett.* 25, 5185-5190 (DOI: 10.1021/acs.orglett.3c01614)

6. Overall Conclusion and Future Scope

6.1 Conclusion

The focus of this thesis is on developing a novel strategy for C–C bond formation via harnessing the power of visible light-photo-redox catalysis for C–H functionalization of 2-aryl heterocycles. Specifically, we have explored the C–H functionalization of the 2-phenyl-4H-pyrido[1,2-a]pyrimidin-4-one scaffold, employing a dual catalytic approach that synergistically merges photo-redox and transition metal catalysis to provide a greener and more sustainable pathway under mild conditions. These approaches not only enhance the efficiency of heterocyclic scaffold functionalization but also offer an environmentally friendly and operationally efficient pathway for sustainable synthetic transformations.

*In **Chapter 1**, we discussed an overview of synthetic methods and the advantages and limitations of cross-coupling reactions. Then we discussed transition metal catalysts, highlighting their role, particularly in C–H activation and functionalization processes, and their limitations. Further, visible light-mediated C–H functionalization overcomes the has been discussed. Additionally, the merging of transition metal catalysis with photo-redox that converts inert C–H bonds into C–C bonds, thereby enhancing the efficiency of bond-forming reactions has been discussed. This chapter also covers the significance of pyridine as a versatile core structure in the synthesis of various biologically active and pharmacologically relevant heterocyclic compounds. Finally, we delve into the bioactive scaffold 4H-pyrido[1,2-a]pyrimidin-4-one, summarizing its synthetic methodologies and the advancements in its functionalization reported to date.*

*In **Chapter 2**, a metal-free, organic dye-catalyzed direct C3–H arylation of pyrido[1,2-a]pyrimidin-4-ones using visible light under mild*

conditions has been discussed. This straightforward C–H functionalization method efficiently produces C3-arylated pyrido[1,2-*a*]pyrimidin-4-one and thiazolo[3,2-*a*]pyrimidin-5-one derivatives, including medically relevant endothelial cell dysfunction inhibitors and anti-inflammatory agents, in good to excellent yields. The approach demonstrates good functional group tolerance, and it is suitable for scale-up synthesis.

In **Chapter 3**, we presented a novel ortho C–H decarboxylative arylation of pyrido[1,2-*a*]pyrimidin-4-one using phenyl glyoxylic acid. This methodology employs a synergistic catalytic system combining a ruthenium-photocatalyst with a palladium catalyst under visible light irradiation in the presence of greener oxygen as an oxidant using extremely mild conditions for C–H functionalization. The developed protocol efficiently delivers aryl ketone-functionalized pyrido[1,2-*a*]pyrimidin-4-one derivatives in yields up to 91%, showcasing excellent functional group tolerance and a broad substrate scope under mild, environmentally friendly conditions.

In **Chapter 4**, a visible-light-induced, photocatalyst-free, site-selective C–H arylation of 2-phenyl-4H-pyrido[1,2-*a*]pyrimidin-4-one and related 2-aryl heteroarenes, achieving ortho-arylated products in 41–95% yields at room temperature has been discussed. Mechanistic studies, including controlled experiments, UV-visible analysis, and DFT calculations, suggest that an *in situ* generated Ag-palladacycle complex absorbs visible light, facilitating aryl radical generation from aryldiazonium salts, leading to efficient C–H arylation under mild conditions. This approach is suitable for the scalable synthesis of the desired product.

In **Chapter 5**, we described a visible-light-induced, ortho-selective C–H alkylation and alkenylation of 2-aryl heteroarenes with maleimides using dual catalysis, merging a rhodium-catalyst with eosin Y in the presence of water as reaction solvent. This mild, silver-free protocol achieves up to 92% yield with a broad substrate scope. Mechanistic

studies, including the KIE study, H/D labelling study, light on-off experiments, and quantum yield calculations, H₂O₂ detection tests, were performed to understand the reaction pathway. The approach is also suitable for scalable synthesis of the desired alkylated and alkenylated products.

6.2. Future scope

The functionalization of 2-aryl heterocycles and nitrogen-containing fused heterocycles continues to be a compelling area of research in organic synthesis due to its broad applications across various fields, including medicinal chemistry, agrochemicals, pharmaceuticals, and materials science. The methodologies developed in this context offer versatile pathways for synthesizing bioactive molecules and drug candidates with diverse pharmacological properties such as anti-inflammatory, antitubercular, antiallergic, antioxidant, and antipsychotic activities. By streamlining synthetic routes, these approaches can significantly reduce the number of steps needed to access complex molecules. Furthermore, structural modifications of key bioactive scaffolds can enable the creation of compound libraries, facilitating the discovery and optimization of new therapeutic agents. Through comprehensive screening and structure-activity relationship (SAR) studies, these modifications can lead to the development of new lead molecules or drug candidates with improved efficacy and selectivity.

List of Publications:

Thesis work:

1. **Bhawale R.T.**, Kshirsagar U. A. (2023), Visible Light Assisted C-3 Arylation of Pyrido[1,2-*a*]pyrimidin-4-ones and Thiazolo[3,2-*a*]pyrimidin-5-ones, *J. Org. Chem.* 88, 9537-9542 (DOI: 10.1021/acs.joc.3c00780).
2. **Bhawale R. T.**, Sarothiya D., Kshirsagar U. A. (2022), Synergistic Approach for Decarboxylative Ortho C–H Aroylation of 2-Aryl-pyrido[1,2-*a*]pyrimidin-4-ones and Thiazolopyrimidinones by Merging Palladium Catalysis with Photo-catalysis, *Asian J. Org. Chem.* 11, e202200134 (DOI: 10.1002/ajoc.202200134).
3. **Bhawale R. T.**, Chillal A. S., Ghosh S., Kshirsagar U. A. (2024), Visible-Light Induced Ag-Palladacycle-Complex-Mediated Regioselective C–H Arylation, *Adv. Synth. Catal.* 366, 3603-3609 (DOI:10.1002/adsc.202400466).
4. **Bhawale R. T.**, Chillal A. S., Kshirsagar U. A. (2025), Visible-Light-Enabled Regioselective C–H alkylation and alkenylation of 2-Aryl Heterocycles using Dual Catalysis, *Adv. Synth. Catal.* 367, e202401294 (DOI: 10.1002/adsc.202401294).
5. **Bhawale R. T.**, Chillal A. S., Kshirsagar U. A. (2023), 4*H*-Pyrido[1,2-*a*]pyrimidin-4-one, biologically important fused heterocyclic scaffold: Synthesis and functionalization, *J. Heterocycl. Chem.* 60, 1356-1373 (DOI: 10.1002/jhet.4637).

Additional work:

1. Sarothiya D., **Bhawale R. T.**, Kshirsagar U. A. (2022), Organic-Dye-Catalyzed Visible-Light-Mediated Regioselective C-3 Alkoxyacylation of Imidazopyridines by Carbazates, *J. Org. Chem.* 87, 14915-14922 (DOI: 10.1021/acs.joc.2c01742).
2. Chillal A. S., **Bhawale R. T.**, Kshirsagar U. A. (2023), Photo-induced Regio-selective Chalcogenation and Thiocyanation of 4*H*-

- Pyrido[1,2-*a*]-pyrimidin-4-ones Under Benign Conditions, *Eur. J. Org. Chem.* 26, e202300665 (DOI: 10.1002/ejoc.202300665).
3. Chillal A. S., **Bhawale R. T.**, Kshirsagar U. A. (2024), Oxone[®] Mediated Regioselective C(sp²)-H Selenylation and Thiocyanation of Pyrazolo[1,5-*a*]pyrimidines at room temperature, *Chemistryselect* 9, e202304815 (DOI: 10.1002/slct.202304815).
 4. Chillal A. S., **Bhawale R. T.**, Kshirsagar U. A. (2024), Regioselective C(sp²)-H halogenation of pyrazolo[1,5-*a*]pyrimidines facilitated by hypervalent iodine(III) under aqueous and ambient conditions, *RSC Adv.* 14, 13095-13099 (DOI: 10.1039/d4ra02090a).
 5. Chillal A. S., **Bhawale R. T.**, Sharma S., Kshirsagar U. A. (2024), Electrochemical Regioselective C(sp²)-H Bond Chalcogenation of Pyrazolo[1,5-*a*]pyrimidines via Radical Cross Coupling at Room Temperature, *J. Org. Chem.* 89, 14496-14504 (DOI: 10.1021/acs.joc.4c00856).

Erratum





Mr. Rajesh T. Bhawale was born in Beed, Maharashtra, India, in 1995. He completed his B.Sc. (2016) and M.Sc. in Chemistry (2018) from Dr. Babasaheb Ambedkar Marathwada University, Chhatrapati Sambhajinagar (Aurangabad), India. In 2019, he qualified UGC-NET, GATE, and SET examinations. He pursued his doctoral studies in Chemistry at the Indian Institute of Technology Indore (2020–2024) under the supervision of Dr. Umesh A. Kshirsagar. His research focused on “Visible Light-induced Photo-redox Catalysis and Dual Catalysis for C–H Functionalization of 2-Phenyl-4H-pyrido[1,2-a]pyrimidin-4-one and 2-Aryl Heterocycles,” a culmination of dedicated research over five years.